Advances in Earthquake Engineering

Earthquake Geodynamics

Seismic Case Studies

Editor: E.L. Lekkas

WIT PRESS

Earthquake Geodynamics:

Seismic Case Studies

WITPRESS

WIT Press publishes leading books in Science and Technology.
Visit our website for new and current list of titles.
www.witpress.com

WITeLibrary

Making the latest research accessible, the WIT electronic-library features papers presented at Wessex Institute of Technology's prestigious international conferences.
To access the library and view abstracts free of charge please visit www.witpress.com

Advances in Earthquake Engineering

Objectives

The objectives of this series are to provide clear accounts of both basic and applied research in the various fields of earthquake engineering with particular reference to earthquake resistant analysis and the design of structural systems.

The series consists of books concerned with state-of-the-art developments in earthquake engineering and as such comprises volumes covering the latest developments and applications. Each book is composed of authored works or edited volumes of several chapters written by leading researchers in the field.

The scope of the series covers almost the entire spectrum of earthquake engineering and as such the following topics are covered: engineering seismology, strong ground motions and site effects, seismic hazard evaluation and design earthquake loads, soil-structure interaction, numerical methods in earthquake engineering, stochastic analysis methods, principles of earthquake resistant design, reinforced concrete structures, steel structures, masonry and masonry infill structures, historical buildings and monuments, bridges, earth and concrete dams, underground and lifeline structures, storage tanks, silos and other industrial structures, offshore structures, seismic isolation and control, vulnerability and risk assessment of structural systems, repair and retrofit, seismic code regulations and case studies in earthquake engineering.

Series Editors

D.E. Beskos
University of Patras
Greece

E. Kausel
Massachusetts Inst. of Technology
USA

Honorary Editors

Associate Editors

Earthquake Geodynamics:
Seismic Case Studies

Editor: E.L. Lekkas

WIT PRESS Southampton, Boston

Earthquake Geodynamics: Seismic Case Studies

Series: Advances in Earthquake Engineering

E.L. Lekkas
University of Athens, Greece

Published by

WIT Press
Ashurst Lodge, Ashurst, Southampton, SO40 7AA, UK
Tel: 44 (0) 238 029 3223; Fax: 44 (0) 238 029 2853
E-Mail: witpress@witpress.com
http://www.witpress.com

For USA, Canada and Mexico

Computational Mechanics Inc
25 Bridge Street, Billerica, MA 01821, USA
Tel: 978 667 5841; Fax: 978 667 7582
E-Mail: infousa@witpress.com
http://www.witpress.com

British Library Cataloguing-in-Publication Data

A Catalogue record for this book is available
from the British Library

ISBN: 1-85312-996-8
ISSN: 1361-617X

Library of Congress Catalog Card Number: 2003106796

The texts of the papers in this volume were set individually by the authors or under their supervision. Only minor corrections to the text may have been carried out by the publisher.

Printed in Great Britain by Athenaeum Press, Gateshead.

Contents

Preface ..... **xiii**

Chapter 1 The 1999 earthquake in Izmit – the study of actualistic strike-slip tectonic forms **1**
E.L. Lekkas

1 Introduction 1
2 Geodynamic – seismotectonic setting 4
3 General description of seismic faults 5
4 Detailed description of fault segments 6
5 Tectonic forms and structures 10
6 Discussion and conclusions 15

Chapter 2 The Gujarat, West India Earthquake (26 January 2001): A geodynamic episode in an intra-plate compressional regime **23**
S.G. Lozios, E.L. Lekkas & G.D. Danamos

1 Introduction 24
2 The geodynamic regime of India 25
3 The seimotectonic regime of the major area 26
4 The tectonic structure of the affected area 28
5 Seismic ruptures and seimic fault 29
6 Discussion and conclusions 31

Chapter 3 Contribution of GIS to analysis of the 7 September 1999 Athens earthquake **35**
N. Voulgaris

1 Introduction 35
2 Data 36

2.1 Seismological data 36
2.2 Additional data 37
3 Data analysis 38
4 Discussion 43

Chapter 4 The neotectonic macrostructures and the geological basement, the main factors controlling the spatial distribution of the damage and geodynamic phenomena resulting from the Kalamata (13 September 1986) and Athens (7 September 1999) earthquakes **45**
I. Fountoulis

1 Introduction 45
2 The case of Kalamata 46
2.1 Geology – tectonics 46
2.2 Neotectonics – fault-zones – faults 48
2.3 Geographical distribution of damage and geodynamic phenomena ... 50
2.4 Conclusions 54
3 The case of Athens 55
3.1 Geology – tectonics 55
3.2 Neotectonics – fault-zones – faults 56
3.3 Geographical distribution of damage and geodynamic phenomena ... 59
3.4 Conclusions 61
4 Discussion and conclusions 63

Chapter 5 A sequence of low magnitude earthquakes as a result of local tectonic activation: the case of the Psachna area, Evia Island, Greece **69**
D. Fountoulis, Ch. Metaxas, S. Lalechos & C. Gountromichou

1 Introduction 70
1.1 Geology – tectonics 70
1.2 Historical and instrumental seismicity 71
2 Methodology 72
3 Data analysis 72
3.1 Current seismicity 72
3.2 Lineament analysis based on Landsat 7 ETM+ data 73
3.3 Gravity data 74
4 Results 75
5 Conclusions 78

Chapter 6 The 26 July 2001 Skyros (north Aegean Sea, Greece) earthquake **81**
G. Drakatos, G. Stavrakakis, A. Ganas, V. Karastathis, N. Melis, M. Ziazia & A. Plessa

1 Introduction 81
2 Data: instrumental seismicity – foreshock activity 84
2.1 The aftershock sequence – aftershocks focal mechanism 85
3 Discussion and conclusions 87

Chapter 7 Surficial expression of seismic faults and urban planning **91**
S.G. Lozios, E.L. Lekkas & L.C. Chatzistavrou

1 Introduction 91
2 The Kalamata earthquake (13 September 1986, M_s= 6.0) 93
3 The Greneva-Kozani earthquake (13 May 1995, M_s= 6.6) 95
4 The Egio earthquake (15 June 1995, M_s= 6.1) 97
5 The Parnitha (Athens) earthquake (9 September 1999, M_s= 5.9) 101
6 Discussion and conclusions 102

Chapter 8 Active faults and seismic hazard assessment at municipality level – the case of Tenea (Corinthia, Greece) **105**
H.D. Kranis, E.L. Lekkas, S.G. Lozios & A.S. Bakopoulou

1 Introduction 105
2 Geology and tectonics 108
3 Seismological data 111
4 Examination of population centres and infrastructure 112
4.1 Hiliomodi - Koutalas 112
4.2 Klenia – Agios Vassileios 113
4.3 Stefanion - Agionorion 114
4.4 Spathovouni – Corinth-Tripolis motorway 114
4.5 Mapsos 116
5 Discussion and conclusions 116

Chapter 9 Seismically-triggered landslide risk assessment **119**
I. Parcharidis, Emm. Vassilakis, Ger. Cooksley & Ch. Metaxas

1 Introduction 119
2 Geological setting of the area 121

3 Data collection and database construction 123
3.1 Analysis method 123
3.2 Static factor of safety 124
3.3 Newmark displacement calculation 125
4 Results and conclusions 127

Chapter 10 Low-strain techniques used for microzoning studies in soft rock areas in Greece **131**
T.D. Papadopoulos, J.D. Alexopoulos & P.J. Kambouris

1 Introduction 131
2 Methodology 132
2.1 Surface methods 132
2.2 Borehole methods 133
3 Elastic moduli determination 134
4 Case histories 135
4.1 Area of Greneva-Kozani 135
4.2 Area of Aegio - Achaia 137
4.3 Area of Thiva Beotia 140
4.4 Area of Athens Attiki 140
4.5 Area of Heraklion Crete 141

Chapter 11 Parameters of intensity distribution in the Izmit and Düzce (Turkey) earthquakes **147**
E.L. Lekkas

1 Introduction 147
2 Seismic faults 149
3 Concomitant geodynamic phenomena 150
4 Intensity evaluation – geographic distribution 153
5 Conclusions 157

Chapter 12 Seismic strike-slip faults on a major boundary transverse to the Apenninic chain; the case of the Molise (S. Italy) earthquake (31 October 2002) **161**
S.G. Lozios, G.D. Danamos & E.L. Lekkas

1 Introduction 162
2 Geodynamic frame of the Italian peninsula 162
3 Geological frame and seismotectonic regime of the wider affected area .. 164
4 The earthquake parameters 169
5 Tectonic structures, geotechnical effects and damage distribution 170
6 Discussion and conclusions 174

PREFACE

This book brings together a number of papers discussing various aspects of earthquake geodynamics in seismically active regions. It is the twelfth volume in the series *Advances in Earthquake Engineering,* which has gained broad acceptance from the scientific world. The main concept behind this compilation is to bring together a number of papers dealing with the geological, tectonic, seismological and engineering geological aspects of earthquakes. It has been realized, often painfully, that unless all these are mastered, constructions (be it private houses, lifelines or even nuclear power plants) will never be safe, even if they are designed to meet the strictest safety standards. What is more, a thorough knowledge of earthquake geodynamics is vital in increasing the safety/cost ratio of every construction.

The contributions include 'lessons learnt' from earthquakes which struck urban areas in the past two decades and cover a wide variety of topics within earthquake geodynamics such as the analysis of seismic sequences, the study of surficial deformation, G.I.S. integration of multi-disciplinary studies and geophysical techniques for microzonation purposes. The authors are renowned geoscientists who have had first-hand experience of earthquake events in seismically active regions such as Greece and Turkey.

The opening chapter is by Lekkas who sees the Izmit and Düzce earthquakes in Turkey (August and November 1999) as case studies for the better understanding of tectonic deformation in strike-slip regimes. He illustrates the current deformation pattern of one of the most active fault zones in the world, the North Anatolian Fault Zone, and correlates it with recent results from experimental studies in strike-slip deformation environments.

In Chapter 2 Lozios et al. discuss the consequences of one of the most devastating earthquakes in the past 100 years, especially in terms of the human toll paid. The Gujarat event is placed in the geodynamic context of the active plate margin between the Indian subcontinent and the Eurasian tectonic plate. The authors describe the patterns of surficial deformation and the geological site effects that aggravated the consequences of the earthquake, which resulted in extensive damage even hundreds of kilometres away from its epicentre.

Chapter 3 is by Voulgaris who utilises specialized GIS database structures to perform a multi-parameter analysis of the aftershock sequence of the 7 September 1999 earthquake of Athens. This contribution combines seismic and tectonic data from all the research groups involved in the post-earthquake surveys in order to provide better insight into earthquake activity and potential in the broader area of the capital of Greece.

The contribution by Fountoulis I. in Chapter 4 makes illuminating associations between the Athens earthquake in 1999 and the Kalamata event, 13

years earlier. The paper focuses on the selective distribution of catastrophic phenomena and correlates it with the prevailing neotectonic and geological conditions. One of the most didactic results of this work is that the seismic parameters, as the focal depth and mechanism, are not the only factors that need to be taken into account when considering the earthquake risk of an active area, as damage and the suite of earthquake-related phenomena are controlled by the existing pre-quaternary tectonic grain, such as blind thrusts, Mesozoic discontinuities and so forth.

The importance of knowledge of the geological and tectonic conditions is also demonstrated by Fountoulis D. et al. (Chapter 5) who focus on a swarm of low-magnitude that occurred within a two-month spell in Evia, central Greece. The integration of seismic data, the processing of Landsat ETM+ images and the interpretation of local gravity anomalies suggest that the active tectonics in the area is controlled by a relatively shallow Mesozoic structure. Furthermore, they discuss the complex deformation history of the area, which is expressed in the form of micro-block displacements.

Drakatos et al. in Chapter 6 analyse the earthquake sequence of the Mw=6.5 event which took place in the central Aegean Sea, close to the island of Skyros, in the summer of 2001. Their analysis suggests that the current westerly termination of the North Anatolian Fault Zone may be found within the central Aegean tectonic basin.

The significance of integrating scientific knowledge with decision-making is shown by Lozios et al. (Chapter 7) who re-examine the subject of the adequacy of current regulations for safe constructions in tectonically active zones, in the light of recent results from earthquake-stricken areas. They describe the variations in the surficial expression of earthquake faulting, which are dependent both upon the seismic characteristics of the shock and the local geological and tectonic conditions.

In Chapter 8 Kranis et al. deal with the pre-catastrophic stage and use a G.I.S.-based multi-disciplinary approach to assess the earthquake risk at municipality level. They combine the results of geological, tectonic, seismic, geotechnical and building vulnerability studies and define the localities most prone to the various earthquake-related site effects, including liquefaction, landslides, local intensity amplification and so on. The possibility of disruption of transportation and other lifelines is also examined and the locations where such failures are likely to occur are spotted.

On the subject of earthquake-related destructive phenomena, Parcharidis et al. focus on a very common site-effect of an earthquake, that of seismically-triggered landslides (Chapter 9). They incorporate geophysical and remote-sensing data on a G.I.S. platform and, using a Newmark method, assess the landslide risk of the prefecture of Achaia, southern Greece, in the case of an earthquake.

Focusing on the foundation medium (Chapter 10), Papadopoulos et al. make a comprehensive overview of the geophysical techniques utilized for microzonation projects in soft rock areas. Every technique is outlined and illustrated through appropriate case studies in which the usefulness of the method

is analysed in terms of the clarification of the structure and properties of the foundation medium, especially as far as the spatial distribution of Vs is concerned.

In Chapter 11 Lekkas examines the factors that contributed to the damage distribution in the devastating Izmit and Düzce earthquakes in Turkey of August and November 1999, respectively. He makes use of the updated European Macroseismic Scale (EMS_{1998}) to assess the extent and severity of damage in both earthquakes. The use of EMS_{1998} has proven particularly useful in this case, as the different types of construction are accounted for and the results of the macroseismic records can be better analysed, both qualitatively and quantitatively. He also describes the geological and other earthquake-related site effects that led to local intensity amplification, even at long distances from the fault trace.

In the chapter that concludes this volume, Lozios et al. describe the results of the field survey that was conducted soon after the October 2002 earthquake in southern Italy (Mw=5.9). They also describe the patterns of surficial deformation and relate them to the current seismotectonic setting of the area. This last-minute addition to this volume shows clearly how our knowledge of earthquake geodynamics is constantly updated as seismic events never stop occurring.

All these contributions do nothing but depict the urgent need for better knowledge of the ever-changing surface of our planet, upon which we have built our homes and based our hopes for a happy and prosperous future. And it is not only geoscientists who must broaden and deepen their knowledge on the subject; engineers, too, will be greatly benefited, for the earth awaits being better understood by us.

Concluding, I should like to express my gratitude to WIT Press and the Series Editor, C.A. Brebbia, who gave me the opportunity to compile this book and invaluably assisted me throughout the process of compilation. My sincere thanks also to all the contributors and researchers who did their utmost to produce high-standard work.

E. L. Lekkas
2003

CHAPTER 1

The 1999 earthquake activity in Izmit – The study of actualistic strike-slip tectonic forms

E.L. Lekkas
Faculty of Geology, University of Athens, Greece.

Abstract

The 1999 earthquake activity in the area of Izmit – Bolu, Turkey, which included two major shocks, on 17 August and 12 November 1999, was caused by the reactivation of fault segments that belong to the North Anatolian Fault Zone (NAFZ). The two main earthquakes, measuring Mw=7.4 and 7.1, caused surficial faulting for more than 150 km. The mean fault strike was E-W and the horizontal (right-lateral) offset locally exceeded 5 m. Our field research was focused on fault geometry and slip characteristics, and allowed us to distinguish seven successive right-stepping reactivated segments and the related oversteps that developed between the consecutive segments. Our investigations showed a good match between the observed structures and those produced by experimental modeling. Finally, an estimation is made as to the percentage of seismic and aseismic slip on the reactivated segment of the fault zone.

1 Introduction

On 17 August 1999 (03:01:37 local time), a major earthquake hit NW Turkey. The epicentre was located at 40.702N, 29.987E (USGS), the magnitude was Mw=7.4 (USGS, Kandilli Observatory) and the focal depth was h=15-17 km (USGS). The earthquake caused considerable damage to numerous population centres including Adapazari, Izmit, Gölcük and Yalova, all lying along an E-W axis. The main bulk of the damage was within a 140 by 15 km zone, which also included the surficial occurrence of the seismic fault, which belongs to the NAFZ (Figures 1, 2). Damage was also reported in other locations outside the zone, in Istanbul, Bursa, Eskisehir, Düzce, Bolu for example.

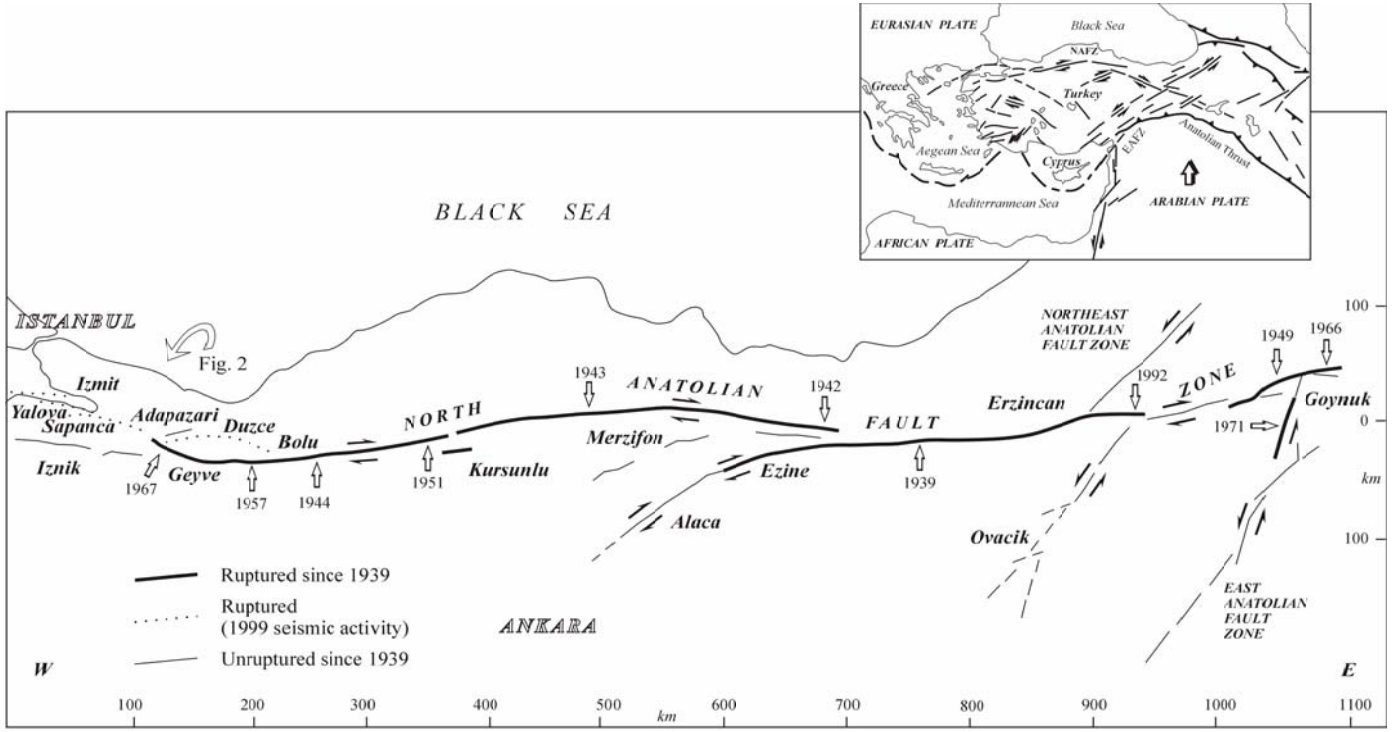

Figure 1: Tectonic sketch map showing the parts of the NAFZ reactivated since 1939 (heavy lines), according to Stein et al. [11], and the Bolu, Düzce, Adapazari, Sapanca, Izmit and Yalova segments ruptured in the 17 August and 12 November 1999 earthquakes (dotted lines).

The post-earthquake damage evaluation reported approximately 17,000 deaths, 45,000 injuries and 600,000 people homeless, while some 45.000 people were reported missing. During the earthquake 2,600 buildings collapsed partially or totally and 20,000 more were heavily damaged. Major industrial facilities and technical constructions were also destroyed, such as motorways, bridges and ports (Lekkas et al. [1]).

About three months later, on 12 November 1999 (19:57:21 local time), the area was hit by a Mw=7.1 earthquake (h=10 km), located at 40.768N, 31.148E (USGS), approximately 100 km east of the August shock. The towns of Bolu, Düzce, Hendek, Gölyaka and Adapazari, among others, were severely damaged; all of them lay on an 80 km long and 10 km wide E-W trending zone. That zone also hosted the surficial occurrence of the seismic fault, located on the eastward prolongation of the 17 August rupture.

The shock killed approximately 1,300 people and injured another 10,000, while some 200,000 became homeless. Five hundred buildings collapsed totally or partially and 5,000 more suffered significant damage. Infrastructure and other facilities were also damaged in this earthquake.

Both earthquakes were accompanied by a suite of earthquake-related effects such as lateral extension, soil fractures, liquefaction, settlement, coastline change and tsunamis. On top of all these, the fires that broke out completed the picture of devastation (Lekkas et al. [1]).

The 150 kilometres of surficial faulting (Figure 2) in the Izmit and Düzce earthquakes gave us a chance to study the real-time deformation in strike-slip zones. This is a rare opportunity because, except for a few cases (the San Andreas Fault being a prime example), the study of strike-slip deformations is based mainly either on laboratory, analog or numerical experiments, or on the examination of tectonic structures formed in the geological past.

In the following sections, we shall give first a brief outline of the regional seismotectonic – geodynamic setting; the earthquake faults and related events will also be presented. Next, we will focus on the reactivated fault segments and associated structures. Finally, a comparison between our observations and the results of previous studies will be attempted.

2 Geodynamic - seismotectonic setting

The Middle East region corresponds roughly to the Arabian Plate (Figure 1), which moves northwards, towards the Eurasian Plate, squeezing the Anatolian Plate out and to the west, while a portion of eastern Turkey, Armenia, Azerbaijan and northern Iran are driven eastwards (Oral [2], Reilinger et al. [3]). The westward extrusion of the Anatolian Plate is accommodated mainly through the NAFZ, which has a mean E-W trend, running from Armenia to the Sea of Marmara. It is a first order tectonic structure within the Eurasian Plate (Ambraseys [4], Sengor [5], Sengor et al. [6], Barka et al. [7], Barka [8]). The right-

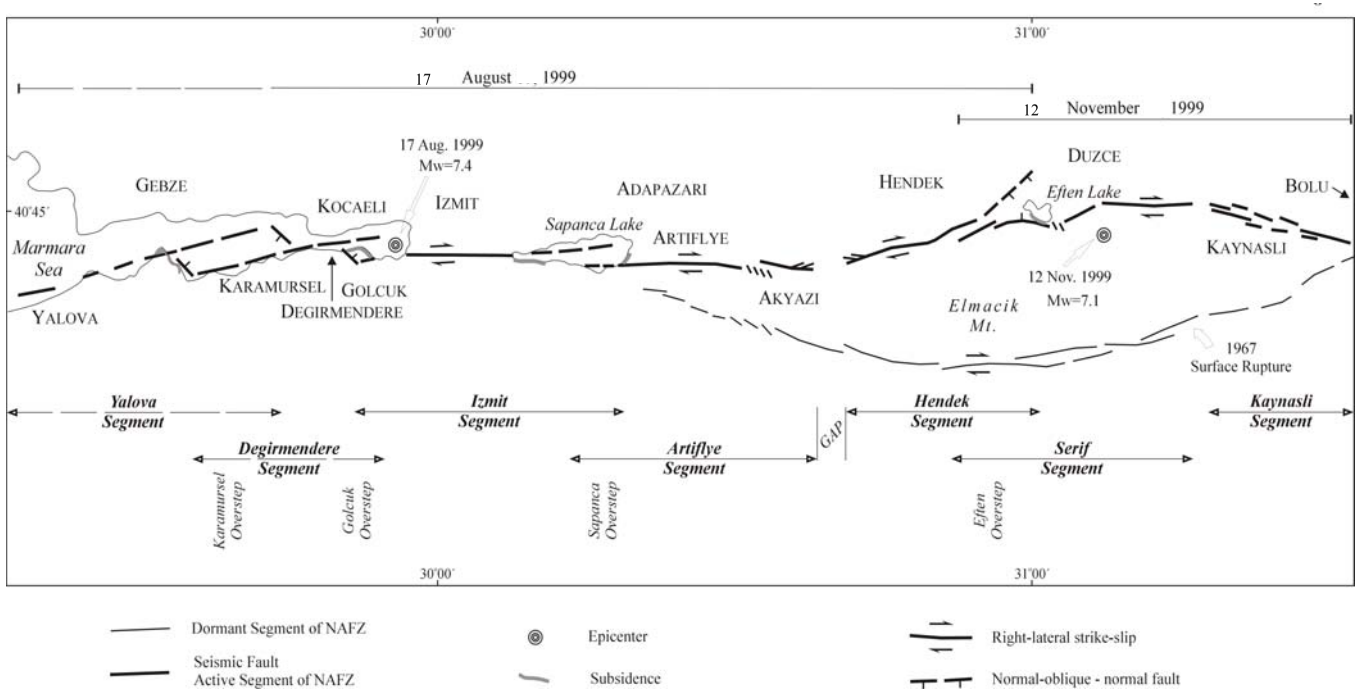

Figure 2: The traces of the segments reactivated in the 17 August and 12 November 1999 earthquakes.

lateral strike-slip motion (Figure 1) of the NAFZ has given birth to a series of major earthquakes, many of them exceeding magnitude 7 (Barka [9], Barka & Kadinsky-Cade [10]). Ten such large earthquakes have occurred since 1939, causing considerable damage to the population centers lying on its traces (Stein et al. [11]).

The existence of the NAFZ is also evident in the modification it has caused to the relief and drainage (Chorowicz et al. [12]). Strike-slip deformation has created, among other things, a series of depressions, or pull-apart basins, such as the Sapanca and Izmit lakes; another example is the Sea of Marmara (Wong et al. [13], Armijo et al. [14]) which, according to more recent research, is characterized as an escape basin with co-linear symmetrical flower structures above a single buried master fault (Aksu et al. [15]).

The outcrops of the neogene and quaternary formations along the NAFZ have also been affected by the strike-slip deformation; they are elongated along a general E-W trend and a smooth relief has developed on these outcrops (Sengor et al. [6], Barka [16], Andrieux et al. [17], Dhont et al. [18]). On the contrary, on both sides of the deformation zone, pre-neogene formations are characterized by high relief and significant differentiation in their tectonic fabric.

The 17 August and 12 November 1999 earthquakes were the outcome of the reactivation of two parts of the NAFZ, located close to its western inland termination. These segments had remained dormant in the twentieth century and their reactivation had been anticipated (Stein et al. [11]). The same authors reported that since 1939 tectonic activity has been migrating westwards, a fact that forewarned seismologists for the 1999 activity (Reilinger et al. [19]).

3 General description of seismic faults

The part of the NAFZ that gave rise to the 17 August 1999 earthquake had not ruptured in the twentieth century (Stein et al. [11]) (Figure 1). GPS surveys had detected aseismic movement on this part, in the order of 10-15 mm/yr (Straub et al. [20], Armijo et al. [14]). USGS has reported that the rupture plane was almost vertical, oriented E-W, and the slip vector was right-lateral (NP1: strike 92, dip 68, slip 178; NP2: strike 183, dip 88, slip 22). It has also been suggested that earthquake fractures were produced in the 1719 and 1754 earthquakes that were located in the same area.

Field reconnaissance and mapping showed that the surficial faulting occurred between Lake Eften and Gölcük, for an overall distance of 100 km; the maximum observed offset was locally more than 5 m (Figure 2). Additionally, there is evidence that faulting continued offshore to the west of Gölcük and in the Sea of Marmara, for another 50 km (Youd et al. [21]).

The epicentre of the 12 November 1999 earthquake was located south of Düzce. The shock was also caused by a part of the NAFZ that had not ruptured in the twentieth century (Stein et al. [11]). GPS measurements have also found a 10-15 mm/year aseismic movement on this part of the fault (Straub et al. [20], Armijo et al. [14]). The focal mechanism solution calculated by the USGS gave

an E-W trending rupture plane with steep southerly dip (NP1: strike 265, dip 65, slip –158, NP2: strike 166, dip 70, slip –27).

Post-earthquake field mapping showed that surficial faulting occurred between Lake Eften to the west and Kaynasli-Bolu to the east, for a distance of over 50 km, and a maximum right-lateral offset that locally exceeded 4.5 m (Figure 2).

The identification and measuring of the geometrical and kinematic characteristics of the reactivated segment (Figure 3) were facilitated by the displacement of man-made features (fences, tree-lines, roads and pavements, power lines, etc.).

Figure 3: Surface break in Gölcük displacing posts by 4 m during the 17 August earthquake.

4 Detailed description of fault segments

The reactivated fault zone in the 17 August earthquake was 100 km long; about 50 km, half of the length of the August reactivated zone, was the rupture caused by the 12 November shock, which means that a total of 150 km were affected by surficial faulting onshore, while within the Sea of Marmara faulting may have continued for a few tens of km (Youd et al. [21]).

It is therefore obvious that the Izmit and Düzce earthquakes are linked not only in time, but also geodynamically, since they were caused by reactivation of consecutive parts of the NAFZ, which had not ruptured in the twentieth century, and share geometrical and kinematic characteristics. Having taken this into

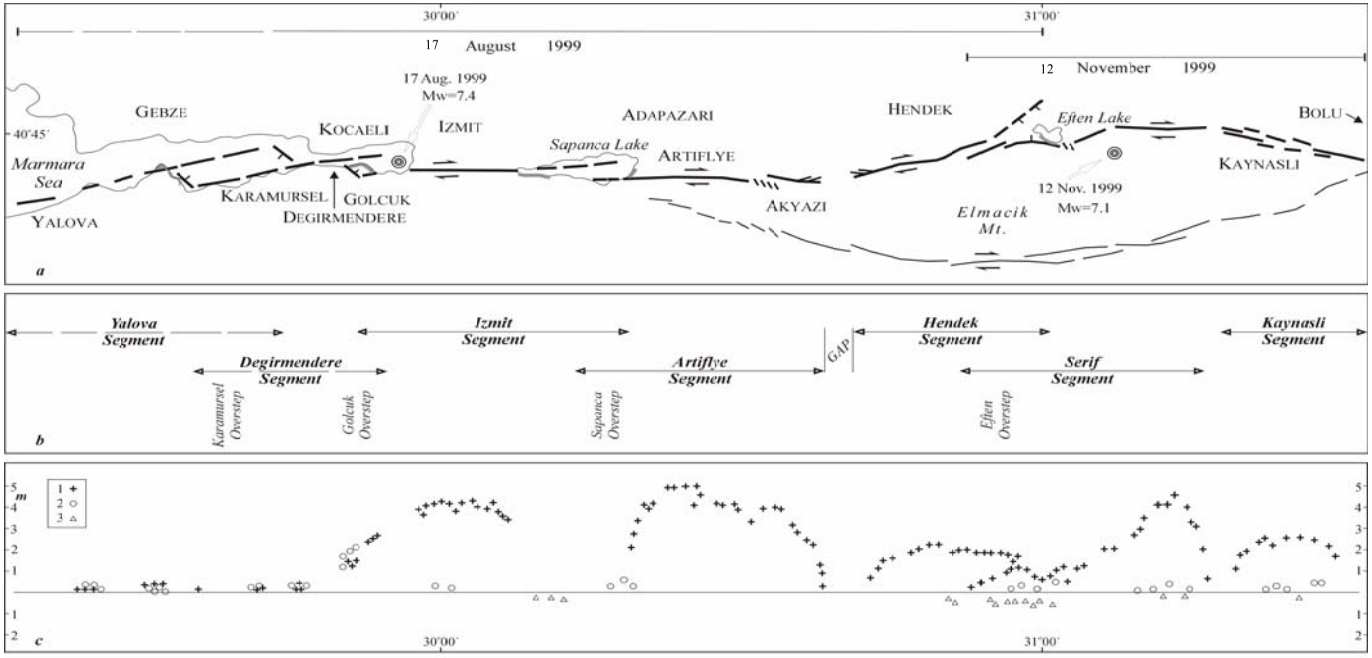

Figure 4: a. Slip map of the surface ruptures associated with the 17 August and 12 November 1999 earthquakes; b. Segment and overstep names; c. Along strike-slip distribution. 1: strike-slip, 2: dip-slip (northern-side-down), 3: dip-slip (southern-side-down).

consideration, it was thought purposeful that all reactivated segments should be studied together.

The surficial ruptures are distinguished in segments (Figure 2), which are characterized by their own geometry and kinematics (Figure 4). Our description is based on field observations along the seismic fault (Lekkas [22], Lekkas [23]) and data taken from Dolan et al. [24], Hartleb & Dolan [25] and Lettis et al. [26].

Yalova segment. This is located within the Sea of Marmara (Youd et al. [21]). It strikes N75°E, parallel to the coastline, which is probably cut by the fault NE of Yalova. At this particular site, there are abundant soil fractures and lateral spreading in the formations that outcrop on the coastal zone, giving rise to ENE-WSW (N75°E) gaps that display horizontal (right-lateral) offset that does not exceed 15 cm. It cannot be confirmed, however, whether these cracks are dynamically related to the Yalova segment or have resulted from seismic shaking. At any rate, the Yalova segment is estimated to be more than 25 km long. The occurrence of numerous submarine slides and tsunamis may indicate that the segment continues further offshore.

Degirmendere segment. The occurrence of this segment is more certain than that of the previous one, since is marks several parts of the coastline between Karamursel and Gölcük. Its overall strike is N70°E and its length is approximately 20 km. Coseismic slip amounted to 20 cm. The separation distance between this segment and the Yalova segment is 4 km, with the Karamursel overstep developing between these two segments.

Karamursel overstep. A 16 by 4 km pull-apart basin has formed within this extensional overstep. However, its occurrence within the Sea of Marmara obstructed further more detailed observation.

Izmit segment. This has a general E-W trend and a length of 27 km, and stretches between Gölcük in the west and Lake Sapanca in the east. At its western end, close to Gölcük (Ford factory) there is a N45°W, 2 km long surficial trace with 2.3 m vertical throw (NE side down) and 1.7 m of dextral offset. Towards the east and for the next 4 km, the fault strike is N85°E and the strike-slip offset reaches 2.8 m. The fault then enters the sea, to be found again south of Izmit at the eastern flank of the gulf; at this location the strike-slip offset reaches its maximum value of 4.6 m and the trend is N85°-90°E, with only minor deviations. The segment can be traced up to Lake Sapanca and its continuation within the lake is deemed highly possible.

Gölcük overstep. A second releasing overstep with the northern part lying under sea level, between the Izmit and Artiflye segments. Its length is ~ 6 km and its width is ~ 2 km.

Artiflye segment. This can be traced from the southern coast of Lake Sapanca up to Akyazi, where the fault trace splays into numerous minor sub-parallel fractures. It maintains a nearly steady E-W trend for about of 37 km. Throughout its length the right-lateral displacement component is predominant, amounting to 5.2 m, while the vertical offset rarely exceeds 20-40 cm. This segment can be distinguished into two constituent faults: the western one displays the maximum, 5.2 m, horizontal offset, accompanied by several en echelon fractures; and the

eastern one, smaller displacement (>4 m). Towards the east, the displacement decreases and the fault trace breaks up into five en echelon fractures with gradually decreasing throw. Note also that a gap exists between the termination of this segment and the adjacent one to the east (Hendek segment).

Sapanca overstep. This develops between the Izmit and Artiflye segments. This strike-slip basin has a length (overlap distance) of 8 km and a width (separation) of 2.5 km.

Hendek segment. This has a length of ~35 km and an initial N80°E trend at its western part, bending eastwards to N60°E. It is traced from Akyazi up to Lake Eften, where it forms the northern flank of the lake. It displays a certain variety in its kinematic characteristics: at the western, N70-80°E trending, part the right-lateral component amounts to 2.6 m and the vertical component does not exceed 0.5 m. At the eastern part, the horizontal offset gradually decreases and the vertical throw reaches 0.5 m, with the southern block downthrown.

Eften overstep. This corresponds roughly with Lake Eften, developing between the Hendek and Serif segments that overlap for ~13 km, being offset by 1-5 km.

Serif segment. This was reactivated in the 12 November 1999 earthquake. Its length is 33 km and strikes N85°-90°E. The strike-slip offset in this segment reaches up to 4.6 m, while locally we measured 0.6 m of vertical throw. Its western part must also have moved in the 17 August 1999 event, with a right-lateral offset of less than 0.5 m.

Kaynasli segment. This is the easternmost fault reactivated in the 12 November earthquake. It stretches from the town of Kaynasli up to Bolu and is characterized by predominant dextral strike-slip offset (maximum observed: 2.8 m) and secondary dip-slip (max: 0.5 m). Its length is 17 km and it has a mean E-W trend. This segment is also characterized by the existence of a broad deformation zone, especially at the locations where it cuts loose surficial deposits. At these sites, the width of the deformation zones, which include suites of minor fractures sub-parallel to each other, is up to 200 m. Its throw steadily decreases towards the E.

The distinction of the segments that ruptured in the 1999 earthquakes gives a picture of the deformation along the NAFZ on the macro-scale; and this has shown that the mean trend of these segments was E-W and their average length was 40 km. The maximum strike-slip displacement was more than 5 m, but it was significantly smaller on the NW-SE or NE-SW trending parts, where the dip-slip component reached its maximum value (~1.5 m). The distinction of the surficial traces is also in good agreement with the observed displacements, which invariably decrease towards the edges of the mapped surficial fault traces (Figure 4).

All segments are consistently right-stepping and the pull-apart basins that have developed have a W/L ratio of 1:3 to 1:4, a figure indicative of a mature stage of strike-slip deformation (Mann et al. [27]).

It should also be noted that there is another branch of the NAFZ in the area, lying to the south of the reactivated segments, passing from Mudurnu. This arc-shaped branch, which meets the reactivated fault between Artiflye and Bolu,

remained dormant in the 1999 earthquakes although it was activated in 1967 (Ambraseys & Zatopec [28]).

5 Tectonic forms and structures

It has been proven that the theoretical and experimental models of strike-slip faulting cannot provide a comprehensive and accurate picture of the structural features that develop in nature. Two main reasons have been suggested for this (Hancock [29]): first, it is the anisotropy of the geological formations, not only because of their lithostratigraphical configuration, but also because of their inherited deformation and tectonic grain. Second, a long-existing strike-slip zone with a progressive deformation history may overprint brittle and ductile structures and affect rotated elements within the zone of varying obliquity and sense of displacement.

The Izmit and Düzce earthquakes gave us a chance to study the ongoing strike-slip deformation related structures that developed; this is of great importance, as our knowledge so far has come either from experimental modeling or the study of older, pre-existing forms (Woodcock & Fischer [30]). The following structures have been distinguished:

Riedel shears, P shears and S lenses. These are structures that develop at the initial stages of strike-slip deformation (Tchalenko [31], Naylor et al. [32]) (Figure 5). They were found mostly within recent, albeit relatively compact formations (alluvium and artificial fill) that had undergone no previous tectonic deformation. The observed R shears formed an angle of 15° to the main line of faulting, while the angle formed by the R' and the trend of the primary deformation zone (PDZ) was 75°. Also, P shears had developed at a small acute angle of <15° to the PDZ; S lenses were formed between consecutive restraining and releasing bends (Figure 5).

En echelon, relay and anastomozing fractures. En echelon describes a consistently overtopping and overlapping arrangement at structures, sub-parallel to each other but oblique to the planar zone in which they occur (Campbell [33]). From all these fracture patterns, the most common was the en echelon arrangement. In this pattern, the fractures usually formed an angle of 35° to the PDZ, oriented roughly NW-SE. Such patterns were observed on the Artiflye and Serif segments, developing within the Plio-quaternary cover (some tens of m thick). Relay patterns were not so common; they were found at Artiflye and Eften. The fractures that constitute the pattern were some tens of m long, developing parallel to the PDZ, while at certain locations they were anastomozing, as at Eften and Kaynasli.

Restraining and releasing bends. It has been long recognized that differentiation in shear stresses caused by the existing lithostratigraphy and the inherited

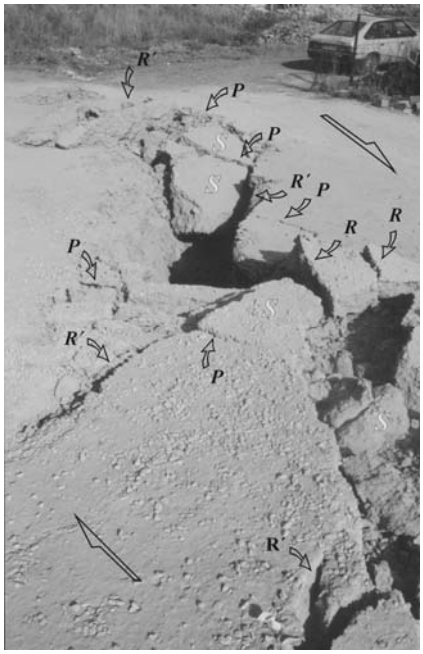

Figure 5: R, R', P shears and S-lenses along a surface break in Gölcük (17 August earthquake).

Figure 6: Restraining and releasing bends at the Izmit segment (17 August earthquake) caused by minor changes in fault trend.

tectonic fabric may lead to localized compression or extension. This, in turn, leads to the formation of restraining and releasing bends (Crowell [34]). Deformation at releasing bends is dominated by extension, and especially normal faulting, whereas at restraining bends shortening is achieved through thrusting and folding. Such structures were abundant along the reactivated segments of the NAFZ, and particularly at the Izmit and Artiflye segments. The dimensions of these structures ranged between a few m to a few tens of m, and topographic subsidence (or uplift) was up to 3 m (Figure 6).

Horsetail splays. These curved faults that merge with the main fault near its end (Biddle & Christie-Blick [35]) were, in this case, in the form of open fractures with a length of several tens of m. They were found mainly where the fault entered thick loose surficial formations, such as the western termination of the Artiflye segment.

Flower structures. Such structures were commonly found close to Kaynasli after the 12 November earthquake. The 17 August shock also produced flower

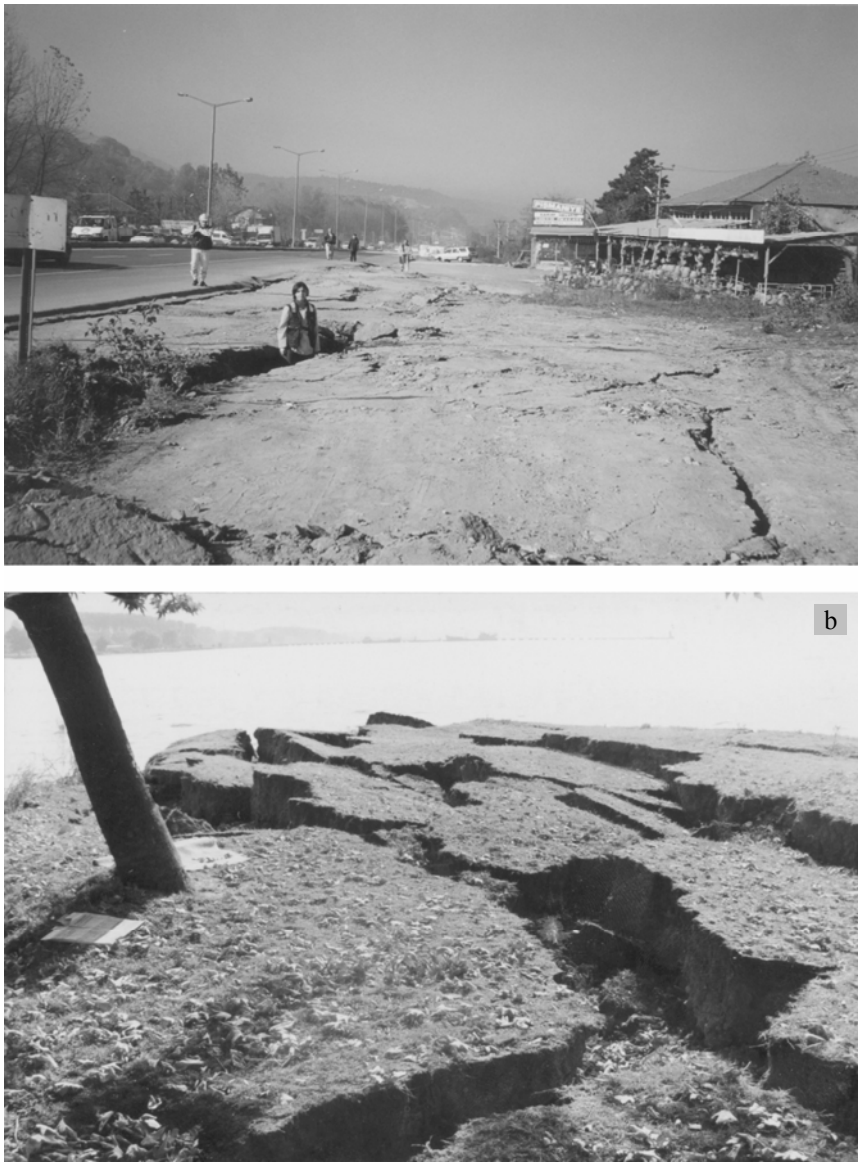

Figure 7: Flower structures along the Kaynasli (a) and Izmit (b) segments.

structures along the coastal zone of Gölcük. Both negative and positive forms were produced, reaching a maximum length of 2,000 m and width of 150 m. Such structures, which have also been observed in other seismic events of similar character (Lade & Cole [36], Fenton & Bray [37], Harding [38]), are the surficial expression of a strike-slip fault that branches upwards into a series of secondary surfaces. They were observed within the loose sedimentary cover (Plio-quaternary formations), and especially within alluvial or coastal deposits, the thickness of which was certainly several tens of m. More usual were the negative flower structures which marked characteristic complex depressions, 50-100 m wide, on the ground surface. The damage caused by the formation of flower structures was impressive, as whole buildings appeared to have sunk into the ground (Figure 7).

Micro & macro pull-apart basins. Impressive pull-aparts (Burchfiel & Stewart [39], Aydin & Nur [40], Mann et al. [27]) were formed at several locations along the fault trace. Such structures had been studied at a number of cases in the field (Burchfiel & Stewart [39]) and later, in laboratory experiments; however, few actualistic models, formed by active faulting, exist. This opportunity (to study actualistic pull-apart basin formation) was provided in the 1999 earthquakes. Pull-apart basins were formed on a variety of scales, ranging from a few m to several hundreds of meters. Two cases will be presented, each on a different scale. The first is a pull-apart basin, 200 by 60 m, located south of Izmit (Figure 8). Here, two fault splays define a lens-shaped area (approximately 50 by 200 m) that subsided for as much as 50 cm. Each of the two splays, which comprise smaller-order faults, displays its own kinematics. The northern one consists of right-lateral faults which towards the east are replaced by normal ones that downthrow their southern part; these, in turn, are replaced by oblique-normal faults towards the east, before the two branches merge (Figure 9). The kinematics of the southern splay are a 'reverse' image of the northern one: from oblique-normal faults in the west, we pass on to normal ones at the central and right-lateral faults at the eastern part. On the whole, the structure represents a typical pull-apart basin. The second case is a km-scale pull-apart basin that develops between the Degirmendere and Izmit segments. The maximum estimated subsidence was 5 m, which caused many residential blocks of Gölcük to sink. It could be confirmed that the E-W trending faults that bound the pull-apart are pure strike-slip, while the NW-SE trending ones are oblique-normal. The overall dimensions of the pull-apart basin are 2 by 6 km.

Trasform-parallel strike-slip basins. This elongated type of pull-apart basin differs from a typical one, in that there are no visible faults connecting the overlapping segment, which remain parallel to each other (Ben-Avraham & Zoback [41]). One such case is Lake Sapanca, with an elongated (E-W) shape, approximately 8 km long and 2.5 km wide. In the 17 August earthquake the coasts of Lake Sapanca subsided as much as 0.5 m, which resulted in several buildings now being under water.

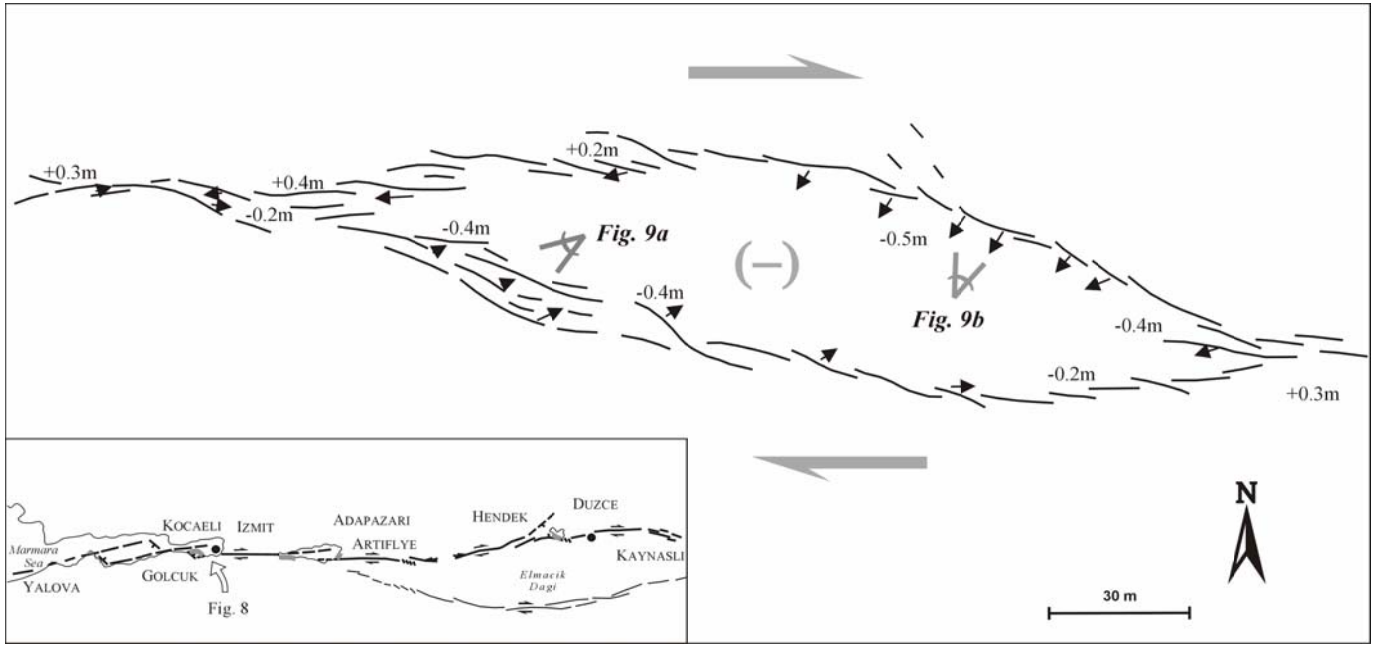

Figure 8: Tectonic map of a typical small-scale pull-apart on the Izmit segment. Arrows show direction of slip.

Figure 9: Oblique-normal (a) and normal (b) faults that bound the pull-apart basin of Figure 8.

6 Discussion - conclusions

The 1999 earthquake activity in NW Turkey, which culminated in the two major shocks of 17 August and 12 November (the Izmit and Duzce earthquakes), was caused by the reactivation of two consecutive parts of the NAFZ which had not ruptured in the twentieth century; however these segments were expected to break (Stein et al. [11]). This reactivation produced surficial faulting for over 150 km. The sense of slip was predominantly strike-slip (dextral) and locally exceeded 5 m, while the mean trend was E-W. The data collected from the field reconnaissance are in good agreement with the instrumental recordings and focal mechanism solutions which, in turn, comply with the kinematic and dynamic setting that controls the NAFZ. Certain deviations in the geometry and kinematics of some fault segments are due to localized transtension or transpression. Additionally, it seems that the 12 November earthquake was caused by the 17 August event, which triggered the adjacent eastern non-reactivated part of the fault zone. It should also be noted that the Mudurnu branch, which lies south of the reactivated segments and had ruptured in the 1967 event, was not reactivated in the 1999 activity.

The study of surficial faulting and deformation produced in these events was a rare chance to investigate ongoing strike-slip related structures. This actualistic model can be compared to the results of laboratory experiments and previous investigations on similar/relevant structures formed in the geological past.

Field reconnaissance showed that the overall 150 km of surficial faulting can be broken into seven right-stepping segments. This distinction is in good agreement with the observed slip distribution (Figure 4).

The W/L ratio of the oversteps is around 1:3 to 1:4. This is indicative of strike-slip deformation that has reached a mature stage and has formed pull-aparts that were either well-defined and bounded on all sides by faults (i.e. the Gölcük pull-apart basin) or were of transform-parallel type (e.g. Lake Sapanca). In general picture push-up structures were small (in the order of a few m), while pull-aparts were frequent and observed at all scales.

The onset of strike-slip deformation is placed at 5 Ma BP (Armijo et al. [14]). The finite deformation has reached a mature stage and this is confirmed by the comparison of the W/L ratio (W/L= 1:3 to 1:4) of the pull-apart basins (Aydin & Nur [40]). In addition, the overall strike-slip displacement is more or less equal to the length of the Sapanca pull-apart basin, which is 16 km. The average annual displacement is thus estimated at 3.2 mm/yr (16 km/ 5 Ma).

Taking into account that the last (prior to 1999) reported surficial faulting at this part of the NAFZ was in the events of 1719 and 1754, we can estimate that in this 250+ year interval the cumulative residual deformation that had not been accommodated by creep was between 2.5 – 5 m (0 – 20 mm/year). On the other hand, it is noteworthy that the annual displacement along the fault trace (on both fault blocks) is estimated at 10-15 mm/yr by GPS measurements (Youd et al. [21], Armijo et al. [14]). So, comparing the above slip rates, it is obvious that

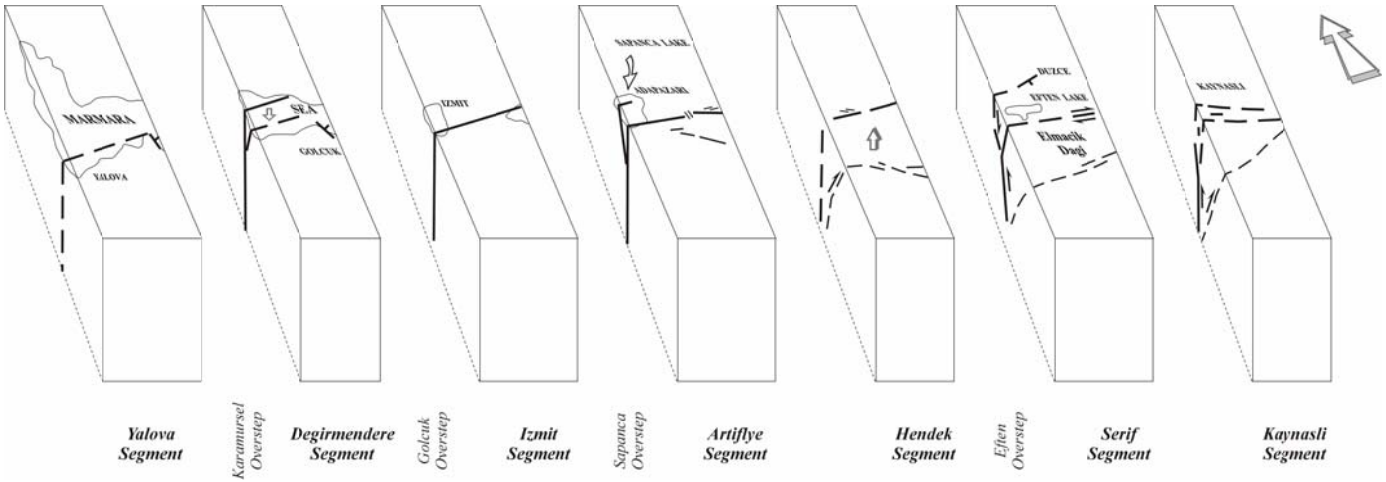

Figure 10: Schematic block diagram to show the consecutive segments (heavy lines) that broke in the 17 August and 12 November 1999 earthquakes. The Mudurnu branch, which had ruptured in the 1967 event, is also shown (thin line).

the mean discontinuous (seismic) deformation and the creep deformation are of the same order a fact that verifies relative observations on strike-slip faults.

The amount of subsidence within the Sapanca pull-apart can be approximated (Sylvester [42]) and this should be more or less equal to the offset length, which is 5 km. This value reflects the displacement of the substratum formations and not the picture we get from the local morphology: sediments which have accumulated in depressions and ridges have been eroded, which tends to eliminate the surficial expression of the actual tectonic displacement.

In addition to the large-scale structures, smaller ones also developed, a fact indicating that deformation is expressed on a variety of scales. The R, R´, P and S fractures, the en echelon and relay patterns, the horsetails splays and flower structures observed are in good agreement with the results of the theoretical modeling and laboratory experiments that have been presented so far. From the observations on all these structures, we can conclude that their existence, development and form are governed by the anisotropy of the affected host formations. Is should also be noted that most of the aforementioned structures were found in undeformed sediments.

On the macro-scale and disregarding the localized deviations caused by secondary factors, it is the existence of the seven consecutive segments that has controlled coseismic deformation. These segments must meet the master fault at a depth of 2 – 5 km, which is inferred from the overall width of the deformation zone (Sylvester [42]) (Figure 10).

References

[1] Lekkas, E., Dandoulaki, M., Ioannides, K., Lalechos, S. & Kiriazis, A. Izmit earthquake, Turkey 1999. Seismotectonic settings – Earthquake and Ground motion characteristics – Geodynamic phenomena – Damage typology and distribution. *13th Hellenic Concrete Conference*, Special Issue, Rethimno, 1999.

[2] Oral, M.B. Global Positioning System (GPS) Measurements in Turkey (1988-1992): Kinematics of the Africa-Arabia-Eurasia Plate Collision Zone. Ph. D. Thesis, Mass. Inst. Tech, 1994.

[3] Reilinger, R.E., McClusky, S.C., Oral, M.B., King, R.W., Toksoz, M.N., Barka, A.A., Kinik, I., Lenk, O. & Sanli I. Global Positioning System measurements of present-day crustal movements in the Arabia-Africa-Eurasia plate collision zone. *Journal of Geophysical Research*, **102**, pp. 9983-9999, 1997.

[4] Ambraseys, N. Some characteristic features of the North Anatolian Fault Zone. *Tectonophysics*, **9**, pp. 143-165, 1970.

[5] Sengor, A. The North Anatolian transform fault: its age, offset and tectonic significance. *Journal of the Geological Society of London*, **136**, pp. 269-282, 1979.

[6] Sengor, A.M.C., Gorur, N. & Saroglu, F. Strike-slip faulting and related basin formation in zones of tectonic escape: Turkey as a case study. In: Strike-

slip deformation, basin formation and sedimentation, eds K.T. Biddle & N. Christie-Blick, *Spec. Publ. Soc. Econ, Paleont. Miner.*, Tulsa, **37**, pp. 227-264, 1985.

[7] Barka, A.A., Hancock, P.L. & Robertson, A.M.F. Neotectonic deformation patterns in the convex-northwards arc of the North Anatolian Fault zone. In: The Geological Evolution of the Eastern Mediterranean, ed. J.F. Dixon, *Geological Society of London*, Special Publication, **17**, pp. 763-774, 1984.

[8] Barka, A. The North Anatolian Fault Zone. *Annales Tectonicae*, **6**, 164-195, 1992.

[9] Barka, A. Slip distribution along the North Anatolian fault associated with the large earthquakes of the period 1939-1967. *Bull. Seism. Soc. Am.*, **86**, pp. 1238-1254, 1996.

[10] Barka, A.A. & Kadinsky-Cade, K. Strike-slip fault geometry in Turkey and its influence on earthquake activity. *Tectonics*, **7**, pp. 663-684, 1988.

[11] Stein, R., Barka, A. & Dieterich, H. Progressive failure on the North Anatolian fault since 1939 by earthquake stress triggering. *Geophysical Journal International*, **128**, pp. 594-604, 1997.

[12] Chorowicz, J., Dhont, D. & Gundogdu, N. Neotectonics in the eastern North Anatolian fault region (Turkey) advocates crustal extension: mapping from SAR ERS imagery and Digital Elevation Model. *Journal of Structural Geology*, **21**, pp. 511-532, 1999.

[13] Wong, H.K., Ludmann, T., Ulug, A. & Gorur, N. The Sea of Marmara: A plate boundary sea in an escape tectonic regime. *Tectonophysics*, **244**, pp. 231-250, 1995.

[14] Armijo, R., Meyer, B., Hubert, A. & Barka, A. Westward propagation of the North Anatolian fault into the northern Aegean Sea: Timing and kinematics. *Geology*, **27(3)**, pp. 267-270, 1999.

[15] Aksu, A., Calon, T. & Hiscott, R. Anatomy of the North Anatolian Fault Zone in the Marmara Sea, Western Turkey: extensional basins above a continental transform. *GSA Today*, Publ. Geol. Soc. America, **10(6)**, pp. 3-7, 2000.

[16] Barka, A. Geology and tectonic evolution of some Neogene-Quaternary basins in the North Anatolian Fault Zone. In: *Ketin Symposium*. Geological Society of Turkey, Special Publication, pp. 209-227, 1985.

[17] Andrieux, J., Over, S., Poisson, A. & Bellier, O. The North Anatolian Fault Zone: distributed Neogene deformation in its northward convex part. *Tectonophysics*, **243**, pp. 135-154, 1995.

[18] Dhont, D., Chorowicz, J., Yurur, T. & Kose, O. Polyphased block tectonics along the North Anatolian Fault in the Tosya basin area (Turkey). *Tectonophysics*, **299**, pp. 213-277, 1998.

[19] Reilinger, R., Toksoz, N. & McClusky, S. 1999 Izmit earthquake, Turkey was no surprise: *GSA Today*, **10(1)**, pp. 1-6, 2000.

[20] Straub, C., Kahle, H.G. & Schindler, C. GPS and geological estimates of the tectonic activity in the Marmara Sea region, NW Anatolia. *Journal of Geophysical Research*, **102**, pp. 27587-27601, 1997.

[21] Youd, T., Aschheim, M., Basoz, N., Gulkan, P., Imbsen, R.A., Johnson G.S., Love J., Mander J.B., Mitchell W., Sezen H., Sozen M., Swan F. & Yanev, P. The Izmit (Kocaeli), Turkey Earthquake of August 17, 1999. *EERI Special Earthquake Report*, pp. 1-12, October 1999.
[22] Lekkas, E. The 1999 earthquake activity in the broader area of Izmit. An actualistic deformation study on strike-slip faults. *Asian Seismological Commission 2000 (ASC)*, Abstract, Tehran, 2000.
[23] Lekkas, E. The 1999 earthquake activity in the broader area of Izmit. An actualistic deformation study on strike-slip faults. *International Earth Sciences Colloquium on the Aegean region (IESCA 2000)*, Abstract, p. 191, Izmir, 2000.
[24] Dolan, J.F., Hartleb, R.D., Akyuz, S., Barka, A.A. & Altunel, E. The August 17, 1999 Izmit, and November 12, 1999 Duzce, Turkey, earthquakes. *Seismological Society of America*, 95th Annual Meeting, Abstract, San Diego, 2000.
[25] Hartleb, R.D. & Dolan, J.F. Surface rupture mapping of the Karadere segment of the 17-August-1999 Izmit, Turkey earthquake and the western section of the 11-November-1999 Duzce, Turkey earthquake. *Seismological Society of America*, 95th Annual Meeting, Abstract, San Diego, 2000.
[26] Lettis, W.R., Barka, A.A., Bachhuber, J.L., Witter, R.C., Brankman, C.M. & Hengesh, J.V. Influence of pull-apart basins on rupture mechanics of the August 17, 1999 Kocaeli earthquake. *Seismological Society of America*, 95th Annual Meeting, Abstract, San Diego, 2000.
[27] Mann, P., Hampton, M.R., Bradley, D.C & Burke, K. Development of pull-apart basins. *Journal of Geology*, **91**, pp. 529-554, 1983.
[28] Ambraseys, N. & Zatopec, A. The Muduryu Valley, Western Anatolia, Turkey earthquake of 22 July 1967. *Bull. Seismological Society of America*, **59**, pp. 521-589, 1969.
[29] Hancock, P. Continental deformation. Pergamon Press: Oxford, 1994.
[30] Woodcock N.H. & Fischer M. Strike-slip duplexes. *Journal of Structural Geology*, **8**, pp. 725-735, 1986.
[31] Tchalenko, J.S. Similarities between shear zones of different magnitudes. *Bull. Geol. Soc. Am.*, **81**, pp. 1625-1640, 1970.
[32] Naylor, M.A., Mandl, G. & Sijpesteijn, C.H.K. Fault geometries in basement-induced wrench faulting under different initial stress states. *Journal of Structural Geology*, **8**, pp. 737-752, 1986.
[33] Campbell, J.D. En echelon folding. *Econ. Geol.*, **53**, pp. 448-472, 1958.
[34] Crowell, J.C. Sedimentation along the San Andreas Fault. In: Modern and Ancient Geosynclinal Sedimentation, ed. R.H.Jr. Dott, *Spec. Publs. Soc. Econ. Paleont. Miner.*, Tulsa, **19**, pp. 292-303, 1974.
[35] Biddle, K. & Christie-Blick, N. Glossary – Strike-slip deformation, basin formation and sedimentation. In: Strike-slip deformation, basin formation and sedimentation, eds K.T. Biddle & N. Christie-Blick, *Soc. Econ. Paleon. & Min., Sp. Publ.* **37**, pp. 375-386, 1985.

[36] Lade, P. & Cole, D.Jr. Influence zones in alluvium over dip-slips faults. *Journal of Geotechnical Engineering*, ASCE, **110**, May, pp. 599-615, 1984.
[37] Fenton, J. & Bray, J. Relationship of surficial earth materials to the characteristics of the 1992 Landers earthquake surface rupture. *Geotechnical Engineering – Dept. of Civil Engineering*, University of California, Berkeley, UCB/GT/94-05, September 1994, 1994.
[38] Harding, T.P. Seismic characteristics and identification of negative flower structures, positive flower structures and positive structural inversion. *Bull. Am. Ass. Petrol. Geol.*, **69**, pp. 582-600, 1985.
[39] Burchfiel, B.C. & Stewart, J.H. "Pull-apart" origin of the central segment of Death Valley, California. *Bull. Geol. Soc. Am.*, **77**, pp. 439-442, 1966.
[40] Aydin, A. & Nur, A. Evolution of pull-apart basins and their scale independence. *Tectonics*, **1**, pp. 91-105, 1982.
[41] Ben-Avraham, Z. & Zoback, M.D. Transform-normal extension and asymmetric basins: An alternative to pull-apart models: *Geology*, **20**, pp. 423-426, 1992.
[42] Sylvester, A.G. Strike-slip faults. *Bull. Geol. Soc. Am.*, **100**, pp. 1666-1703, 1988.

CHAPTER 2

The Gujarat, West India Earthquake (26 January 2001): A geodynamic episode in an intra-plate compressional regime

S. G. Lozios, E. L. Lekkas & G. D. Danamos
Faculty of Geology, University of Athens, Greece

Abstract

A very strong catastrophic earthquake (Ms=7.7) occurred on 26 January 2001, in the Gujarat district of W. India, some hundreds of kilometers away from the active plate boundary (collisional zone) between the Indian subcontinent and the Asian plate. Historical catastrophic earthquakes have also been reported from the same region, such as the 1819 Ms=7.7±0.2 earthquake. A zone of co-seismic E–W surface ruptures, 30-40 km long and 15-20 km wide, was observed near the epicentral area and seems to be associated with pre-existing reverse faults and thrust folds, which were partially reactivated during this earthquake. Apart from the reverse vertical movement, a significant right-lateral displacement was also observed along these E-W surface ruptures. This seismic event could have been also accompanied by a large-scale flexural-slip folding, as the absence of significant co-seismic fault displacement and fault scarp indicated. This type of compressional tectonic deformation is also confirmed by the focal mechanism of the earthquake and the seismo-tectonic "history" of the area. The NW–SE open cracks, also observed in the affected area, either represent en echelon structures, due to the right-lateral shear component of the reactivated fault (or branch faults), or they are associated with the local extensional stress field in huge anticline hinges of the co-seismic flexural-slip folds. A large number of ground ruptures, failures and open cracks are also associated with extensive sand boils, liquefaction phenomena and lateral spreading.

1 Introduction

On 26 January 2001 (at 8:46 local time) a strong earthquake struck the Gujarat district of West India. The epicenter was located near the city of Bhachau

(23˚40′ N, 70˚32′ E). The calculated magnitude was Ms=7.7 and the depth of the epicenter was 23.6 km (data from USGS). This earthquake was the strongest seismic event in India in the last 150 years. The previous strongest earthquake occurred almost within the same epicentral area on 16 June 1819 (Bilham et al. [1], Bilham & Gaur [2]).

The last earthquake in Gujarat was so strong that it was recorded even in cities as far away as Bombay, Delhi and Karatsi, about 1500 km from the epicenter. It was also felt in several areas in Nepal. It is worth mentioning that the affected region is the heart of the Indian industrial area for oil refining and the steel industry and the main supplier of electricity, and the damage from this event were huge in relation to the income per capita of the population. The cities located at the epicentral area, such as Bhachau, Bhuj, Anjar and Kandla sustained complete or almost complete destruction. The city of Bhachau and several other neighbouring villages were totally destroyed, while multi-story buildings collapsed in cities located at a distance of more than 350 km from the epicentral zone, the capital of Gujarat, Ahmedabad. The *Times of India* reported, on 1 February, that there were at least 35,000 dead, while the final estimate was around 100,000.

As is well known, the majority of earthquakes that have occurred in collisional geotectonic environments are distributed along an orogenic arc, which means either within the trough zone and areas of the island arc or within the back-arc and volcanic-arc. These are the areas where the most important geodynamical processes of the orogene can be observed. In general, earthquakes that occur along the collisional plate-boundaries are observed mainly in active arcs (Greece, Japan, Taiwan etc.). The difference between these and the rest of the other orogenic arcs is the fact that in the area of the Himalayan and India microplate the geotectonic environment corresponds to a supercollision state between the two continental crust fragments. This process is directly correlated to the high seismic activity that is observed along the entire zone of collision.

The epicenter of the earthquake (23˚40′ N, 70˚32′ E) indicates that the rupture occurred within the Indian microplate at a distance of 400 to 800 km from the axis of the Himalyan mountain range where the deformed continental margins of the India and Asia plates are located and the peak of the horogenetic processes take place. This seismic event occurred in a stable continental region. As is indicated from the event, the collisional processes, generated in the internal part of each plate, create the conditions responsible for the occurrence of several types of faults (mainly reverse or strike-slip faults and rarely normal faults) along distinct zones responsible for seismic activity, such as the Gujarat district. It should be noted that for several researchers (Bilham et al. [1], Bilham & Gaur [2], Jain et al. [3]) the tectonic regime of the Gujarat area is still problematic, indicating both a marginal as well as a within-plate geodynamical setting. The presence of a zone with several active reverse faults and folds (pointed out by the large magnitudes and the fault plane solutions of the earthquakes), shows that this area represents a transitional zone between the stable part of the Indian microplate and the margin under collision.

The aim of this study is to describe and translate into geological terms the focal mechanism of the Gujarat earthquake following our fieldwork in the affected region just after the seismic event.

2 The geodynamic regime of India

The Indian microplate, which is a segment of continental crust detached from Gondwana, has already collided with Asia (Bassoulet et al. [4], Bossart & Ottiger [5], Boulin & Bouyx [6], Crawford [7], Fuchs [8]). The important seismic activity along the front of the collision indicates that the there is still active northward movement of the Indian microplate. New geodetical data imply that the length of the Indian continent is being reduced by 3 mm/year along a NNE–SSW direction. On the other hand, the Himalayan belt and the Tibetan plateau are shrinking by 20 mm/year and 9 mm/year respectively due to the compressional regime (Bilham et al. [1], Bilham & Gaur [2]).

The Gujarat earthquake as well as the majority of the earthquakes which have struck India during recent years, are correlated with the compressional regime over the Indian plate while is drifting towards the NNE. The present shrink of the Himalayan belt and the northernmost part of the Tibetan plateau (Transhimalaya) belongs to the latest stage of a long process – initially a subduction of an oceanic crust, later a collision between continental crust fragments and finally a supercollision – which started during the Late Cretaceous period (Gansser [9], Le Fort [10], Le Fort [11], Le Fort [12]).

The collision between the two fragments of continental crust, and the deformation along their margins, created the Himalayan belt from the sediments that were squeezed and which drifted from the north to the south towards the Indian micro-continent (Fuchs [13], Fuchs [8], Heim & Gansser [14], Le Fort [12]).

It is pointed out that the geometry of the Himalayan belt is not constant along its entire length but is changing in the west (towards Pakistan) as well as in the East (towards Burma) from NW–SE to N–S. Thus, a change in the kinematical characteristics is observed and the drifting to the NE takes place through a lateral subduction with a velocity as high as 52 mm/year (Burma–Andaman Arc) while that towards the NW takes place through strike-slip faults which have a direction perpendicular to the Arc (e.g. the Chaman Fault) and a rate of drift of 40 mm/year (Malik et al. [15]). At the southern part of the collisional front, the present drift of the Indian plate causes deformation not only at the front of the MBT but also in the internal part of the Indian plate, as the Gujarat earthquake indicates. On the other hand, in the northern part of Himalaya the thick continental crust of the Tibetan plateau is under the control of extensional forces, which give rise to normal and/or strike-slip faults.

3 The seismotectonic regime of the major area

The Gujarat earthquake is related to a within-plate geodynamical setting, especially within the Indian plate which is characterized by a Pre-Cambrian crystalline basement. The latter consists of gneisses and granites and is overlaid by a

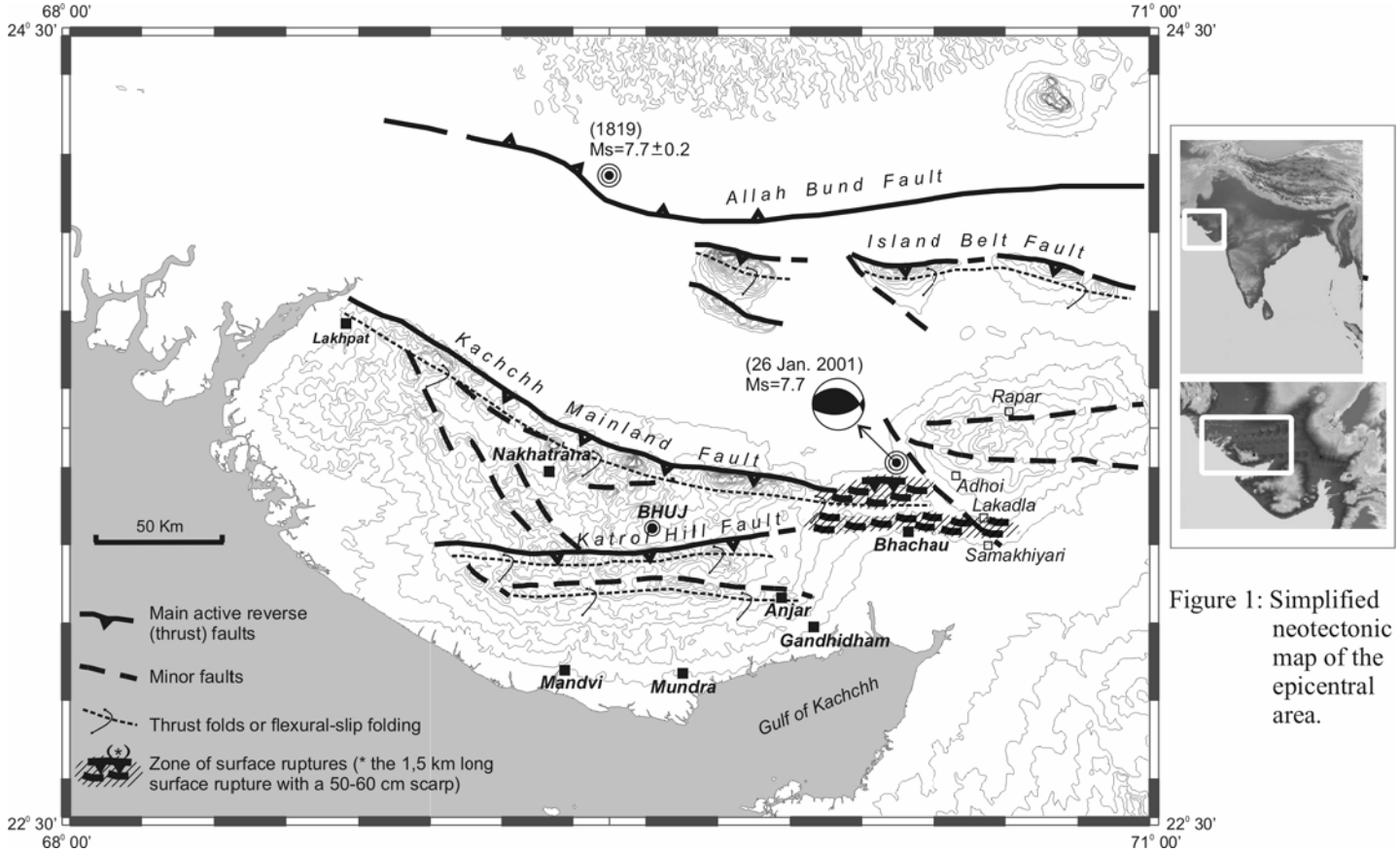

Figure 1: Simplified neotectonic map of the epicentral area.

thick continental sedimentary sequence. The latter contains continental and marine sediments, very often separated by several unconformities which have been caused by horogenetic movements.

The last earthquake was not the only one during the history of this region. In Kachchh (Gujarat district) a seismic event of an equivalent magnitude (7.7±0.2) occurred in 1819. Other events of minor importance have occurred and have caused major damage.

The focal mechanisms have shown the activation of reverse faults with a low participation of strike-slip movement, with an E–W direction due to the northward collisional movement of the Indian plate. The greater area of Kachchh, which is under a seismic reactivation, is characterized by the presence of horizontal to sub-horizontal Mesozoic and Cainozoic sediments which are folded along distinct zones. In these zones the seismic activity is manifested by the formation of open anticlines and synclines of large scale which are correlated with large-scale thrust-belts with the same E–W direction (Malik et al. [15]).

From the seismotectonic point of view the greater region is limited northward and southward by two major fault zones with an E–W directional trend, well known as the Nagar–Parkar Fault (to the north) and the Kachchh Mainland Fault (to the south).

Smaller scale fault zones with the same direction cross the internal part of the region. The fault zone activity has created a characteristic topography of high hills in contrast with the flattened general picture of the adjacent area. Several generations of screes, alluvial cones and valleys are some of the elements that characteristically indicate the intensive erosion.

Very characteristic are also the Quaternary terraces which are crossed by deep valleys as well as the isolated branches of the hydrographic network, forming small basins where water accumulates. The relief is under the control of the active tectonism of the area. In particular, the series of hills, the terraces and the morphological discontinuities are developed in an E–W direction, parallel to the fault zones as has been mentioned above. The tectonic structure in the field, which has been confirmed by the geodetic data (Bilham & Gaur [2]), indicates that these fault zones are characterized by a reverse oblique-slip movement resulting in the formation of characteristic tectonic grabens, the E–W graben of Kachchh, which is bounded by two marginal fault zones, the Allah Bund Fault to the north and the Kachchh Mainland Fault to the south (Figure 1).

It should be noted that the Allah Bund fault zone was created during the earthquake of 1819 (Ms=7.7+0.2). The activation of this zone produced a fault scarp in the alluvial deposits of the order of 6 to 9 m and with an overall length of 80 to 90 km. During the Anjar earthquake in 1956 (Ms=6.1), which is correlated with the reactivation of other active fault zones to the south, the fault scarp was about 1 m (Bilham & Gaur [2]).

The dynamic regime of the entire area is also responsible for the upward movements of large-scale blocks which are formed in a composite and complex way, resulting in the appearance of the Mesozoic rocks at the surface. The smaller-scale blocks also show complex uplifting with important or less important bending of the sediments near the margins of the blocks and in their internal

parts respectively. This has resulted in the formation of elliptical domes, asymmetric anticlines, large-scale kink-folds (flexures) but also questas and mesas-type structures with a general E–W trend. It has also been observed, for most of the blocks, that one of their margins is been defined by a reverse fault (usually the northern one) while the other has been defined by bending and deformation of the rocks with open asymmetrical folds or kink-bands (flexural kink-folding).

As was mentioned above, the greater area of Kachchh shows continuous seismic activity, at least during the last 200 years. This activity is manifested by earthquakes with magnitudes of the order of 3.5 to 8 on the Richter scale.

4 The tectonic structure of the affected area

The most affected area coincides with the epicentral area, situated northward from the gulf of Kachchh, and covers a zone of an E–W direction (of the order of 100 km southward and northward from the epicenter), from Nakhatrama and Bhuj in the west towards Bhachau and Rapar in the east. The major fault zone in this area is known as the Kachchh Mainland Fault, of an ESE–WNW to E–W direction, and is more than 200 km long. It borders a flattened area, known as Great Rann of Kachchh, to the north, and the hilly semi-mountainous region of the hinterland in the south.

Figure 2: Panoramic view of the Katrol Hill Fault and the uplifted asymmetric anticline of the rocky mainland (thrust fold and fault and flexural-slip folding).

Southward, two more fault zones of smaller scale are detected, with similar characteristics and an E–W direction. The first of these zones is located south of the town of Bhuj (known as the Katrol Hill Fault, Figures 1 and 2) and the second is north of Anjar city. Between these zones and towards the western part of the hilly semi-mountainous area, there are a few smaller faults (between 20-50 km long), trending mainly in the SE–NW and rarely in the E–W direction. Northward, in the region of Adhoi and Rapar, E–W faults of a similar importance are also observed. The trace of the Allah Bund Fault, which reactivated in 1819 and caused an earthquake of similar magnitude, is located 100 to 150 km north of the affected area and the Kachchh Mainland Fault.

All the above-mentioned faults and fault zones totally control the morphology of the area, creating characteristic geomorphological structures such as allu-

vial fans, screes, talus cones, scarps and intense linear erosion. The morphological picks in most cases are related to uplifted blocks where folding of rocks is observed as huge asymmetrical open synclines and anticlines with a prominent E–W hinge direction. This folding is in accordance with the geometry of the reverse faults.

From the geometrical and kinematical point of view, most of the faults in the epicentral area are almost vertical or very steep, plunging to the south at an angle of 60-80 degrees and showing a reverse motion. Faults of minor importance, which were detected within the same area, also show a reverse-type movement (and rarely strike-slip), confirming the observations for the large-scale fault zones. In several cases these faults are the result of flexural-slip folds.

5 Seismic ruptures and seismic fault (?)

The extensive research which was carried out in the greater epicentral area revealed an important number of ruptures and fractures at different scales that seem to be in direct correlation or not to the seismic fault that produced the seismic event of 26 January. All these fractures and ruptures are observed along an E–W to ENE–WSW trending zone at a distance of 50 km from Bhachau and within the epicentral area (Figure 1).

Figure 3: The main E-W surface rupture (1.5 km long with a 60 cm scarp), located at the eastern prolongation of the Kachchh Mainland Fault.

The longest rupture (1-1.5 km long) has an E–W to ENE–WSW trend (approximately 80 degrees) and was observed almost 20 km NNW of Bhachau, in the eastern prolongation of the Kachchh Mainland Fault. This rupture demon-

strates an en-echelon arrangement and forms a scarp in the surface of more than 60-70 cm (Figure 3). No particular opening has been observed along this rupture, which dips 60-80 degrees to the south. The overall geometry and kinematics also indicate a reverse type movement with the southern part uplifted in relation to the northern one.

Not only a vertical movement has been observed but also a dextral strike-slip motion. The hanging wall has been moved to the west whereas the footwall has moved to the east, giving as a result a reverse oblique-slip kinematical character to the rupture.

No other rupture with such a big displacement is observed in the major area, but many other fractures, less important, cross the alluvial deposits and the unconsolidated sediments as well as the asphalt road that connects the cities of Bhachau and Bhuj with the adjacent villages. Their length appears to be of the order of few meters up to several tens or, rarely, hundreds of meters and they have an E–W, WNW–ESE and NW–SE as well as (in few cases) a NE–SW direction.

It should be noted that the fractures of a general E–W trend have shown similar kinematic and dynamical characteristics the great rupture that was previously described (compressional regime and a reverse oblique-slip motion).

A typical fracture of this type is shown in Figure 4, where it cuts the asphalt road and the adjacent sediments of the road from Bachau to Bhuj. The principal surface of the rupture dips 70-75 degrees towards the south, with the southern block uplifted about 3-4 cm. This movement is also accompanied by a right-lateral displacement of 1 cm. About half a meter apart from this main rupture, a conjugate surface has also been detected, with no clear fracture but only flexural folding. Its dip is approximately at 60-65 degrees towards the north and the uplifted northern block has been slightly moved, compressing and deforming the area between the two conjugate surfaces.

In the greater area, these fractures dip either to the south or to the north with the uplifted part the southern or the northern block respectively. The displacement is usually of the order of a few centimeters and is rarely bigger. The development of these fractures is systematic and follows, most of the time, an en-echelon structure. Two principal zones of these fractures have been detected. The first and bigger one follows the Bhachau–Lakadla line and is developed in the prolongation of the Katrol Hill Fault. The second is located more to the north, at the greater area of the easternmost ends of the Kachchh Mainland Fault, in the same area where the most important, in terms of length and displacement, fracture occurs (Figure 1).

Unlike the E–W fractures, the NW–SE or WNW–ESE ones represent a totally different kinematic and dynamic character, since they are followed, in most cases, by an opening that shows an extensional character. Their size is between 1-2 m and several tens of meters (rarely greater), and they are not randomly distributed. Two distinct cases have been recognized.

In the first case, the NW–SE fractures are systematically developed in distinct zones, with an E–W general trend in direction. They are characterized by an

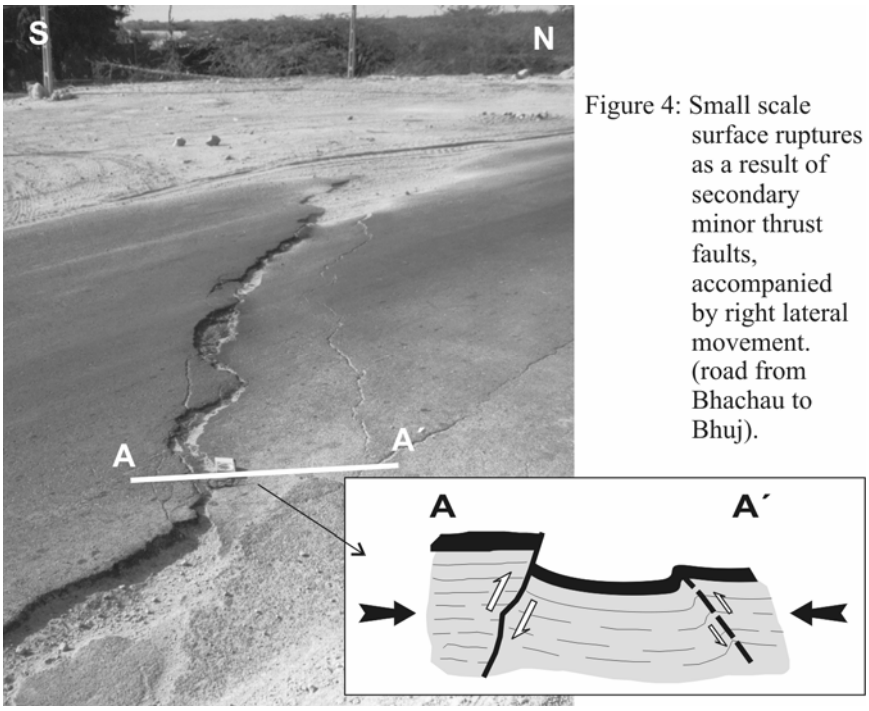

Figure 4: Small scale surface ruptures as a result of secondary minor thrust faults, accompanied by right lateral movement. (road from Bhachau to Bhuj).

en-echelon arrangement and represent the open cracks that are developed in a dextral shear zone with an E–W general trend.

These zones outcrop mainly north of Bhachau, in the greater area of the eastern prolongation of the Kachchh Mainland Fault and of the fractures with an E–W direction, and rarely more to the south in the prolongation of the Katrol Hill Fault zone, along the line Bhachau–Lakalda.

In the second case these fractures do not indicate any distinct distribution and in most cases they tend to lie in different directions (NW–SE, WNW–ESE, NE–SW and rarely N–S). Most of them appear mainly in the greater area of Bhachau and, rarely, more to the north, and they are associated with extensive sand boils, liquefaction phenomena and lateral spreading.

6 Discussion – conclusions

The greater area of Gujarat district, while it is situated far from the Himalayan collisional belt, is characterized by high seismic activity with focal mechanisms indicating mainly a compressional stress field. This is also argued directly through field observations since the region is crossed by large-scale reverse faults which, in combination with the huge asymmetrical anticlines (flexural folds), exclusively control the morphology of the region.

The first question is whether the main seismic fault, which caused the earthquake, was expressed on the surface with kinematical and dynamic characteristics which coincide with those defined by the earthquake focal mechanism (reverse fault accompanied by strike-slip movement). This question becomes more important since the previous very strong earthquake which struck this region (1819), created a 90 km long and 9 m high fault scarp, which showed similar geometric, kinematic and dynamic characteristics.

The above question has created a long debate (Jain et al. [3]), since no fracture of similar size and displacement (to the 1819 one) has been observed after the recent earthquake. Thus, there is skepticism as to whether these observed smaller-scale fractures are directly connected to the seismic fault or to secondary effects that usually follow an earthquake (liquefaction, landslides etc.).

The epicenter of the earthquake was located north of Bhachau, approximately 50-70 km south of the epicenter and the fault trace of the 1819 earthquake. It coincide, in general, with the eastern ends of the two other important E–W fault zones, the Kachchh Mainland Fault and the Katrol Hill Fault, which partially converge in this area (Figure 1).

The position of the epicenter in combination with the damage distribution and the concomitant geodynamic phenomena (liquefaction, landslides, water level changes etc.), which have been observed within an E–W trending zone in the major epicentral area, generally define the expected position of the trace of the seismic fault.

The geometrical, kinematical and dynamical characteristics (en-echelon arrangement, reverse oblique-slip movement etc) of the main E–W trending seismic rupture (length of 1-1.5 km and total vertical displacement of 60 cm, Figures 1 and 3), which has been observed 15-20 km northern of Bhachau, at the eastern prolongation of the Kachchh Mainland Fault zone, as well as of the smaller E–W ones which follow this zone (Figures 1 and 4), show that they represent the expression at the surface either of the seismic fault or of a secondary branch fault (Figures 1 & 5).

Similar characteristics are present in several other seismic fractures south of the Bhachau area, in the eastern prolongation of the Katrol Hill Fault zone; they are probably related to a second reactivated surface (Figures 1 and 2).

The reverse character of these ruptures and fractures, together with the right-lateral displacement, which is confirmed by the measurements in the field as well as by the en-echelon arrangement of the fractures, coincides with the focal mechanism of the recent earthquake (but also of the past earthquakes) as well as with the general tectonic state of the major area.

The absence of greater scale movements along the surfaces which have been reactivated (as was expected due to the magnitude of the earthquake, and as happened in the 1819 earthquake), could be explained by the flexural type deformation (and uplift) along the anticline structures of the Kachchh Mainland Fault and the Katrol Hill Fault.

It is noted that this type of deformation (flexural folding) at an even smaller scale, has been observed in several ground fractures after the last earthquake and is quite common with this "tectonic style" of deformation.

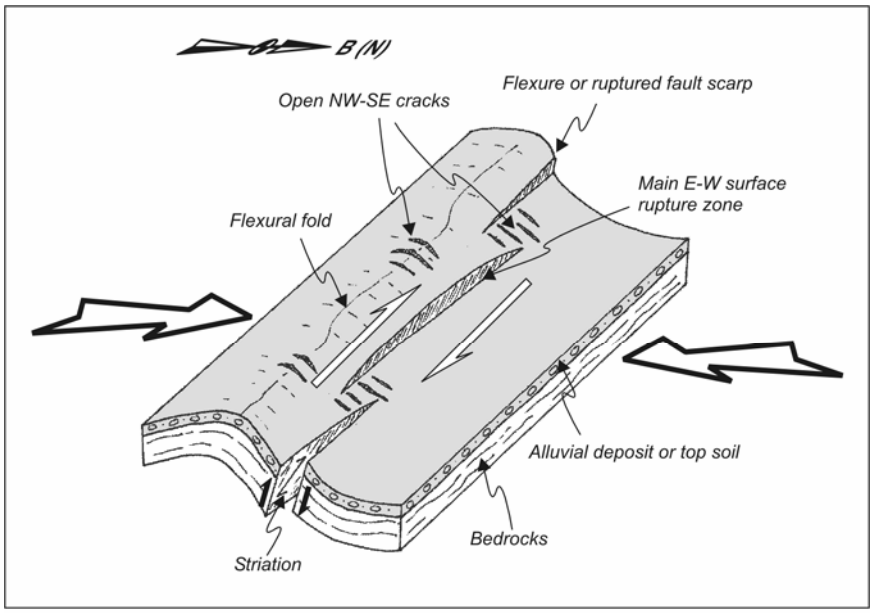

Figure 5: Schematic diagram showing the surficial features associated with the E-W surface rupture zone.

The NW–SE open cracks, also observed in the affected area, either represent en-echelon structures, due to the right-lateral shear component of the reactivated fault (or branch faults), or they are associated with the local extensional stress field in huge anticline hinges of the co-seismic flexural-slip folds (Figure 5).

Finally, a large number of ground ruptures, failures and open cracks (mainly in the region of the topmost parts of the anticline structures**)** are also associated with extensive sand boils, liquefaction phenomena and lateral spreading.

References

[1] Bilham, R., Blume, F., Bendick, R. & Gaur, V. Geodetic constraints on the Translation and Deformation of India: Implications for future great Himalayan earthquakes. *Current Science*, **74(3)**, pp. 213-229, 1998.

[2] Bilham, R. & Gaur, V. Geodetic contributions to the study of seismotectonics in India. *Current Science*, **79(9)**, pp. 1259-1268, 2000.

[3] Jain, S.K., Lettis, W.R., Jaswant A., Ballantyne, D., Chaubey, S.K., Dayal, U., Goel, R., Gcyal, A., Hengesh, J., Malhotra, P., Murty, C.V.R., Narula, P.L., Saikia, F.C.K., Singh, M. & Vatsa, K. Preliminary observations on the origin and effects of the Jan. 26, 2001 Bhuj (Gujarat, India) earthquake. *EERI Special Earthquake Report,* pp. 1-16, April 2001.

[4] Bassoulet, J.P., Colchen, M. & Mouterde, R. Esquisse paléographique et essai sur l'évolution géodynamique de l'Himalaya. *Mem. h. ser. Soc. Geol. Fr.*, **8**, pp. 213-234, 1977.

[5] Bossart, P. & Ottiger, R. Rocks of the Murree formation in Northern Pakistan: indicators of a descending foreland basin of Late Paleocene to Middle Eocene. *Eclog. Geol. Hlv.,* **82(1)**, pp. 133-165, 1989.
[6] Boulin, J. & Bouyx, E. Introduction à la géologie de l'Hindou Kouch occidental. *Mem. h. ser. Soc. geol. Fr.,* **8**, pp. 87-105, 1977.
[7] Crawford, A. The Indian suture line, the Himalaya, Tibet and Gondwanaland. *Geol. Mag.,* **III**, pp. 369-383, 1974.
[8] Fuchs, G. The terrain map of the Himalaya. Explanatory notes. *Ann. Geol. Pays Hell.,* **37**, pp. 575-599, 1996-97.
[9] Gansser, A. *Geology of the Himalaya s*, Interscience Publishers, John Wiley and Sons: West Sussex, 1964.
[10] Le Fort, P. Les leucogranites à tourmaline de l'Himalaya sur l'exemple du granite du Manaslu (Nepal central). *B.S.G.F.,* **7**, **XV(5/6)**, pp. 555-561, 1973.
[11] Le Fort, P. Himalaya: The collided range. Present knowledge of the continental arc. *Am. Journ. Scinc.,* **275(A)**, pp. 1-44, 1975.
[12] Le Fort, P. The Himalayan orogenic segment. *Tectonic Evolution of the Tethyan Region*, Sengor & A.M.C., eds. Kluwer Academic Publishers, pp. 289-386, 1989.
[13] Fuchs, G. The geological history of the Himalayas. Rep. 22th Intern. *Geol. Cong. Prague*, **3**, pp. 174-181, 1968.
[14] Heim, A. & Gansser, A. Central Himalaya: geological observations of the Swiss expedition 1936. *Mem. Soc. Helv. Sc. Nat.,* **73**, 1939.
[15] Malik, J.N., Sohoni, P.S., Merh, S.S. & Karanth, R.V., Palaeoseismology and neotectonism of Kachchh, Western India: Active Fault Research for the New Millenium, *Proc. of the Kokudan Intern. Symp. & School on Active Faulting*, eds. K.Okumura, H. Goto, & K. Takada, 2000.

CHAPTER 3

Contribution of GIS to analysis of the 7 September 1999 Athens earthquake

N. Voulgaris
Faculty of Geology, University of Athens, Greece.

Abstract

On 7 September 1999 at 11:56 GMT a M_w=6.0 earthquake occurred near Athens, causing 148 deaths, injuries and considerable damage. Several institutes, universities and research groups have been involved in field surveying and analysis in order to investigate the tectonic characteristics and seismic potential of the affected region. In the present paper an attempt is made to elaborate further on available tectonic and seismological data using the support provided by GIS in order to improve our understanding of the seismic activity in the area. The definition of specialized GIS database structures has enabled multi-parameter analysis facilitating additional observations leading to better insight into the evolution of the aftershock sequence and its tectonic implications.

1 Introduction

The application of computers in geosciences for the management of geographically referenced information began during the late 1960s. The rapid advances in computer technology during the 1980s, both in terms of processing power and storage capacity, enabled the development of expert software for the management of geographical referenced information known as Geographical Information Systems (GIS). Geological and tectonic mapping were among the first applications of GIS in the geosciences, while seismological applications followed later. The high uncertainties associated with seismological data was one of the main reasons for the relative delay in the application of GIS techniques in seismology. However, once the advances in computer technology were transferred to seismograph station development, resulting in the new-generation digital recorders, and enabled the development of advanced

processing algorithms, the overall accuracy of seismological data was greatly improved.

On 7 September 1999 a strong earthquake of magnitude M_w=6.0 occurred in the vicinity of Athens. The main event was followed by a large number of aftershocks, which were recorded by a local, digital network of eight portable stations, which had been installed in the epicentral area by the Athens University Seismological Laboratory the day after the main shock (Figure 1), and which remained in operation until December 1999 (Papadimitriou et al. [1], Papadimitriou et al. [2], Voulgaris et al. [3]).

A large number of aftershocks were recorded, and a total of 3,261 were analyzed. The application of GIS techniques for the processing, analysis and evaluation of this aftershock sequence represents a good example of the new capabilities offered by the increased level of accuracy.

2 Data

Data architecture and organization probably represent the most important factor of a GIS implementation. In the present study all available data can be subdivided into two main categories: the seismological data acquired during the field campaign following the Athens earthquake and additional data collected from various sources such as topographic maps and satellite images.

2.1 Seismological data

The local, digital network of eight portable stations with GPS timing and location support (Figure 1) was installed in the area the day after the main shock and operated during a period of three months on a continuous recording basis, in order to maximize the efficiency of seismic activity monitoring. Following data acquisition on a regular basis, the focal parameters of the aftershocks were determined using standard seismological procedures and algorithms, as described in detail in Papadimitriou et al. [2] and Voulgaris et al. [3]. The resulting aftershock epicenters were next introduced in a GIS platform. Special attention was given to designing the corresponding focal parameter database of the GIS system in order to encode all available information in a way that would facilitate further processing and query definition, selection and expandability within the system.

In addition, as a first step for the seismotectonic analysis of the aftershock sequence, 1,051 events were selected and their focal mechanism solution was calculated using P-wave first motion polarities. The selection was based on the number of available observations, which for the selected events was greater than six with sufficient azimuthal coverage. Following the determination of focal mechanisms (see Voulgaris et al. [3], Voulgaris et al. [4]) the aftershock database of the GIS was updated to include additional parameters such as azimuth and dip of the fault and the auxiliary plane, the P and T axes, the slip

vector orientation and dip parameters and the type of the fault plane solution according to the rake value calculated.

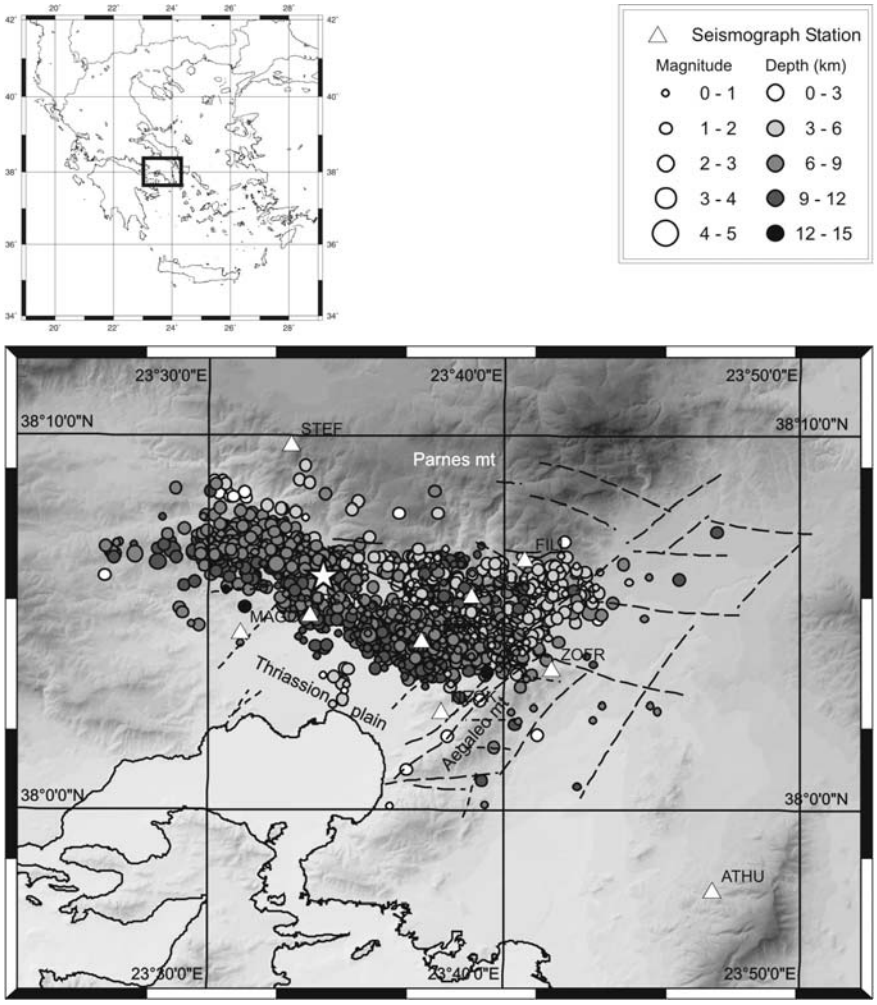

Figure 1: Epicenter location of the 7 September 1999 (M_w=6.0) Athens earthquake (star) and distribution of better located aftershocks recorded by the portable digital seismograph network (triangles). Tectonic elements depicted have been derived from Mariolakos & Foundoulis [5].

2.2 Additional data

In order to support further analysis of the aftershock sequence within the GIS environment, the introduction of all available data layers for the investigated

area is also required. Initially, the digital elevation model (DEM) of the area with a cell size of 15 meters was constructed by digitizing the 1:50 000 scale topographic maps of the area (Figure 1). This procedure also included the digitization of all available altimetry points in order to improve the accuracy of the resulting DEM. Using this DEM as input, data layers representing the distribution of morphological parameters such as slope and aspect were also derived. Next, the geological map of the area was digitized and all the available tectonic data provided by the work of Lekkas [6] and Mariolakos & Foundoulis [5] were also introduced into the system.

Using available Landsat 7 image data, a pseudochromatic image of the area was also created with a pixel resolution of 15 m by combining channels 4, 3, 1 with the panchromatic channel. This was accomplished by applying a geometric correction to each channel based on a number of control points and nearest neighbor resampling and subsequently merging the multispectral and panchromatic images.

Finally, the differential interferogram kindly provided by the Earthquake Planning and Protection Organization (E.P.P.O.) was also introduced into the GIS system as an additional georeferenced data layer in order to provide an expression of the coseismic surface deformation following the Athens earthquake. This was produced using two SAR images on 15 July and 23 September 1999; each cycle corresponds to a 28 mm ground movement in the line of sight.

3 Data analysis

In figure 1 the distribution of selected aftershock epicenters is presented and the general conclusions proposed by Papadimitriou et al. [2] and Voulgaris et al. [3] can be verified. The aftershock epicenter locations appear to be constrained mainly within the Thriassion basin by the Parnes mountain to the north and the Aegaleo mountain to the east. The epicenter distribution displays a general WNW–ESE orientation, along both sides of the 7 September 1999 main shock. Epicenter depths appear to be increasing along a SE direction while the shallower aftershock depths are observed mostly in the NE near the Fili fault zone area and the convergence of the Parnes and Aegaleo mountains. In addition, the westwards extension of the aftershock distribution along a slightly varied E–W direction must also be mentioned.

In order to compare the spatial distribution of the aftershocks with the pattern of coseismic surface deformation expressed by the interferogram, figure 2 was prepared with the approximate boundaries of the three main fringes outlined and the projection of the selected epicenters corresponding to the time period covered by the interferogram. The first observation which can be made during the analysis of figure 2 is the one initially made by Papadimitriou et al. [2] regarding the proximity of the epicenter of the 7 September 1999 earthquake to the area of maximum coseismic surface deformation expressed by the inner fringe. An additional observation is associated with the similarity observed between the spatial (geographical and depth) distribution of the aftershock

epicenters and the geometry of the interferogram fringes. The majority of epicenters appear to be constrained within the boundary defined by the second fringe, while the third and outer fringe represents the final boundary for the distribution of all epicenters.

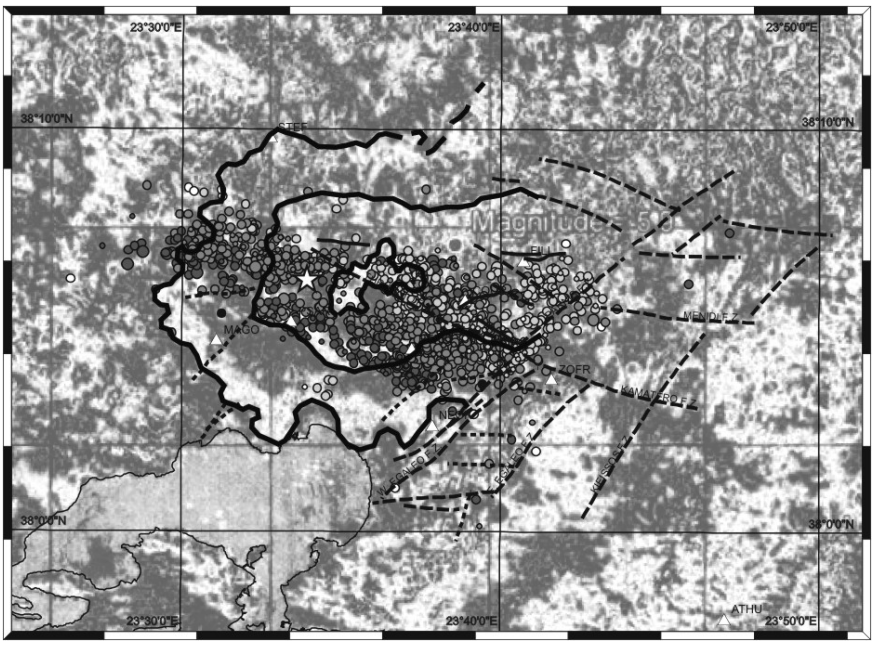

Figure 2: Aftershock epicenter distribution overlaying the interferogram provided by E.P.P.O. Digitized thick black lines indicate approximate fringe geometry and extent.

Following the investigation of the spatial characteristics of the aftershock distribution, the assessment of the temporal evolution of the sequence was next attempted. Examination of the overall time evolution of the aftershock sequence, displayed in figure 3, reveals that the rate of seismic activity decreases exponentially after the main shock, with the maximum observed daily aftershock number reduced in half within two days (10/9–12/9). Slight deviations from the above general observation appear to be associated with the occurrence of aftershocks of relatively higher magnitude, indicating a change in seismic energy release rate probably related to local stress build-up.

Additional analysis was performed using the possibilities offered by the GIS system, which allowed the combined assessment of the spatial and temporal evolution of the aftershock sequence, through the creation of epicenter distribution maps at successive time intervals (Figure 4). The decrease in seismicity can be verified from the three daily maps in this figure, where the

number of aftershocks 12 days after the September 7 earthquake appears to be significantly lower. Further examination of these maps, however, indicates that clustered aftershock activity near the location of the epicenter of the main shock persists. A second area of high aftershock activity is located further east along the Thriassion fault zone extending to the east up to the region where the Parnes and Aegaleo mountains converge. It should be noted that epicenter distribution alignment in this area appears to be in good agreement with both the direction of the Thriassion fault zone (Mariolakos & Foundoulis [5]) and the direction of several transverse faults located north and south of the latter.

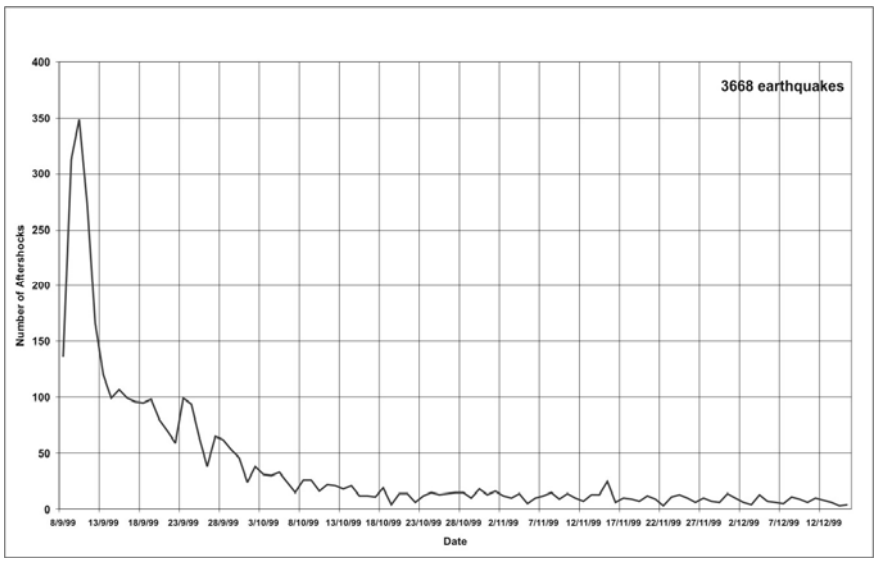

Figure 3: Rate of seismic activity, expressed in terms of daily number of aftershocks recorded by the temporary digital seismographic network during the three months of operation.

In an effort to correlate the seismological observations expressed by the calculated focal mechanisms for selected aftershocks (Voulgaris et al. [4]) with the available tectonic data provided by Mariolakos & Foundoulis [5], an attempt was made to project these focal mechanisms to the surface, along the fault plane, taking into account the calculated azimuth and dip. The results of this operation are presented in figure 5, where the projected fault planes have also been rotated according to the azimuth values calculated for each focal plane. However, before examining these results, it must be clarified that the obtained image is based on the assumption that the calculated dip for each mechanism remains constant from the earthquake focus to the surface.

The validity of this assumption cannot be controlled or expressed quantitatively. This must be taken into account along with the errors involved in

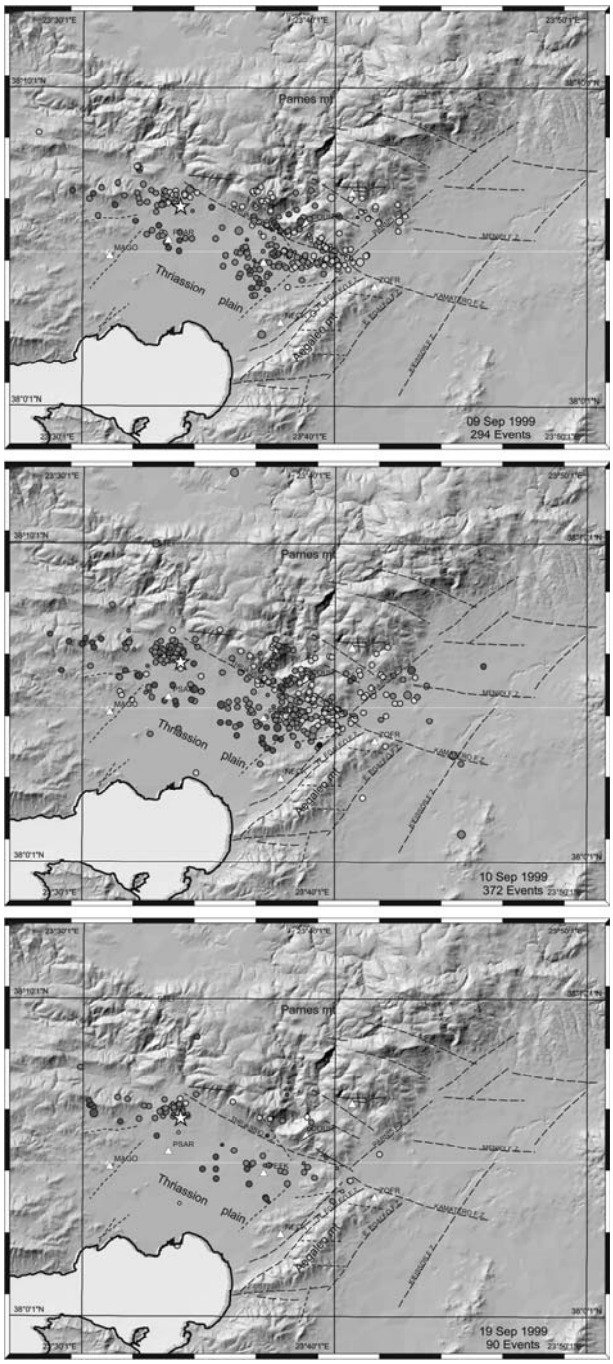

Figure 4: Daily seismic activity maps 2, 3 and 12 days after the 7 September 1999 M_w=6.0 Athens earthquake (star).

the calculation of both the focal mechanisms and the earthquake locations in an attempt to interpret the results of figure 5.

Based on the statistical analysis of the calculated fault plane presented by Voulgaris et al. [4], the projected focal mechanisms were divided into three main groups. In the first group, focal mechanisms with azimuths 90° to 120°, similar to the one calculated by Papadimitriou at al. [2] for the main shock (105°), were included. Focal mechanisms with azimuths between 130° and 160°, representing the primary azimuth concentration in the rose diagram of figure 5, were included in the second group. Finally, the third was formed by focal mechanisms with azimuths between 60° and 90°, represented by the third and smallest concentra-

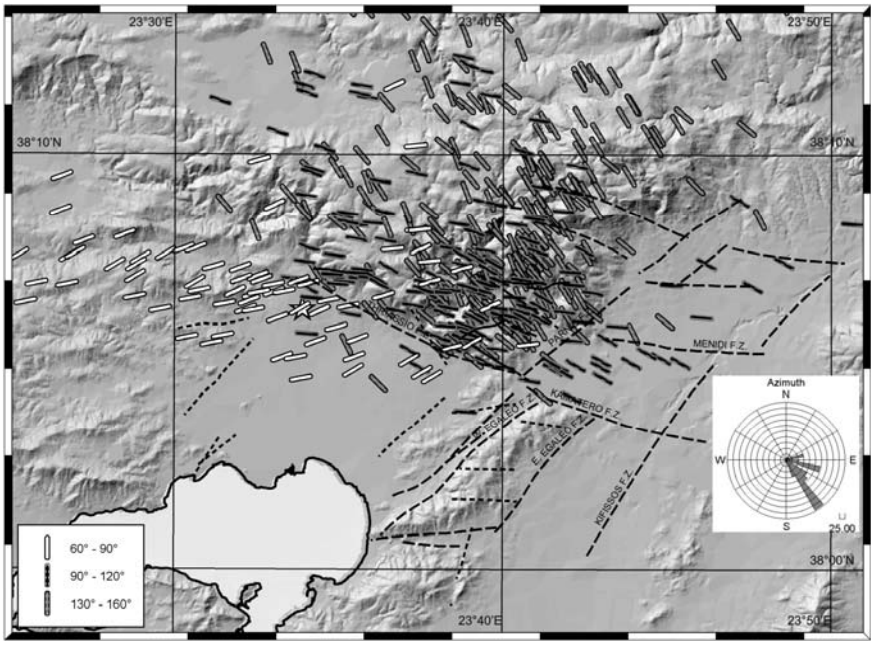

Figure 5: Projected fault planes derived from focal mechanisms calculated by Voulgaris et al. [4] and divided into three groups according to the categories illustrated in the rose diagram.

tion observed in the rose diagram.

Analysis of figure 5 reveals that the majority of projected focal planes are located north and west of the Thriassion plane. The projected focal planes of the third group (60°–90°) appear to dominate the western part of the area. The projected focal planes of the second group (130°–160°) are concentrated to the north of the Thriassion plain and especially to the eastern part of the mountain of Parnes. Finally, the first group (90°–120°) appears again concentrated north of the Thriassion plain but mostly along the southern part of Parnes.

4 Discussion

In the present paper an effort has been made to elaborate further on the results presented by Papadimitriou et al. [2], Voulgaris et al. [3] and Voulgaris et al. [4] regarding the 7 September 1999 earthquake and aftershock sequence. This effort was based primarily on the application of GIS techniques to the analysis of the spatial and temporal distribution of seismological data in association with additional information. The definition of specific GIS database structures, capable of encoding all available earthquake information parameters, was required in order to accomplish this task.

The combined examination of the spatial distribution of epicenters, and the patterns of coseismic surface deformation as expressed by the differential interferogram, revealed that apart from the proximity of the epicenter of the main shock to the area of maximum deformation first indicated by Papadimitriou et al. [2], fringe geometry and orientation appears to be in very good agreement with the aftershock distribution, since most of the epicenters appear to be constrained within the outer third fringe. In addition, the persistent seismic activity located around the epicenter of the main shock (Figure 4) appears to coincide with the maximum deformation area. The combination of the above two observations probably represents an important argument supporting the validity of the location of the main shock calculated by Papadimitriou et al. [2].

Detailed analysis of the image obtained by projecting the calculated focal mechanisms to the surface (Figure 5), allows for some interesting comments. A very good correlation between the orientation of the projected fault planes and the tectonic structure of the area is displayed. The geographical distribution diversity of the projected fault planes reveals the existence of three sub-areas characterized by different tectonic orientations. In the westernmost part of the investigated region, ENE–WSW to E–W oriented tectonic activity is dominant. Along the Thriassion fault zone tectonic activity is mainly expressed by ESE–WNW directions, similar to the calculated fault plane for the main shock. Furthermore, NW–SE orientations appear to reflect tectonic activity in the north–eastern part of the mountain of Parnes. This transition from an ENE–WSW to a NW–SE direction verifies the results of Papanikolaou & Lozios [7]. Finally, it is also important to note that convergence between the ENE–WSW and ESE–WNW directions is observed near the epicenter of the main shock in the area of maximum deformation according to the previous interferogram interpretation.

Acknowledgements

The author is grateful to E.P.P.O. for providing the differential interferometric image and to Dr. I. Parcharidis for his support in interpreting it.

References

[1] Papadimitriou P., Kaviris G., Voulgaris N., Kassaras I., Delibasis N. & Makropoulos K. The September 7, 1999 Athens earthquake sequence recorded by the CORNET network: preliminary results of source parameters determination of the mainshock. *Annales Geologiques des Pays Helleniques, 1e serie, t. XXXVIII, fasc. B,* Athens, pp. 29-40, 2000.

[2] Papadimitriou P., Voulgaris N., Kassaras I., Kaviris G., Delibasis N. & Makropoulos K. The Mw=6.0, 7 September 1999 Athens earthquake. *Natural Hazards,* **27**, (**1-2)**, pp.15-33, 2002.

[3] Voulgaris N., Kassaras I., Papadimitriou P. & Delibasis N. Preliminary results of the Athens September 7, 1999 aftershock sequence. *Annales Geologiques des Pays Helleniques, 1e serie, t. XXXVIII, fasc. B,* Athens, pp. 51-62, 2000.

[4] Voulgaris N., Pirli M., Papadimitriou P., Kassaras J. & Makropoulos K. Seismotectonic observations for the area of western Attica derived from the study of the September 7, 1999 Athens earthquake aftershock sequence. *Bull. Geol. Soc. of Greece,* **XXXIV**, **4**, pp. 1645-1654, 2001.

[5] Mariolakos I. & Foundoulis I. The Athens earthquake September 7, 1999: Neotectonic regime and geodynamic phenomena. *Integration of Earth Science Research on the Turkish and Greek 1999 Earthquakes, Kluwer Academic Publishers, Amsterdam,* pp. 113-126, 2002.

[6] Lekkas E. The Athens earthquake (7 September 1999): Intensity distribution and controlling factors. Engineering Geology, 59, pp. 297-311, 2001.

[7] Papanikolaou D. & Lozios S. Comparative neotectonic structure of high (Corinth) and low (Attica-Cyclades) level activity. *Bull. Geol. Soc. of Greece,* **XXVI**, pp. 47-65, 1990.

CHAPTER 4

The neotectonic macrostructures and the geological basement, the main factors controlling the spatial distribution of the damage and geodynamic phenomena resulting from the Kalamata (13 September 1986) and Athens (7 September 1999) earthquakes

I. Fountoulis
Faculty of Geology, University of Athens, Greece.

Abstract

Substantial destruction in construction plants, as well as many rockfalls, were observed and mapped in the Kalamata and Athens regions after the earthquakes of 13 September 1986 and 7 September 1999 respectively. These destructive phenomena were located mainly in places in which: (i) fault reactivation, (ii) creation of new ground seismic fractures (Kalamata, Eleohori, Parnitha Mt. etc.) and (iii) small faults without reactivation, were observed. This paper attempts to interpret this selective distribution of the destructive phenomena, paying special attention to the influence of the neotectonic macrostructures, the fractures and the geological substratum of the affected area and also of the wider region.

1 Introduction

Greece is one of the most seismically active areas of Europe since it is near the Hellenic Trench. Kalamata and Athens were damaged by the 13 September 1986 M=6.2 R, and 7 September 1999 Ms=5.9 R, earthquakes. Damage, seismic fractures and rockfalls were observed in both seismic events.

The areas affected by the earthquake activity, belong to different geotectonic regimes regarding to their position in relation to the Hellenic Arc system, as Kalamata is located very close (<70 km) to the Hellenic (Ionian) Trench region in which the subduction zone of the African plate below the European (Aegean)

plate exists, while Athens is located far (>250 km) from the Hellenic Trench (Figure 1).

In this paper, an attempt is made not only to describe but also to compare the distribution of the damage, the rockfalls and generally the geodynamic phenomena in both cases, taking into account the geological and mainly the neotectonic data as well as the geotechnical characteristics of the formations outcropping in the affected areas.

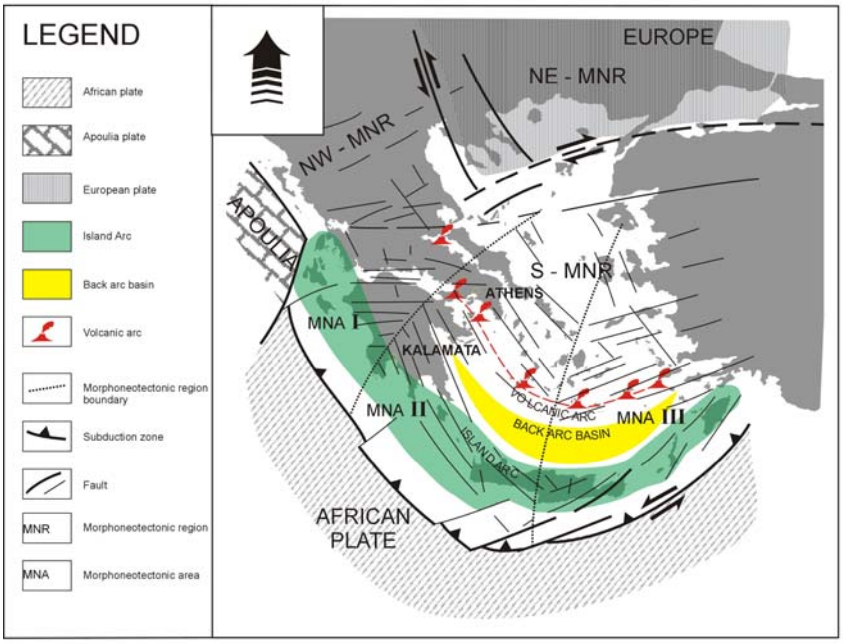

Figure 1: The Hellenic Arc system and the location of the earthquake-affected areas (Kalamata 13 September 1986 and Athens 7 September 1999).

2 The case of Kalamata

2.1 Geology - tectonics

In the broader Kalamata area the following four alpine geotectonic units Psonis [1], Mariolakos et al. [2] from lower to upper occur: (a) the Mani unit consisting mainly of marbles, (b) the Arna unit consisting of quartzites and phyllites, (c) the Tripolis unit which consists of neritic carbonates and flysch formation and (d) the Pindos unit consisting of thin-bedded pelagic carbonates and clastic formations. From the structural point of view, the four above-mentioned geotectonic units form a succession of three nappes. The Mani unit (slightly

metamorphosed) is considered to be the relatively autochthonous one. The Arna unit overthrusts the Mani unit, the Tripolis unit (the second nappe) overthrusts the Arna unit and the Pindos unit (third nappe) overthrusts the Tripolis unit (Figure 2).

The Late Pliocene-Early Pleistocene deposits consist of marls, sandstone and conglomerates Marcopoulou-Diacantoni et al. [3]. The total thickness of the deposits varies from place to place and in the central part of the basin, where Kalamata is located, it is over 1200 m thick Mariolakos et al. [4], Mariolakos et al. [5]. The Middle-Late Pleistocene deposits consist mainly of red colored siliceous sands – sandstone and conglomerates. Alluvial deposits, unconsolidated or consolidated clastic material and talus represent the Holocene.

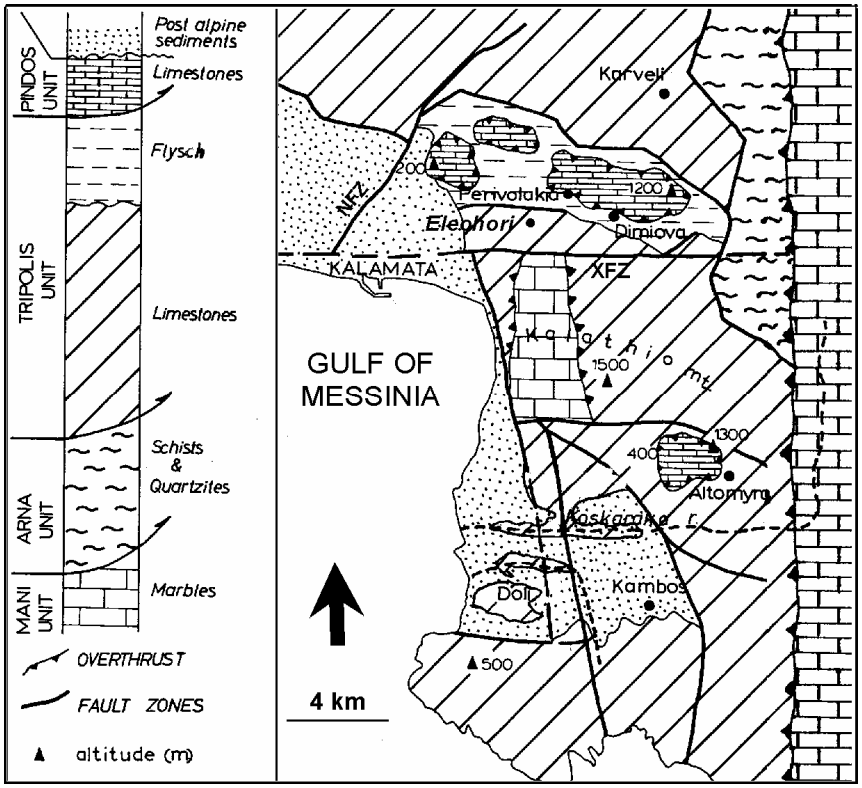

Figure 2: Simplified geological map showing the four alpine geotectonic units overthrust one on top of the other, as well as the post-alpine sediments of the region of the Kalamata area XFZ:Xerilas Fault Zone, NFZ: Nedon Fault Zone (after Mariolakos et al. [2]).

2.2 Neotectonics – fault zones – faults

The study area is located at the eastern margin of the Kalamata – Kyparissia graben (first neotectonic macrostructure) and constitutes the northward prolongation of the Gulf of Messinia (Figure 3).

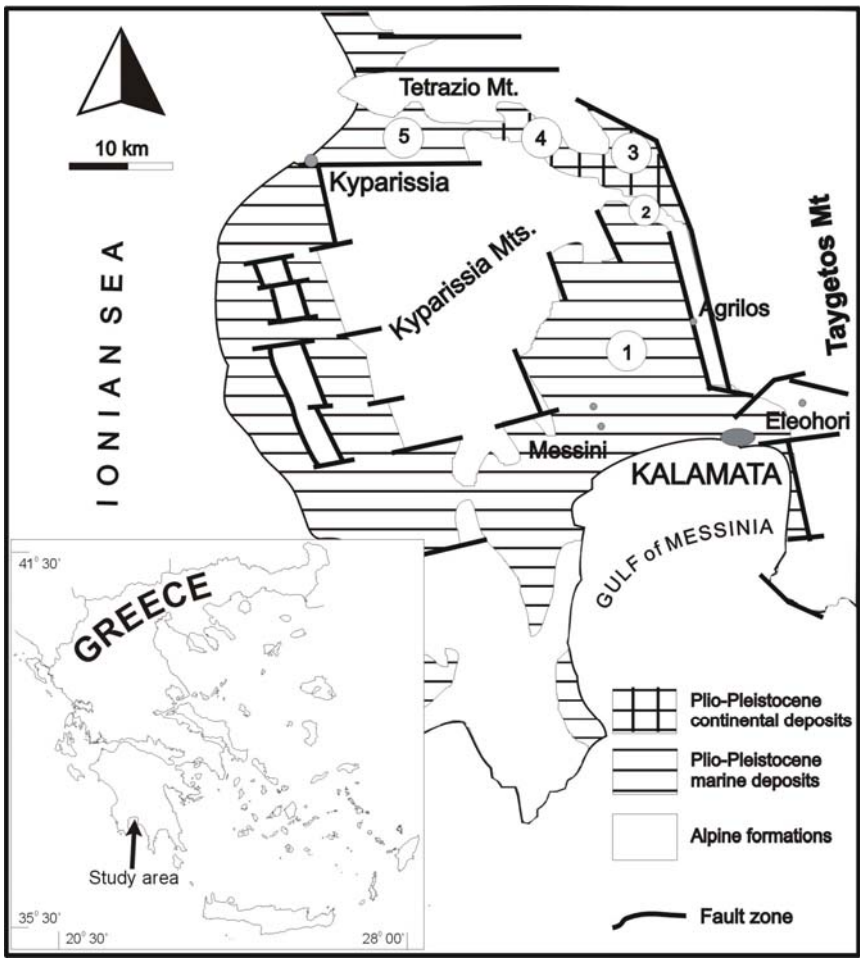

Figure 3: The second order neotectonic macrostructures within the first order neotectonic macrostructure of the Kalamata-Kyparissia graben. The numbers correspond to the following second order neotectonic macrostructures: 1: Kato Messinia sub-graben, 2: Meligalas horst, 3: Ano Messinia graben, 4: Dorion basin, 5: Kyparissia-Kalo Nero graben (after Mariolakos & Fountoulis, [6]).

Large and composite fault zones define the margins of the first order neotectonic macrostructure. Within, as well as at the margins of, the graben there are second order macrostructures, which are smaller grabens and horsts (Figure 3) Mariolakos & Fountoulis [6]. The kinematic evolution of these fault zones is very complicated and is differentiated in each fault zone. The most intensive kinematic activity is focused mainly along these fault zones, outlining the rock mass properties in these areas.

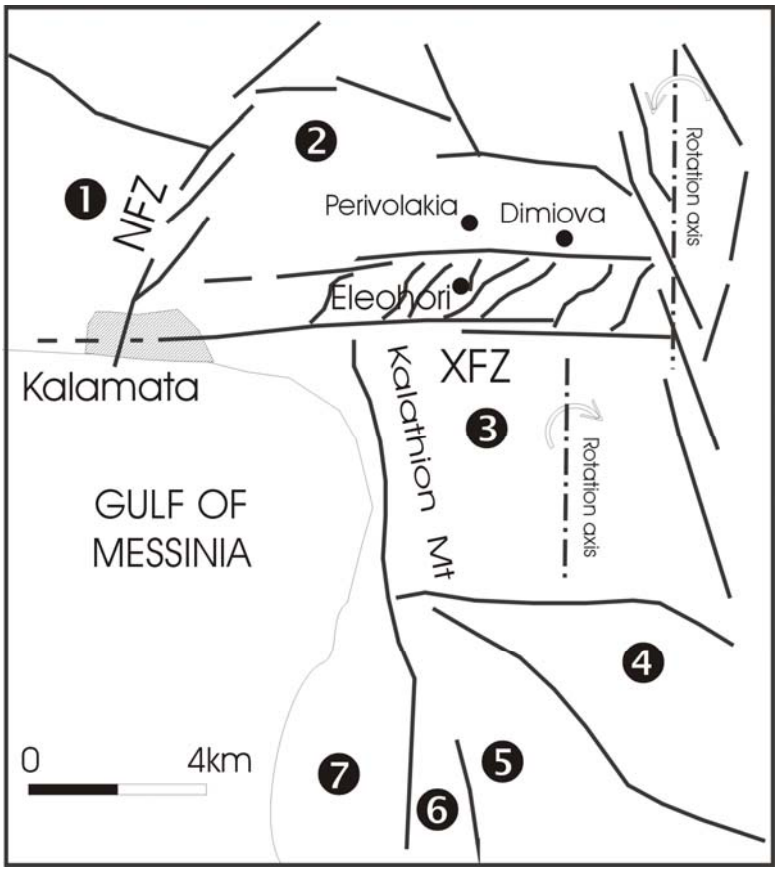

Figure 4: Sketch map of smaller order neotectonic macrostructures of the Kato Messinia sub-graben 1: Asprochoma-Koutalas horst, 2: Dimiova-Perivolakia graben, 3: Kalathion Mt. horst, 4: Altomyra semi-graben, 5: Kambos graben, 6: Vardia-Koka horst, 7: Kitries-Mantinia sub-graben, XFZ:Xerilas Fault zone, NFZ:Nedon Fault Zone (after Mariolakos & Fountoulis [6]).

At the south-eastern margin of the Kalamata – Kyparissia graben, a great number of smaller order structures are present, striking in different directions. Some are parallel, whereas others are perpendicular to it. These second-order neotectonic macrostructures east of Kalamata are the following Mariolakos & Fountoulis [6] (Figure 4): (a) Asprochoma-Koutalas horst, (b) the Dimiova – Perivolakia graben, (c) the Kalathion Mt. Horst, (d) the Altomyra semi-graben, (e) the Kambos graben, (f) the Vardia-Koka horst and (e) the Kitries-Mantinia sub-graben.

The E-W striking Dimiova – Perivolakia graben is bounded by the Kato Karveli – Venitsa fault zone to the north, by the Arahova to the east, by the Xerilas fault zone (XFZ) to the south and by the Nedon fault zone (NFZ) to the west (Figure 4).

This macrostructure constitutes one of the most interesting minor order neotectonic macrostructures, because of the occurrence of the Pindos unit, which give us the opportunity to interpret the kinematic regime during the neotectonic period. Mariolakos et al. [4] interpreted the kinematic regime of this macrostructure suggesting that this graben rotates around an N-S axis located at the area of Arahova westwards. At the western part of the fault zone the total throw is more than 2,000m Mariolakos et al. [5], Mariolakos et al. [4]. Within this graben during the seismic activity of September 1986, most of the seismic fractures, fault reactivation, damage, landslides and rockfalls were observed.

The marginal fault zones consist of many faults, which are not continuous and differ on strike even when they belong to the same fault zone, as they form conjugate fault systems.

2.3 Geographical distribution of damages and geodynamic phenomena

2.3.1 Seismic faults – seismic fractures

During the above-mentioned seismic activity, fault reactivation (seismic faults), new faulting and seismic fracturing were observed (the latter distinguished by no displacement) (Figure 5).

Regarding the seismic faults, the following must be noted:

[a] Generally, they are the result of the reactivation of the older neotectonic faults. However, in one case, (in the area of a small village, Diasello), a totally new fault was created in the upper nappe (Pindos unit).

[b] Most seismic faults occurred during the main shock (13 September 1986, M=6.2.R); only one (west of Eleohori village) occurred during the main aftershock (15 September 1986, M=5.6 R). It must be mentioned that during the main aftershock many faults were reactivated, although they had not been reactivated during the main shock, on the slopes of the Tzirorema gorge, an area that is located north of the damage area.

[c] The reactivated faults strike in different directions.

[d] The throw of the faults due to the reactivation is generally small (max=20 cm) and of normal character. The maximum throw has been observed at a seismic fault caused by the main aftershock Ms=5.6 R.

[e] Seismic faults observed in all kinds of alpine (carbonates of Tripolis unit, pelagic deposits of Pindos unit), and post-alpine formations (Early Pleistocene marine deposits).
[f] No seismic faults were observed in the other Quaternary deposits, and in the flysch of the Tripolis unit.
[g] In many places with high gradient the fault reactivation was accompanied by rockfalls.

Regarding the seismic fractures (ruptures without visible throw) the following must be noted:

[a] Seismic fractures were created in almost all geological formations (alpine or post-alpine). Most of the fractures are relatively small (4-5 meters in length); however, some may be longer (10-50 meters).
[b] The seismic fractures form a zone or zones. The arrangement of the seismic fractures within the zones is typical en echelon. In some areas, these fracture zones are of right lateral, and in some other areas of left-lateral character.
[c] Seismic fractures were created during both the main shock and the main aftershock. In some cases, two separate fractures created by the main shock were intersected by a new fracture created during the main aftershock.
[d] Many fractures created during the main shock were enlarged in width and length by the main aftershock.
[e] The seismic fractures are not planar and so their shape on the ground is not straight but is a crooked line.
[f] The density of the fracture zones containing large fractures varies from place to place. In one area, the fracture density was estimated (measured) as ten fracture zones per 100 meters.

2.3.2 Disasters

As mentioned in the previous section, the disasters were limited to an area of triangular shape, which is defined to the south by the fault zone of the Xerilas river, to the east by the fault zone of Nedousa – Arahova, and to the west by the fault zone of the Nedontas river (Figure 5).

No disasters were recorded to the west of the Nedon fault zone (e.g. the villages of Amfeia, Thouria, Sperxogeia, Messini) and south of the Xerilas fault zone (the villages of Verga, Sotirianika, Kampos, Stayropigi,Doloi, Nea Mantinia) and especially in areas where geological beds have the same seismo-geological behavior as those in the city of Kalamata and Eleohori village, which caused serious damage.

It is worth mentioning that during the earthquakes of 1944, disasters where recorded in the villages of Verga and Kampos, while no damage was recorded in the city of Kalamata and Eleohori village (this information was collected by the resident of the settlements).

Similar conditions have been observed during past earthquakes. The earthquake that took place on 10 June 1846, which was of great macroseismic intensity (was felt in Asia Minor), destroyed many villages in Messinia, among

others Messini, Mikromani and Aslanaga (west of the Nedon river) but in Kalamata only a few houses collapsed, Galanopoulos [7].

The geological basement on which the various constructions were founded varies. Kalamata, for example, has a basement that is composed of coastal, loose riverbed sediments (gravel, sand, clay etc), or red siliceous clastic formations that are relatively more consolidated than those previously mentioned, or marls, sandstones, conglomerates, sediments even more consolidated than those previously mentioned, of Plio-Pleistocene age, or even alpine basement. The depth of the free water table from the surface also varies from one location to another, determined mainly by the distance of the area from the shore.

In Eleohori, which was nearly totally destroyed, the foundation ground is composed of massive unbedded neritic limestone-dolomite of the Tripoli unit. In the villages of Ladas and Karveli, the basement is composed of dolomites of the Tripoli unit while in Nedousa and Artemisia the basement is composed of phyllites – quartzites, that is, metamorphosed rocks of the Arna unit.

It seems from field observations that have taken place that the disasters and the damage as a whole are not determined only from the age, type, height and other characteristics of the buildings. For example, there were cases where two nearly identical constructions in the same area, one remained intact while the other was destroyed.

During the same seismic activity, old constructions such as the historical monastery of Mardaki (near Nedousa village), which dated back to the eighteenth century, and the monastery of Velanidia (north of Kalamata) were nearly destroyed. Of course we have no detailed data for the damage that previous earthquakes have caused to historical buildings and as a result it is not possible to extract relevant conclusions.

In many other cases the building destruction is linked to zones of seismic fracturing that were observed in the construction basement. Of course, this is not the rule. For example, in the area of the old Municipality Flea Market, where the main and surrounding buildings were damaged or destroyed (e.g. the temple of Ag. Apostoloi), no surface fracturing was observed. On the other hand, in the area of Giannitsanika, where surface fracturing was observed, disasters also occurred, while where no surface fracturing existed no disasters occurred. Furthermore, at the beach of Kalamata, the damage to buildings was minor in spite of the poor founding conditions (loose gravel, sand, high water table). However, exceptions still exist. Seismic fracturing must have been created during previous earthquakes in areas where disasters occurred, but they were not recorded except in special cases such as the aforementioned earthquake of the 10 June 1846. For this meizoseismal area, A. Galanopoulos (1947 p. 43) [7] reports, *"Near the village of Mpaliaga soil raptures were observed from which water and sand were released forming a small lake. Near the Mikromani village soil ruptures were observed that had a width of nearly 3-5 cm with sand cones that had a width of nearly 10 cm. From the openings of these cones, fluid materials were released. Next to the banks of the river Pamisos the ruptures were of greater width and partly filled by mud…"* From this description it can be

concluded that the observed phenomenon is liquefaction, something that was not recorded during the earthquakes of 1986.

2.3.3 Rock falls

The geographical distribution of the rock falls is focused mainly at several locations along a section of the Tzirirema, Karveliotiko, Xerilas streams, the Nedon river and in the greater area of the villages of Eleohori, Karveli and Ladas (Figure 5).

The largest percentage of the rock falls was observed in areas where the average dip is greater than 50 per cent, without regarding this as a rule since rock falls were observed also in areas where the average dip was less than 50 per cent. It is worth mentioning that in isolated cases movement or even overturning of relatively large blocks was observed (e.g. a limestone block with dimensions 60 cm x 40 cm x 30 cm) even in nearly horizontal relief (morphological dip 0-10 per cent) This was observed in the greater area of Eleohori and more specifically by the side of the road from Kalamata to Eleohori at an altitude of 300 meters, on limestone of the Tripoli unit. Nearly everywhere the rock falls are related to small or large faults where some have been reactivated and some have not. The reactivation is not related to the movement of blocks but only to fracturing.

As is known, the rock falls are theoretically linked to a reduction of consistency and internal friction of the rock, the increase of the slope gradient and so on, that is from the number of and the angular relationship between unconformable surfaces and the morphology of the slopes. The rock falls observed in the greater area of Kalamata during the seismic activity of September 1986 differ in relation to the aforementioned conditions. This is because rock falls were observed in sections of the area in which the conditions did not reinforce their creation, while in sections of the area where suitable conditions existed rock falls did not occur. Prompted by this fact, a detailed study of the rock falls took place, from which the following results were extracted Mariolakos et al. [8]: (a) In several sections of the area, rock falls were observed during the first (13 September 1986) and during the second (15 September 1986) earthquake, for example in the greater area of Eleohori, Ladas and so on, while in other areas rock falls were observed only during the second earthquake (15 September 1986), for example in the area of Tzirorema, (b) The sizes of the rock blocks that fell range from the size of an agglomerate to a size of many cubic metres, (c) It was observed that nearly all the rock falls are related to the reactivation of active faults and tectonic zones of extension.

Therefore, the intense relief and the geometry of the unconformable surfaces played an assisting contribution and nothing more than that.

From field observations that took place on the SE slope of the Tzirorema stream, it can be said that the geographical spreading of rock falls can be related to the frequency of tectonic unconformities, and the extensional tectonic zones present, which were activated in the area in a NW direction Mariolakos et al. [8] (Figure 5).

It is worth mentioning that at the northern side of the Tzirorema, although the conditions for rock falls exist (balanced dipping of bed surfaces to slope gradient etc.) such faults were significantly few.

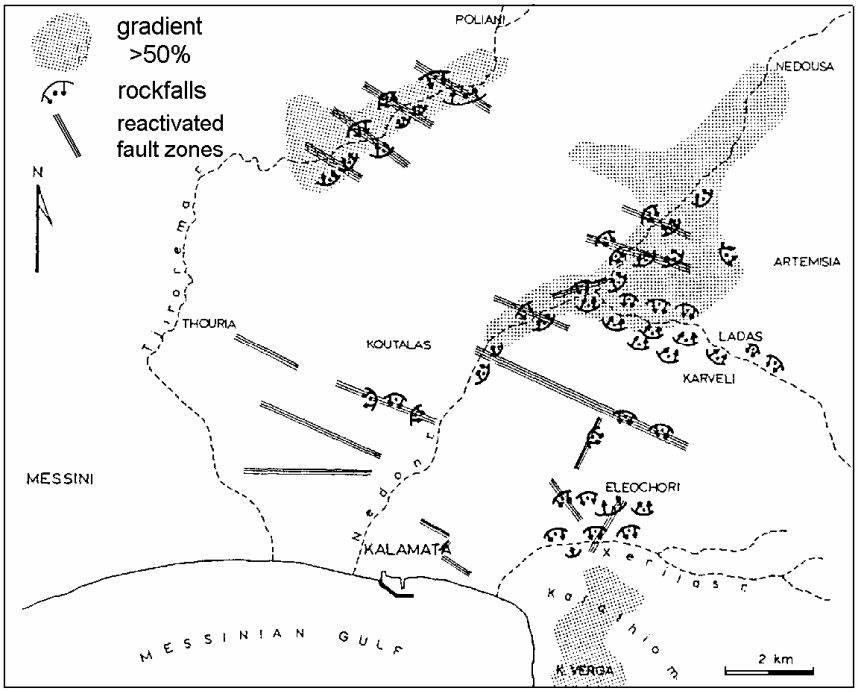

Figure 5: The geographical area within which disasters, rock falls and fault reactivations were observed during the earthquakes of Kalamata (after Mariolakos et al. [8]).

The rock falls in the whole distribution area are due to the same reasons. At this point we should mention that at a small distance southwards (nearly 2 km), at the tectonic horst of Kalathi Mt., no rock falls were observed nor movement of agglomerates, although the most favorable conditions dominate scree and steep slopes. According to our view, this fact is related to the non-existant reactivation of the fault zones in the area.

Therefore, according to the aforementioned, we believe that we are dealing with seismic rock falls and seismic scree, depending on the size of the material.

2.4 Conclusions

Taking into account the aforementioned we can draw the following conclusions:

i. The disasters were limited to the area that can be regarded as a transitional area between the tectonic basin Kalamata – Kyparissia and the tectonic horsts

of Asprohoma – Koutala to the north and the Kalathio Mt. to the south. On the contrary, in Messini and in Verga, disasters of that magnitude were not observed because those areas belong to different neotectonic macrosturctures that were not reactivated during the earthquakes of 1986 (central region of the tectonic basin of Kato Messinia and tectonic horst of Kalathio Mt respectively).

ii. Rock falls were observed mainly in the tectonic basin that was activated and also north of it, at Tzirorema, an area that was activated only during the second large earthquake (15 September 1986, M=5.6R). On the other hand, on the steep slopes of the Kalathio Mt. that belong to the homonymous neotectonic macrostructure, which was not reactivated, no rock falls were observed.

iii. An important factor in the distribution of the disasters and rock falls in the greater area was the reactivation of old faults or the creation of new soil ruptures. In this way, the fact that the destruction of buildings was observed in Gianitsanika and not near the coast can be explained, although the foundation ground – red siliceous clastic formation – in the first case theoretically presents better geotechnical characteristics in comparison to the loose coastal deposits.

3 The case of Athens

3.1 Geology - tectonics

The area affected by the earthquake presents a complex alpine structure, consisting mainly of two basic rock types, the Mesozoic metamorphics of the Attica geotectonic unit, occurring mainly at Penteli the Imittos mountains and the wider eastern Attica area, and the Mesozoic non-metamorphics of the Eastern Greece unit, occurring mainly in the Parnitha and Aegaleo mountains (Figure 6). It is important that the affected area is located at the boundaries of the above-mentioned units and towards Parnitha Mt., but their tectonic relation is yet to be determined in this area, since a thorough and detailed geological mapping has not hitherto been carried out. Furthermore, this old tectonic contact is covered by an allochtonous system, called “Athens schists”, as well as Neogene and Quaternary deposits. All that is certain is that the allochtonous system is tectonically overlaid on the two previously-mentioned units (Kober [9], Katsikatsos [10], Petrascheck & Marinos, [11]). The tectonic contact between the metamorphic and non-metamorphic units must have a NE-SW direction and its location must coincide with the bed of the Kifissos river (Figure 6).

The following comments can be made concerning the deposition period for the post-alpine sediments of the western part of the Athens basin:

Today, one can observe the remains of the deposits of a great lake during Late Miocene times, since lacustrine deposits of a similar age are found north of Parnitha Mt. (the Malakasa and Avlona areas etc.), as well as to the south (the Megara basin). It is very likely, therefore, that beneath the Quaternary deposits of the Thriassio plain, there are lacustrine deposits of the same age. This

indicates that the wider area of Parnitha was surrounded by one (?) great lake or lakes, and it must have been far from the sea, since no trace of sea influence is observed, while there is some evidence indicating that the lake water level of that age did not present a significant difference in elevation from the sea level of that time.

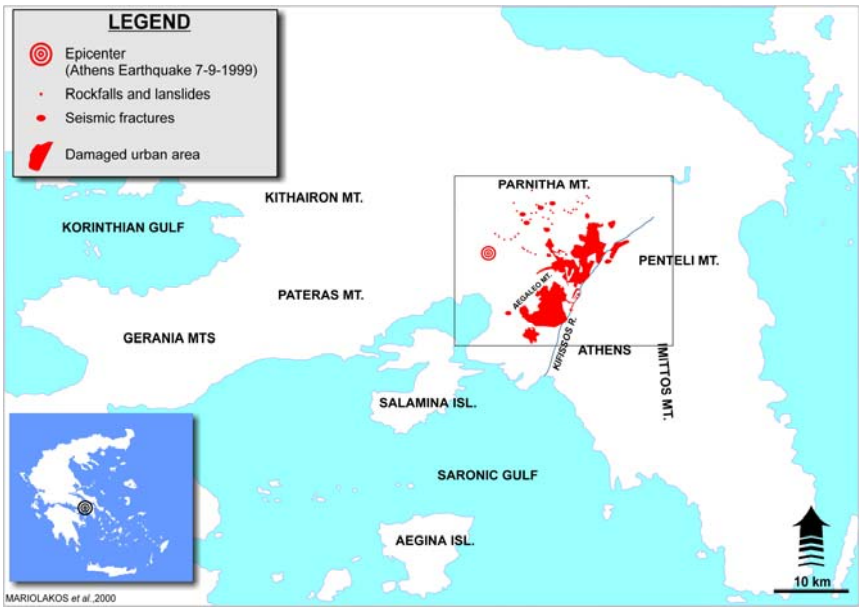

Figure 6: The study area.

The low tectonic activity of the Late Miocene was followed by a phase of intense tectonic activity of the Pliocene, which seems to affect only the eastern part of the basin, since the pebbles originated exclusively from rocks of the metamorphic units. So, during the Pliocene, Parnitha Mt. must have had the lowest relief energy compared to the Penteli and Imittos Mts, and did not supply the basin with erosional material, since no pebbles of the formations of Parnitha have been found in the Pliocene conglomerates Mariolakos, I. & Fountoulis [12].

3.2 Neotectonics – fault zones – faults

The broader Attica area represents a complex post-alpine morphotectonic structure, formed by the following great blocks of first order: the tectonic horsts of Parnitha, Aegaleo, Imittos and Penteli mountains and the tectonic grabens of Thriassion plain and that of the W. Athens basin (Figure 7). Within these major first order structures, smaller horsts and grabens are distinguished (second, third order etc.). The geometry of these structures is very complex. Their main directions are E-W and NE-SW.

The major fault zones of the meisoseismal area are the following (Figure 7).

i. Kifissos fault zone
ii. W. Aegaleo - Parnis fault zone
iii. Thriassion - Kamatero fault zone

The two first fault zones strike NE-SW and the third strikes WNW-ESE (Figure 7). The two last fault zones are typical scissor fault zones. That is, the Aegaleo segment downthrows west whereas the Parnis segment downthrows east, and the Thriassion segment downthrows south whereas the Kamatero segment downthrows north.

Taking into account (i) all the above elements, (ii) the detailed geological mapping of the Neogene formations carried out by B. v. Freyberg [13] and (iii) the morphotectonic study, the following conclusions can be drawn regarding the movements of the different blocks, as well as their internal deformation.

- The earthquake-affected area constitutes a "block mosaic" defined mainly by faults of NE-SW and WSW-ENE directions.
- Striations on fault surfaces have been observed in several cases, both on the marginal faults of the Athens basin and on Neogene formations, showing a significant horizontal component.
- The lignite horizons found within the Late Miocene deposits are folded, both at the eastern margin -N. Irakleio area- B. v. Freyberg [13], and the western margin -Peristeri area- O. De Pian [14] with axes again trending WNW-ESE. Folds are also found in the Neogene deposits with a low angle axial plane with a NE dip that indicates a local compressional stress field with $\sigma 1$ directed from NE to SW.
- Most of the blocks are rotated around axes trending E-W, while Parnitha Mt., with its blocks, rotates around a NE-SW axis, to the west. Using morphotectonic evidence, Parnitha Mt. appears to dip at its NW extremities relative to its SE part, where it appears to have the maximum uplift. That is the reason why Parnitha Mt. presents the highest altitudes in this area, with the consequence of high erosion, high relief energy and slope gradient.
- The throws of the faults defining the margins of the blocks are different; for example, between the blocks of Petroupoli and Menidi the throw has been greater than 400 m since the Pliocene, while the throw between Menidi and Fyli blocks has been greater than 600 m since the Pliocene.
- The Ano Liosia-Menidi area belongs to a graben which, as a whole, presents greater subsidence during the last 5Ma, within an area that rotates around an horizontal axis, trending NE-SW and dipping to NE, gradually decreasing the surface of the lake to the NW, remains of which exist even today, since, periodically, a small lake forms in the same area (see the area which is known today as "Limni" lake at Ano Liosia).
- The actual alpine basement of many blocks (neotectonic horsts and grabens) is below the present sea level, which indicates a continuous subsidence, in spite of the fact that the whole area is lifting up.
- The highest altitude of the lacustrine occurrences (500 m approx.) is located in the Thrakomakedones area, that is, at the margins of Parnitha Mt., where the highest mountain altitudes occur (more than 1100 m). In this area the

dip of the lacustrine beds is 35^0 to the NE. This means that the uplift of Parnitha must have occurred after the deposition of the Pliocene lacustrine sediments, during Pleistocene times. The result of this movement is the formation of a large talus, with material supplied exclusively from Parnitha Mt.. Within the Fyli basin, the same lacustrine deposits have uplifted, up to an altitude of 350 m.

- The area of the first order tectonic graben, apart from the rotation of each block, shows an overall continuous rotation throughout the whole period between the Pleistocene to the present time.
- Parnitha Mt. is uplifting, forming one of the active margins of the great Parnis-Kithairon complex morphotectonic multi-block, and specifically at its south-easten extremity. The north-western margin, located close to the Korinthian Gulf, is uplifting in the same way, forming the Kitheron Mt. horst.

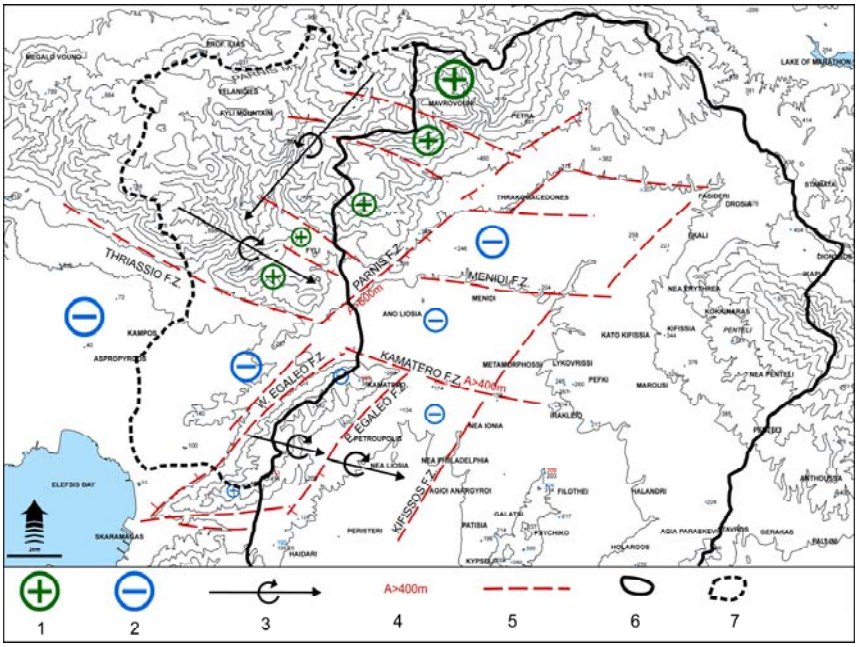

Figure 7: Sketch map depicting the major fault zones of the earthquake-affected area: 1: uplift, 2: subsidence, 3; rotational axis, 4: estimated vertical throw, 5: fault zone, 6: watershed of Kifissos r. basin, 7: watershed of Giannoulas r. basin. The relative size of the markers for uplift or subsidence indicates respective rate (after Mariolakos & Fountoulis [12], [15]).

- The above-analyzed complex kinematic evolution is the result of complex dynamics and, therefore, a more complex stress field, difficult to interpret by the existence of a simple tensional regime, which is unable to explain the continual uplift of Parnis Mountain.

3.3 Geographical distribution of damage and geodynamic phenomena

3.3.1 Seismic faults – seismic fractures

Seismic fractures were mainly observed within the SE part of Parnitha Mt. They occurred at the transition zones between the horsts and the grabens and they had two main trends that are WNW-ESE and N-S.

The most impressive seismic fractures were observed at the area of Parnitha Mt. located NE of the Kleiston Monastery and SW of the cave of Pan (Figure 5, location 2). In this site, the seismic fractures had an average trend WNW-ESE, occurred within the Mesozoic neritic carbonates, had a length of at least 250 m and showed a maximum vertical displacement of about 40 cm. In the broader area, many smaller fractures occurred, mainly in en-echelon arrangement, trending WNW-ESE (80^o-110^o), NNW-SSE (350^o) and NW-SE (120^o-135^o).

It is worth noticing that this seismic fracture runs parallel to an older one. It is very possible that this has to do with a gravity fault, as it is difficult to see any horizontal component and/or the geometry of the fracture.

Other major seismic fractures were found on the northern margin of the Fyli graben, in the Agios Kyprianos Monastery area (Figure 5, location 1). Two main fracture trends were measured. The longer one, with a length of approx. 100 m, which caused damage inside the monastery, presents a trend of 350^o. Smaller fractures (15-20 m) were observed to be parallel to the tectonic contact of the clastic Triassic rocks and the neritic limestones of the Eastern Greece unit, trending 80^o-100^o.

Other fractures of a similar direction were observed in the Fyli castle, as well as on forest roads, often at fault or thrust extensions, functioning today as normal faults and affecting the alpine rock mass of SE Parnitha Mt.

It must be pointed out that along a fault surface occurring on neritic carbonates, there is a light band defining a displacement probably due to an older earthquake event (Figure 7) This fault surface trends 158^o and dips 64^o towards the SW.

Some seismic fractures were also found in the Thrakomakedones area and the broader Amygdaleza area (Figure 5, location 4). Both directions (E-W and 352^o) were found in this area too, the latter being predominant. It is important that these fractures are closed; they present no displacement but have cut through pebbles found within the asphalt.

On the road leading to Agia Triada and near the church (the area between the Xenia Hotel and the Parnis Casino) (Figure 5, location 3) a fracture was observed, trending E-W, near the tectonic contact of the Triassic sediments and the neritic limestone, cutting through the small cement wall at the side of the road, which shows a displacement of reverse character.

3.3.2 Disasters

The damage caused by the earthquake was very serious for the buildings, with large fractures and/or cross-fractures on structural elements, collapses and so on, etc, mainly in the area of Ano Liossia and the Menidi basin Mariolakos & Fountoulis [15], Mariolakos et al. [16], as well as in the area of Thrakomakedones, whereas in the epicentral area (Aspropyrgos, Elefsis, Magoula, Mandra in the Thriassion basin) the damage was limited. Furthermore, the earthquake caused 143 fatalities and 700 injuries, and more than 70,000 people became homeless. It has to be remarked that the spatial distribution of site effects and damage is relevant not only to the distribution of seismic energy, but also, indirectly, to urbanization, which is diachronically controlled by the geomorphology and the tectonics of the area.

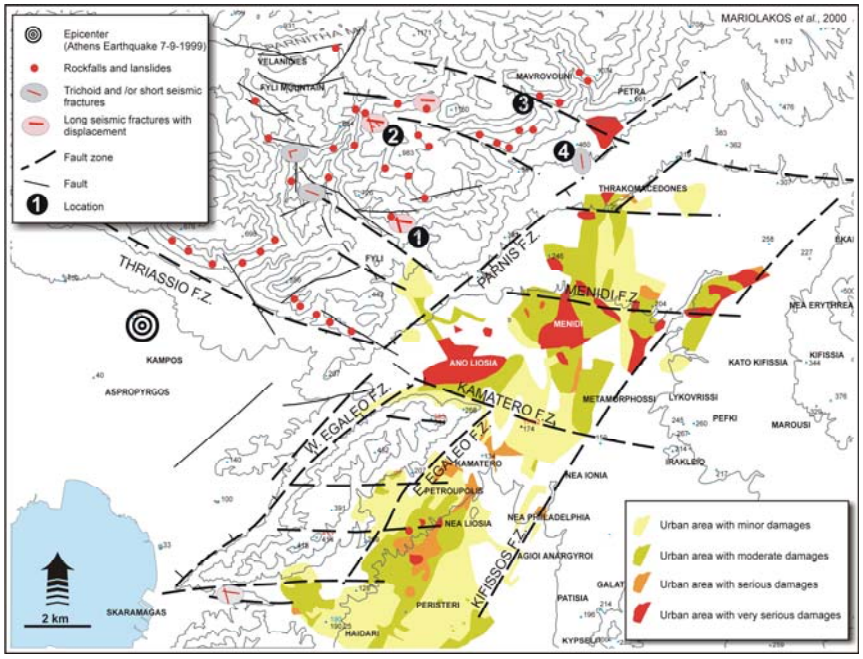

Figure 8: Map showing the distribution of the damage and geodynamic phenomena observed during the Athens earthquake (7 September 1999). Damage distribution has been based on Marinos et al. [17]).

The large-scale urbanization of Athens had originally developed within the homonymous basin, while during the recent decades it has developed towards the margins of the basin and the foothills of the surrounding mountains (Parnitha, Penteli etc.) (Figures 6, 8). However, these margins are formed as a result of the activity of the marginal faults of the basin.

The mainly stricken urban area includes the majority of the regions between the axis of the Kifissos riverbed and, westwards, the foothills of the mountains of Aegaleo and Parnitha, as well as the grabens between these mountains (Figure 5). In other words, the damage was located in the minor order tectonic grabens of the western-northwestern part of the Athens basin, that is, areas of low relief, covered by post-alpine deposits, which is also the reason for the development of urbanization towards these regions. These grabens are tectonic structures consisting of cohesive and loose deposits of recent age (Neogene - Quaternary), and thus they are considered tectonically active. Furthermore, they are bounded by fault zones with varying displacement, several hundred meters in some cases Mariolakos & Fountoulis [15].

3.3.3 Rockfalls and landslides

The seismic activity of 7 September 1999 caused rockfalls, which were especially noticeable in the cases where they caused problems on the road network.

The rockfalls were located at the SE part of Parnitha Mt., that is, south of its basic water divide and in the hydrologic basin of the Giannoulas river to the west, and partially in the NW part of the Kifissos hydrologic basin (Figures 7, 8).

It is known that rockfalls are directly related to, among other factors, a reduction of cohesion and the angle of internal friction and an increase in the slope gradient.

Practically all rockfalls are a function of the angular relationship between the surfaces of discontinuities and the slope gradient, as well as the density of the discontinuities within the rock-body.

It is important to note that the rockfalls did not occur in all favorable areas (broken brecciated rockmass, favorable conditions of the geometry of discontinuities surface etc.), but they were observed only in narrow strips along faults or fissures, which were reactivated by this earthquake event.

More specifically, the rockfalls were observed mainly in areas where one of the fractures trends WNW-ESE or N-S and the slope gradient dips to the north or the south (Figure 8).

3.4 Conclusions

Taking into account all the above, the following can be mentioned:

1. The serious damage and the majority of the geodynamic phenomena were restricted to between the Kifissos riverbed to the east, the Giannoulas riverbed to the west, and the watershed dividing Parnis Mt. in to its north and south parts (Figure 9).
2. This area is controlled by two main sets of fault zones trending NE-SW, WNW-ESE and/or E-W.
3. Through these fault zones the whole area is divided in to several blocks, with different kinematics.

4. Although reactivation of pre-existing faults has been observed, no displacement has been observed so far, apart from a small one at the area of the caves of Pan (Figure 8 location 2).
5. Many rockfalls have been observed, always connected with major or minor alpine fractures or faults.
6. It is worth noting that all these reactivated fractures are of alpine age, and they have most likely been reactivated more than once in the past.
7. In some cases, it is certain that the kinematics of these alpine structures have changed through time, that is, an initially reverse fault or thrust now behaves as a normal or oblique slip fault. The same has also been observed in the case of the Egion earthquake of 1995 in the Eratini area, Mariolakos et al. [18].
8. Damage to buildings was restricted to the area of the multi-fractured neotectonic graben filled in with a thick sequence of Plio-Pleistocene clastic sediments.

4 Discussion - conclusions

After the recent earthquake events, it has been generally realized that both the areas studied are not only tectonically active areas, but they are also seismically active.

Although both areas belong to different geotectonic regimes due to their distance from the Hellenic Trench (Kalamata belongs to the Island Arc region whereas Athens belong to the back arc basin region), they presented similar behaviour in the damage, and secondary geodynamic phenomena, distribution. More specifically, based on the above, we can come to the following conclusions for both cases:

i. The disasters occurred within graben structures oriented by fault zones
ii. No damage or very limited damage was observed in the epicentral areas.
iii. Rockfalls did not occur in all favorable areas (broken brecciated rock mass, favorable conditions of the geometry of discontinuities surface etc.), but were observed only in narrow strips along faults or fissures, which were reactivated by this earthquake event. On the contrary, no rockfalls were observed on brecciated rock mass on slopes with high gradient belonging to a neotectonic macrostructure, which was not reactivated by the earthquakes.
iv. The reactivation of existing faults or the creation of new fractures played very important role in the spatial distribution of the damages and the rockfalls in the broader area.

Taking into account all the above concerning the damage and the rockfalls induced by both earthquakes, it is necessary to underline that during proposed geological mapping of tectonically seismically active areas for engineering geological purposes, special attention has to be given to the mapping of the active faults. This is because active faults have the highest potential for dangerous rockfalls to occur, even in areas where, from a theoretical point of view, the slopes could be considered stable. Consequently, the traditional analytical work in structural geology as described in rock mechanics is without a

doubt necessary, but not enough for tectonically active areas, as found in Greece and throughout the world, if we want to approach as well as possible the problem of the prediction of rockfalls. Furthermore we have to distinguish the rock mass in loose and cohesive rock mass units. This distinction is very useful because it permits us to locate areas vulnerable to damage and rockfalls, even when, according to the geotechnical characteristics of the rocks and the slope gradient, they could be considered stable.

More specifically, in spite of the technicogeological characteristics of the ground, the relief, the water table and the technical properties of the structures, the following have played a very important role in the distribution of damage and rockfalls: (a) the neotectonic structure that was reactivated, (b) the reactivated faults regardless of the distance of the affected area from the epicenter, (c) the seismic fractures that were created and present a specific arrangement in space, especially in cases where they are not related to liquefaction phenomena, (d) some old minor faults, which were not reactivated but were classified, taking into account their geometry in respect of the active ones, (e) the density of the discontinuities of the rock mass, which is controlled by the older and the younger tectonism.

The detailed study of the fault pattern in all scales of observation gave us information on the "behavior" of the different types of faults and fractures during a seismic event and consequently on the "seismo-geological" behavior of the various formations. The main characteristics of these faults are the following:

a. The density of faulting seems to be irregular in major areas and is independent of the strata age.
b. The density of the neotectonic faults intersecting the neritic carbonates of the Tripolis and Eastern Greece units is much higher than that of the Cretaceous limestones of the Pindos unit and in Parnitha Mt.
c. The density of the faults in the post-alpine deposits is relatively lower than in the alpine age carbonates.
d. The density of the neotectonic faults varies from place to place within the same lithological units.

Most of the faults intersecting the carbonates of the Tripolis unit are old faults of which some were possibly created during the initial stages of the neotectonic period. Some of these faults, which in many cases have been reactivated more than once, as indicated by the successive slickensides generations, cannot be considered as active faults, Mariolakos et al. [19]. Studying the faults within the carbonate rock mass, areas can be distinguished that are intensively fractured and others that are much less fractured. In the study the difference in the grade (frequency + density) of fracturing can be easily understood, and in the neighboring areas as well. These faults present the following characteristics (Figure 9):

a. The fault surfaces are not planar but curved. As a result, strike and dip varies significantly. These surfaces have been created in the latest alpine orogenic stages or in the very early stages of the neotectonic period; hence, they are considered as inactive, Mariolakos et al. [5], Mariolakos et al. [4].

b. The fault surfaces are not always continuous; indeed, most terminate when they meet a more dominant fault surface. The smaller-order fault surfaces are limited (bounded) by greater-order faults; they usually have an "s" shape and occur in an en echelon arrangement. This is evidence of the dynamic and kinematic dependence of the smaller-order fault surfaces on the greater ones (Figure 9).
c. The fault size differs from place to place, and a local classification as first, second etc. order may be made. In many cases, the genetic relationship between faults of greater order and those of lesser is apparent.
d. These faults show an en echelon arrangement.
e. Usually the fault surfaces are polished and more than one slickenside generation occurs on the surfaces. They are characterized by the absence of tectonic breccia or looseness zone along the fault zone.
f. From the kinematic point of view, these faults should be considered as oblique slip faults, with movement normal and/or reverse. Generally, the normal or reverse character of these faults is not apparent because of the complex shape of the fault surface.

Those areas that are faulted by older neotectonic activity are fractured again by younger faults that transverse the whole rockmass (Figure 9). These younger faults should be considered to be active, since the earthquakes of 13September 1986 and 7September 1999 reactivated some of them, although the observed displacement was very small. These faults are named seismic faults bearing in mind that they could be reactivated during a future earthquake but they do not seem to cause any seismic event.

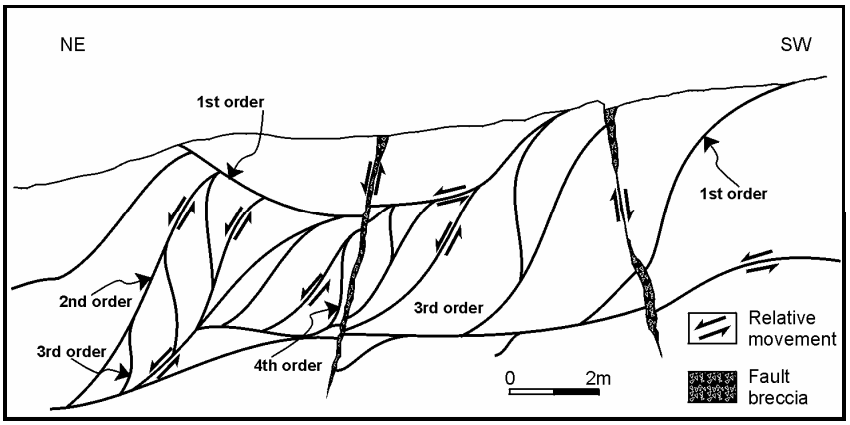

Figure 9: Schematic depiction of older (inactive) neotectonic faults of various orders intersected by younger active faults (after Mariolakos & Fountoulis [6]).

The density of the neotectonic faults of all orders is generally very high. It is observed in many sites of the Hellenic territory and is related to the local dynamic and kinematic regime of the neotectonic deformation of each area. The high density of the active neotectonic faults by itself makes it very difficult to transform the massive rock mass into a loose one (soft rock). The transformation of the mechanical properties of the rock mass is a more complicated phenomenon relating to the kind of movement along the surfaces of the active faults and to their geometry. If there are some presuppositions, some inactive blocks may be displaced due to passive reactivation of inactive faults. These small passive displacements cause new displacements to other minor blocks and so on. Due to the geometry of the inactive fault surfaces, even a very small displacement causes sites of compression and tension locally, which in their turn cause reactivation of other inactive blocks. Following this, and because the reactivation has taken place many times in the past, mountainous areas can be fractured in various sized blocks with various degrees of looseness. Hence, areas that have suffered such a type of deformation are transformed to huge size tectonic macro-breccia. Within this loose rock mass there are some parts of various sizes that can still remain massive. All the processes described take place mainly in the transition zones between the positive and negative neotectonic structures (horsts, grabens).

Taking into account all the above regarding the disasters and the rock falls that were observed during the earthquakes of September 1986, we believe that during geotechnical mapping of a seismically active region, emphasis should be given to the mapping of the active faults as well as to the distinguishing of the rock mass into loose and massive tectonic units. Such data are necessary since they allow the location of areas where the development of catastrophic phenomena are likely to occur, even if they could be regarded as stable according to the geotechnical characteristics of the rocks and the morphology of the relief.

References

[1] Psonis, K. *Geological map of Greece, Kalamata sheet, scale 1/50,000*, Geological Survey of Greece: Athens, 1986.

[2] Mariolakos, I., Schneider, H., Fountoulis, I. & Vouloumanos, N. Paleogeography, sedimentation and neotectonic implications at the Kambos depression and Kitries Bay area (Messinia, Peloponnese, Greece). *Bull Geol. Soc. Greece*, **XXVIII/1**, pp. 397-413, 1993.

[3] Marcopoulou-Diacantoni, A., Mirkou, M.R., Mariolakos, I., Logos, E., Lozios, S. & Fountoulis, I. Stratigraphic observations in the post alpine deposits in Thouria-Ano Amfia area (Messinia Province, Greece) and their neotectonic interpretation. *Bull. Geol Soc. Greece*, **XXIII/3**, pp. 275-295, 1989 (in Greek).

[4] Mariolakos, I., Fountoulis, I., Logos, E. & Lozios, S. (a), Surface faulting caused by the Kalamata (Greece) earthquakes (13.9.1986). *Tectonophysics*, **163**, pp. 197-203, 1989.

[5] Mariolakos, I., Sabot, V., Alexopoulos, A., Danamos, G., Lekkas, E., Logos, E., Lozios, S., Mertzanis, A. & Fountoulis, I. *Microzonic study of Kalamata (Geology, Tectonics, Neotectonics, Geomorphology).* Report of EPPO (Earth Planning Protection Organization), 1986 (in Greek).

[6] Mariolakos, I. & Fountoulis, I. Is it safe to built on fault surfaces in a seismically active area? *Proc. 8th International IAEG Congress*, pp. 665-670, Balkema, 1998.

[7] Galanopoulos, A. The seismicity in Messinia province. *Ann. Geol. Pays Hellen.,* **I**, pp. 38-59, 1947.

[8] Mariolakos, I., Fountoulis, I. & Nassopoulou, S. The influence of the neotectonic macrostructures, fractures, and the geological basement in the distribution of the damages in the kalamata earthquake (13-9-1986). *Proc. 1st greek Congress on Antiseismic Engineering and Technical Seismology Technical Chamber of Greece*, **1**, pp. 55-68, 1992 (in Greek).

[9] Kober, L. Beitrage zur Geologie von Attika. *Sitzungsb. Akad. Wiss. Mat-Nat. Kl.*, **138**, pp. 299-327, 1929.

[10] Katsikatsos, G., La structure tectonique d' Attique et l' île d' Eubée, Proc. Vth Coll. On the Aegean Region, Athens, *IGME Publ.*, **1**, pp. 211-228, 1977.

[11] Petrascheck, W.E. & Marinos, G. Zur Geologie von Attika, *Kober Festschr.*, pp. 52-59, 1953.

[12] Mariolakos, I. & Fountoulis, I. The Athens earthquake September 7, 1999: The neotectonic regime of the affected area, *Ann. Geol. Pays Hellen.*, **38(B)**, pp. 165-174, ISSN: 1105-0004, 2000.

[13] Freyberg, B.V., Das Neogen-Gebiet nordwestlich Athen. *Ann. Geol. Pays Hellen.,* **III**, pp. 65-86, 1951.

[14] O. De Pian, Peristeri, *IGME Unpublished Report*, Athens, 1950.

[15] Mariolakos, I., & Fountoulis, I., The Athens earthquake September 7, 1999; Neotectonic regime and geodynamic phenomena, In *Integration of Earth Science Research on the Turkish and Greek 1999 Earthquakes*, Kluwer Academic Publishers: pp. 113-126, 2002.

[16] Mariolakos, I., Fountoulis, I., Mariolakos, D., Andreadakis, Em. & Georgakopoulos, A. Geodynamic phenomena observed during the Athens earthquake (Ms=5.9) 7-9-1999. *Ann. Geol. Pays Hellen.*, **38(B)**, pp. 175-186, ISSN: 1105-0004, 2000.

[17] Marinos, P., Boukouvalas, G., Tsiambaos, G., Protonotarios, G., Sabatakakis, N. and collaborators, Damage distribution in the western part of Athens after the 7-9-99 earthquakes. *European Centre on Prevention and Forecasting of Earthquakes Newsletter*, December 1999, Issue No 3, pp. 37-39, 2000.

[18] Mariolakos, I., Fountoulis, I. & Mariolakos, D. Deformation structures at the Gulf of Corinth, Greece, induced by the Egion earthquake of 15-6-1995. *Proc. 8th IAEG Congress*, pp. 789-795, 1998.

[19] Mariolakos, I., Logos, E., Lozios, S. & Fountoulis, I. Neotectonic deformation of the Zimbeli fault surface (East of Kalamata, South

Peloponnese). *Bull. Geol. Soc. Greece*, **XXIII/3**, pp. 241-258, Athens 1989 (in Greek).

CHAPTER 5

A sequence of low magnitude earthquakes as a result of local tectonic activation: the case of the Psachna area, Evia Island, Greece

D. Fountoulis, Ch. Metaxas, S. Lalechos & C. Gountromichou
Department of Seismotectonics, Earthquake Planning and Protection Organisation (E.P.P.O.), Athens, Greece.

Abstract

A sequence of low magnitude shallow earthquakes occurred in January – February 2002, in the central part of Evia Island, Greece. Most of these earthquakes were felt locally in the town of Psachna and in the adjacent area. For monitoring the seismic activity, a temporary seismological network of four digital instruments was deployed and operated in the area. The coordinates, magnitude (from M_S=2.5 to M_S=4.2) and focal depth (1 – 30 km) of 258 earthquakes were determined. The geological map of the area (scale 1:50 000), a lineament map derived from processed Landsat ETM+ images, and a deep fault map based on the qualitative interpretation of the Bouguer gravity map, were integrated into a Geographic Information System (GIS) environment in order to comprehend the cause of the local seismicity. The current geodynamic regime of the area is characterized by the activation of primary SW-NE and secondary SE – NW deep faults, creating a system of small dimensions blocks (up to 20 km) of the pre-alpine basement. The foci are located on the activated deep fault planes and are mainly concentrated along two levels, at 1.0 and 3.0 km depth. These levels correspond to a thrust plane of the ophiolites above the carbonate series of Upper Triassic – Upper Jurassic and to a transgressive overlap of the Triassic sedimentary series above Paleozoic formations, respectively. The clusters of foci terminate at a depth of 8.0 km, which represents the thrust plane of the Pelagonian zone above the metamorphic formations of the Attico-cycladic zone. This characteristic distribution of the foci indicates the complicated movement of tectonic microblocks along the pre-existing horizontal and vertical geological discontinuities in accordance with the present N – S extension of the area.

1 Introduction

A sequence of low magnitude shallow earthquakes occurred in January – February 2002, in the central part of Evia Island, Greece. Most of these earthquakes were felt in Psachna town and within a radial distance of 10 km. Such a worrying phenomenon has been observed in Greece repeatedly, especially during the last five to six years (Nysiros Island, 1996, Zante Island, 1998, Corfu Island, 2001, Meligalas, South Peloponnesus, 2001 and 2002).

The present paper concerns the study of this seismic sequence, based on multi-source data integration (seismicity, geology, remotely sensed data and gravity data) and provides a complete framework for interpretation of the seismic activity in the area.

1.1 Geology – tectonics

The greater area belongs to the Pelagonian zone, which upthrusts the metamorphic formations of the Attico-cycladic zone. The latter forms a tectonic window in the south-eastern part of Evia Island (Figure 1). Post-alpine sediments cover the tectonic contact between the two units. The pre-alpine basement of the Pelagonian zone consists of schists and phyllites of the Upper Paleozoic (Permian). The alpine unit presents a continuous sedimentation from Lower Triassic (sandstones) to Upper Jurassic (limestones and dolomites) (IGME [1]).

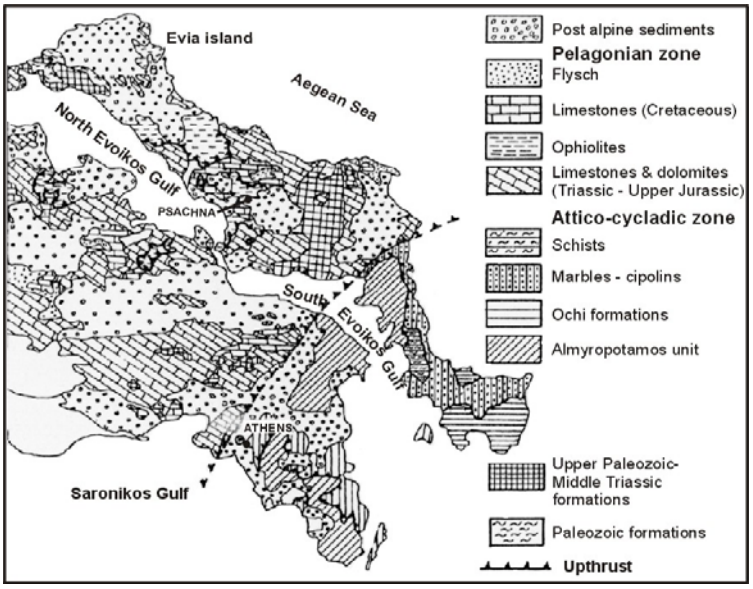

Figure 1: Schematic geological map of Evia Island (modified from Vergely [2]).

The aforementioned series are overthrusted by serpentinised ophiolites accompanied by shists-chert formations. The overthrusting of these ophiolites took place after the Upper Jurassic – Lower Cretaceous and before the Upper Cretaceous (Cenomanian) (Katsikatsos [3]). The alpine formations continue with transgressive carbonates of Upper Cretaceous age and they end up with Maastrichtian – Paleocene flysch. The post-alpine sediments correspond to alternations of marine and lacustrine deposits consisting of bedded conglomerates, marls, marly limestones and sandstones of the Pliocene. The post-alpine sediments cover a large area and overlay the alpine formations uncomformably.

Various tectonic phases, from alpine napping to the opening of neotectonic basins, have led to a complicated fracturing of the area. The two main alpine tectonic phases in the area are: (a) the overthrusting of the ophiolites towards the east (~ N – S strike of thrust faults), which took place after the Upper Jurassic - Lower Cretaceous and before the Upper Cretaceous (Cenomanian) and (b) the overthrusting of the Pelagonian zone above the Attico-cycladic zone towards SSW (~ WNW – ESE strike of folds and thrust faults) during the Middle Eocene (Katsikatsos [3]). After the alpine movements, the main geodynamics of the broader area, as of the whole Aegean area, is characterized mainly by a tensional regime causing normal faults with remarkable displacements in the relief. There are three phases in the neotectonic history of the area: (a) NE-SW tensional regime during the Pliocene, (b) a short period of NW-SE compressional regime during the Upper Pliocene-Lower Pleistocene and (c) the N – S tensional regime from the Middle Pleistocene to date (Lemeille [4], Mercier et al. [5]). The last period is responsible for the opening of the North Evoikos Gulf as tectonic graben and could have caused earthquakes of large magnitude in ancient and recent times (Thermopiles, 426 BC, M=7.0, Orchomenos, 426 BC, M=6.6, Thiva, 1853, 1893, 1914, M=6.3-6.8, Atalanti, 1894, M=7.0).

1.2 Historical and instrumental seismicity

The historical seismicity in central Greece, and consequently in central Evia, is imperfectly known. The historical seismicity catalogues (Papazachos & Papazachou [6], Ambraseys & Jackson [7], Ambrasays [8], Papazachos et al. [9]) provide data relating to earthquakes that occurred at some distance from the capital of Greece, Athens. Some of them are located close to the Psachna area, Evia Island, the case study, within a distance of no more than 50 km, and could be related to the study area. The data diminish for the period back in time from 1800 and further (Table 1).

The lack of complete historical records of earthquakes may plead for an apparent low earthquake hazard in the area. However, in analyzing further the instrumental seismicity of the area for the period from 1920 to 2000 some remarkable seismic episodes were observed, 11-13 September 1931 (six events, Ms = 4.9-5.3, V-VIII MMS), 5 September 1961 (2 events, Ms = 4.5, VI MMS) and 8 November 1971 (three events, Ms = 4.1 – 4.5). The epicenters of these episodes are located close to the town of Psachna. Moreover, the earthquakes

which related to these episodes could be characterized as events with medium magnitude and relatively high macroseismic intensity.

Table 1: Historical earthquakes in the Psachna area and surroundings.

Date – Time	*Coordinates – Epicenters*	*Magnitude*	*Intensity*	*Ref.*
426 BC – Winter – (427 BC)	38.5˚ N, 23.1˚ E – Orchomenos	M=(6.6)	VIII	[6], [8]
426 BC – Summer	38.8˚ N, 22.6˚ E – Thermopiles	M=(7.0)	IX	[6], [8]
1853 Aug 18 – 08:30:00	38.3˚ N, 23.5˚ E – Thiva	M=(6.8)	X	[6], [8]
1902 Apr 11 – 18:35:30	38.5˚ N, 23.5˚ E – Chalkida	M=(5.5)	VI	[9]
1914 Oct 17	38.3˚ N, 23.5˚ E – Thiva	M=(6.2)	IX	[7], [8]
1916 May 10 – 21:05:59	38.4˚ N, 23.5˚ E – Chalkida	Ms=4.9	IV	[9]
1916 May 20 – 22:14:11	38.4˚ N, 23.5˚ E – Thiva	Ms=5.3	V	[9]
1919 Nov 02 - 05:02:20	38.5˚ N, 23.7˚ E – Psachna	Ms=4.9	V	[9]
1938 July 20 – 00:23:00	38.3˚ N, 23.8˚ E – Oropos	Ms=6.1	VIII	[6], [7]

2 Methodology

The study of the of the cause of these low magnitude earthquakes in the area is based on the analysis of multi-source data and their integration in a GIS, in order to define possible map associations and understand this phenomenon.

The input data used in this study are processed with ILWIS V. 3.1 software (ILWIS [10]) and are the following:

- The epicenters of the earthquakes plotted in a point map.
- The geological map of the area with the known normal faults.
- The lineament map, which has been produced based on visual interpretation of advanced processed Landsat ETM+ data.
- The deep fault map, which contains the deep structure as it was identified in the area based on qualitative interpretation of gravity data.

3 Data analysis

3.1 Current seismicity

For monitoring the local seismic activity, a temporary seismological network of four GPS controlled, digital 24-bit instruments TELEDYNE DL 24-A, seismometer MARK PRODUCTS L-4-3D, was deployed in the area. The network was operated for the period 22 January - 22 February.

For the seismic data processing SEISAN V. 7.1 software (SEISAN [11]) was used. The velocity model (Table 2) was constructed using geological data of the area, as well as the results of a wide aperture reflection/refraction profiling (WARRP) seismic survey which was carried out along the North Evoikos Gulf (Makris et al. [12]).

The coordinates, magnitude and focal depth of 258 earthquakes were determined. Calculated magnitudes range from Ms = 2.5 to 4.2, and focal depths

from 1.0 to 30.0 km. Some spatial characteristics of foci distribution are the following:

1. The seismic activity appears to be expressed locally around Psachna.
2. A diffused pattern of local seismicity is observed, which means that there are several clusters of epicenters in the area which do not show a predominant linear distribution.
3. The foci seem to be concentrated generally at a depth from 1 to 8 km, being distributed horizontally mainly along two levels: at 1.0 and 3.0 km depth. Vertical distribution of the foci along narrow zones is also observed, and most of the foci terminate at a depth of 8.0 km.

Table 2: Velocity model

Velocity (km/sec)	*Depth (km)*
1.85	0.0
3.80	1.0
5.15	1.5
5.70	2.0
6.15	3.0
6.70	8.0
8.00	18.0
8.25	50.0
8.50	80.0

3.2 Lineament analysis based on Landsat 7 ETM+ data

In order to produce the most refined lineament map of the Psachna area, a subscene of Landsat 7 ETM+ image was used (acquired date 21.06.02, 183 path, 33 row). First, the image was georeferenced to UTM zone 34 by a first order polynomial transformation model using ground control points (GCP) from a 1:50 000 recent topographic map of the area. The image processing was then split into two parts for lineament analysis: (a) filtering techniques and (b) image fusion techniques (Gountromichou & Pohl [13]). The filters were run in a panchromatic band of Landsat 7 data, band 8, and after that the produced lineament map was corrected using as background the fused images.

Applying filters is the most common technique for lineament detection and it is the most preferable of any of the automatic or semi-automatic methods. For this study, the following filters were used: Sobel directional filters in four directions (N – S, NE – SW, E – W, NW – SE), edge enhancement 5x5, a run-once directional filter 5x5 (Gountromichou & Pohl [13]) and interpretation on Principle Component 1 (PC1). Image fusion was applied to the single-sensor spatial data in order to obtain the maximum spectral and spatial information, improving interpretability as well. The following techniques were used: Principal Component Analysis (PCA), Brovey Transform, Intensity Hue Saturation (IHS) and RGB combinations merging the high resolution band 8 (Figure 2). The final lineament map consists of 258 lineaments and it contributes to the delineation of the tectonic pattern of the area.

3.3 Gravity data

Qualitative interpretation and zoning of the gravity field allow understanding of some features of deep tectonic structures of the study area and the determination

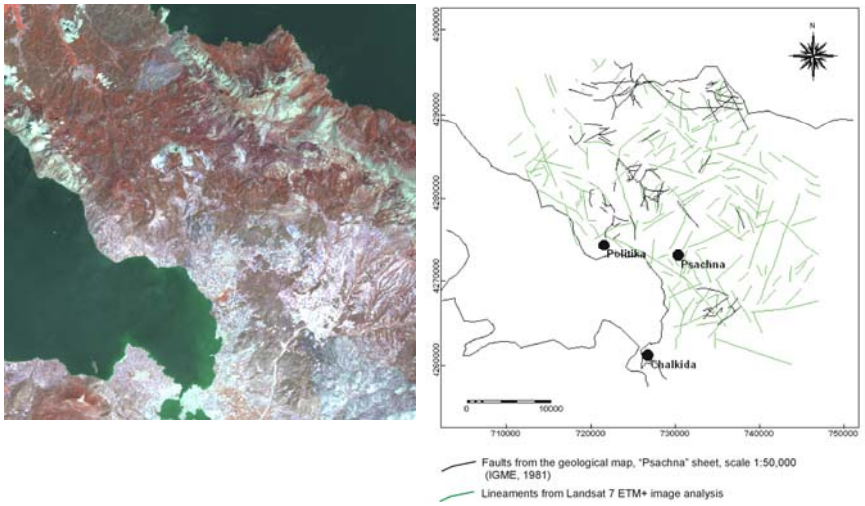

Figure 2: Fused image R,G,B (4,3,8) from Landsat 7 ETM+ as product of image processing for lineament analysis and the map, produced with the lineaments overlaid by the faults.

of possible "blind" faults zones. Zoning of the gravity field and related tectonic zoning are based on the relation to the peculiarities of field pattern over the geological or structural heterogeneity (object), as well as on theoretical anomalies over "simple" bodies (Khesin et al. [14]). Various "blind" fault zones could be determined in potential fields from their different linear features, which are related to fault origin and development. It is possible to find different linear features (indications) in the gravity field along the fault zone, due to fault segmentation. An arrangement of indications along the same direction allows the tracing of the fault.

For determining the characteristics of the deep tectonic structure of the Psachna area, the Bouguer gravity map, ρ= 2.67 gr/cm^3, topographic correction from 100 m to 167 km (Angelopoulos & Noutsis [15]) was used (Figure 3). The deep fault zones have been identified based on the following indications: (a) elongated zones of high field gradient, (b) abrupt closure or contraction of isolines, (c) offset of anomalies belonging to the elongated anomalous zone, and d) en echelon displacement of zones with linearly elongated anomalies. The gravity fields of the Psachna and Parnitha areas appear to have similarities due to their tectonic position at the tectonic contact between the Pelagonian and Attico-

cycladic zones. Thus, the gravity field of the Psachna area is probably defined by the structure of the pre-alpine Paleozoic basement, as in the Parnitha area (Metaxas et al. [16]).

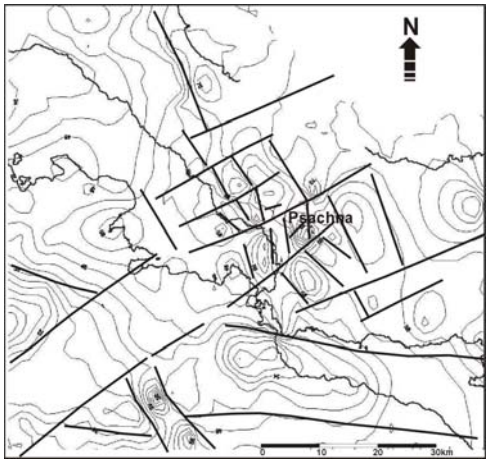

Figure 3: Gravity map of the Psachna area (modified from Bouguer gravity map of Greece, scale 1:500 000 (Gountromichou & Pohl [13]). Solid lines are probable deep faults.

4 Results

The spatial analysis of the lineaments, the surface and deep faults, as well as the seismicity, highlights the relation between deep and surface structures, and contributes to the interpretation of current seismic activity in the area. Most of the epicenters of seismic sequence studied are distributed in the area around Psachna (Figure 4). Based on the interpretation of gravity data, the main characteristic of the deep structure of this area is the microblock (up to 20 km) tectonics of the pre-alpine basement. Clusters of epicenters fit in either with some deep faults or with their intersections, and the reactivation of these structures seems to be the principal reason for the local seismicity in the Psachna area.

According to the geological map, surface faults are not mapped in the activated area; however, there are lineaments which have been identified in that area. These lineaments have two dominant directions based on their statistical analysis, one striking NW – SE and the other NE – SW (Figure 5a). Both sets of lineaments are considered as surface expression of the same directions of deep faults, which are responsible for the current seismic activity in the area (Figure 5b). In addition, the kinematics of the NW – SE and NE – SW faults has been tested in relation to the actual stress tensor of the area using the method of Carey (Carey [18]). Several sets of dip and rakes were tried as input in this method, and finally faults with 65^{o} dip and 60^{o} rake (oblique-slip normal movement) were considered to be the most compatible with the N – S tensional regime in the area from the Late Pleistocene up to present time.

Lateral distribution of the epicenters and deepening of the foci seem to reflect the activation of some “blind” faults, as well as tectonic boundaries between the different geological units (Figure 6). The spatial distribution of the foci

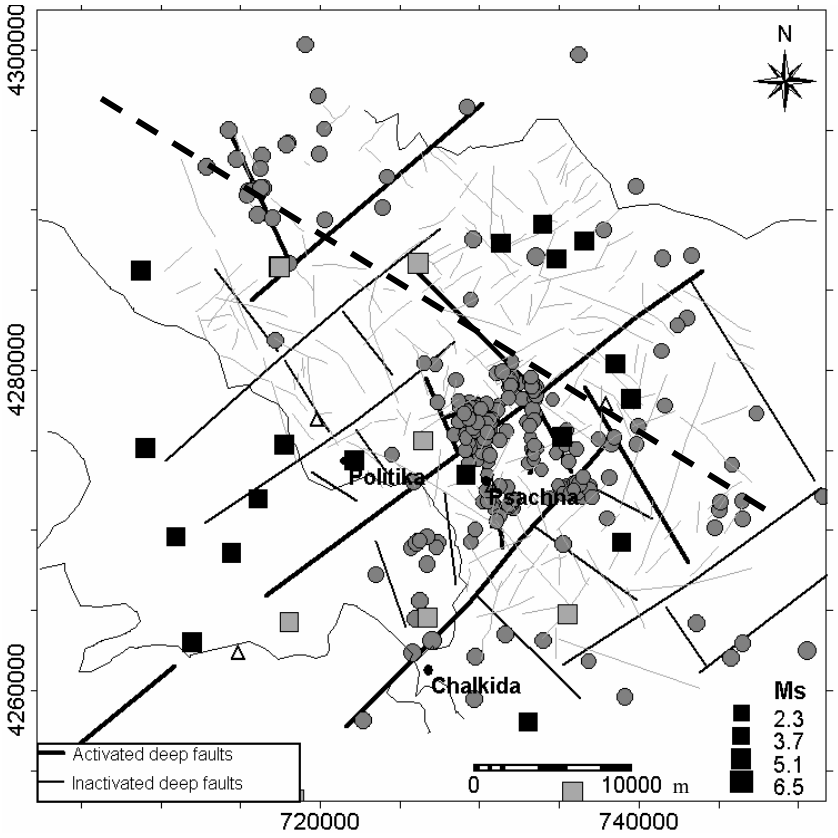

Figure 4: Final map illustrating the spatial distribution of the epicenters (gray circles for current seismicity, gray squares for events before 1961 (Papazachos et al. [9]) and black squares for earthquakes after 1961 (Papazachos et al. [9], NOA [17]), and its relation to the deep faults and the lineaments (thin lines). Triangles indicate the temporal seismological network and the dashed line the location of the schematic geological-geophysical cross-section.

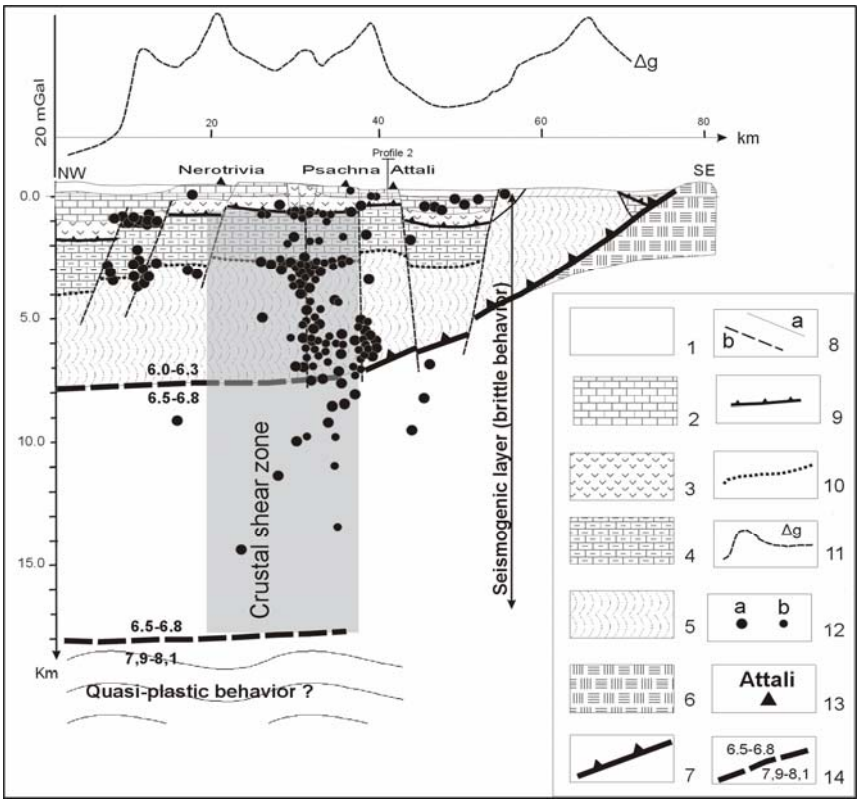

Figure 5: Schematic geological – geophysical cross section 1. Post alpine sediments, 2. Cretaceous limestones, 3. Ophiolites, 4. Upper Triassic – Upper Jurassic limestones and dolomites, 5. Upper Paleozoic cipolius and shists (pre-alpine basement), 6. Mesozoic metamorphic formations, 7. Upthrust, 8. Faults: A – from geological and remotely sensed data, B – from gravity data, 9. Overthrusting of ophiolites, 10. Transgressive contact of Mesozoic and Paleozoic formations, 11. Bouguer gravity curve, 12. Earthquakes of local sequence, 13. Temporal seismological stations, 14. Crustal velocity discontinuities and velocity rates in km/sec^2 (Makris et al. [12]).

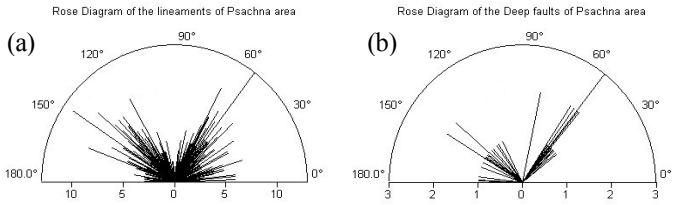

Figure 6: Statistical diagrams of the lineaments (a) and deep faults (b), indicating almost the same predominant directions: NE – SW and NW – SE.

on the sub-horizontal geological discontinuities and the deep fault kinematics indicate that the seismic activity is mainly associated with NE – SW horizontal movement, which may determine a shear zone.

These geological boundaries are either thrust planes or transgressive overlaps, such as:

– Thrust plane of the ophiolites above the carbonate series of Upper Triassic – Upper Jurassic (foci distribution at 1.0 km depth).

– Transgressive overlap of the Triassic sedimentary series above Paleozoic formations (foci distribution at 3.0 km depth).

– Thrust plane of Pelagonian zone above the metamorphic formations of Attico-cycladic zone. The prolongation of this plane to the depth corresponds to the velocity discontinuity. Most of the foci are concentrated at the shear zone and end up at this boundary (at 8.0 km depth).

The aforementioned pre-existing discontinuities are very favorable for reactivation and associated movements. However, the reactivation of such a low-angle discontinuities implies an increased heat flow and an associated hydrothermal circulation in order to facilitate the movement. Indeed, the measured heat flow in the northern part of Evia Island is relatively high (60 – 80 mW/m^2) according to (Čermak & Rybach [19]).

5 Conclusions

Multi-source data integration as a method of studying seismicity in the Psachna area provides a complete framework concerning understanding of the tectonic pattern and the geodynamics of the study area.

The pattern of the lineaments on the surface represents not only the overprints of the deep tectonic structure, but also the results of the geodynamic evolution of the area.

The characteristic distribution of the foci indicates the complicated movements of tectonic microblocks along the pre-existing sub-horizontal and vertical geological discontinuities. The geodynamic regime of the area, which is responsible for the local seismicity, is characterized by the activation of primary

NE – SW and secondary NW – SE deep faults. Estimation of their kinematics provides useful information about the sense of movement, which could be characterized as an oblique-slip normal movement and is in good agreement with the current N – S extension of the area.

Microblocks are prone to this activation due to their low inertia, and in the case of an earthquake even with medium magnitude in adjacent areas, it is possible for a local seismic sequence to be triggered. Thus, the study earthquake sequence was probably triggered by the recent strong earthquake in Skyros Island, July 2001, M=5.8, which is located in the close vicinity (80 km to the NE) and on the prolongation of the activated NE – SW primary fault structures of the Psachna area.

Acknowledgements

The authors are grateful to Dr. A. Angelopoulos, who kindly provided the Bouguer gravity map of Greece (1:500 000).

References

[1] *Geological map of Greece, Sheet Psachna, Scale 1:50 000*, IGME: Athens 1981.

[2] Vergely, P. *Tectonique des ophiolites dans les Héllénides internes – Conséquences sur l' évolution des régions téthysiennes occidentales*, Thèse d' État, Université de Paris-Sud, **2**, 1984.

[3] Katsikatsos, G. *Geology of Greece*, Athens 1992.

[4] Lemeille, F. *Etudes néotectoniques en Grèce centrale nord-orientale (Eubée centrale, Attique, Béotie, Locride) et dans les Sporades du Nord (île de Skiros)*, Thèse de 3^{e} cycle, Université de Paris-Sud, Orsay 1977.

[5] Mercier, J.L., Sorel, D., Vergely, P. & Simeakis, K. Extensional tectonic regimes in the Aegean basins during the Cenosoic. *Basin Research*, **2**, pp. 49-71, 1989.

[6] Papazachos, B. & Papazachou, K. *The earthquakes of Greece*, Ziti: Thessaloniki 1989.

[7] Ambraseys, N.N. & Jackson, J.A. Seismicity and associated strain of central Greece between 1890 and 1988. *Geophs. J. Int.,* **101**, pp. 663-708, 1990.

[8] Ambraseys, N.N. Material for Investigation of the Seismicity of Central Greece, *EC project "Review of Historical Seismicity in Europe" (RHISE)* 1989 - 1993. Source:http://www.globalnet.gr/seismoi_k_ell.html (19.08.02).

[9] Papazachos, B.C., Comninakis, P.E., Karakaisis, G.F., Karakostas, B.G., Papaioannou, Ch.A., Papazachos, C.B. & Scordilis, E.M. *A catalogue of earthquakes in Greece and surrounding area for the period 550BC-1999*, Geophysical Laboratory: University of Thessaloniki, **1**, 2000.

[10] ILWIS, V., 3.1. International Institute for Geo-Information Science and Earth Observation (ITC), the Netherlands 2002.

[11] SEISAN V., 7.1. *The earthquake analysis software*, Institute of Solid Earth Physics, University of Bergen, Norway 2000.
[12] Makris, J., Papoulia, J., Papanikolaou, D. & Stavrakakis, G. Thinned continental crust below northern Evoikos Gulf, central Greece, detected from deep seismic soundings. *Tectonophysics*, **341**, pp. 225-236, 2001.
[13] Gountromichou, C. & Pohl, C. Detection of active faults using data fusion techniques – Case study: Psachna - Island of Evoia, Greece. *Proc. of the 9th International Symposium on Remote Sensing*, ed. E. Manfred, SPIE Conference: Crete, Greece 2002, in press.
[14] Khesin B., Alexeyev, V. & Metaxas Ch. *Interpretation of magnetic anomalies in the conditions of oblique magnetization and rugged topography*, Nedra: Moscow 1983 (in Russian).
[15] Angelopoulos, A. & Noutsis, V. *Bouguer gravity map of Greece 1:500 000*, IGME: Athens, 2000.
[16] Metaxas, C., Angelopoulos, A., Lalechos, S. & Foundoulis, D. Deep Tectonic Structure of Northwestern Attica, Greece: Geodynamic Pattern of Athens Earthquake. *Geological Soc. of Greece*, **XXXIV**/1, pp. 259-265, 2001.
[17] National Observatory of Athens (NOA), *Seismicity of Greece, Earthquake database of Greece*, Source: http://www.gein.noa.gr/Greek/home-gr.html (19.08.02).
[18] Carey, E. *Analyse numérique d'un modèle mécanique élémentaire appliqué à l'étude d'une population de failles; calculs des caractéristiques d'un tenseur moyen des contraintes à partir des stries de glissement*, Thèse de 3e cycle, Université de Paris-Sud, Orsay 1976.
[19] Čermak, V. & Rybach, L. (eds.). *Terrestrial Heat Flow in Europe,* Inter-Union Commission of Geodymanics, Scientific Report 58, Springer Verlag: Berlin, 1979.

CHAPTER 6

The 26 July 2001 Skyros (north Aegean Sea, Greece) earthquake

G. Drakatos, G. Stavrakakis, A. Ganas, V. Karastathis, N. Melis, M. Ziazia & A. Plessa
National Observatory of Athens, Institute of Geodynamics, Greece.

Abstract

On 26 July 2001 a strong earthquake of magnitude M_w=6.5 hit the central Aegean Sea at 00:21:39 GMT. The event took place off shore Skyros Island at a distance of 135 km NNE of Athens. A sequence of many aftershocks followed with the magnitude of the largest of them reaching Ms = 5.4. The temporal and spatial characteristics of the aftershock sequence are investigated as well as the focal mechanism of the main shock and of the 47 largest aftershocks. The fault plane solution determined by the Institute of Geodynamics (National Observatory of Athens) implies that the main shock rupture is associated with sinistral strike slip faulting. In contrast to the general NE – SW strike of the principal planes of strong earthquakes in the North Aegean region, the strike of Skyros earthquake rupture zone has a NW-SE direction, supported from the distribution and the fault plane solutions of the strongest aftershocks. Therefore, the rupture zone of the 26 July 2001 earthquake probably defines the western end of the North Anatolian Fault.

1 Introduction

On 26 July 2001 a strong earthquake of magnitude M_w=6.5 hit the north Aegean Sea at 00:21:39.1 GMT. The event, according to the Institute of Geodynamics, National Observatory of Athens (NOAGI), took place off shore Skyros Island at a distance of 135 km NNE of Athens (39.046^0N – 24.338^0E, depth = 17 km; Figure 1). The epicentral region is situated at the westward extension of North Anatolian fault (NAF) into the Aegean Sea. This is an area of intense deformation, characterized by high seismicity with earthquake magnitudes up to about 7.5 (Papadopoulos et al. [1]). Strike-slip and normal faulting are predominant (Papazachos et al. [2], Taymaz et al. [3], Kiratzi and Papazachos

[4]). The primary cause of the deformation is the motion of the Arabian plate in a NNW direction which causes the westward escape of Turkey (Anatolian plate) relative to Eurasia, towards the Aegean.

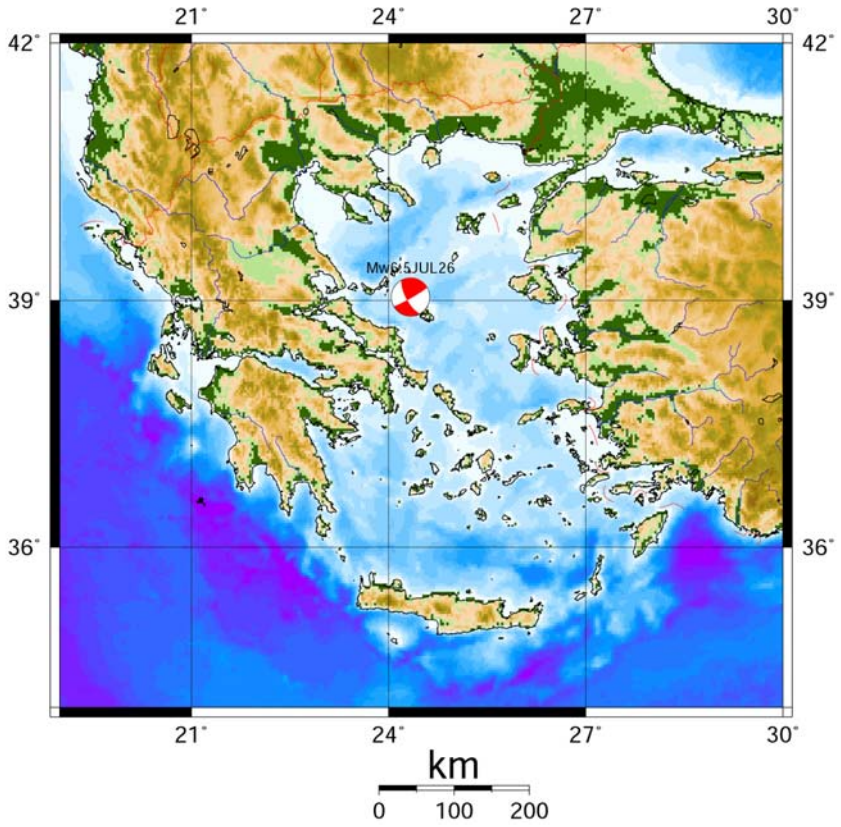

Figure 1: Tectonic setting of the Skyros earthquake. Background map is a raster digital elevation model of the Hellenic Arc and Back-arc areas. Thin lines are major rivers and political boundaries. Beach ball shows the focal mechanism solution according to several solutions (Table 1); black denotes compression quadrants.

It is important to note that the 26 July 2001 event was felt in a wide region (about 200 km radius) around the epicentral area. No severe damage was reported; however, almost 350 non-reinforced houses, mostly old traditional dwellings in the capital of Skyros suffered minor damage. Among them, an almost 1000 year old monastery was badly damaged. The strong motion resulted in massive rock falls which crashed onto many parked cars beneath the steep hill of the Skyros castle. The biggest effect to the population was the blockage of the

spring which supplies the capital with water. The seismic intensity did not exceed I_{max} = VII (modified Mercalli) in Skyros town. Minor damage was reported on the islands of Skopelos and Alonissos, about 50 km to the north-west of the epicenter (Figure 2). An intense sequence of aftershocks followed, with the magnitude of the largest of them reaching Ms = 5.3.

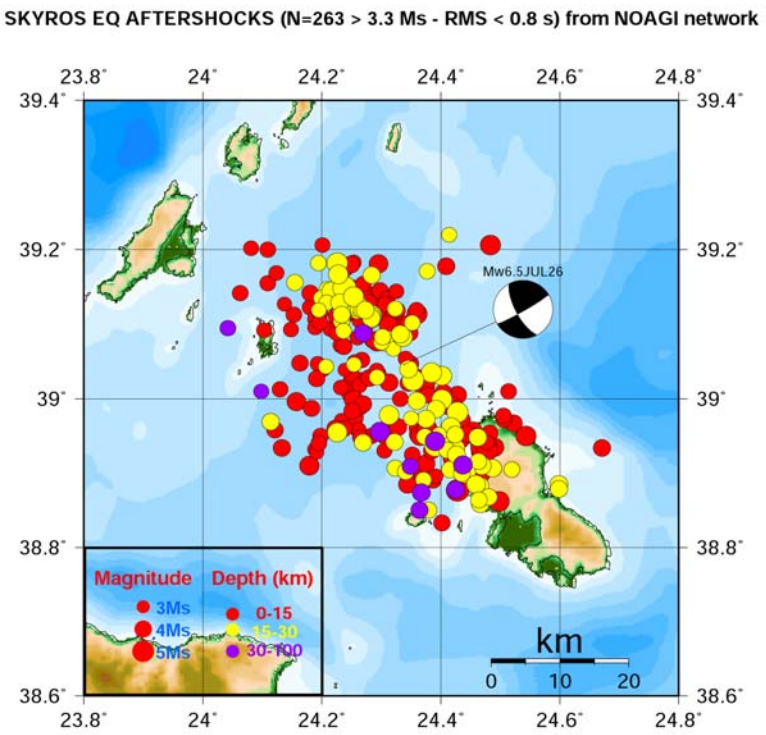

Figure 2: Map of aftershocks and focal mechanism solution of the Skyros 26 July 2001 earthquake. The aftershock colours and sizes follow depth and magnitude distribution, respectively.

The Skyros earthquake occurred two years after the Izmit earthquake (17 August 1999, Mw=7.4), in an area where several investigators claimed that strong events should be expected as a result of NAF westward movement (Papazachos et al. [5]). In the present study, the focal mechanisms of the main shock, of the three foreshocks and of the forty-seven (47) largest aftershocks as well as the spatial and temporal characteristics of the aftershock sequence are

presented, in an attempt to illuminate the complicated seismotectonic regime of the region.

2 Data: instrumental seismicity - foreshock activity

The fault-plane solution for the main shock that was determined from NOAGI when plotted together with the aftershock sequence implies that the main shock rupture is associated with strike-slip faulting (Figure 2). The solution was determined using 17 broadband NOAGI stations (at 20 s) and provides strike=150, dip=70 and rake=5 (Figure 2). The scalar moment is $Mo=4x10^{18}$ Nm. In addition, a detailed study of the focal properties of the main event has been done by NOAGI (Melis et al. [6]). Using the ASPO method (Zahradnik et al. [7]), based on amplitude spectra of complete three-component waveforms and first motion polarities, they calculated strike=150, dip=70, rake=10 and $Mo=4.1x10^{18}$ Nm. Both solutions are in agreement with those announced by USGS and other research centers (e.g. Benetatos et al. [8]). Table 1 summarizes the focal parameters, the magnitude and the fault-plane solutions according to different organizations. The main shock was preceded by three significant foreshocks (Table 2; Figure 3), which occurred on 21 July (M_L=4.1 and M_L=4.6) and on 25 July 2001 (M_L=4.2), very close to the epicenter of the main shock.

The largest event, closer to the epicenter of 26 July earthquake, occurred on 4 March 1967 (17:58:09 GMT, M=6.8), almost 30 km to the East (Delibasis and Drakopoulos [9]). According to the NOAGI seismicity catalog during the last 3.5 years seismicity has been very low in the region (Chouliaras and Stavrakakis [10]). Therefore, seismic quiescence was detected before the Skyros earthquake, concerning large events as well as small events.

2.1 The aftershock sequence – aftershocks focal mechanism

The Skyros earthquake was followed by intense aftershock activity. After careful examination of the digital records we processed 263 events of which 47 are presented in Table 2. At least six P-wave and S-wave phases for each event, recorded by the digital array of NOAGI, were used to locate the aftershock sequence using the HYPOINVERSE algorithm. For the Greek seismicity catalog the M_L=3.2 is proposed by Drakatos and Latoussakis [11] as the minimum magnitude (threshold magnitude). But in the investigated region the detectability of the NOAGI network reaches smaller magnitudes (Chouliaras and Stavrakakis [10]). We note that the aftershock distribution (Figure 2) implies a bilateral rupture, with the major axis of the aftershock area striking in a NW-SE direction. The above mentioned direction becomes quite clear from the epicenter distribution of the aftershocks with determined focal plane solutions (Figure 3). In general, the aftershocks are well defined in a relatively narrow zone along the fault as can also be shown in the aftershock distribution with respect to depth (Figure 2). We suggest that the processed, largest aftershocks define the rupture zone of Skyros earthquake (Figure 3). Their strike, NW – SE, coincides with that of the main shock nodal plane. Within the first day (26 July 2001) the rupture

zone was defined with the long axis trending NW-SE and extending for almost 28 km. At the end of the aftershock sequence (end of October 2001) the long axis of the rupture zone extends for about 45 km (Figure 4 bottom).

Table 1: Focal parameters and fault-plane solutions for the 26 July 2001 earthquake. Time is GMT. Capital phi and lambda are latitude and longitude coordinates, respectively. M is earthquake magnitude. Mo is seismic moment. Focal plane parameters are strike ξ, dip δ and rake λ.

Organization	**Time**	**Φ (^{0}N)**	**Λ (^{0}E)**	**L (km)**	**M**	**M_0 (Nm)**	**$\xi(^0)$ NP1 NP2**	**$\delta(^0)$ NP1 NP2**	**$\lambda(^0)$ NP1 NP2**
NOA GI	00:21:39	39.046	24.338	19	Ms=5.8	$4x10^{18}$	150 60	70 85	5 160
ASPO	00:21:39	39.06	24.34	17	Mw=6.5	$4x10^{18}$	150	70	10
USGS	00:21:38	39.06	24.34	14	Mw=6.5 Mb=6.0 Ms=6.6	$5.4x10^{18}$	145 55	85 86	4 175
CSEM	00:21:37	39.07	24.14	10	Mw=6.4 Mb=5.8	$5.2x10^{18}$	128 37	81 84	6 171
SED	00:21:37	39.06	24.34	21	Mw=6.6	$8.7x10^{18}$	238 148	90 73	-163 0
HRV	00:21:44	38.93	24.30	15	Mw=6.5	$5.4x10^{18}$	148 238	71 89	1 -161
THE	00:21:38	38.99	24.38	14	M=6.4	—	—	—	—

The cross sections drawn both parallel and perpendicular to the fault strike show several events reaching depths of 30 km, which is deeper than the main shock hypocenter depth (17 km). These events define a narrow zone of earthquake occurrence in the lower crust beneath the main shock hypocenter. We note that crustal thickness around Skyros is estimated as 30 km (Tsokas and Hansen, [12]).

Table 2: Focal plane solution (preferred plane) of the 50 well-determined shocks of the Skyros earthquake sequence (3 foreshocks – 47 aftershocks). MAG is surface magnitude.

DATE	LAT	LONG	DEPTH	STRIKE	DIP	RAKE	MAG
721	39.071	24.318	20.89	135	40	-20	4.6
721	39.065	24.387	3.50	130	60	0	5.1
725	39.082	24.349	7.32	245	75	-170	4.7
726	39.025	24.359	13.79	155	75	-30	5.3
726	39.107	24.309	9.55	100	55	-50	4.8
726	38.965	24.431	7.87	0	60	50	4.9
726	39.112	24.283	19.47	100	70	-50	4.9
726	39.078	24.308	29.34	135	85	10	5.0
726	38.949	24.412	28.58	55	90	-140	5.2
726	38.929	24.470	11.87	230	85	170	5.3
726	39.035	24.384	17.85	300	85	0	4.7
726	38.999	24.402	17.75	125	85	-30	4.7
726	38.937	24.391	28.28	60	85	-160	5.1
726	38.907	24.487	21.29	125	55	110	4.2
726	38.986	24.392	27.95	325	90	10	4.3
726	39.010	24.514	10.63	15	30	20	4.2
726	39.067	24.320	29.75	240	55	170	4.1
726	39.076	24.293	6.20	245	60	180	4.3
726	38.944	24.404	26.07	325	85	0	4.8
726	38.943	24.390	30.20	55	90	-140	4.6
726	39.025	24.353	27.16	55	90	-140	5.1
726	39.111	24.284	18.97	130	40	0	4.3
726	39.018	24.373	6.09	60	90	-150	4.5
726	39.083	24.336	19.10	220	85	-170	4.5
726	39.125	24.258	16.19	115	70	-30	5.1
726	38.962	24.417	25.23	60	90	-160	4.5
726	38.910	24.469	26.27	330	90	30	4.4
727	38.862	24.498	6.39	50	85	-140	4.8
728	38.901	24.440	29.95	60	90	-130	5.1
730	39.126	24.244	19.68	140	85	-70	4.4
730	39.119	24.233	22.11	110	85	0	4.3
730	39.181	24.295	13.65	325	80	-50	4.4
730	39.114	24.360	9.11	160	70	-30	4.8
731	38.876	24.425	32.50	170	60	-30	4.3
8 2	39.206	24.483	7.41	120	65	30	4.8
8 3	38.996	24.157	7.95	90	80	120	4.4
8 3	39.117	24.268	14.89	330	90	30	4.4
8 3	39.098	24.272	13.93	150	85	-50	4.0
8 8	38.931	24.478	12.52	50	70	-140	4.9
810	38.991	24.263	10.33	145	75	30	4.6
812	38.999	24.253	6.64	150	75	-30	4.4
827	39.137	24.253	21.93	45	75	-150	4.8
9 4	38.941	24.269	18.66	315	85	-10	4.0
9 7	38.955	24.226	24.87	325	85	0	4.5
910	38.960	24.223	12.26	330	90	30	4.1
919	38.949	24.459	13.89	345	70	60	4.3
10 7	38.953	24.443	13.23	110	65	-70	4.0
1012	39.176	24.239	13.87	320	80	10	4.3
1029	38.877	24.428	13.70	75	75	-150	5.3
1029	38.874	24.367	33.30	85	85	-140	4.2

3 Discussion - conclusions

The primary cause of the deformation in the investigated region is the motion of the Arabian plate in a NNW direction which causes the westward escape of Turkey (Anatolian plate) relative to Eurasia, towards the Aegean (e.g. Taymaz et al. [3]).

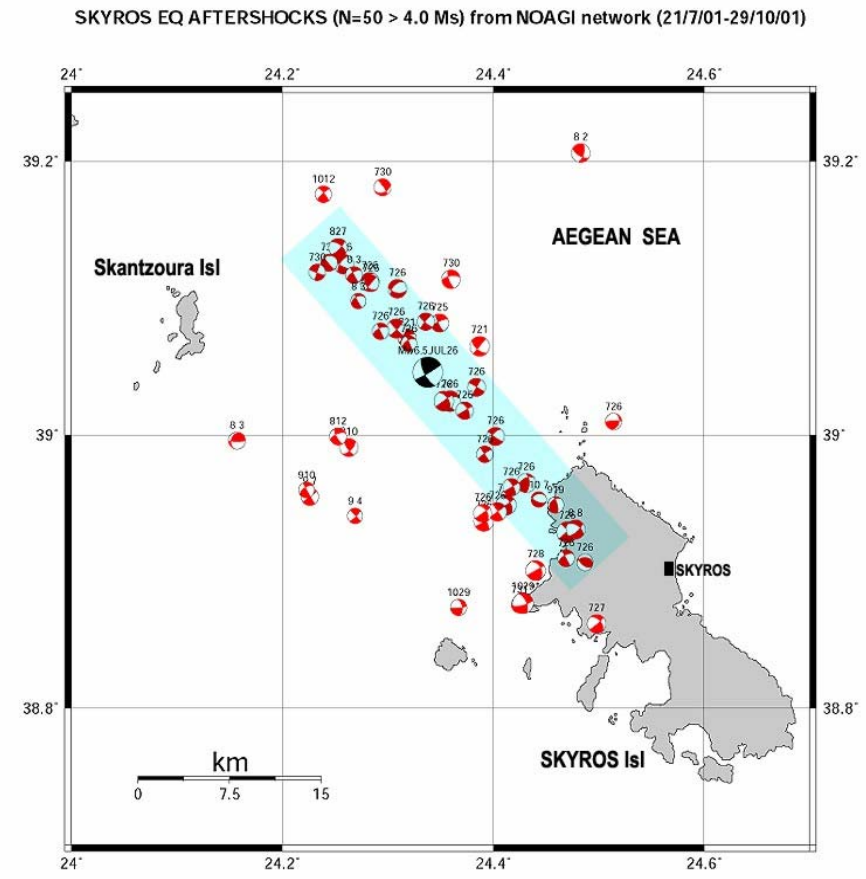

Figure 3: Map of focal plane solutions of major aftershocks of the Skyros 26 July, 2001 earthquake. Black denotes compression quadrants. Large, black beachball indicates solution for the main event. Shaded rectangle indicates extent of rupture zone and possible location of the seismic fault.

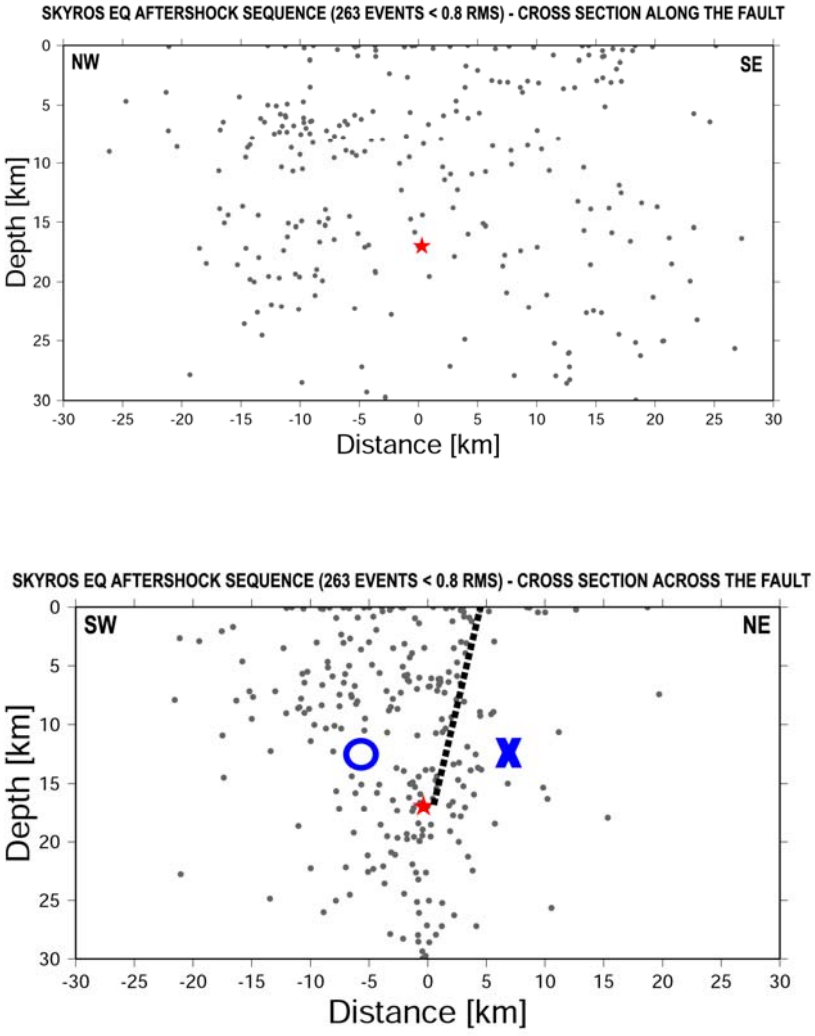

Figure 4: Cross sections of the hypocenters of the aftershock sequence. Top: along the fault, Bottom (across the fault). Star indicates the mainshock hypocenter. Dashed line indicates geometry of the seismic fault. X indicates motion away from the observer.

The North East Anatolian strike-slip Fault accommodates this escape (Sengor et al. [13]). In turn, the counter-clockwise rotation of Anatolia causes an extensional stress field in the Aegean area (Pavlides and Tranos [14]). In its western termination, the NAF splits into two main branches. The northern branch is predominant in the region of the north Aegean Sea. The southern branch is less clear in the sea bottom morphology (Figure 1). It crosses north-western Asia Minor, and then it turns south-west and reaches the Skyros Basin, where the epicentral area of the Skyros earthquake (26 July 2001) is located. However, the extension of the NAF to the west (Greek mainland) is not well defined. The geological data suggest that this area is deformed primarily by normal faulting (e.g. Roberts and Ganas [15]). It is supposed that its continuation ends at the Cephallonia Transform Fault (CFT), which is considered as a triple junction of the Aegean, Eurasian and Adriatic plates (King et al. [16]).

On the contrary, our fault-plane solutions of the Skyros main shock show strike slip faulting striking NW-SE with a small, thrust component (see also Melis et al. [6], Benetatos et al. [8]). These results document the existence of a major, left-lateral strike-slip fault in the area between Skyros Island and the Sporades basin (Figure 2). This fault appears to accommodate deformation between central Greece (to the west) and Skyros basin (to the east). In addition, it should be mentioned that the fault-plane solution of the 4 March 1967 event (the largest in the vicinity of the epicentral region) indicates normal faulting (Delibasis and Drakopoulos [9]), striking NW-SE, as well.

This strong earthquake ends a long period of seismic quiescence in this region, since the previous strong event, of Ms=6.8, took place on 4 March 1967 at a distance of about 30 km from the epicenter of 26 July 2001 earthquake. Moreover, the strike of the seismic fault (NW-SE) is not optimally oriented to the general trend of the North Anatolian Fault. In this point, the critical question to be answered is whether the Skyros earthquake was an expected or an unexpected event. The progressive failure of NAF during the second half of the twentieth century has triggered strong earthquakes in the Aegean Sea, as supported by several investigators (Stein et al. [17], Nalbant et al. [18]). Therefore, from this point of view this event was an expected one. But its focal mechanism suggests that the activated rupture zone may define the western end of the NAF inside the Aegean Sea. And from this point of view the Skyros earthquake was an unexpected event.

References

[1] Papadopoulos, G.A., Ganas, A. & Plessa, A., The Skyros earthquake (Mw 6.5) of 26 July 2001 and precursory seismicity patterns in the North Aegean Sea. *BSSA*, **92(3)**, pp. 1141–1145, 2002.

[2] Papazachos, B.C., Kiratzi, A. & Papadimitriou, E., Regional focal mechanisms for earthquakes in the Aegean Sea. *PAGEOPH*, **136(4)**, pp. 405– 420, 1991.

[3] Taymaz, T., Jackson, J. & McKenzie, D., Active tectonics of the north and central Aegean Sea. *Geophys. J. Int.*, **106**, pp. 433– 490, 1991.

[4] Kiratzi, A. & Papazachos, C.B. Active crustal from the Azores triple junction to the Middle East. *J. Geodynamics*, **19(1)**, pp. 65–78, 1995.
[5] Papazachos, B.C., Karakaisis, G.F., Papazachos, C.B., & Scordilis, E.M. Earthquake triggering in the North and East Aegean plate boundaries due to the Anatolia westward motion. *Geophys. Res. Lett.*, **27**, pp. 3957– 3960, 2000.
[6] Melis, N. S., Stavrakakis, G.N. & Zahradnik, J. Focal properties of the Mw=6.5 Skyros, Aegean Sea, earthquake. *ORFEUS Newsletter*, **3(2)**, 2002.
[7] Zahradnik, J., Jansky. & Papatsimpa, N. Focal mechanisms of weak earthquakes from amplitudes spectra and polarities. *PAGEOPH*, **158**, pp. 647–655, 2001.
[8] Benetatos, C., Roumelioti, Z., Kiratzi, A. & Melis, N. Source parameters of the M 6.5 Skyros island (North Aegean Sea) earthquake of 26 July, 2001. *Annali di Geofisica*, **45(3/4),** pp. 513-526, 2002.
[9] Delibasis. N. & Drakopoulos, J. Focal mechanism of earthquakes in the north Aegean Sea, 1965 – 1968 and related problems. *Geophys. Prospecting*, **N10**, pp. 149–167, 1974.
[10] Chouliaras, G. & Stavrakakis, G. N. Current seismic quiescence in Greece: Implications for seismic hazard. *Journal of Seismology*, **5**, pp. 595-608, 2001.
[11] Drakatos, G. & Latoussakis, J. Some features of Aftershock Patterns in Greece. *Geophys. J. Int.*, **126**, pp. 123–134, 1996.
[12] Tsokas, G. N., and Hansen, R. O., 1997. Study of the crustal thickness and the subducting lithosphere in Greece from gravity data. *Journal of Geophysical Research*, **102 (B9),** pp. 20585-20597.
[13] Sengor, A., Gorur, N., & Saroglou, F. Strike-slip faulting and related basin formation in zones of tectonic escapes:Turkey as a case study, eds. Biddle, K.T. & Christ-Blick, N., *Strike slip formation, basin formation and sedimentation. Soc. Economic Paleontologist and mineralogists.* Special Publ., **37**, pp. 227–265, 1985.
[14] Pavlides, S.B. & Tranos, M.D. Structural characteristics of two strong earthquakes in the North Aegean: Ierissos (1932) and Agios Efstratios (1968). *Journal of Structural Geology*, **13(2),** pp. 205-214.
[15] Roberts, G. P. & Ganas, A. Fault-slip directions in central and southern Greece measured from striated and corrugated fault planes: comparison with focal mechanism and geodetic data. *Journal of Geophysical Research*, **105(B10)**, pp. 23443-23462, 2000.
[16] King, G., Sturdy, D. & Whitney, J. Landscape geometry and active tectonics of northwestern Greece. *Geol. Soc. Am. Bull.*, **105**, pp. 137–161, 1993.
[17] Stein, R.S., Barka, A., & Dieterich, J.H. Progressive failure of the North Anatolian fault since 1939 by earthquake stress triggering. *Geophys. J. Int.*, **128**, pp. 594–604, 1997.
[18] Nalbant, S., Hubert, A., & King, C.P. Stress coupling between earthquakes in northwest Turkey and the north Aegean Sea. *J. Geophys. Res.*, **103(B10)**, pp. 24469–24486, 1998.

CHAPTER 7

Surficial expression of seismic faults and urban planning

S. G. Lozios , E. L. Lekkas & L. C. Chatzistavrou
Faculty of Geology, University of Athens, Greece

Abstract

In the most developed countries with high seismic risk, the existing seismic design codes include specific legal regulations for building near active faults. These regulations in most cases refer to a zone of a specific width along the fault trace. Within this area, construction is either forbidden or controlled by specific requirements. Such a way of prevention and control of seismic risk presupposes a linear damage distribution along the seismic fault. The aim of this study is to define the damage distribution caused by the most catastrophic earthquakes during the last 20 years in Greece, in comparison to the geotectonic setting of the affected area and the local geological conditions. The neotectonic and seismotectonic regime of these earthquakes (magnitude, depth, focal mechanism, etc.) has been very different and thus the expression of the seismic fault in the surface differs in each case. There is therefore, a discussion as to whether or not the existing legal regulations for building near active faults provide substantial protection or not.

1 Introduction

It is well known that Greece faces a high seismic risk, and many catastrophic events have taken place during the last 20 years, producing severe damage on large scale. The increasing losses are due to intensive urbanism and the development of economic, industrial and administrative activities near urban areas. The Greek state is extremely interested in managing this problem and taking decisions according to the increasing need. An example is that seismic design codes and the legal framework are becoming more stringent, following the increasing demand for protection. In trying to manage the seismic risk more efficiently, specific patterns for building near active faults have been implemented.

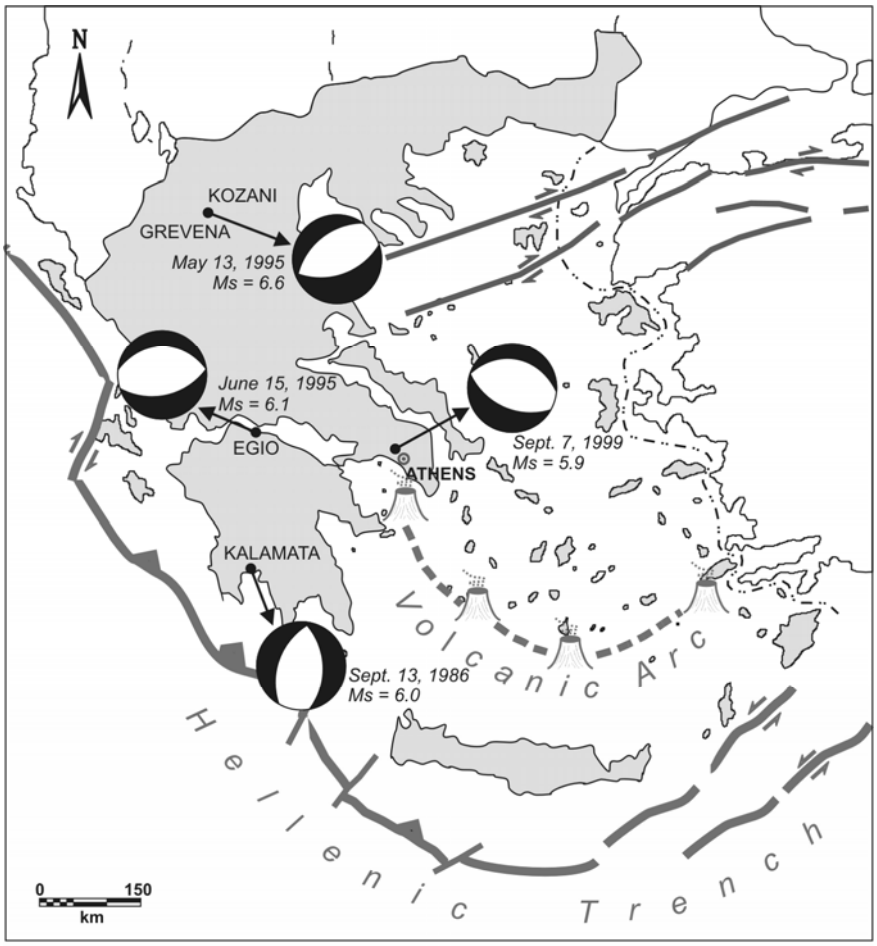

Figure 1: Geotectonic position of the four catastrophic earthquakes which have occurred during the last 20 years in Greece.

More particularly, in the zone along side an active fault, building activity is forbidden or is controlled by specific requirements. As has been seen from detailed neotectonic studies and mapping at 1:100 000 scale, a great number of active faults in the Greek region are found in specific areas or zones. Relative to the present active Hellenic Arc, these faults are found in several geotectonic regimes, resulting in many differences in the character and the consequences of earthquakes.

This work focuses on four catastrophic earthquakes which have occurred in Greece over the past 20 years. More particularly, the damage distribution is analyzed and correlated relative to the seismotectonic setting of each earthquake but

also to the local geological and neotectonic conditions. The four catastrophic events are the following (Figure 1):

1. The earthquake at Kalamata, in the broader area of the Messinian Gulf, which represents a NNW–SSE neotectonic structure, parallel to the present Hellenic arc.
2. The earthquake at Kozani–Grevena within the mainland, in a region considered more or less as inactive, far from the present active arc.
3. The earthquake at Egio, which occurred in the southern active margin of the central Corinthian Gulf, which represents an E–W neotectonic basin perpendicular to the present hellenic arc.
4. The earthquake at Parnitha (Athens), in the easternmost part of Greece and behind the present volcanic arc.

For each of these earthquakes the characteristics and the parameters of the seismic event have been analyzed and correlated with the neotectonic structure of the region, the expression of the seismic fault at the surface, the presence and the distribution of seismic fractures and surface ruptures and the secondary catastrophic phenomena, as well as the distribution and the cause of damage.

2 The Kalamata earthquake (13 September, 1986, M_S= 6.0)

On 13 September 1986 at 19:24:33.8 local time, a destructive shallow (depth 5 km) seismic event struck the wider area of the city of Kalamata (South Peloponnesus, Greece) and resulted in 20 casualties. The epicenter of the main earthquake was located at 37°10΄N, 22°19΄E, 10 km ENE of the city, and its magnitude was M_S= 6.0R (National Observatory of Athens). Two days later, at 13:41:30.5 local time, a second shock of M_L= 4.8R magnitude occurred closer to the city at the same depth. Its epicenter laid at 37°08΄N, 22°07΄E (National Observatory of Athens). In the same area, the epicenters of the aftershocks plotted in a NNE–SSW direction.

The main shock focal mechanism, strike 201° (+10º, -20º), dip 45º±5º, rake 283º (+10º, -25º), show an E–W normal faulting (Figure 1). The greater focal area coincides with the active fault zone of the eastern margin of the Messinian Gulf which represents a NNE–SSW marine neotectonic basin (Mariolakos et al. [2]).

The surficial expression of the seismic fault (Lyon-Caen et al. [1]) probably coincides with a larger NNE–SSW zone of seismic ruptures which appears east of Kalamata near the margin with the tectonic horst of the mountain of Kalathio (Figure 2). Besides this zone, numerous N–S, NE–SW, E–W and NW–SE seismic ruptures were observed in the affected area, in most cases in an en echelon arrangement (Mariolakos et al. [2]). These seismic ruptures had a vertical offset of several mm up to 25-30 cm, while they were often accompanied by an horizontal component, showing a sinistral or dextral displacement.

In addition to the ruptures mentioned above, numerous faults were observed in the wider area whose surfaces exhibited a minor reactivation with a normal or

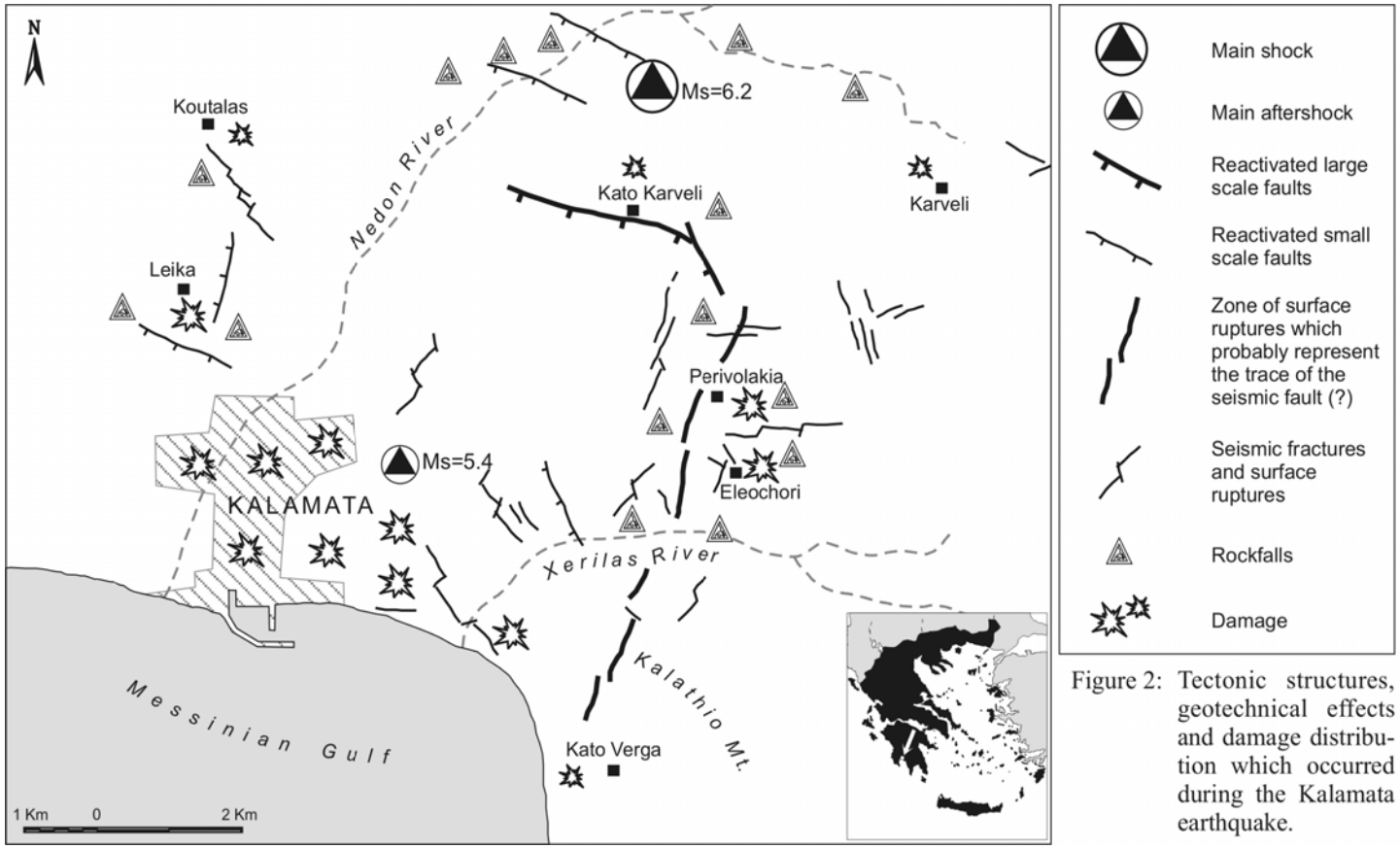

Figure 2: Tectonic structures, geotechnical effects and damage distribution which occurred during the Kalamata earthquake.

oblique slip (sinistral or dextral) displacement of 20-30 cm. It is important to notice that these faults also had various directions, either N–S or approximately NNE–SSW and E–W. These faults represent either large scale fault zones, longer that 5-10 km, or smaller faults some tens of meters in length.

All the above observations indicate that the surficial expression of the seismic fault occurred through a number of smaller faults with various directions, which coincided with the main neotectonic lines of the area.

Secondary destructive phenomena, mainly rockfalls and landslides, were located in many sites in the affected area and they appear to be directly connected with the reactivation of the faults and seismic fractures (Figure 2).

The earthquake caused much damage. Two apartment blocks collapsed and many other buildings, monuments, churches, infrastructures and lifelines were severely damaged. A preliminary examination of the damage distribution shows that it was limited to a specific neotectonic block with a NNE–SSW trend. It is important that to the NNE of the city of Kalamata the destruction spread to a distance greater than 20-25 km. On the other hand, west and east of the city was very limited since neither the town of Messini (10 km west of Kalamata) nor the community of Verga (5 km east of Kalamata) suffered serious damage (Gazetas [3], Mariolakos et al. [2]).

Locally, the type of constructions, as well as the soil formation (type and thickness of loose sediments) are of great importance for the damage distribution, although in the case of the Kalamata earthquakes there were important exceptions. Modern buildings founded on soil of good geotechnical properties collapsed, while other neighboring buildings (modern or not) suffered no or minor damage.

The detailed analysis of the tectonic structures which occurred during the earthquake, and the correlation with the damage, shows that the most important factor in their damage distribution was the existence of reactivated faults, seismic fractures and surface ruptures, since in most cases of damage such a structure cross-cut the damaged construction.

3 The Grevena–Kozani earthquake (13 May 1995, M_S=6.6)

On 13 May 1995 at 10:47:17.0 local time an earthquake of M_S=6.6R magnitude hit the Grevena–Kozani region (NW Greece, 130 km west of Thessaloniki) following two minor foreshocks. Its epicenter lay at 40°18΄N 21°67΄E and the estimated focal depth was 39Km (NOA), (Harvard: 40°08΄N, 21°68΄E, depth 16 km; University of Thessaloniki: 40°16΄N, 21°67΄E, depth 9 km). Almost 1,000 houses collapsed and 10,000 buildings were severely damaged, but no deaths were reported (Carydis et al. [4]).

According to the focal mechanisms (strike 240º, dip 31º, rake -98º) of Harvard University, the earthquake was attributed to the reactivation of a NE–SW fault with a NW dip. The broader affected area was, up the time of the earthquake, considered to be aseismic, given the fact that the only active neotectonic structure was the NE–SW Servia fault which is located SSE of the affected area (Figure 3). It is also noted that the pleistoseismal area as well as most of the

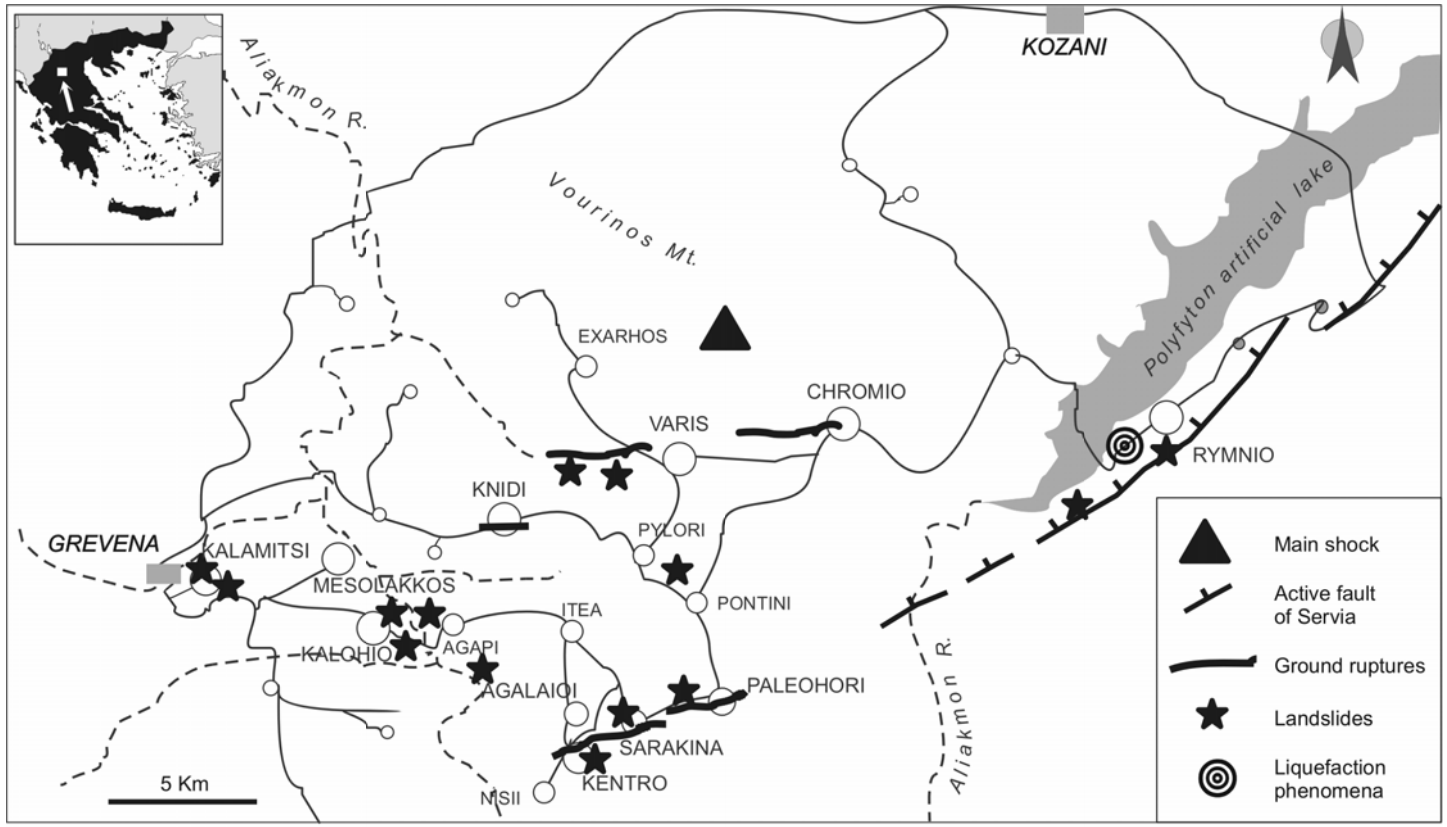

Figure 3: Tectonic structures, geotechnical effects and damage distribution which occurred during the Grevena - Kozani earthquake.

destruction are located on the SW prolongation of the Servia fault, which is buried under the molassic and neogene deposits without any important morphological or other anomaly as indication of its existence (Lekkas et al. [5]).
After the main shock there was no evidence of a surficial expression of the seismic fault (Carydis et al. [4], Lekkas et al. [5]), since the displacement reached a depth of 4-15 km (Drakatos et al. [6]). Only a few seismic fractures, in the NE–SW and E–W directions, were observed in the major area (Lekkas et al. [5]). Surface ruptures were also observed in several sites as a result of secondary catastrophic phenomena, such as landslides, subsidence and liquefaction phenomena. The latter ones were found mainly near the artificial lake of Polyfyton.

By examining the destruction locally, it was clear that beside the quality of the construction of the buildings, the topography and the secondary catastrophic phenomena, the foundation soil was also an important factor (Christaras et al. [7]). There were constructions founded on molassic formations that sustained no damage while newer ones on neogene formations collapsed (Lekkas et al. [8]).

4 The Egio earthquake (15 June 1995, M_S= 6.1)

On 15 June 1995, a strong shallow (depth 26 km) seismic event occurred in the sea between Egio (Northern Peloponnesus) and Erateini (Southern Sterea Hellas) at 03:15:51.0 local time. According to the calculations of the National Observatory of Athens, its magnitude was M_S=6.1R and its epicenter 38°37΄N, 21°15΄E. A strong M_S=5.7R aftershock was registered 15 minutes later; its focus lay at a depth of 5 km and the position of its epicenter was 38°33΄N, 21°93΄E (NOA).

Harvard proposes a fault plane solution (strike 287º, dip 32º, rake -78º) which indicates a normal E–W fault, dipping to the N. The submarine data show that the earthquake was probably produced by a submarine fault at the southern border of the Corinthian Gulf, a few km north of the town Egio. The Egio E–W fault, which also reactivated during this earthquake (Lekkas et al. [9]), represents a secondary branch fault (Figure 4).

Fractures caused by this seismic event were observed mainly on the north (E–W strike) but also on the western (WNW–ESE strike) flanks of the town, up to Rododafni at the base of a 100 m high, E–W trending escarpment, whose height decreases eastwards (Lekkas et al. [10]). To the north of the scarp there is a flat area with a mean altitude of 30 m, while to the south it meets hilly terrain with altitudes of more than 120 m. The scarp must have been created by the Egio fault; its hanging wall consists of loose alluvial and fluvial deposits and its footwall comprises Late Pleistocene – Holocene consolidated conglomerates.

Seismic fractures occur along the foot of the scarp and display a small vertical offset of 1-2 cm (north side downthrown). They are visible at the western end of the fault, from the western outskirts of Egio up to Rododafni (Lekkas et al. [11]). To the east of Egio such fractures are hard to locate, mostly because of the densely built area and the fact that their occurrence can be deduced only through the damage distribution. It is characteristic that these fractures cut and offset alluvial deposits, river terraces recent fluvial deposits, Late Pleistocene conglomerates (at Rododafni) and artificial landfill as well as small-scale constructions

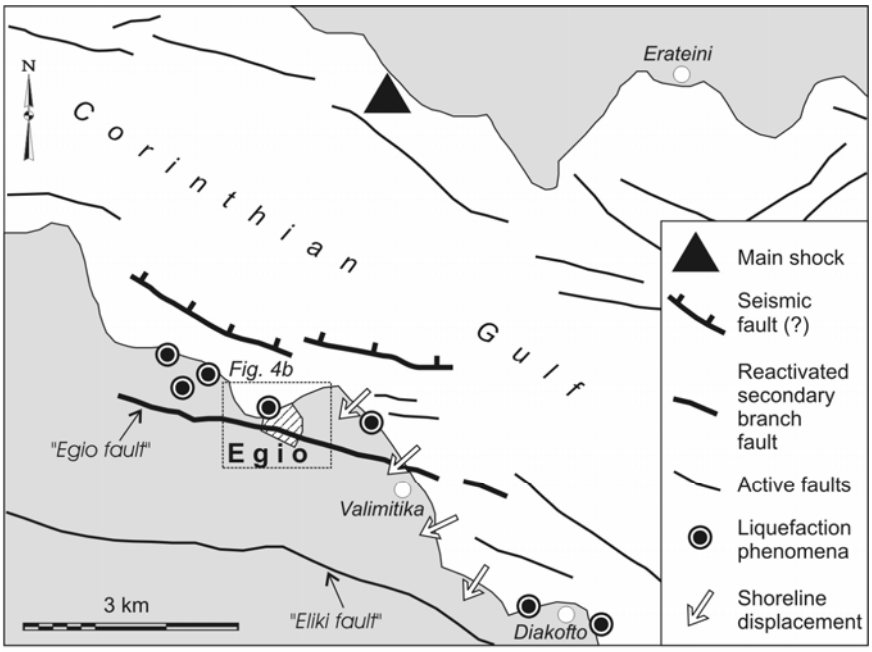

Figure 4a

Figure 4b

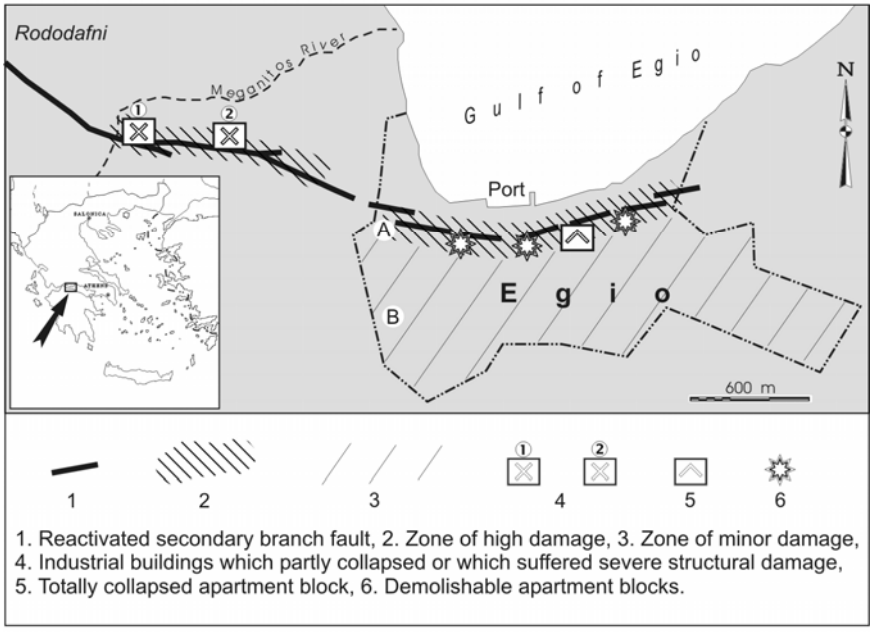

1. Reactivated secondary branch fault, 2. Zone of high damage, 3. Zone of minor damage,
4. Industrial buildings which partly collapsed or which suffered severe structural damage,
5. Totally collapsed apartment block, 6. Demolishable apartment blocks.

Figure 4: Tectonic structures, geotechnical effects and damage distribution that occurred during the Egio earthquake.

(property walls, gutters, pavements, etc.). Liquefaction phenomena and coastline changes were also reported (Lekkas et al. [10]).

In total, 2,000 buildings collapsed or were damaged beyond repair, 2,801 were rendered uninhabitable and about 10,000 more suffered minor damage. In an apartment block in the city of Egio and a hotel at Valimitika 26 people lost their lives (Lekkas et al. [11]). The total cost of the earthquake amounted to $ 600 million (Carydis et al. [12]).

Examination of the damage distribution clearly shows a density of destruction near the center of the town of Egio, at the broader area of the northern coast of Peloponnesus (Eleonas, Rodia, Valimitika, Rododafni, Avytos and Selianitika). In the southern Sterea Hellas (Erateini), where the earthquake was also felt, the damage was smaller. There was both extensive damage (building collapse or severe structural failure) and lighter damage. Several building types were damaged, both old and modern constructions (Lekkas et al. [11], Lekkas et al. [13]).

Inside the town of Egio the intense damage forms a narrow E–W to WNW–ESE zone which coincides with the prolongation of the fractured zone outside the town. More specifically, the zone is parallel to the coast (northern part of the city) and lies at the footwall of the Egio fault. The morphology of the zone is characterized by the prominent escarpment of the tectonically-controlled terrace on which Egio was built. There was an increasing trend in the intensity of damage at locations of steep topographic gradient. Most of the reinforced concrete frame structures in this area sustained severe damage (collapsed apartment block), while the foundation formations (consolidated conglomerates) are more or less uniform and of good geotechnical properties. In the case of the collapsed apartment block, the most important factor was the presence of seismic fractures and a secondary was the morphological gradient (Carydis et al. [12]).

In the western part of the town (in the vicinity of Hellenic Weapons Industry) the occurrence of seismic fractures and liquefaction phenomena was responsible for severe damage to high-standard buildings.

In the central and southern part of the town the building type was crucial, and in the port area strong seismic shaking created subsidence phenomena. In the southern Sterea Hellas, damage was due mainly to seismic shaking as well as liquefaction phenomena and in some cases the occurrence of ground fissures.

5 The Parnitha (Athens) earthquake (9 September 1999, M_S = 5.9)

On 7 September 1999, at 14:56:50.5 local time, a M_S=5.9R shallow (depth 29 km) earthquake hit the north-western part of the basin of Athens, causing about 140 deaths and a large number of injuries, as well as extensive damage to structures. Its epicenter lay at 38º15´N, 23º60´E (NOA).

The focal mechanism computed by Harvard (strike 114º, dip 45º, rake -73º) gives a normal WNW–ESE fault with a S dip. No trace of the seismic fault was located at the surface (Lekkas et al. [14], Papanikolaou et al. [15]), which is why it is referred to as a ‘blind’ fault that reaches up to 4-12 km depth (Papazachos et

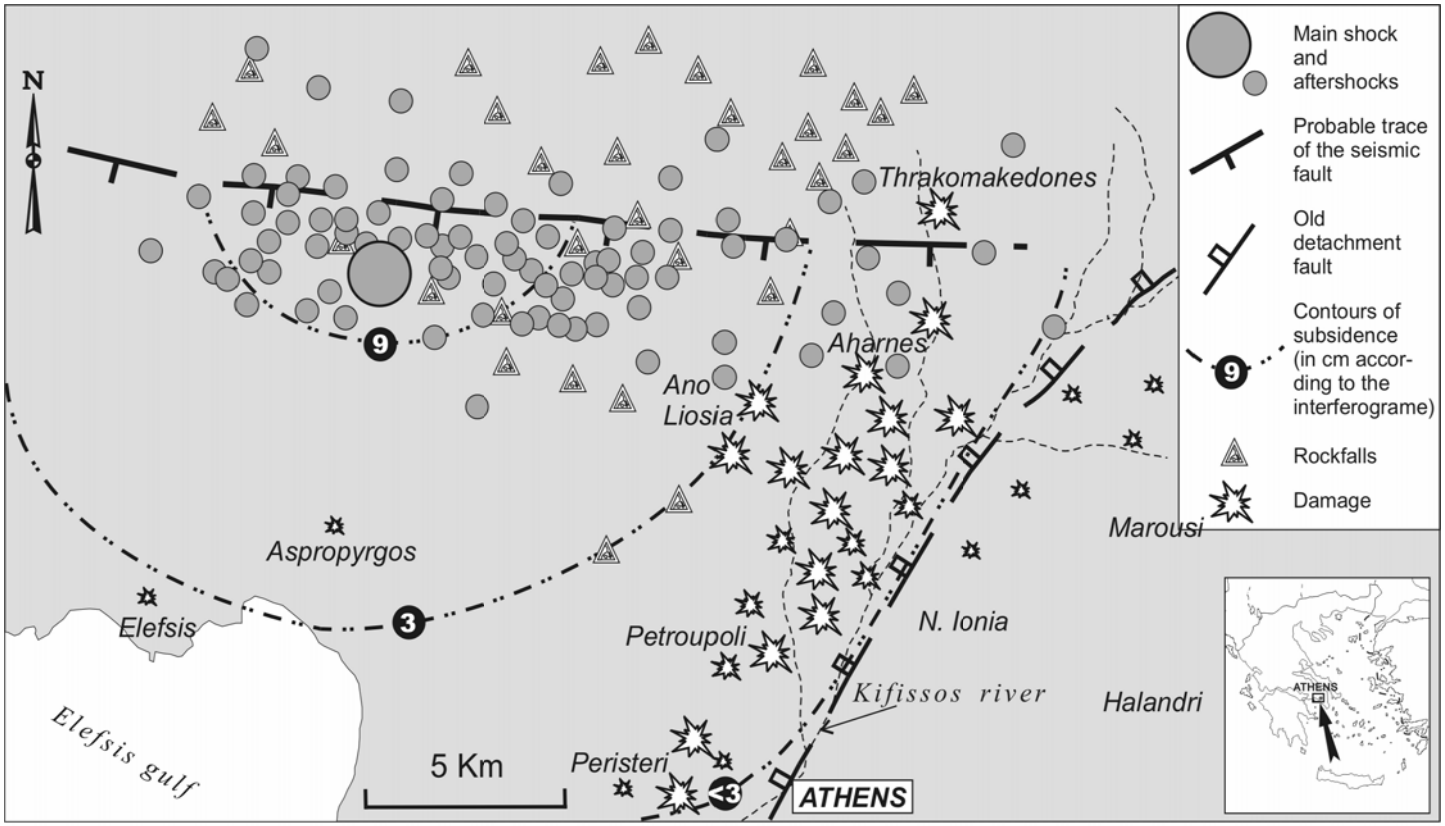

Figure 5: Tectonic structures, geotechnical effects and damage distribution that occurred during the Parnitha (Athens) earthquake.

al. [16]), although the Parnitha fault is visible in aerial photographs and satellite images (Papadimitriou et al. [17]).

Based on (i) the location of the epicenter, the aftershock sequence and the focal mechanism solution (Stavrakakis [18]), (ii) the interferogram compiled after the earthquake, and (iii) the distribution of the secondary destructive phenomena, it is concluded that the seismic fault had a mean WNW–ESE strike and a SSW dip and was located under the mass of Mt Parnitha (Figure 5).

This fault lies at the prolongation of fault zones of the same strike, such as the active faults of the Eastern Corinthian Gulf (80 km West of Athens), which are responsible for the destructive earthquakes which have taken place since the historical times (Ancient Corinthos, Corinthos, Alkyonides, etc.) (Lekkas et al. [14], Papanikolaou et al. [15]).

Secondary destructive phenomena, such as rockfalls, landslides, settlement and soil fractures, were observed. The damage caused by the earthquake is all located east of the epicenter and the seismic fault, in the western part of the Athens basin, which is a graben filled with post-alpine formations.

In spite of the WNW–ESE strike of the seismic fault, the damage distribution follows a NNE–SSW trend, coinciding with that of the basin of Athens, and the strike of a large detachment fault, buried under the post-alpine sediments (Papanikolaou et al. [15]). This fault brings metamorphic alpine rocks in contact with non-metamorphic.

Correlation between the damage distribution and the geological and structural data from the major area showed that the most serious damage took place on loose foundation formations, which were either the unconsolidated members of the talus cones, or the alluvial deposits and river terraces (Lekkas et al. [19], Marinos et al. [20]).

However, this was not the only factor that affected the damage distribution, since the heaviest damage was located: (i) along the trace of the tectonic contact between the alpine units of the area, (ii) in the areas with higher fault density, usually close to the basin margins, but also locally within the basin. These faults were not reactivated in the September earthquake, but “channeled” the seismic energy into specific zones (Lekkas et al. [14], Papanikolaou et al. [15]).

Moreover, hanging wall effects, effects of sedimentary basins, basin edge effects and focusing effects (Somerville [21]) probably played a significant role the damage distribution at the locations where the fault geometry and the basin structure acted as reflectors, magnifying the effects of shaking and thus maximizing the strong ground motion values.

6 Discussion – conclusions

As has been mentioned before, it is quite clear that the problem of damage distribution after an earthquake is related to several factors that define whether the damage follows a linear distribution along the activated fault, a linear distribution but in a different direction relative to the activated fault or is scattered within a large area limited by several geological or tectonic structures such as the following:

- The geotectonic setting of the area in relation to the present active Hellenic Arc.
- The neotectonic macrostructure of the area, focusing in the kinematical and dynamic characteristics of the fault blocks.
- The seismotectonic setting and the parameters of the earthquake, such as its magnitude, depth, focal mechanism and aftershock distribution.
- The surface expression of the activated fault with a specific trace and displacement.
- The reactivation of several faults and fault zones.
- The expression of the activated fault at the surface through a number of smaller faults with less important displacement, and a direction constant or not.
- The distribution of seismic fractures and surface ruptures in a direction parallel or not to the seismic fault.
- The combination of two or more of the above-mentioned factors.
- The presence of large scale tectonic structures, active or not, acting as barriers to the damage distribution.
- The regional geology and the tectonic structure, which can control the propagation and the amplification of the seismic energy.

Building problems in regions with high seismic risk are therefore complex, and the simple limitation of a zone along an active fault with implementation of seismic design codes is not the most suitable solution, given that in several cases the seismotectonic patterns in several cases could not give a linear damage distribution along the reactivated fault trace.

Detailed studies on seismic hazard in various affected areas in Greece, as well as research studies on earthquake effects, are the necessary tools to define specific patterns for seismic building codes that could provide substantial protection against seismic risk. These tools could definitely contribute to better earthquake protection planning.

References

[1] Lyon-Caen, H., Armijo, R., Drakopoulos, J., Baskoutas, J., Delibassis, N., Gaulon, R., Kouskouna, V., Latoussakis, J., Makropoulos, K., Papadimitriou, P., Papanastassiou, D. & Pedotti, G. The Kalamata (South Peloponnesus) earthquake: detailed Study of a Normal Fault, Evidences for East-West Extension in the Hellenic Arc. *Journal of Geophysical Research*, **93(B12)**, pp. 14,967-15,000, 1988.

[2] Mariolakos, I., Fountoulis, I., Logos, E. & Lozios, S. Surface faulting caused by the Kalamata (Greece) earthquakes (13-9-1986). *Tectonophysics*, **163**, pp. 197-203, Amsterdam 1989.

[3] Gazetas, G. Experience and questions from the geotechnical investigation of Kalamata. *Bulletin of the Public Works Research Center*, **4**, pp. 241-243, Athens 1987.

[4] Carydis, P., Holevas, K., Lekkas, E. & Papadopoulos, T. The Grevena (Central–North) Greece Earthquake Series of May 13, 1995. *EERI Newsletter*, Special Earthquake Report, June 1995, **29(6)**, pp.1-4, California 1995.

[5] Lekkas, E., Fountoulis, I., Lozios, S., Kranis, Ch. & Adamopoulou, E. Neotectonic implications of Grevena–Kozani Earthquake (May 13, 1995, W. Macedonia, Greece). *International meeting on results of the May 13, 1995 earthquake of West Macedonia: One year after*, INQUA, pp. 76-80, Kozani 1996.

[6] Drakatos, G., Papanastassiou, D., Voulgaris, N. & Stavrakakis, G. Observations on the 3-D crustal velocity structure in the Kozani–Grevena (NW Greece) area. *J. Geodynamics*, **26(2-4)**, pp. 341-351, 1998.

[7] Christaras, B., Dimitriou, An. & Lemoni, Hel. Soil quality as a factor of the distribution of damages at the meizoseismal area of the Kozani–Grevena 1995 earthquake, in Greece (Ms=6,6). *J. Geodynamics*, **26(2-4)**, pp. 393-411, 1998.

[8] Lekkas, E., Kranis, Ch., Fountoulis, I., Lozios, S. & Adamopoulou, E. Spatial Distribution of damage caused by the Grevena–Kozani earthquake (W. Macedonia) of May 13, 1995. *International meeting on results of the May 13, 1995 earthquake of West Macedonia: One year after*, INQUA, pp. 89-92, Kozani 1996.

[9] Lekkas, E.L., Lozios, S.G., Skourtsos, E.N. & Kranis, H.D. Egio earthquake (15 June 1995): An episode in the neotectonic evolution of Corinthiakos Gulf. *J. Geodynamics*, **26(2-4)**, pp. 487-499, 1998.

[10] Lekkas, E., Lozios, S., Skourtsos, E.N. & Kranis, Ch. Liquefaction, ground fissures and coastline change during the Egio earthquake (15 June 1995; Central–Western Greece). *Terra Nova*, Blackwell Science Ltd.: Oxford, **8(6)**, pp. 648-654, 1996.

[11] Lekkas, E., Lozios, S., Kranis, H. & Skourtsos, E., Linear damage distribution and seismic fractures at the Egio earthquake (15 June 1995, Greece). *Advances in Earthquake Engineering, Earthquake Resistant Engineering Structures*, Computational Mechanics Publications: Southampton, **2**, pp. 37-46, 1997.

[12] Carydis, P., Holevas, K., Lekkas, E. & Papadopoulos, T., The Egion, Greece, Earthquake of June 15, 1995. *EERI Newsletter*, Special Earthquake Report, July 1995, **29(7)**, pp.1-3, California 1995.

[13] Lekkas, E.L. The Role of Earthquake-Related Effects in Urban Complexes. *Natural Hazards*, **25**, pp. 23-35, 2002.

[14] Lekkas, E.L., Lozios, S.G. & Danamos, G.D. Geotectonic regime and damage distribution at the city of Ano Liosia (Athens, Greece) during the earthquake of September 7, 1999. *XXVII General Assembly of the European Seismological Commission (ESC)*, pp. 155-159, Lisbon 2000.

[15] Papanikolaou, D.I., Lekkas, E., Sideris, Ch., Fountoulis, I., Danamos, G., Kranis, Ch., & Lozios, S. at the contribution of Antoniou, I., Vassilakis, E., Vasilopoulou, S., Nomikou, P., Papanikolaou, I., Skourtsos, E. & Soukis, K. Geology and tectonics of Western Attica in relation to the 7-9-

1999 earthquake. *Newsletter of the European Centre on Prevention and Forecasting of Earthquakes*, **3**, pp. 30-34, December 1999.

[16] Papazachos, C. B., Karakostas, B. G., Karakaisis, G. F. & Papaioannou Ch. A. The Athens 1999 mainshock (Mw=5.9) and the evolution of its aftershock sequence. *Proceedings of the 9th International Congress*, Athens, September 2001. Bulletin of the Geological Society of Greece, **XXXIV/4**, pp. 1581-1586, 2001.

[17] Papadimitriou, P., Kaviris, G., Voulgaris, N., Kassaras, I., Delibassis, N. & Makropoulos, K. The September 7, 1999 Athens earthquake sequence recorded by the cornet network: preliminary results of source parameters determination of the mainshock. *Annales Géologiques Des Pays Helléniques*, **XXXVIII(B)**, pp. 29-39, 2000.

[18] Stavrakakis, G. Some seismological aspects of the Athens earthquake of Sept. 7, 1999. *Newsletter of the European Centre on Prevention and Forecasting of Earthquakes*, **3**, pp. 26-29, December 1999.

[19] Lekkas, E. The Athens earthquake (7 September 1999): Intensity distribution and controlling factors. *Engineering Geology*, **59**, pp. 297-311, 2001.

[20] Marinos, P., Boukovalas, G., Tsiambaos, G., Protonotarios, G., Sabatakakis, N. and collaborators Damage distribution in the western part of Athens after the 7-9-99 earthquake. *Newsletter of the European Centre on Prevention and Forecasting of Earthquakes*, December 1999, 3, pp. 37-39, 2000.

[21] Somerville, P. Seismic Hazard Evaluation. *12th World Congr. On Earth. Eng.*, Aukland, New Zealand, Pres. No. 2833, 2000.

CHAPTER 8

Active faults and seismic hazard assessment at municipality level – the case of Tenea (Corinthia, Greece)

H.D. Kranis, E.L. Lekkas, S.G. Lozios and A.S. Bakopoulou
Faculty of Geology,University of Athens, Greece.

Abstract

We present the results of the multidisciplinary study on earthquake planning and protection for the municipality of Tenea, Corinthia. The paper focuses on the population centres and describes the geological effects in the case of activation of the fault structures that cross the area. The locations most prone to the occurrence of ground fracturing, liquefaction, rockfalls, landslides and local intensity amplification, caused by the basin edge effect, are presented. Moreover, we examine the cases where the road or railway connections may be disrupted because of fault reactivation and suggest the locations most susceptible to this.

1 Introduction

The topic of earthquake hazard assessment has been the focus of numerous studies applying deterministic and probabilistic methods (see Yeats et al. [1] for a comprehensive review).

In this paper we try to address the same issue using a quasi-deterministic technique, and to predict the problems that may arise from the occurrence of a medium or large earthquake within, or close to, the administrative boundaries of the municipality of Tenea, prefecture of Corinth, north-eastern Peloponnesus, Greece (Fig. 1). The administrative division (municipality) of Tenea has a total area of 162.4 km^2, lies between 37º30’43’’S, 37º30’53’’N, 22º30’44’’W and 22º30’55’’E and is the result of a recent public administration law merging the multitude of small townships into larger administrative divisions, for the sake of simpler and more effective administration. However, this new law entailed the reconsideration of local emergency planning, as local authorities have now to

face an increased variety of contingencies in the event of a destructive earthquake.

Another aspect that we have taken into consideration is the fact that Tenea is crossed by major lifelines: the main Tripolis-Korinthos-Athens motorway, the trunk line of the Peloponnesian railway network and the main powerlines that transport electricity from the power plants of the central Peloponnessus to Athens, Korinthos, Loutraki and other population centres (Fig. 1).

The central and northwestern parts of the area are rather flat-lying, save for the odd hill, while the relief becomes rougher at the northern and north-eastern part, with steeper slopes, cliffs and prominent mountain tops (highest peak: Profitis Ilias, alt. 701 m) The southern part is mountainous, with steep terrain and altitudes as high as 1,078 m (Psili Rahi).

The capital is Hiliomodi (population 1,750), built at the eastern extremity of the administrative division. Other population centres (towns, villages) are Agios Vassileios, Klenia, Spathovouni, Koutalas and Mapsos (Figs 2 & 3).

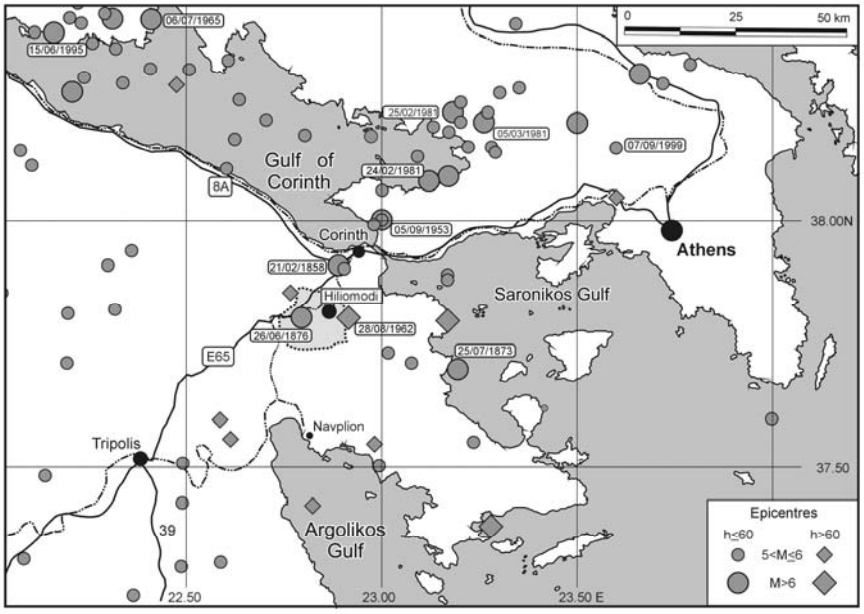

Figure 1: Map of the north-eastern Peloponnessus, with the epicentres of the medium and large earthquakes (Nat. Observatory of Athens, revised catalogue; Papazachos and Papazachou, [2]). The dates in boxes refer to the earthquakes discussed in the text. The shaded area corresponds to the municipality of Tenea. The major road (continuous line) and railroad (dash-and-dot line) networks are also shown.

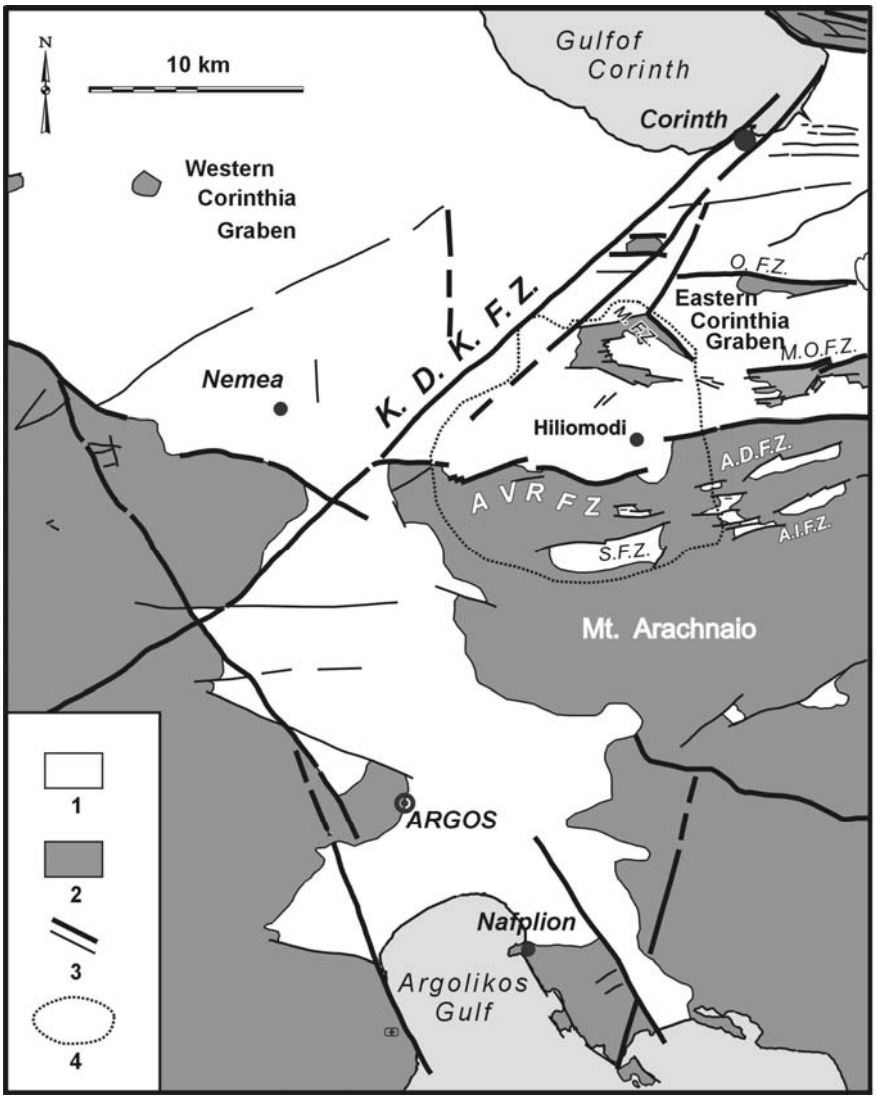

Figure 2: Tectonic sketch map of the broader study area, modified from Papanikolaou et al. [3]. 1: Neogene-quaternary sediments; 2: alpine rocks; 3: major (thick line) and secondary (thin line) faults; 4: administrative boundaries of Tenea. KDKFZ: Korinthos-Dervenakia-Kaparelli F.Z.; AVRFZ: Agios Vassileios-Ryton F.Z.; ADFZ: Agios Dimitrios F.Z.; SFZ: Stefanion F.Z.; AIFZ: Agios Ioannis F.Z.; MFZ: Mapsos F.Z.; OFZ: Oneia F.Z.; MOFZ: Mavri Ora F.Z.

The procedure we followed consisted of the well-established steps of field reconnaissance and mapping (geological and geotechnical), satellite image and aerial-photograph interpretation and examination and evaluation of local and regional seismicity patterns. All data were administered on a GIS platform (ArcGIS).

The examination of historically and instrumentally recorded seismicity, earthquake source modelling and the determination of response spectra are invaluable sources of information for the study of the behaviour of constructions. All these were seamlessly integrated with the field survey of active faults and the mapping of pre-existing landslides, liquefaction sites, and so forth.

In the following sections we shall first give an outline of the geological and the neotectonic conditions of the study area. Then we shall present the current local and regional seismicity pattern, as it is derived from instrumental recordings and historical references. We shall then examine the population centres, infrastructure and lifelines of Tenea, in respect to their seismic vulnerability. Finally, we shall discuss the results of this study and the implications for seismic hazard assessment.

2 Geology and tectonics

The geological formations that crop out in the area comprise both Neogene – Quaternary deposits (post-alpine formations) and Tertiary rocks (alpine formations). The latter outcrop mainly at the southern, mountainous part. In the northern part, the alpine substratum is usually exposed in neotectonic horsts and/or bedrock ridges (Fig. 2). The post-alpine ("synrift") deposits cover most of the northern part of the area and cover unconformably the alpine basement; their thickness is highly variable and ranges between a few tens of metres and (probably) more than 200 m. This variability is explained by the fact that the study area belongs within the Eastern Corinthia Graben (ECG, Fig. 2) (Papanikolaou et al. [3]), in which the synrift deposits have either covered a highly tectonized basement and/or have been faulted against alpine rocks. This situation is rather less obvious in the Western Graben, where the thickness of the synrift sediments is much higher and the alpine substratum is only sporadically exposed (Fig. 2).

Both the Eastern and Western Corinthia Grabens form the onshore prolongation of the present-day Gulf of Corinth, an active rift structure with very high deformation rates and seismicity (e.g. Davies et al. [4], Hatzfeld et al. [5], and references therein).

The study area hosts a range-bounding fault zone, the Agios Vassileios-Ryton F.Z. (Table 1; Figs 2 and 3) and numerous other second- and third-order faults. Besides a first-order transverse tectonic structure, the Korinthos-Dervenakia-Kaparelli F.Z. (KDKFZ) has been identified by Papanikolaou et al. [3] and it is held responsible for the geologic a tectonic differentiation between the Eastern and the Western Corinthia Graben. The fault characteristics are summarized in Table 1.

Table 1: Active fault and fault zone characteristics in the vicinity of Tenea and environs, modified from Papanikolaou et al. [3].

Fault name	Population centres	Order*	Length (km)	Strike	Kinematics†	Throw (m)	Potential (Ms) §
Korinthos-Dervenakia-Kaparelli F.Z.	Korinthos, Nemea, Spathovouni, Kleonai	1	48	N 045	Oblique-dip slip, left-lateral	> 150	6.4 R
Oneia Mts F.Z.	Solomos, Kenchraii, Xylokeriza	1	~ 9	E-W	Normal	> 150	5.5 R
Agios Vassileios-Ryto F.Z.	Agios Vassileios, Klenia, Hiliomodi	1	~ 24	NW-SE**	Normal	> 150	6.3 R
Mapsos F.Z.	Mapsos	1	3.5	NW-SE	Normal	>150	4.7 R
Mapsos horst faults	Mapsos	2	0.5-1	E-W	N/A	<100	N/A
Mavri Ora F.Z.	Athikia, Myrtea	1	~ 9	E-W**	Normal	> 150	5.5 R
Agios Dimitrios F.		2	~ 6	††	Normal	< 100	5.2 R
Stefanion F.	Stefanion, Agionorion	2	~ 7	N 080 E	Normal	< 100	5.3 R
Agios Ioannis F.	Agios Ioannis, Agionorion	2	~ 5	ENE-WSW	Normal	< 100	5.0 R

* 1: Main fault or marginal, 2: second order fault.

† Refers to the last reactivation. In a number of cases, the kinematic character of the zone has changed during its existence. Classification after Mariolakos and Papanikolaou [6].

§ After Papazachos [7] .

Comprises E-W and ENE-WSW en echelon segments.

** Mean strike; it consists of en echelon segments.

†† Four WSW-ENE en echelon segments linked through NNW-SSE linking faults.

3 Seismological data

The narrow area itself has not hosted many large earthquake epicentres; however, several seismic events have affected the existing infrastructure. The nearest seismogenic areas are the Gulf of Corinth and its easternmost extremity, the Alkyonides Gulf (Fig.1). The most notable earthquakes are shown in Table 2.

Table 2. The most destructive earthquakes that have affected Tenea in the past 150 years. Data from Papazachos and Papazachou [2] and the revised catalogue of the National Observatory of Athens.

Date	Longitude (E)	Latitude (N)	Magnitude (Ms)(*)	Notes
21 Feb 1858	22.90	37.90	6.5	Io=X at Corinth, 21 casualties
25 Jul 1873	23.20	37.7	6.0	Io=VII at Epidauros
26 Jun 1876	22.80	37.8	6.1	Imax= at Nemea
22 Apr 1928	23.00	37.90	6.3	Io=IX at Corinth
6 Jul 1962	37.80	22.90	6.6	Io=VIII+ at Ancient Corinth. Medium depth eq. (h=95 km)
24 Feb 1981	22.90	38.10	6.8	Io=IX at Perachora

(*) Estimated magnitude for the 19th century events.

The 21 February 1858 earthquake ravaged the city of Corinth and caused extensive damage to the surrounding population centres, including Hiliomodi. The maximum recorded intensity was Io=X at Corinth and this must be the most serious seismic event in the recent history of the study area. Fifteen years later (25 July 1873) a M=6.0 shock took place; its epicentre must have been approximately 30 km to the east of the administrative division of Tenea, which is included in the I=VI isoseismal of the shock. Another strong earthquake occurred in 1876 (26 June); this time, the epicentre lay within the area of the municipality, approximately 7-8 km west of Hiliomodi, at Nemea. Again, as in the 1858 event, damage was widespread. The maximum recorded intensity was Io=VIII at Nemea, located a few km west of Hiliomodi.

Unfortunately, for all the aforementioned events only a small amount of reliable data are available and especially when it comes to our knowledge of surficial faulting, geological site effects and so on, we have almost no information, save for vague second-hand reports, documented in the works of Schmidt [8], Papazachos & Papazachou [2] and Ambraseys [9].

In the twentieth century, three significant events occurred, for all of which the available data are plentiful and more accurate. The 22 April 1928 earthquake razed Corinth, killed more than 20 people and wreaked havoc in numerous towns

and villages, including most of the population centres within the administrative boundaries of Tenea. In 1953 (13 June), the epicentre of the earthquake lay along the south-eastern coast of the Gulf of Corinth and caused moderate damage. The most serious event of the last century was the Alkyonides earthquake (24 February 1981), which was followed by a series of destructive aftershocks, the most important of which was on 4 March 1981 (Ms= 6.4).

Bearing in mind all the above, we can have an estimate of the maximum intensities, the depth, focal mechanism and epicentral distance of the medium and large earthquakes which have affected the study area in the last 150 years. Smaller events (M<5.0) have not been considered in this study; we believe that only a M>5.0 (possibly M>5.5), shallow earthquake with an epicentral distance of no more than 30 km is capable of seriously disrupting the functions, lifelines and services and, most of all, pose a serious threat to human lives in the municipality of Tenea. The large shocks that occur on either of the margins of the Gulf of Corinth (e.g. the 1965 Erateini (Ms=6.5) and the 1995 Egion (M=6.5) earthquakes), with an epicentral distance of 80-90 km have left the area unharmed; the same goes for major events (M>7.0) that occur sporadically along the southwestern part of the Hellenic Arc.

4 Examination of population centres and infrastructure

4.1 Hiliomodi – Koutalas

The capital is located within the Eastern Corinthia Graben (ECG), close to the Agios Vassileios – Ryto Fault Zone (AVRFZ), which is an E-W range-bounding structure (Table 1; Figs 2 & 3). It should also be noted that the town lies within the ECG in which numerous active small faults have been mapped, bounding second- and third-order horsts and graben. The most prominent neotectonic feature is the Koutalas horst, bounded on the south by the namesake fault (Fig. 3), striking WNW-ESE and with a visible trace of 4 km. In the same area and NW of the town (Profitis Ilias), another NE-SW fault set has been mapped, consisting of overlapping faults of 1-2 km visible length. Hiliomodi is located within the hanging wall of these normal faults. The Koutalas fault presents all the signs of late Quaternary activity (fresh slickensides, loose debris, sharp morphologic discontinuity, etc.) and is considered active. The Profitis Ilias fault set seems to be less active, with the exception of one strand that interacts with the Koutalas Fault and is active. All these faults are prone to reactivation in the sense that they can accommodate differential movements of fault-bounded blocks in the event of a shallow, near-field earthquake originating in one of the seismogenic structures of the area.

Reactivation of the aforementioned faults can lead to a suite of geological site effects. Rockfalls and slides are highly probable, especially along the fault traces, due to high topographic gradient and intense pre-existing fracturing of the host rock. Liquefaction is also likely at the eastern and southern outskirts of the town, where the topography, lithology and the hydrogeological conditions (very

shallow aquifer) are favourable. Note that the railway line is founded on these loose, liquefaction-prone formations.

Another serious threat for Hiliomodi is posed by possible reactivation of the range-bounding AVRFZ, an active, 25-km long structure with an accumulated vertical throw of more than 150 m and seismic potential M=6.3 R (Table 2). The available data of historical seismicity suggest that the AVRFZ may have ruptured in the 1876 event (Table 2), judging from the presumed epicentre and distribution of macroseismic intensities. The effects from the reactivation of this fault will be analogous to those already mentioned before, though in this case their magnitude and extent are expected to be much greater. The road connections between Hiliomodi and the towns to the south may be seriously disrupted (especially the road leading to Klenia, Agionori and Stefani). Liquefaction is highly likely to occur in the soft alluvial sediments within and around the town and this will seriously affect the railway line. Fortunately enough, the town hall and the elementary and secondary school complex are founded on more competent formations and are not expected to suffer damage caused by liquefaction. However, the possibility for ground fracturing is very high, as the town lies just west of the tip of an active fault strand that belongs to the AVRFZ (Fig. 3).

4.2 Klenia – Agios Vassileios

These two villages are located at the foot of the faulted mounted front of Psili Rahi – Dafnias, which occupies the southern sector of the study area and belongs to the neotectonic horst of Mt. Arachnaio (Figs. 2 and 3). Both villages lie on the trace of the AVRFZ and this, coupled with the fact that the geological and topographic conditions are unfavourable, makes them more vulnerable.

More specifically, the topographic gradient at both Agios Vassileios and Klenia is rather high (25-55%) and this factor, combined with the lithology of the area, adds to the risk of rockfalls and landslides. The villages are built on the surface of highly heterogeneous talus cones, which, although they are covered by a well-indurated carapace, artificial and natural cuts have exposed extended lenses of loose sand and gravel, interlayerings of silt and finer sediment, as well as cavities of various sizes. This type of geological formation is prone to differential settlement because the lithological heterogeneity occurs rapidly both in the vertical and the horizontal sense. Also, if the AVRFZ is reactivated extensive ground fracturing is expected to occur; the fracture sets will most probably develop parallel or sub-parallel to the fault zone, i.e. along the E-W and ENE-WSW directions, although connecting fractures, striking approximately NNW-SSE will also be present. Ground fracturing will cause small-scale (up to some m.) depressions and culminations of the free surface, while open gashes are also likely to develop. All these may cause serious problems to the foundations of the buildings, especially the older ones, and the local road network.

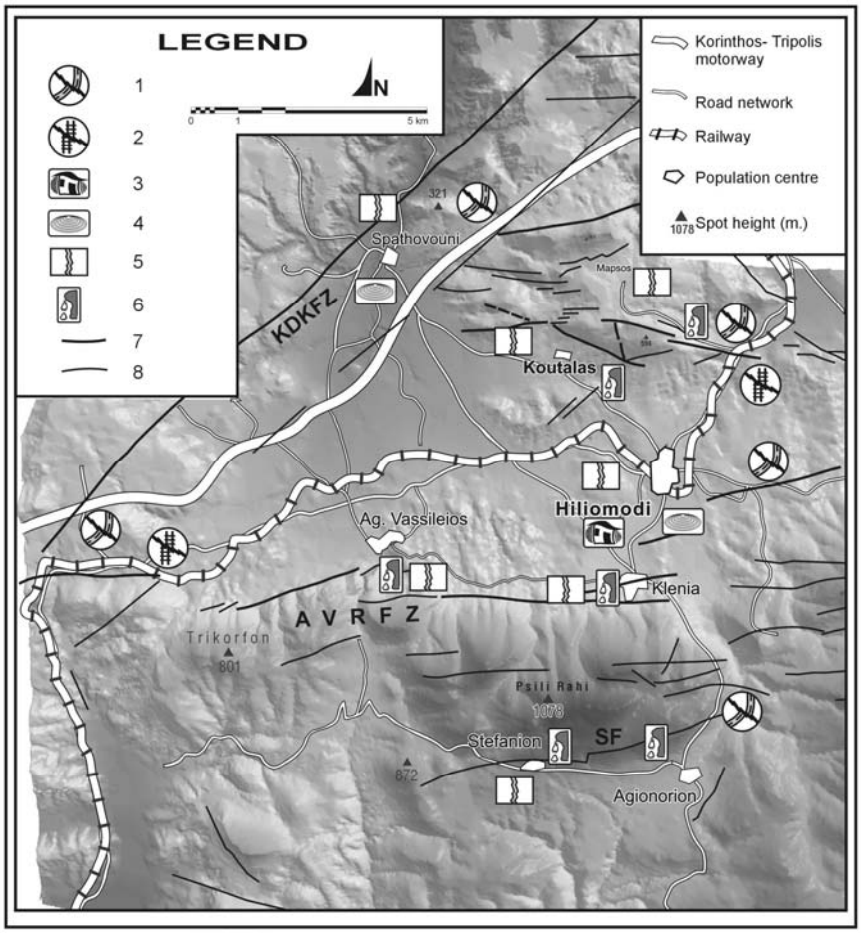

Figure 3: Shaded relief map, lit from the NE, of the municipality of Tenea, showing the active faults in the area (same annotation as in Figure 2) and the possible occurrences of geological effects induced by reactivation of the tectonic structures shown here. 1. disruption of traffic due to fault displacement; 2. disruption of rail transport due to fault displacement; 3. amplified ground shaking; 4. liquefaction; 5. soil fracturing; 6. rockfalls; 7. major fault; 8. secondary fault.

Figure 4: The Mapsos Fault. View to SW.

4.3 Stefanion – Agionorion

The southernmost villages of the area are located within the mountainous area, on the flanks of a plateau. The nearest fault is the Stefanion Fault (SF) (Fig. 3), with E-W to ENE-WSW strike and a visible length of 7 km. It consists of two en echelon segments, linked with a small N-S fault. Debris, with various degrees of cohesion, occur all along its trace, on a 50-150 m-wide zone. The fault does not display signs of recent activity (i.e. in the past 10,000 years), however, and judging by the form of the morphological discontinuity and the extent and degree of cohesion of the slope wash material we can assume that it has moved in the Quaternary. Any reactivation on this fault will have immediate effects on Stefanion, which lies practically on the trace of the fault; Agionorion is also expected to be affected by ground (subsidiary) fracturing. Rockfalls are also very likely, especially at Stefanion. Note also that the SF runs across the road connecting the two villages with the other population centres. The most crucial intersection point is NE of Agionorion, and displacement on the fault may seriously impede transportation.

4.4 Spathovouni – Corinth-Tripolis motorway

The village of Mapsos lies at the NW part of the municipality and is founded partly on the plioquaternary formations of the ECG and partly on alluvium. The main neotectonic structure in the vicinity is the first-order Korinthos-Dervenakia – Kaparelli Fault Zone (KDKFZ), a transcurrent fault, which is the critical boundary between the eastern and western basins of Corinthia (Fig. 2). It has a length of approximately 50 km, striking NE-SW. Its degree of activity is still unclear, as it displays a certain north-eastward migration in the Quaternary (Papanikolaou et al., [3], with its SW segment being dormant or possibly active and the NE active. The part KDKFZ that crosses the area of interest is actually the transfer region (not in the structural sense) between the dormant and active segments. Its topographic expression is subdued, partly due to its kinematic character (strike-slip) and partly because the geomorphic processes in the Late Quaternary may have outpaced its degree of activity. Nonetheless, it separates an area of very low relief to the north-west from a hilly area in the south-west that corresponds to the north-eastern sector of the municipality. All the hills are either bedrock ridges and/or small horsts bounded by the faults described in this paper (Fig. 3). This difference in the morphology between the two blocks of the KDKFZ reflects its tectonic significance: the ECG is a shallow basin, while the thickness of the synrift deposits in the greater Western Corinth Graben (WCG) is much higher. It is therefore expected that the basement morphology under the study area will be highly uneven and probably the synrift deposits have buried small horsts and graben; unfortunately, no systematic geophysical investigations have been conducted in order to clarify the basement morphology and this could be of high value in the estimation of strong motion parameters, as the uneven basement morphology is bound to produce multiple inter-basin reflections of seismic waves (Takemiya and Adam [10]).

The trace of the KDKFZ is parallel to the Corinth-Tripolis motorway in the study area and also crosses it at the west of the municipality boundaries (Fig.3). Besides, another suspected fault strand, parallel to the KDKFZ almost coincides with the motorway; the latter is little more than a photo-lineament and there are no available data for better estimations.

The motorway could be affected if the E-W faults at Mapsos (Fig. 3) are reactivated. These second- and third-order normal faults are active and at least three of these cross the motorway just east of Spathovouni. The most important of these is the Mapsos fault (Fig. 4), which may affect not only the road network, but also the village of Spathovouni, which lies very close to its visible western tip. This fault has a visible length of 3.5 km and its estimated cumulative throw may exceed 150 m.

Apart from problems arising directly from fault displacement, Spathovouni and its environs are susceptible to other geological site effects, namely liquefaction, soil fracturing and lateral spreading. Liquefaction is highly likely, due to the nature of the surficial geological formations.

4.5 Mapsos

The small village of Mapsos is located within a tectonic horst (actually a multi-block), dissected by a multitude of active and probably active faults. The area is sparsely populated and no critical infrastructure facilities are located there. However, the main problem at this north-eastern part of the municipality is the possibility of the disruption of road and railway connections caused by the reactivation of the Mapsos fault, which was described in the previous section, and another, WNW-ESE, fault system located approximately 2.5 km north of Hiliomodi. If these faults are reactivated, problems will arise from possible displacement of the ground surface and from rockfalls that are highly likely to occur on the steep NE and eastern slopes, blocking the existing transportation lines.

5 Discussion and conclusions

The municipality of Tenea is located within a zone of medium to medium-high seismicity. Historical and instrumental records show that is has been affected by at least six medium and large earthquakes in the past 150 years with epicentral distances ranging from a few to 45-50 km. The most destructive of these was the 1876 event (M=6.1), the epicentre of which was only 3-5 km west of Hiliomodi, and the available data allow us to associate it with reactivation of the KDKFZ. The 1962 event, although its epicentre lay only 2-4 km north of Hiliomodi, produced relatively little damage, as it was a medium-depth (h=95 km) earthquake.

The completion of the new Corinth-Tripolis motorway in the last decade, and the ongoing upgrading of the railway connection between Athens and the Peloponnesus, have made Tenea a key location for these lifelines in the event of an earthquake. The most serious threat, as far as near-field tremors are

concerned, is posed by the KDKFZ which has been quiescent for the past 125 years. Both the motorway and the railrway cross the KDKFZ and this makes them susceptible to direct damage from fault displacement. Furthermore, a large stretch of these lifelines is constructed on the hanging-wall basin of the KDKFZ, which corresponds roughly with two-thirds of the area of the municipality. This area, which is a part of the ECG hosts bedrock ridges and tectonic horsts bounded by active or probably active faults, some of which cross the lifelines, such as the MF. Within this part of the ECG, and especially where loose geological formations occur (mainly alluvial silt and sand), liquefaction is highly likely, especially where the aquifer is shallow, as is the case east of Hiliomodi and south of Spathovouni (Fig. 3).

Rockfalls and landslides are a threat for the areas of relatively high relief (the villages of Agios Vassileios and Klenia) and may also disrupt traffic on the secondary artery which connects Hiliomodi with Korinthos.

Earthquakes with epicentral distances from 15-45 km have also been destructive for Tenea. In such a case, the major lifelines are not expected to be seriously hit; private and public buildings will, however, be threatened.

Bearing in mind all the aforementioned, we can say that the population centres and lifelines in the study area will have to withstand both the direct and the indirect (concomitant) effects of an earthquake. In most cases, experience has shown that the related (geological) site effects can prove more destructive than surficial fault displacement or ground shaking themselves. Especially with regard to the first parameter, human and property loss is usually confined within a narrow zone that may coincide with the fault trace or lie parallel to it (Lekkas and Kranis [11]; Lekkas et al. [12]). However, geological site effects can prove much more harmful if local conditions favour them. In the case of Tenea, the soil characteristics, the shallow water table and the unevenness of the alpine substratum of the ECG can trigger liquefaction, lateral spreading, soil fracturing and rockfalls at several locations (Fig. 3).

We believe that this type of approach for seismic hazards can help the administrators towards more effective risk management. The types of hazard, as well as the locations most prone to them, have been located; there remain, however, some aspects to be clarified, such as the detailed imaging of the alpine basement, which is essential for the clarification of the expected patterns of seismic wave propagation through the ECG.

References

[1] Yeats, R.S., Sieh, K. & Allen, C.R. *The Geology of Earthquakes*, Oxford University Press: New York and Oxford, 1997.

[2] Papazachos, B. & Papazachou, A. *The earthquakes of Greece*. Ziti Publications: Thessaloniki, 1989.

[3] Papanikolaou, D., Logos, E., Lozios, S. & Sideris, C. *Neotectonic Map of Greece, 1:100,000 scale, "Korinthos Sheet"* (map and accompanying volume). E.P.P.O & Europ. Centr. for Prev. and Pred. of Earthquakes, 1996.

[4] Davies, R., England, P., Parsons, B., Billiris, H., Paradissis, D. and Veis, G. Geodetic strain in Greece in the interval 1892-1992. *Journal of Geophysical Research*, **102**, B11, pp. 24571-24588, 1997.
[5] Hatzfeld, D., Karakostas, V., Ziazia, M., Kassaras, I., Papadimitriou, E., Makropoulos, K., Voulgaris, N. and Papaioannou, C. Microseismicity and faulting geometry in the Gulf of Corinth (Greece). *Geophysical J. Intern*., **141**, pp. 438-456, 2000.
[6] Mariolakos, I. & Papanikolaou, D. Type of deformation and relationships between deformation and seismicity in the Hellenic Arc. *Bulletin of the Geological Society of Greece*, **XIX**, pp. 59-76, 1986 [in Greek].
[7] Papazachos, B.C. The seismic zones in the Aegean and surrounding area. *Proceedings, European Seismol. Soc., XXI General Assembly*, Sofia, Bulgaria, pp. 82-87, 1989.
[8] Schmidt, J.F. *Studien über Erdbeben*, Leipzig, 1879.
[9] Ambraseys, N.N. Material for the investigation of the seismicity of central Greece. *Archaeoseismicity*, eds. S. Stiros & R.E. Jones, Fitch Lab. Occasional Paper 7, IGME-British School at Athens, 1996.
[10] Takemiya, H. & Adam, M. Why the heaviest damages occurred in Kobe during the Hyogo-ken Nanbu earthquake, Japan, 1995. *Advances in Earthquake Engineering – The Kobe earthquake: geodynamical aspects*, ed. C.A. Brebbia, Computational Mechanics Publications, Southampton and Boston, pp. 39-58, 1996.
[11] Lekkas, E & Kranis, H. Earthquake faulting and human life loss. *Proc.of the Int. Symp. on Eng. Geology and the Environment*, eds. P. Marinos, G. Koukis, G. Tsiambaos & G. Stournaras, A.A. Balkema Publ. Rotterdam, Athens, pp. 835-840, 1997.
[12] Lekkas, E., Lozios S., Kranis, H. & Skourtsos, E. Linear damage distribution and seismic fractures at the Egio earthquake (15 June 1995, Greece). *Advances in Earthquake Engineering: Earthquake Resistant Engineering Structures 2*, eds. G.D. Manolis, D.E. Beskos & C.A. Brebbia, Computational Mechanics Publications: Southampton and Boston, pp. 37-46, 1997.

CHAPTER 9

Seismically-triggered landslide risk assessment

I. Parcharidis[1], Emm. Vassilakis[1], Ger. Cooksley[2] & Chr. Metaxas[3]
[1]*Faculty of Geology, University of Athens, Greece.*
[2]*NPA Group, UK.*
[3]*Earthquake Planning & Protection Organization, Athens, Greece.*

Abstract

Landslides can present a significant risk to people living in earthquake-prone areas. The use of geographical information systems with relevant geophysical data and methods could be used to predict areas according to the risk of landslide occurrence. This study (part of the E.C. project SNAP) presents an application of a simplified Newmark method for modelling the seismically-triggered landslide risk in the broader area of Patras city (Achaia Prefecture) which is characterized of high seismic activity. The final risk map, which was produced using the Newmark method, appears to be highly correlated with landslides mapped on the field, showing a relative overlapping.

1 Introduction

Slopes failures during an earthquake may cause a great number of casualties and damage to structures and facilities. A landslide will occur when the stress acting on a slope exceeds the strength of the material forming the slope. This is expressed as the factor of safety (FoS). Usually the causes of a landslide can be divided into those that (i) increase the stress on a slope and (ii) decrease the strength of the materials that make up the slope. One of the mechanisms by which the factor of safety of a slope can be reduced is the triggering due to earthquakes, traffic, blasting etc. This study describes the development of an information system for seismically-triggered landslide risk assessment in the Achaia area (western Corinthian gulf).

A number of researchers worked on this topic, including the following recent studies. Ambraseys & Srbulov [1] studied the empirical predictive relations that allow an estimation of co-seismic sliding of slopes from the size of energy

released by an earthquake in terms of its magnitude *(Ms)*, its distance from a site *(r)*, and from the critical acceleration ratio *q=Kc/Kmv*. The authors used the sliding block method to calculate permanent displacements. The same authors [2] described a method for estimation of post-seismic sliding for translational slides.

Tibaldi et al. [3] examined landslides triggered by earthquakes and their relations with faults and slope geometry. Landslide distribution shows a correlation with respect to the dip-direction of the faults and the orientation of mountain slopes. Hirotaka et al. [4] examined the landslides induced by the Kobe earthquake in Rokko Mountain. In this case the area of the landslide limit was low in relation to historical worldwide earthquakes of this magnitude, probably as a result of the shallow source of the main shock. The reasons for the low number of landslides were the fairly good bedrock, the dry antecedent condition in winter and the existence of forest cover.

Srbulov [5] estimated sliding of slopes during earthquakes using Monte Carlo simulation based on a semi-empirical attenuation relation and using adopted probability density functions of the parameters in the relation. According to the authors Monte Carlo simulation should be considered for estimations only.

Mankelow & Murphy [6] attempted a landslide hazard zoning using GIS in a probabilistic approach in the assessment of earthquake-triggered landslide hazard.

Luzi & Pergalani [7], basing their studies on the case of the Umbria-Marche earthquake (26 September 1997) tested the prediction accuracy of empirical equations to calculate landslide displacement. Accelerometric records from the permanent and mobile seismic network of the Seismic Survey of Italy were processed and interpolated in order to obtain strong motion parameters at each terrain unit and possible displacements. The results were compared to verify the prediction, given the real landslide occurrences. The method based on Destructiveness Potential was, according to the authors, the most accurate.

Murphy et al. [8] considered three cases of landslides triggered by earthquakes and studied the natural variability of the slope-forming materials and the uncertainties surrounding input ground motions. The results of the analyses show a large scatter into calculated factors of safety for earthquake conditions. The models used in the calculation of seismic slope stability yield acceptable results.

This study describes an assessment of seismically-triggered landslides in the area of Achaia (western Corinthian gulf) using GIS based on the Newmark method [9].

2 Geological setting of the area

The dominant orientation of the mountains of the wider study-area is NW-SE. These mountains were formed during the Alpine orogeny and they are a

recurrence of the mountain ranges of central Greece and Epirus. The main hydrographic network in the Achaia area consists of inflow basins for the rivers Vouraikos, Selinous, Glafkos, Peiros and Foinikas. These rivers flow generally from south to north and are strongly affected by the morphology as this was formed due to high neotectonic activity. Significant quantities of deposits, arising mainly from erosion of Pleio-Pleiostocene formations as well as of later formations, are transported to the coast of the Corinthian Gulf.

The geology of the Achaia consists mainly of alpine sediments of the geotectonic units (from east to west): Pindos, Gavrovo and Ionian. These units are partially covered by Neogene to Quaternary deposits. After studying the geological maps in 1:50 000, the following can be noted:

a) Ionian unit: There is a small appearance in the Western part of the Achaia, due to concealment by Neogene and Quaternary deposits. In particular the internal area of the Ionian unit appears at Manolada where limestone formations from the Upper Jurassic to the Lower Eocene arise, while on these Eocene flysch is deposited.

b) Gavrovo unit: This appears in the western and eastern part of the Achaia. This unit consists of limestone formations, gypsum, dolomitic limestone and schists.

c) Pindos unit: Appearing in the centre of Achaia and consisting of the following alternations: Volcanic tuffs, Triassic – L. Jurassic limestone, L. Cretaceous cherts and radiolarites, Up. Cretaceous limestone and Eocene flysch.

These three units are covered in a large part of the Achaia Perfecture by Pleiocene and other Quaternary formations. These formations can be defined as:

a) Pleio-Pleistocene deposits which consist of marls, clays, sands and conglomerates.

b) Dilouvial deposits which consist of mixed phases of conglomerates with marls and pieces of fragments of erosion, as well as of bigger and smaller pieces of conglomerates and loose or connected material.

c) Holocene deposits which are alluvial deposits and recent silt. These are completed by lagoonal or lake deposits as well as coastal sand formations.

The seismological data which are available for the Achaia area are divided into two periods. The first period consists of earthquakes up to 1889, while the second comprises those from 1900 up to today.

Figure 1 shows the distribution of earthquake epicenters with a magnitude greater than 4.5 Ms for the period 1900-today and within a radius of 100 km around the city of Patras. As shown in Figure 1, there is a concentration of seismicity along the line Lake Trichonis - Gulf of Corinth and there is less seismicity in the immediate vicinity of the city of Patras. The Gulf of Patras corresponds to a seismic gap where according to Hatzfeld et al. [10] there is no observed seismicity at all, even for small magnitude events (microearthquakes).

The focal depths of the earthquakes with epicenters around the Gulf of Patras are in the range 5-20 km.

The wider area of Patras is the westernmost part of an asymmetric graben system striking WNW-ESE, which characterizes the tectonic regime of Central Greece. This system has an age of 3 my and consists of the Saronic Gulf - Gulf of Corinth - Gulf of Patras and Trichonis lake. These grabens were formed under an extensional regime which has been dominant until today in the central Greece area, with strike direction N-S and with a rate of 1.5 cm/y.

Micro-earthquake and tectonic studies in the area of the Achaia and western Greece, showed that the Saronic-Corinth-Trichonis system links to Patras through an asymmetric graben (Rio-Antrrio) which shows complicated rupture characteristics, that is, extensional (normal) and dextral horizontal (strike-slip) (Vassilakis [11]). Armijo et al. [12] suggested that this small graben is the link between Patras and the gulf of Corinth which, according to the spatial distribution of micro-earthquakes in the narrow area from the western Corinth Gulf up to Trichonis to the East, links to Trichonis lake.

An important observation shows that the gulf of Patras is a shallow graben where there is no seismicity of any range of magnitude. On the other hand, the

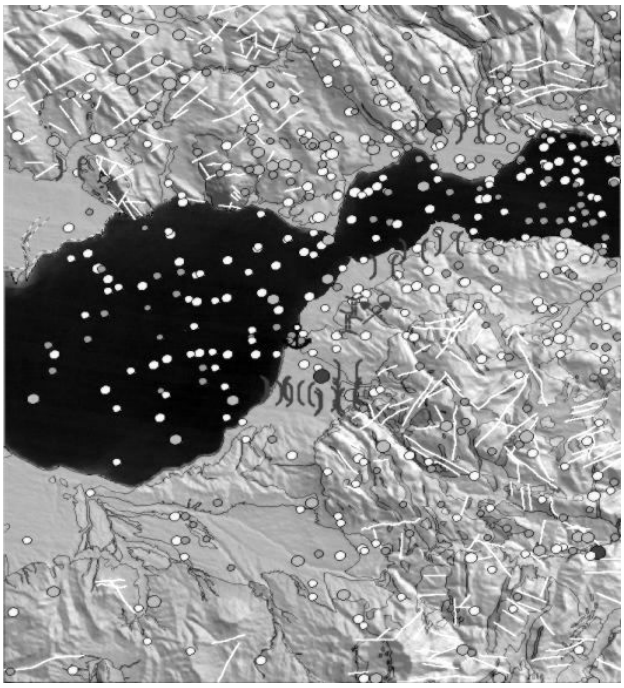

Figure 1: Distribution of earthquake epicenters with magnitude greater than 4.5 Ms for the period 1900-today.

eastern side of the Patras gulf and the area south of Patras city where the link of the Rio-Antirrio system is, historical earthquakes of maximum magnitude 6.7 Ms, as well as seismic records (recorded events) with magnitude 5.5 Ms, have been observed (Tselentis & Makropoulos [13]).

It is also important to note that high seismic activity with small magnitude events has been observed in the Rio-Antirrio area where the graben links to the Corinth-Trichonis system. A maximum magnitude of 6.7 Ms, has also been observed in the recorded incidents and in the historical catalogues.

In this study a database was created containing all the registered mapped neotectonic faults in the Achaia area, and the maximum expected earthquake magnitude was estimated for each of the registered faults. For the wider area of Patras, the maximum expected earthquake magnitude is not more than 5.9 Ms, while it is important to note that there was a historical event of 6.7 Ms in the same area.

3 Data collection and database construction

Seismically triggered landslides can represent a significant risk to people living in earthquake-prone regions. The use of GIS with relevant geophysical data and methods can go some way to predicting and zoning areas according to the risk of landslide occurrence. Such maps can be used by the disaster-prevention community to guide disaster preparedness procedures as well as in making planning decisions to avoid new developments in those regions deemed to be at highest risk from landslides.

3.1 Analysis method

As part of an EC-funded study of the use of InSAR for seismic risk in Greece, the seismically-triggered landslide risk of an area around Patras was examined.

An implementation of the simplified Newmark method by Jibson et al. [14] was used to model seismically-triggered landslide risk. The landslide is modeled as a solid block sliding on an inclined plane. The block begins sliding when the forces exerted on it by the earthquake shaking exceed its critical acceleration threshold (a_c). The critical acceleration threshold of a potential landslide block is a function of the static factor of safety (Figure 2) and slope angle (Figure 3).

The acceleration time-history of an earthquake is normally used to calculate the displacement of the block. Accelerations above the critical threshold cause the block to move while those below the threshold have no effect upon it. The critical acceleration of a block (in terms of the Earth's gravity *g*) is given by:

$$a_c = (FS - 1)g \sin \alpha \quad (1)$$

where *FS* is the static factor of safety and α is the slope angle. The slope angle data were generated from a three arc second resolution DEM of the region.

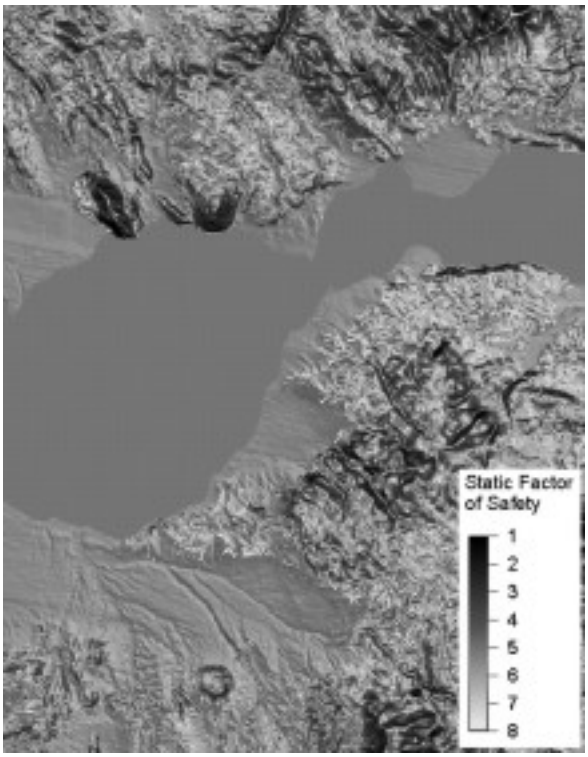

Figure 2: Static factor of safety.

3.2 Static factor of safety

The static factor of safety (FS) is an expression of the balance between resisting and driving forces acting upon the block (Jibson et al. [14]) and can be given by:

$$FS = \frac{c' + c'_r}{\gamma t \sin\alpha} + \frac{\tan\phi'}{\tan\alpha} - \frac{m\gamma_w \tan\phi'}{\gamma \tan\alpha} \qquad (2)$$

cohesive + frictional - reduction of frictional
strength strength strength due to saturation

where c' is the cohesion, ϕ' is the friction angle, α is the slope angle, γ is the material unit weight γ_w is the unit weight of water, t is the thickness of the block, and m is the proportion of the slab that is water saturated. c'_r is an additional

factor included to account for the added cohesion provided by tree roots as suggested by McCalpin [15]. The cohesion, friction angles and material weight were derived from a Geotechnical map (1:50 000, Patras) and applied to the geological units of a same-scale geological map digitized by E.P.P.O. The block thickness was set to 2.4 m following Jibson et al. [14]. A map of tree coverage (Figure 4) was derived from classifying Landsat ETM images; typical values for the added cohesion were as used by McCalpin [15].

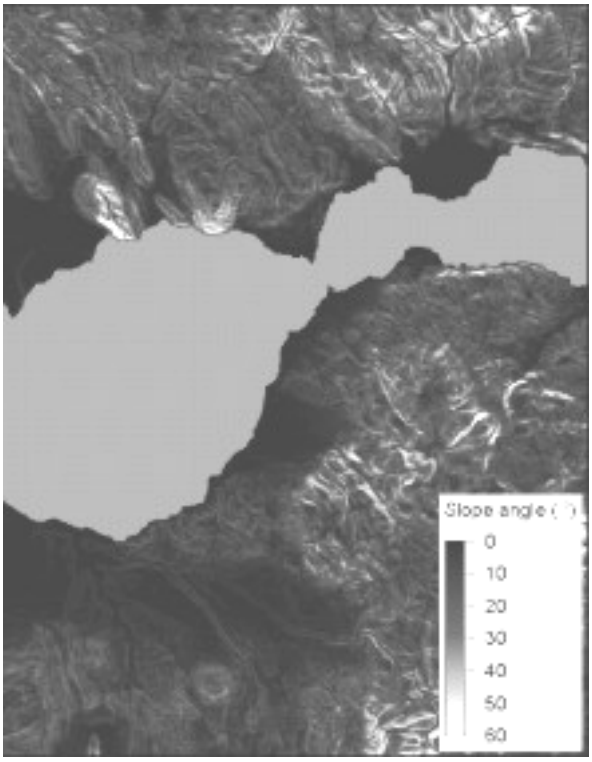

Figure 3: Slope map generated from DEM.

3.3 Newmark displacement calculation

The Newmark displacement calculation method used in this work was based on that presented by McCalpin [15] and utilized methods developed by Jibson [16] and Dobry et al. [17]. These methods use simple formulas developed from the regression analysis of earthquake time histories to provide a relationship

between predicted Newmark displacement (D_n), Arias Intensity (measure of ground motion) (I_a) and critical acceleration a_c:

$$\log D_n = 1.521 \log I_a - 1.993 \log a_c - 1.546 \quad (3)$$

The data available for the Patras region lacked only earthquake strong motion records and groundwater depth data of sufficient density. This necessitated some modification of the above equations. Primarily, since sufficient groundwater data were not available, the proportion of the slab saturated was set to zero so that the third factor was removed from equation 2.

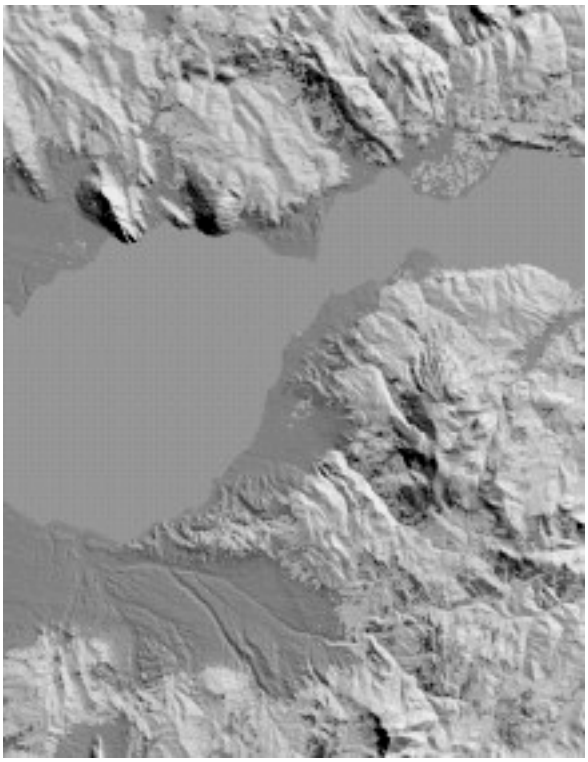

Figure 4: Tree coverage derived from classifying Landsat ETM data.

The second change that had to be made was to use an alternative source of earthquake ground intensity information to derive the Arias intensity. This method, proposed by McCalpin [15], utilized an equation presented by Wilson & Keefer [18] (cited in Jibson [15]) relating PGA with Arias Intensity (I_a):

$$I_a = 0.9(10^{0.432M-1.83})(PGA)^2 \quad (4)$$

where M is earthquake magnitude.

The peak ground acceleration (PGA) data used (Figure 5), were published as part of the GSHAP (Global Seismic Hazard Assessment Programme), Gruenthal et al. [19] of which the Greek element was compiled by Makropoulos K. et al., Athens University. The predicted Newmark displacements were calculated and used to generate a map of seismically triggered landslide risk (Figure 6).

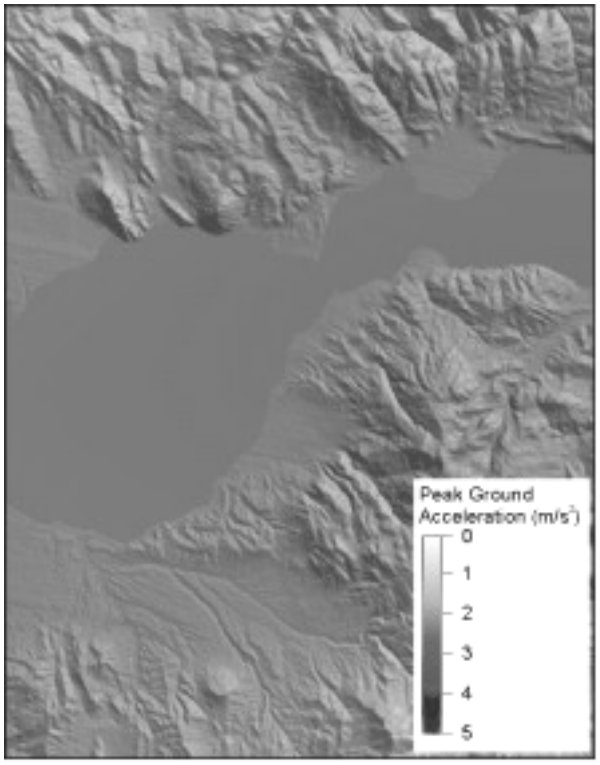

Figure 5: Seismic hazard map overlain on DEM showing the peak ground acceleration (m/s^2) which there is a 10% likelihood of exceeding within 50 years (475-year return period).

4 Results and conclusions

Newmark analysis methods facilitated the production of a seismically triggered landslide risk map (Figure 6). This map could be used as a guide to areas that may need further investigation and could ultimately be used for zoning earthquake risk areas. It would, however, be worthwhile to conduct further Newmark displacement analyses of the region, particularly by using groundwater depth information and actual earthquake strong motion records for the derivation of the Arias Intensity.

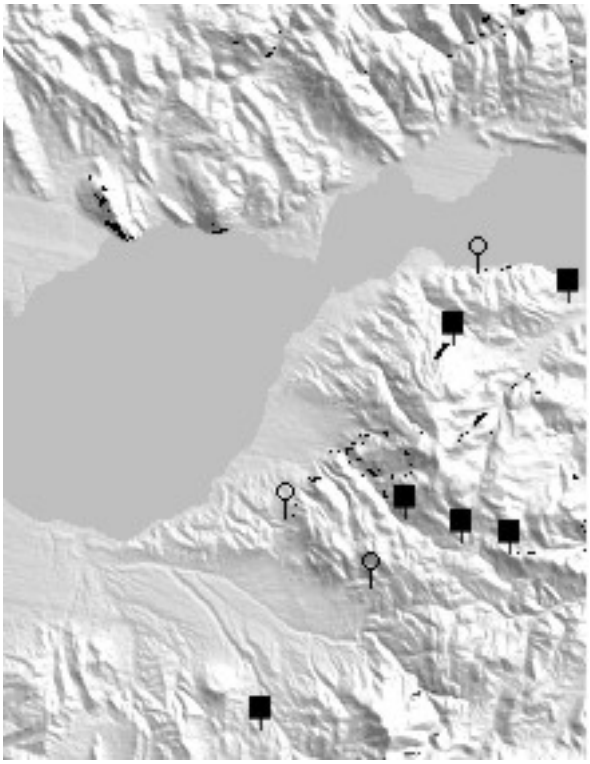

Figure 6: Areas of high seismically-triggered for landslide risk (black pixels). The circles represent landslides triggered by recent earthquakes, while the square symbols represent landslides due to other causes.

References

[1] Ambraseys, N. & Srbulov, M. Attenuation of earthquake induced displacements. *J. Earthq. & Struct. Dyn.*, **23**, pp. 467-487, 1994.

[2] Ambraseys, N. & Srbulov, M. Earthquake induced displacements of slopes. *Soil Dyn. and Earthq. Engineering*, **14**, pp. 59-71, 1995.

[3] Tibaldi A., Ferrari, L. & Pasquare G. Landslides triggered by earthquakes and their relations with faults and mountain slope geometry: an example from Ecuador. *Geomorphology*, **11(3)**, pp. 215-226, 1995.

[4] Hirotaka, O., Hikaru, K., Toshiaki, S. & Kazutoki A. Landslides triggered by the 1995 Hyogo-Ken Nanbu earthquake in the Rokko mountains. *Landslides*, Senneset, Balkema, Rotterdam, 1996.

[5] Srbulov, M. Estimation of co-seismic sliding of slopes. *Landslides*, Senneset, Balkema, Rotterdam. 1996.

[6] Mankelow, M. & Murphy, W. Using GIS in the probabilistic assessment of earthquake triggered landslide hazard. *J. Earth Engin.*, **2(4)**, pp. 593-623, 1998.

[7] Luzi, L. & Pergalani, F. A correlation between slope failures and accelerometric parameters: the 26 September 1997 earthquake (Umbria-Marche, Italy). *Soil Dynamics and Earthquake Engineering*, **20**, pp. 301-313, 2000.

[8] Murphy, W., Petley D.N., Bommer, J. & Mankelow J.M. Uncertainty in ground motion estimates for the evaluation of slope stability during earthquakes. *Quaternarly Journal of Engineering Geology and Hydrology.* **35(1)**, pp. 71-78, 2002.

[9] Newmark, M. Effects of earthquakes on dams and embankments. *Geotechnique*, **15(2)**, pp. 139-160, 1965.

[10] Hatzfeld, D., Karakostas, V., Ziazia, M., Kassaras, J., Papadimitriou, E., Makropoulos, K., Voulgaris, N. & Papaioannou, C. Microseismicity and faulting geometry in the Gulf of Corinth (Greece). *Geophysical Journal International*, **141(2)**, pp. 438-456, 2000.

[11] Vassilakis, Emm. *Neotectonic regime of the Central Aetolia & Akarnania*, MSc Thesis, National & Capodestrian University of Athens, 1998.

[12] Armijo, R., Meyer, B., King, G. and Papanastasiou, D. Quaternary evolution of the Corinth rift and its implications for the late Cenozoic evolution of the Aegean. *Geoph. J. Int.*, **126(1)**, pp. 11-53, 1996.

[13] Tselentis, G. & Makropoulos, K. Rates of crustal deformation in the Gulf of Corinth (Central Greece) as determined from seismicity. *Tectonophysics* **124**, pp. 55-66, 1986.

[14] Jibson, Randall W., Harp, Edwin l. & Michael, John A. A Method for Producing Digital Probabilistic Seismic Landslide Hazard Maps: An example from the Los Angeles, California, Area. *US Geological Survey Open-File Report 98-113*, 1998.

[15] McCalpin, J.P. An Improved Procedure for Mapping Earthquake-Induced Landslide Potential Using a Geographic Information System, with

Application to the Puget Sound Region, Element III.3. *Final technical report, National Earthquake Hazards Reduction Program, US Geological Survey*, 1997.

[16] Jibson, Randall W. Predicting earthquake-induced landslide displacements using Newmark's sliding block analysis. *Transportation Research Record*, **1411**, pp. 9-17, 1993.

[17] Dobry, R., Idriss, I. M. & Ng, E. Duration Characteristics of Horizontal Components of Strong-Motion Earthquake Records. *Bulletin of the Seismological Society of America*, **68(5)**, pp. 1487-1520, 1978.

[18] Wilson R.C. & Keefer D.K. Dynamic analysis of a slope failure from the 6 August 1979 Coyote Lake, California, earthquake. *Bulletin of the Seismological Society of America*, **73**, pp. 863-877, 1983.

[19] Gruenthal, G. & the GSHAP Region 3 Working Group, Seismic Hazard Assessment for Central, North and Northwest Europe: GSHAP Region 3. *Annali di Geofisica*, GHSAP Special Volume, 1999.

CHAPTER 10

Low-strain techniques used for microzoning studies in soft rock areas in Greece

T. D. Papadopoulos, J. D. Alexopoulos & P. J. Kambouris
Faculty of Geology, University of Athens, Greece.

Abstract

For site characterization, and especially in estimating surface strong ground motion, the Vs distribution with depth is a necessary parameter. The distribution also of Vp with depth gives additional information in searching the subsurface conditions, especially when it is related to the structural geometry of the medium. Many geophysical methods have been proposed and have been used worldwide in the past, including surface and borehole techniques. In this paper a synopsis of the methods used by the authors the last few years are presented, and some case histories of particular interest are described, relating to investigations that have been carried out in the framework of microzoning studies in Greek territory and in a soft rock environment.

1 Introduction

In the last two decades, emphasis has been placed by earth scientists and urban planners worldwide on taking into account the effect of soil on buildings during the occurrence of a strong earthquake. The investigation of soil structure and its dynamic elastic characteristics is of primary importance in estimating expected surface strong ground motion. Many papers have been published on the subject including contributions of geophysical investigations by using surface and borehole techniques (Alvarez et al. [1], Bailey & Van Alstine [2], Fertig [3], Helbig & Mesdag [4], Imai & Tonuchi [5], Maurer et al. [6], Moony [7], Stoke & Woods [8], Zhang [9]). Each technique presents its advantages and disadvantages depending on accessibility, depth of investigation, surface conditions (pavement, asphalt, cement, etc.) and the cost of the method used. From surface methods the SASW technique, based on surface waves dispersion, has gained much reliability in the past few years. In Greece there have been conducted a few successful applications in microzoning studies (Pelekis & Athanassopoulos [10],

Pelekis et al. [11]). Since this method cannot be used in all environments, especially in populated areas and in different surface conditions, there is always the need to develop other surface or borehole techniques. Downhole, crosshole and crosshole tomography techniques have been used equally successfully in some areas of Greece (Kambouris et al. [12], Tolis et al. [13]). These techniques are based on the detection and selection of P and S-wave arrivals and the determination of Vp and Vs seismic velocities as well as the associated dynamic elastic parameters. The classical crosshole method of using SPT for Vs determination presents difficulties especially in soft rock environments, and the results obtained are usually doubtful. Nevertheless engineers find useful, and use, empirical graphs showing the relationship between SPT vs Vs values (Bouckovalas et al. [14]) for different geologic formations (clays, sands, clay-sand, marls, etc.).

The scope of this paper is to present the results obtained by the authors in the last few years within the framework of microzoning studies, by developing low-strain surface and borehole techniques in various soft rock environments in Greece.

2 Methodology

Low-strain techniques refer to seismic methods that usually use mechanical sources to produce P and S or PS converted waves. Surface seismic methods utilize mainly SH waves produced by striking a fixed wooden plank (loaded with a heavy weight) on both sides using a sledgehammer. Other modern techniques giving similar results have also been used by utilizing different ways for S wave sources (Deidda & Ranieri [15]). The SASW or Multi-SASW methods are based on the dispersion of surface waves and the dependence of phase and group velocities on their period. The seismic source could be either a sledgehammer or a drop weight. The seismic refraction method, which has been used extensively in the past, gives reliable results for the shallow velocity structure but fails to provide reliable S-wave onsets from deeper horizons. Borehole techniques have been used for detailed structural imaging in areas of special interest. These techniques utilize both surface (sledgehammer) and in-hole (mechanical hammer) seismic sources. Nowadays emphasis is given to developing more sophisticated techniques (e.g. crosshole tomography) in order to obtain detailed, more reliable and 2-D imaging results for Vp, Vs and the dynamic elastic constants, Young's modulus, Ed, rigidity modulus, Gd and Poisson's ratio, σ.

2.1 Surface methods

Different approaches have been used to determine seismic velocities Vp, Vs at depth, which are necessary for the calculation of elastic moduli parameters. The seismic refraction method was the most popular one to have been used routinely in the past, but with limited depth penetration and lower resolution. The seismic reflection method has in the last few years gained much applicability, based on the improvement of seismic sources/instrumentation, the new processing techniques, the deeper depth of penetration and its intrinsic higher resolution. In a

recent paper of Deidda and Ranieri [15], SH-wave seismic reflections were obtained from depths of less than three meters. Surface waves have been used also successfully for stratigraphic structure and seismic velocity distribution at depth (Pelekis et al. [11]).

In this paper, some earlier efforts conducted by the authors using the seismic refraction method will be referred to. A research project has been put forward by the authors in the last three years to investigate the possibility of getting high resolution shallow structures by generating and detecting S-wave onsets, by applying the seismic reflection method, but the study is still in progress. Surface wave method has been developed greatly in the last few years and is nowadays a useful tool for estimating the subsurface distribution of Vs based on the dispersion of mainly Rayleigh waves. Our experience (Papadopoulos et al. [16]) of the subject is strictly limited to only one common project that was carried out in the past including seismic refraction and SASW methods.

2.2 Borehole methods

Borehole methods utilize different techniques such as downhole, uphole, simple crosshole and crosshole tomography techniques. Downhole/uphole techniques are simple and low cost but their applicability presents difficulties based on surface conditions, method of analysis and interpretation and the subsurface structure itself. For the evaluation of soil dynamic properties a new downhole technique was presented recently (Lontzetides [17]) and also a comparison between the results of SASW and crosshole/downhole measurements (Pelekis & Athanassopoulos [10]). An improvement in the method of analysis for downhole measurements has also been presented recently (Kambouris et al. [12]). The simple crosshole technique has been applied basically in two ways. The first configuration utilizes a borehole with a triaxial geophone inside it and the seismic source is set at a distance of 3-4 meters away from the first borehole and at the same depth as the triaxial geophone but as a source the SPT device is used. As the Terzaghi test proceeds deeper, the information for the Vs estimation is obtained whenever the drilling device reaches a predetermined depth and produces seismic waves by freely dropping the weight. This method has been widely used in Greece in recent years (Bouckovalas [18]). The ambiguity introduced by this method comes from its inability to check the arrival of secondary waves, taking into account that P and S wave pulses interfere with each other at short distances.

The other configuration resembles the first but differs in that it uses two boreholes (instead of one) and a mechanical hammer inside one of them is used as a seismic source. The seismic pulse has higher frequency content, and using several triaxial geophones located at different depths for each shot, one can obtain recognizable and more reliable secondary arrivals. This method has been successfully used by the authors (Kambouris et al. [12]). A more sophisticated and effective method is the crosshole tomography method, which utilizes many shot points and geophone locations so that dense seismic traces cover the area between the two boreholes. Thus, a receiver chain of eight triaxial geophones is lowered into one borehole and a number of shots are fired into the other borehole

every two meters by using a mechanical seismic hammer. The seismic source operates by a spring-driven hammer striking an anvil producing signals for P- and S-waves. A converter fixed at the lower part of the hammer transforms the axial movement of the anvil-rod assembly into hydraulic shock. The fluid between the converter plates is pushed into the borehole walls, producing radially directed stresses and consequently compressional and shear waves (Cosma [19]). The frequency content of the waves of the mechanical hammer is in the range 200-1500 Hz. The dominant frequency of the recorded shear waves is in the range 200-350 Hz. In this way it is possible to detect low and high velocity regions between the two boreholes as well as the corresponding distribution of the elastic moduli (Papadopoulos et al. [20]). Limitations to this method can be imposed mainly by two factors, (a) the prerequisite of at least one watertight borehole where the seismic hammer enters and (b) the cost of the two boreholes.

All the above-mentioned techniques have been formulated by the authors and the results obtained from different parts of Greece will be presented below. The measurements have a common character in that they were conducted in lowland areas and in a soft rock environment. The importance of conducting such measurements arises from the need to incorporate the results obtained (e.g. elastic moduli parameters) in microzoning studies that are developed for seismic hazard assessment and protection in vulnerable areas.

3 Elastic moduli determination

The upper 2-3 meters are usually composed of loose material that behaves in an inelastic way and the seismic velocities (Vp, Vs) show much lower values, even below the velocity of sound in the air (340 m/s) for P waves. Reliable results can be obtained below three meters' depth for both surface and borehole geophysical methods. Consequently reliable elastic moduli constants can be obtained at deeper depths where the material starts to behave elastically, although other factors (e.g. water content, fractures) can affect them. The presence of water content in soft rocks can be indicated by the higher Poisson ratio values, σ (Papadopoulos [21]). Under the water table of a formation, the ratio of seismic velocities Vp/Vs will be higher causing a higher Poisson ratio even if the rigidity strength of the rock increases in absolute values. The density of the medium should be known for the rigidity modulus determination. In most cases an average density is obtained, introducing a small error in the calculations since only small density variations are observed in soft rocks (1.6-2.1 gr/cm^3). In earlier times empirical relationships were used to calculate the Young's modulus from seismic velocities, Vp (Brown & Robertshaw [22]). Errors in the determination of elastic moduli parameters are introduced mainly from the errors deriving from the estimation of seismic velocity Vs. Emphasis has been given in recent years to obtaining reliable Vs distribution at depth and laterally by utilizing seismic reflection and crosshole tomography methods.

4 Case histories

Some case histories will be described below for areas where temporary or extensive investigations have been conducted in the framework of site characterization or microzoning studies (Figure 1). For the areas of Grevena-Kozani and Aegio, only surface geophysical investigations were carried out due to the need to provide data for soil conditions in a short time, in order for the local authorities to undertake immediate measures for house repairs or for moving the population to safer regions after the occurrence of the large earthquakes (13 May and 15 June 1995) which struck these areas.

4.1 Area of Grevena-Kozani

A surface geophysical investigation was carried out at selected and heavily damaged sites after the earthquake occurrence of 13 May 1995 of magnitude 6.6R. Macroseismic observations showed that the heavily damaged areas were affected very much by the bad soil conditions. For immediate restoration of

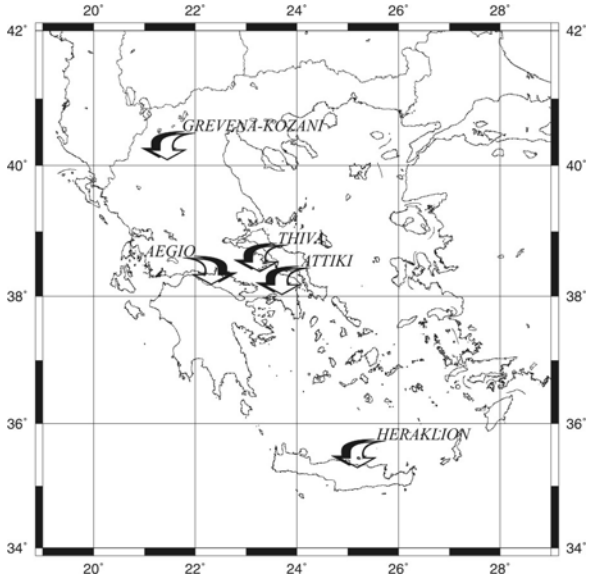

Figure 1: Map of Greece showing the sites where surface and borehole techniques were carried out, in the framework of microzoning studies.

damage or for urban planning decisions regarding whether or not to move the population to other, safer, areas, an integrated geophysical study was proposed among the other investigations including the seismic refraction method and electrical soundings, in order to investigate the thickness of the loose soil material and the presence of the water table at shallow depths. The results obtained could be used for an immediate estimation of the hazard assessment due to landslide or liquefaction phenomena. Since only Vp velocities were determined and in order

to get a gross estimation for at least one elastic parameter, the following empirical formula by Brown, Robertshaw [22] was used to estimate the Young's modulus of soil material:

$$Ed = 1.163 Vp^{2.34} 10^9 \, (Newtons / m^2) \, .$$

In Table 1, the range of Vp seismic velocities for the upper two layers and the corresponding lithologies are shown, obtained from various selected sites of heavily damaged villages in between the Grevena-Kozani area.

Table 1: Range of Vp seismic velocities for the upper two layers and the corresponding lithologies in the Grevena-Kozani area.

Layer no	Seismic velocity, Vp (m/s)	Lithological description
1	550-900	Loose surface material composed of clay, sand, gravel, etc.
2	1250-4500	Alternative layers of conglomerates, sandstone and marls. Higher values correspond to cohesive ophiolitic conglomerates.

In Table 2 the seismic velocities, Vp, and the corresponding values of Young's modulus, Ed, are shown for every investigated village (Figure 2).

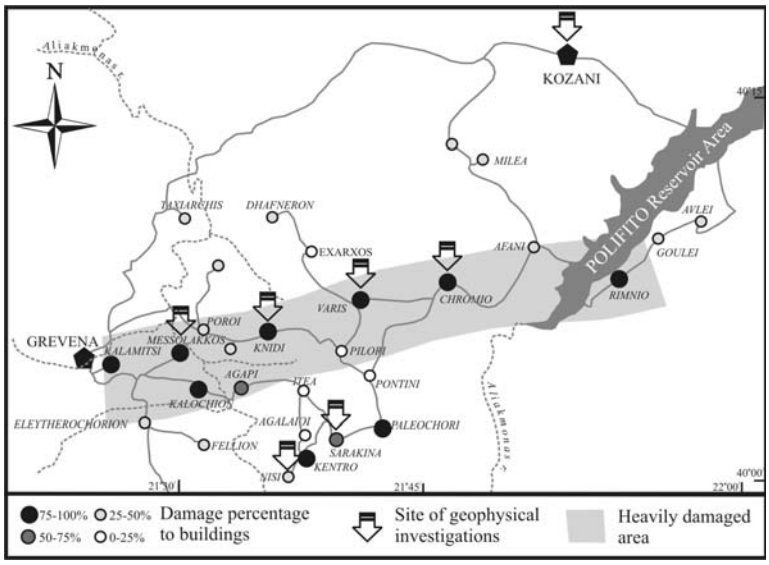

Figure 2: A sketch map of the Grevena-Kozani area, showing the distribution of damage and the investigated geophysical sites.

For loose material composed of clay, sand, gravel, etc., with seismic velocities Vp, 550-900 m/s, the Young's modulus ranges between 0.29-0.91 Nt/m^2 and for conglomerates, sandstone with seismic velocities 1,250-4,500 m/s, the Young's modulus ranges between 2.0-39.3 Nt/m^2. The thickness of the first layer ranges between 13-26 m. The low seismic velocities and the bad geotechnical conditions of the first layer, associated with its relatively small thickness, probably caused the heavy damage that was suffered by the Grevena-Kozani area.

Table 2: The seismic velocities, Vp and the corresponding values of Young's modulus, Ed, for every investigated village in the Grevena-Kozani area.

Village	Layer 1		Layer 2	
	Vp (m/s)	Ed (Nt/m^{2}x10^9)	Vp (m/s)	Ed (Nt/m^{2}x10^9)
Chromio	600-900	0.4-0.9	1250-1350	2.0-2.4
Knidi	800-900	0.7-0.9	3600-4500	23.3-39.3
Baris	550	0.3	1600-1800	3.5-3.9
Nisi	600	0.4	3000-3400	15.2-20.4
Messolakos	650	0.4	1500-1700	3.0-4.0
Sarakina	700	0.5	1550-2000	3.2-5.9
Kozani	500-700	0.2-0.5	1800-1900	3.9-5.2

4.2 Area of Aegio - Achaia

The seismic refraction method was used to investigate the shallow soil conditions in two heavily damaged sites in the Aegio – Achaia area. A five-story apartment building in the city of Aegio and the Eliki Hotel in Valimitika partially collapsed during the large earthquake occurrence on 15 June 1995 of magnitude 6.1R. Among other research studies that were carried out to investigate the causes of the heavy damage to buildings, a geophysical program was executed along traverses close enough or across the damaged buildings wherever possible. According to the results obtained for soil conditions at the five-story building site, a uniform depth (approximately 2 meters thick) of the upper surface and low velocity layer (650 m/s) was detected west of Despotopoulou Street that abruptly deepens eastward to a depth of up to six meters under the damaged L-shaped building (Figure 3a,c). There is a linear trend in isopach lines along a N-S direction, revealing that the western foundation of the building rested on a higher velocity basement (1,300 m/s) that dips eastward (Figure 3b).

The upper surface layer is composed of sand-gravels and clay sand-gravels and the lower layer of clays, clay sands and silty sands. The unfavorable shallow structure, due to the eastward abrupt deepening of the basement and the low seismic velocity values of the overburden, caused extra horizontal forces to be applied to the western foundation of the partially collapsed building, without

ignoring the additional effect of the deeper structure that might modify the strong ground motion as well.

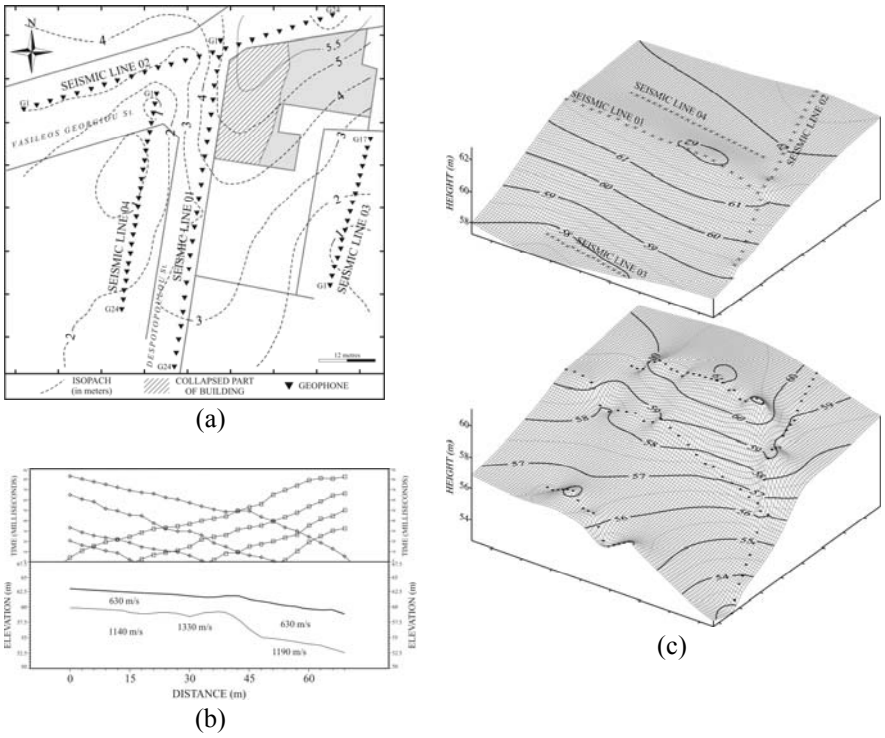

Figure 3: (a) A sketch map showing isopachs and the collapsed part of the five-story building (hatched area), (b) time-distance curves and the corresponding structure along seismic line 03, and (c) 3-D presentation of surface and subsurface (basement) based on seismic results.

At the site of the Eliki Hotel (Figure 4), which also partially collapsed, two distinct subsurface seismic layers were also detected. The upper surface layer with low velocity (700 m/s) is composed of sand gravels, sandy clay and clay sand and the deeper layer had an average seismic velocity 1,550 m/s. This layer corresponds to the sea water front which intrudes from east to west (Corinthian Gulf) which is found at a depth of two meters east of the hotel (G24) and deepens further to six meters' depth west of the hotel (G7). Large Poisson ratio values were determined along Seismic Line 3 (>0.4), where seismic velocities Vs were measured, indicating that the surface materials have been affected by sea water intrusion. In general, the soil formations around the Eliki Hotel area are homogeneous with low values of Young's and rigidity moduli.

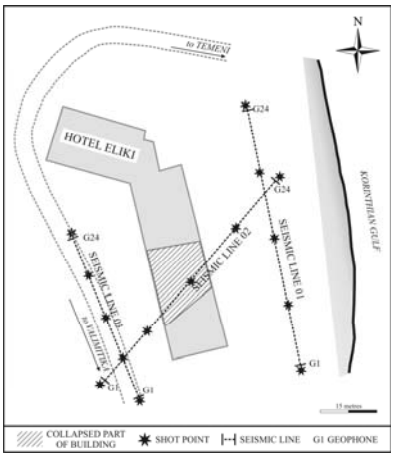

Figure 4: A sketch map showing the seismic lines and the collapsed part (hatched area) of the Eliki Hotel.

4.3 Area of Thiva Beotia

In the framework of the microzoning study for the area of Thiva Beotia, crosshole investigations were carried out at selected sites (Figure 5) based on the existing geological/geotechnical maps.

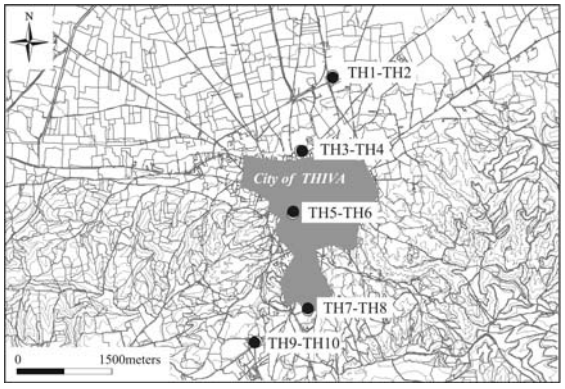

Figure 5: A map showing the broader area of Thiva and the sites of borehole pairs used for crosshole tests.

The crosshole results are shown in figure 6. Higher Vs values (> 500 m/s) are due to fresh marl formation (TH3-TH4 borehole pair) or to the presence of micro-breccia (TH7-TH8, TH9-TH10 borehole pairs) and conglomerates (TH1-

TH2, TH5-TH6 borehole pairs). Seismic velocities, Vs, for micro-breccia and conglomerates are generally low due to fractures and bad rock quality. A slight linear increase in velocity with depth is observed, although local deviations are present.

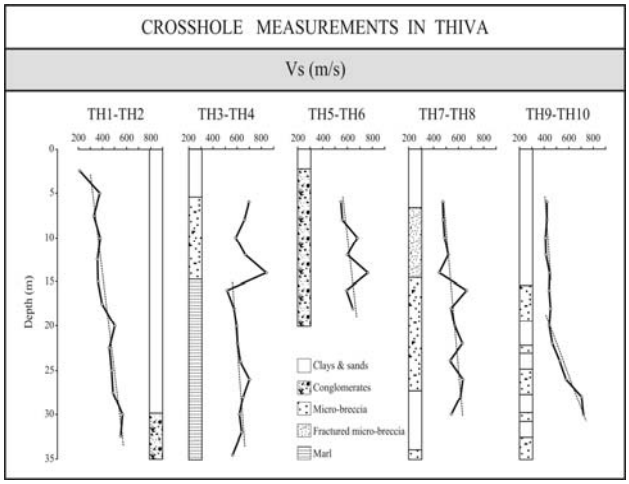

Figure 6: Crosshole results for the area of Thiva and their correlation with lithologic borehole data.

4.4 Area of Athens Attiki

Quite a number of site investigations were conducted (Figure 7) by applying crosshole and crosshole tomography techniques for estimating the seismic velocities Vp and Vs as well as the dynamic elastic parameters of the medium between a pair/s of boreholes. In addition, downhole measurements were also conducted at some sites, in an attempt to correlate and improve modified processing techniques with crosshole and crosshole tomography results.

In figure 8a, compiled crosshole results of Vs distribution with depth for different sites of Attiki are shown. A slight linear increase in velocity with depth is observed for the Ag. Anargiri and Maroussi sites, but a more complicated picture appears for the Elefsis and Thrakomakedones sites. At the Elefsis site the surface material is highly inhomogeneous and in Thrakomakedones the first 15 meters are composed of cohesive breccia. In these two areas the seismic velocities, Vs, are abnormally high at shallow depths. A correlation between crosshole and downhole results for the Thrakomakedones site showed that there is a good agreement for the first 25 meters' depth but weak fit below it (Figure 8c). Crosshole results showed good correlation with borehole data. Classical downhole measurements including data acquisition and processing techniques must be further improved to obtain more reliable results.

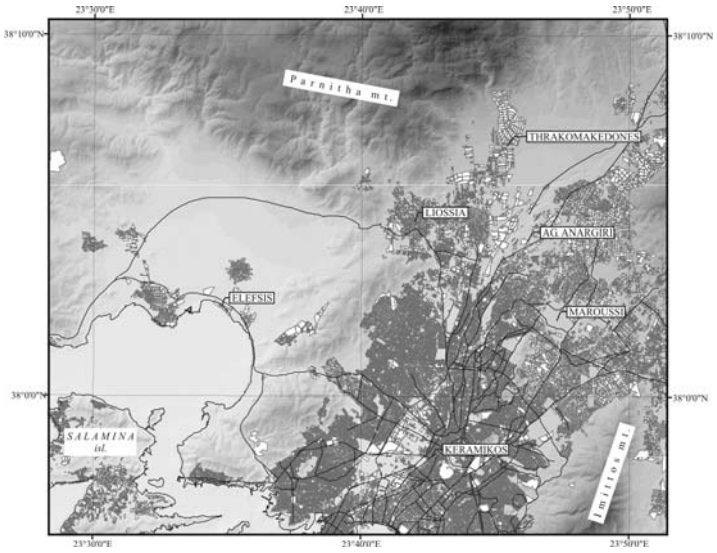

Figure 7: A broader map of the area of Athens, showing the investigated sites.

An effort was made to correlate crosshole tomography results covering a wider area (between boreholes BH1-BH2, 45 meters apart), based on P-wave data and normal crosshole measurements (between borehole pair BH2-BH3) based on S-wave data (Figure 8b). It is obvious that for the upper 10 meters there is no good correlation but for the deeper structure the higher Vs values correspond nicely to higher Vp values. So, we can get a gross estimation of Vs values for the area between the borehole pair BH1-BH2 based on the above-mentioned correlation.

4.5 Area of Heraklion Crete

In the area of Heraklion Crete an integrated geophysical program, including seismic and electrical methods, was conducted in the framework of the microzoning study, carrying out surface as well as borehole techniques. The results obtained from one borehole pair will be presented here, where the crosshole tomography technique was used. The spacing of this borehole pair was 40 m, much longer than the usual one used for normal crosshole measurements (3-4 m apart). The scope of this effort was to investigate the possibility of getting reliable S-wave arrivals in longer distances and in a soft rock environment by using the mechanical hammer as a source. In figure 9 are shown the results obtained for the distribution of Vp, Vs, Poisson Ratio, σ, Rigidity Modulus, Gd and Young's Modulus, Ed. An average density of 2.1 Kg/m^3 was used for the Rigidity Modulus calculation. The estimated Vp and Vs velocities are generally

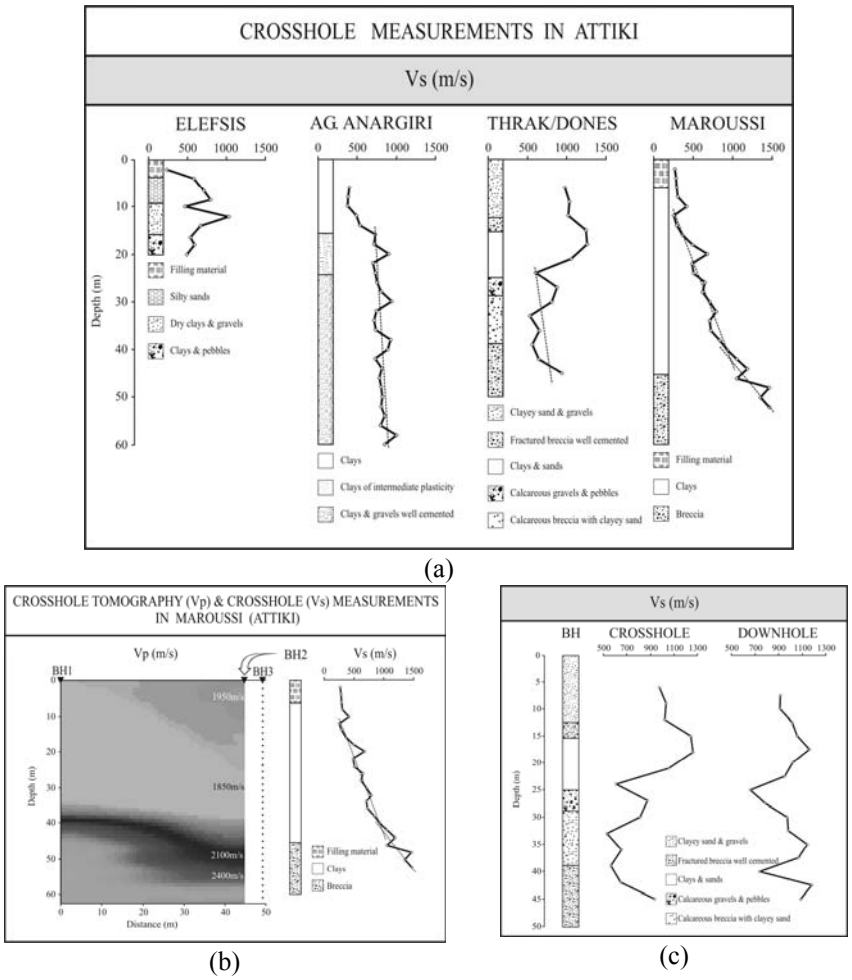

Figure 8: (a) Crosshole results for selected sites in the area of Athens, (b) A comparison between P-wave crosshole tomography results (BH1-BH2) and S-wave crosshole results (BH2-BH3) for extrapolating the S-wave distribution in the area between borehole pair BH1-BH2, and (c) Crosshole/downhole comparison based on modified crosshole processing technique (Kambouris et al. [12]).

low and this is in accordance with the lithology of a medium composed of loose material, clays and locally sands and gravels. The high σ values are attributed to either the shallow depth of water table for areas close to Giofiro torrent or the loose material of the overburden and the bad quality of the upper part, of marl up to 50 meters depth.

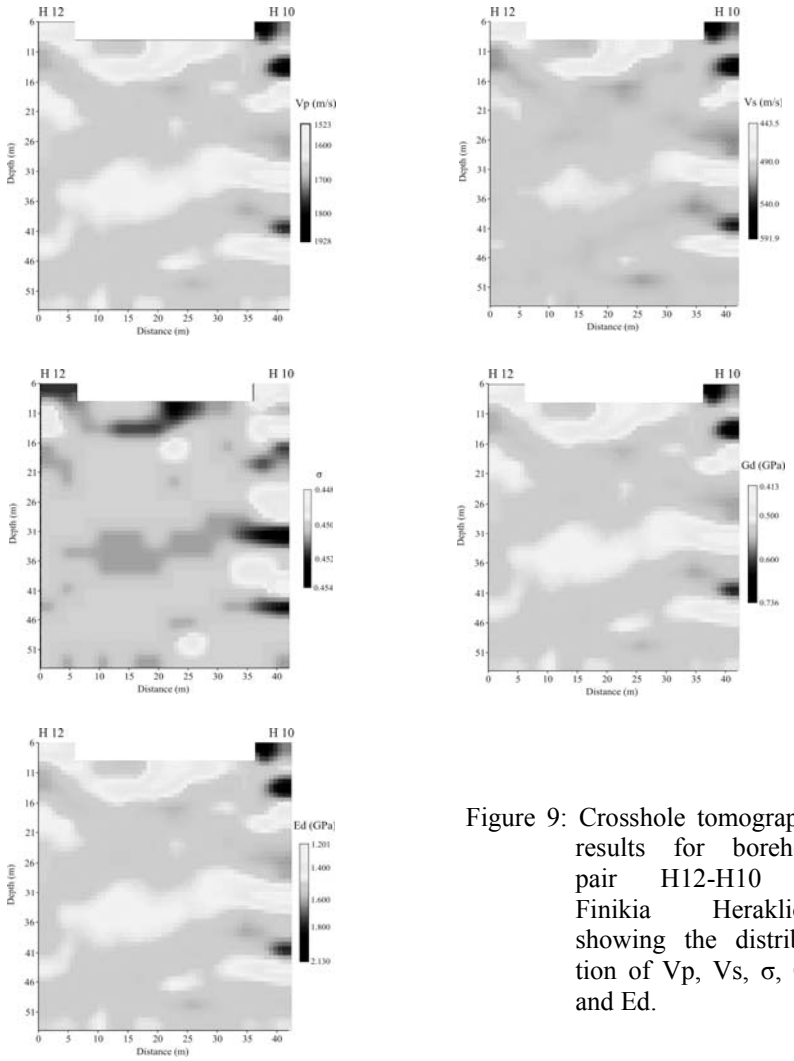

Figure 9: Crosshole tomography results for borehole pair H12-H10 in Finikia Heraklion, showing the distribution of Vp, Vs, σ, Gd and Ed.

References

[1] Alvarez, J., Chavez, R.E. & Lomnitz, C. Shallow SH-refraction survey on Mexico City mud: amplification by wedge effects. *First Break*, **13(12)**, pp. 471-479, 1995.

[2] Bailey, A.D. & Van Alstine, C.L. *Downhole wave and soils study, Nimbus Instruments (Manual)*, West Sacramento, California, 1975.

[3] Fertig, J. Shear waves by an explosive point source. *Geophysical Prospecting*, **31**, pp.873-887, 1984.

[4] Helbig, K. & Mesdag, C.S. The potential of shear wave observations. *Geophysical Prospecting*, **30**, pp. 413-431, 1982.
[5] Imai, T. & Tonuchi, K. Correlation of N value with S-wave velocity and shear modulus. *Proc. Second European Symposium on Penetration Testing*, Amsterdam, 1982.
[6] Maurer, H., Giudici-Trausch, J., Van der Veen, M. & Springman, S. Determining elastic soil properties at small strains. *Proceedings of Annual Meeting of Environmental and Engineering Geophysical Society (SAGEEP)*, pp. 417-423, Oakland, 1999.
[7] Moony, F.M. *Shear waves in engineering seismology. Handbook of Engineering Geophysics*, Bison Instruments: Minneapolis, MN, 1973.
[8] Stoke, K.H. & Woods, R.D. In situ shear wave velocity by crosshole method. *Journal of the Soil Mechanics and Foundations Division, Proceedings ASCE,* **98 (SM5)**, pp. 443-460, 1972.
[9] Zhang, S.H. Shallow SH-wave seismic exploration for subway construction in Shanghai. *Geotechnical and Environmental Geophysics, ed. S.H. Ward, SAGEEP, Proceedings,* pp. 175-179, 1990.
[10] Pelekis, P.K. & Athanassopoulos, G. A comparison between the results of SASW and crosshole/down-hole measurements. *Proceedings of the 4th Hellenic Conference on Geotechnical and Environmental Engineering*, pp. 281-288, Athens, 2001.
[11] Pelekis, P.K., Athanassopoulos, G. & Xenaki, B.K. Utilization of the SASW method for the seismic microzonation of the city of Chania. *Proceedings of the 4th Hellenic Conference on Geotechnical and Environmental Engineering*, pp. 297-304, Athens, 2001.
[12] Kambouris, P.J., Alexopoulos, J.D. & Papadopoulos, T.D. Downhole seismic logging for detailed P-S waves velocity determination. *9th International Congress of the Geological Society of Greece*, pp. 1357-1362, 2001.
[13] Tolis, S.B., Stavrakakis, G., Papadopoulos, T.D. & Cavounidis, S. Estimation of the elastic design response spectra for the new Aghii Anargiri Cancer Hospital at Kifissia. *Proceedings of the 4th Hellenic Conference on Geotechnical and Environmental Engineering*, pp. 345-352, Athens, 2001.
[14] Bouckovalas, G., Marinos, P., Tsiabaos, G. & Sabatakakis, N. Geology effects in the seismic microzonation of Pirgos, Greece. *Proc. XI ECSMFE, 28 May – 1 June*, **4**, pp. 31-36, Copenhagen, 1995.
[15] Deidda, G.P. & Ranieri, G. Some SH-wave seismic reflections from depth of less than three meters. *Geophysical Prospecting*, **49**, pp. 499-508, 2001.
[16] Papadopoulos, T.D., Stavrakakis, G., Bouckovalas, G., Athanassopoulos, G., Tsiampaos, G. & Sabatakakis, N. Comperative and Analytic Study of Ground Seismic Parameters and their Affect on the Buildings (Design Spectra) for the City of Aegio. *Technical Report supported and submitted to EPPO,* Athens, 1996.
[17] Lontzetides, K. Evaluation of the soil dynamic properties utilizing a new down-hole technique. *Proceedings of the 4th Hellenic Conference on Geotechnical and Environmental Engineering*, pp. 209-215, 2001.

[18] Bouckovalas, G. Prediction of soil effects on seismic motions: A comparative case study. *Earthquake Spectra*, **13(3)**, pp. 333-361, 1997.
[19] Cosma, C. Determination of rockmass quality by the crosshole seismic method. *Bull. of the Intern. Assoc. of Engin. Geology*, **26-27**, pp. 219-225, 1983.
[20] Papadopoulos, T.D., Alexopoulos, J., Kambouris, P., Voulgaris, N. & Stavrakakis, G. Combined geophysical methods for subsurface characterization in the framework of microzoning studies. *Proc. of the IAEG Inter. Symp. on Engineering Geology and the Environment*, pp. 1419-1424, Athens, 1997.
[21] Papadopoulos, T.D. Crosshole tomography study for soil characterization in the archaeological area of keramikos Athens. *Technical Report supported and submitted to IGME,* p. 13, Athens, 1996.
[22] Brown, P.D. & Robertshaw, J. The in situ measurement of Youngs Modulus for rock by a dynamic method. *Geotechnique,* 3.7.283, 1953.

CHAPTER 11

Parameters of intensity distribution in the Izmit and Düzce (Turkey) earthquakes

E.L. Lekkas
Faculty of Geology, University of Athens, Greece.

Abstract

On 17 August and 12 November 1999 the wider area of Izmit, Adapazari, Düzce and Bolu (Turkey) was hit by two seismic shocks of magnitudes M_W = 7.4 and M_W = 7.1, respectively. The earthquakes produced surface ruptures over a distance of at least 150 km, as well as settlement, soil fissures, liquefaction, landslides, tsunamis and subsidence. In both cases, the damage was distributed mainly along an E-W aligned zone more than 180 km long and around 25 km wide. Damage and intensity evaluation followed the EMS_{1998} scale. The maximum intensities approached XII in both earthquakes. Intensity maps show alignment parallel to the strike of the seismic faults, with local variations due to geometry and kinematics of certain tectonic structures. Intensities were considerably amplified locally by concomitant geodynamic phenomena. High intensities were also described at long epicentral distances due to a combination of factors, such as earthquake frequency content, local site conditions and construction type.

1 Introduction

On 17 August, 03:01:37 local time, a severe earthquake occurred with its epicenter in the south-western suburbs of the town of Izmit in Turkey. The earthquake's magnitude was M_w = 7.4 and the seismic source depth was estimated at 15-17 km. Extensive damage was recorded along an E-W zone of about 100 km in length that included the towns of Adapazari, Izmit, Gölcük and Yalova. Damage was also reported farther away, in Istanbul, Bursa, Eskisehir and other towns.

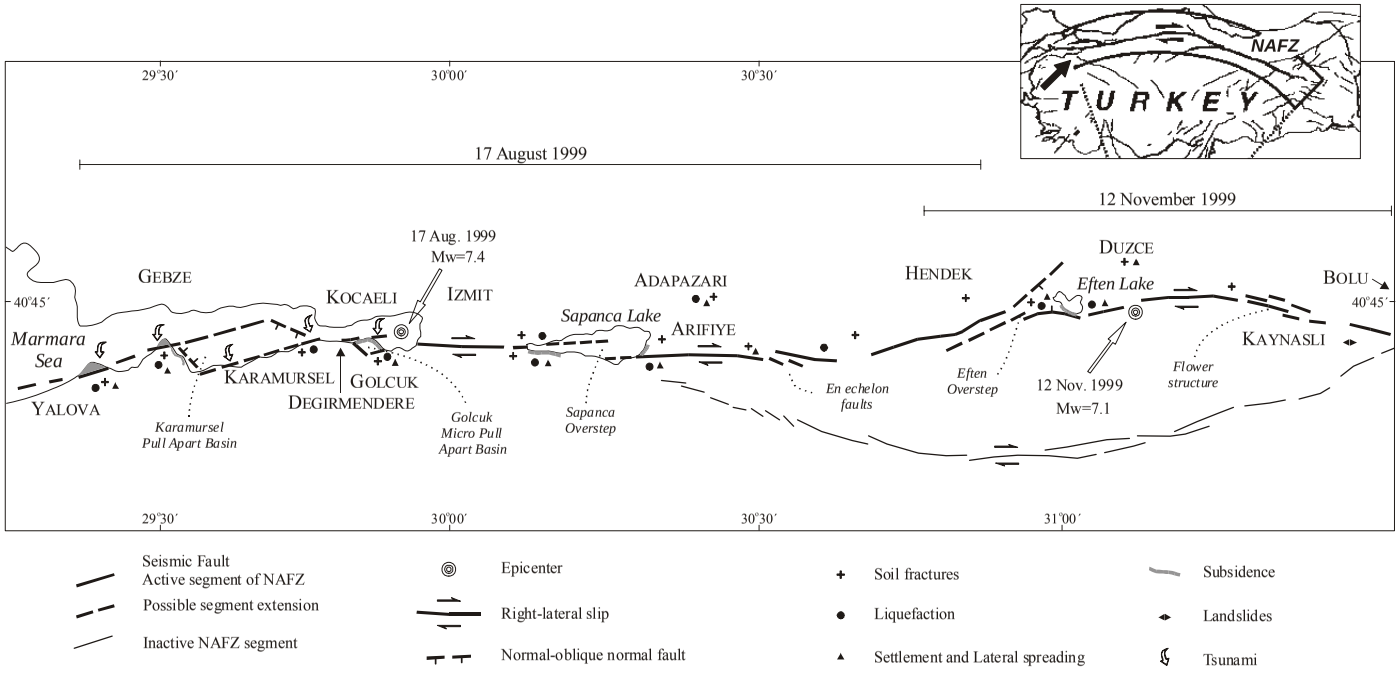

Figure 1: Map depicting the segments of the North Anatolian Fault Zone (NAFZ) reactivated during the earthquakes of 17 August and 12 November 1999, and the concomitant geodynamic phenomena which took place.

Almost three months later, on 12 November 1999, 19:57:21 local time, another severe seismic event of magnitude $M_w = 7.1$ took place with its epicenter about 90 km to the east of the former. The earthquake caused significant damage along an E-W zone about 70 km long, which included Hendek, Düzce, Kaynasli, Bolu and other population centres.

The surficial expression of the seismic fault and the manifestation of concomitant geodynamic effects contributed largely to the damage at both events. The effects included soil fissures, liquefaction, landslides, settlement, lateral spreading, coastline changes, tsunamis, as well as fires (Lekkas et al. [1]). Additionally, tectonic structures relating to strike-slip deformation, such as pull-apart basins, oversteps, en echelon arranged fractures and so on, as well as the local geotechnical conditions and construction type, all played a part in the manifestation and extent of the damage.

The purpose of this paper is to determine the factors that contributed to the amount and type of damage, to damage manifestation and intensity distribution during the earthquakes.

2 Seismic faults

The 17 August 1999 earthquake was centered in the outskirts of Izmit town. The earthquake was the result of the reactivation of the North Anatolian Fault Zone (NAFZ), and particularly of a portion of it that had been dormant in previous seismic events of the twentieth century (Stein et al. [2]). Before the earthquake, repeated GPS surveys indicated an average creep displacement of 10-15 mm in this portion of the fault zone (Armijo et al. [3], Straub et al. [4]). Instrumental data indicate that the fault plane was almost vertical, striking E-W with a right-lateral strike-slip movement.

Field observations show that the surficial rupture was more than 90 km long (Lekkas et al. [1]), vertical with right-lateral displacement in excess of 5 meters, in good agreement with the instrumental data (Figures 1, 2). This seismic fault extended into the submarine area of Marmara bay, west of Gölcük.

The 12 November 1999 earthquake, the epicenter of which was south of Düzce, occurred at the eastern end of the previously activated segment of the NAFZ (Figure 1). This section also had remained dormant during other earthquakes of the last century. Instrumental data showed that the fault plane is almost vertical, strikes E-W and is characterized by a right-lateral slip. Field data showed that the seismic rupture surface was vertical and more than 40 km long and that the horizontal offset locally exceeded 4.5 meters.

The two activated fault segments of the NAFZ caused impressive displacements of rows of trees, fences, roads, pavements and canals, which allowed determination of the geometric and kinematic characteristics of the seismic fault along each section of it. The geometry and kinematics varied locally along the deformation zone; these local variations are attributed to the mode of fracture, the stress field and the occurrence of heterogeneous media -

particularly the differential performance of geological formations under shear stress.

Such variations usually appear along strike-slip faults and are strongly related to oversteps, en echelon structures, flower structures, micro (a few tens of m) and macro (several hundreds of m to a few km) pull-apart basins (Aydin & Nur [5], Harding [6], Lade & Cole [7], Mann et al. [8]) and are held responsible for local differentiation in damage manifestation and intensity distribution (Figures 1, 3).

Figure 2: Surficial occurrence of the portions of the North Anatolian Fault Zone which ruptured during the 12 November 1999 earthquake in Kaynasli.

3 Concomitant geodynamic phenomena

During the earthquakes of 17 August and 12 November 1999, a number of geodynamic phenomena took place in the broader epicentral area (Figure 1). These phenomena are not only of academic interest, as they aggravated the impact, amplified the intensities, and contributed to intensity differentiation from place to place either in the meizoseismal area or at longer distances. These effects are briefly described below:

Soil fissures. Soil fissures were reported in many places where loose recent sediments occur. The most characteristic ones were described around Sapanca

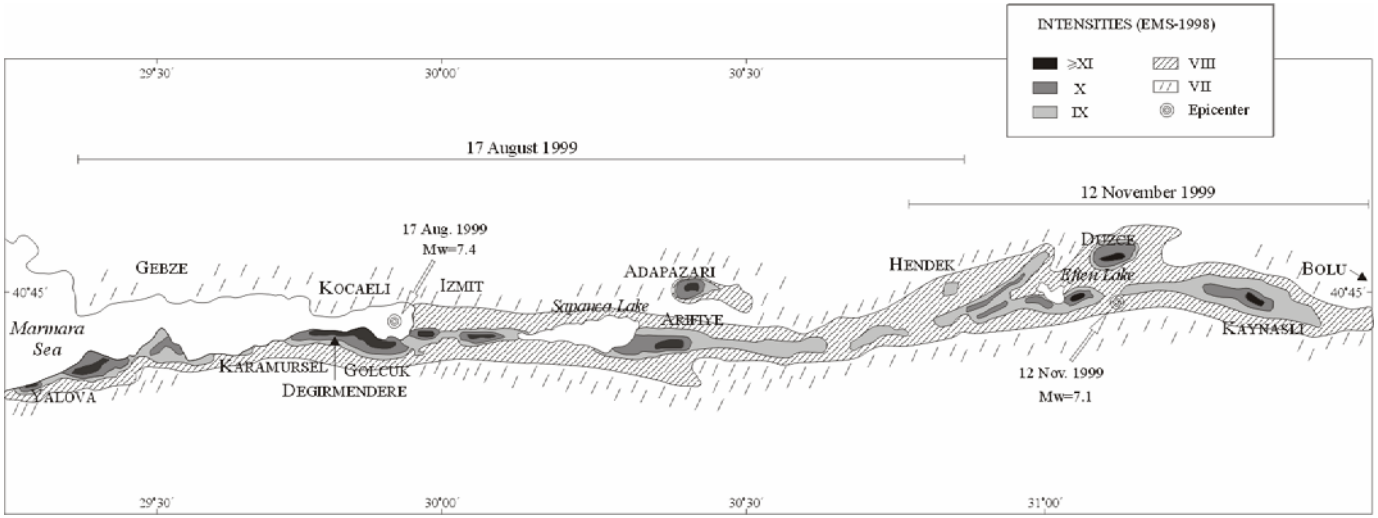

Figure 3: Intensity distribution (EMS-1998) after the earthquakes of 17 August and 12 November 1999.

Lake, along the coastal zone around Gölcük, Degirmendere and Yalova, and in Düzce and Kaynasli.

Liquefaction. This was recorded in the plain area around Sapanca lake, in Adapazari, as well as in the coastal area of Gölcük-Degirmendere-Yalova and in the region of Eften lake.

Landslides. Despite the high magnitude of the 17 August 1999 earthquake, few landslides occurred in the epicentral area. Only few and restricted rockfalls took place along several very steep slopes built of highly fractured rocky formations.

Settlement. This appeared in many places of the epicentral area, mainly where recent loose formations crop out. Lateral spreading and soil fissures were also present, resulting from the differential settlement of the upper geological strata, as was the case in the neighbouring area of Adapazari and around the lakes of Sapanca and Eften.

Tsunamis. The 17 August earthquake generated a tidal wave, which affected the coastal region of Marmara bay, mainly the Gölcük-Yalova area. The submergence of the Gölcük-Degirmendere coastal area is believed to have amplified the influence of the tsunami, the height of which was approximately four meters.

Subsidence. The earthquakes of 17 August and 12 November 1999 produced right-lateral displacements or slip on surface ruptures over a distance of at least 130 km and were nucleated at a depth of 15-17 km. The fault rupture was very often characterised by en echelon, R, R´ and P shear structures, and so on. These structures caused subsidence, uplift and rotation on micro and macroscale (from tens to thousands of m.). The submergence of many coastal areas (from tens of m^2 to some km^2) was the result of pull-apart basin formation (Aydin & Nur [5], Mann et al. [8]). The most representative example is the extended subsidence that occurred in the eastern part of Gölcük. The subsidence of the coast near Gölcük caused a maximum submergence of about 3.5 m so that constructions, port and sport facilities, transportation infrastructure and public beautification works sank into the sea.

The submergence of some regions as well as the manifestation of concomitant geodynamic phenomena were particular cases that aggravated the severity of the earthquake in urban areas and in the environment. In these cases the augmentation of intensities is also attributed to these phenomena especially when occurred at large scale.

4 Intensity evaluation - geographic distribution

Intensity evaluation of the affected area employed the updated European Macroseismic Scale EMS-1998 (Grünthal [9], Grünthal [10]).

Intensity evaluation was based primarily on damage recording elaboration which contributed to the compilation of an intensity map of the affected area for both seismic events (17 August 1999 and 12 November 1999) wherever possible. Additionally, the vulnerability of constructions and the recordings of other effects (not only construction damage) were taken into account into the

final evaluation, according to the given guidelines (Grünthal [9], Grünthal [10]). In order to elaborate damage data, areas with dimensions of about 500x500 m were considered as the basic units, each corresponding to a few urban blocks. Within these blocks the damage grade and the class of vulnerability of the constructions were estimated approximately based on the updated EMS-1998 scale. Airphotos and satellite data were indispensable, particularly in areas that were razed and where almost all of the buildings collapsed (e.g. Adapazari, Gölcük, Kaynasli).

Data recording for the intensity evaluation took place from Yalova to Hendek after the 17 August earthquake and from Hendek to Bolu after the 12 November one. After evaluation of data recordings, an intensity map was obtained according to the EMS-1998 scale, as depicted in Figure 3. The map shows that:

The maximum intensities exceeded I_{EMS98}=XI and locally reached XII (Figure 4) for both earthquakes. During the first earthquake, maximum intensities occurred in the coastal area of Gölcük, in Degirmendere, in Yalova and Adapazari. Particularly, total collapse of the constructions occurred in the coastal area of Gölcük (Figures 5, 6), due to the submergence of the region into the Marmara sea.

Figure 4: Representative view of a portion of Adapazari that suffered total damage (I_{EMS-98} = XII) after the 17 August earthquake.

Figure 5: Reinforced concrete frame structure that collapsed in Gölcük after the 17 August earthquake (grade of damage 5 – class of vulnerability D).

Figure 6: Reinforced concrete frame structure that sustained collapse of ground floor in the area Gölcük – Degirmendere after the 17 August earthquake (grade of damage 5 – class of vulnerability E).

Constructions were affected not only by seismic loading but also by subsidence, tsunamis, lateral spreading and liquefaction. A similar picture was present in the coastal region of Degirmendere. On the other hand, the situation was better in parts of Yalova, because only liquefaction, soil fissures and lateral spreading took place. Parts of Adapazari town were devastated and all buildings collapsed. These sites were dominated by soil fissures, liquefaction, effects of "sedimentary basin" and "basin edge" effects and so on (Kawase [11], Lekkas [12]), which played a significant part in intensity distribution. In Adapazari, tens of buildings sank into the ground, toppled, were partially overturned or collapsed because the soil beneath them liquefied and weakened the foundations (Figure 4). On the other hand, damage was lighter in areas of the town where none of the above phenomena occurred.

Intensities exceeded the I_{EMS-98} = XI degree in a portion of Kaynasli after the 12 November 1999 earthquake, which collapsed thoroughly due to the surface impact of a zone of seismic fissures in the form of a negative flower structure (Lade & Cole [7], Harding [6]), and also due to settlement, lateral spreading and liquefaction. Furthermore, maximum intensities that exceeded degree XI were recorded locally in Düzce.

I_{EMS-98} = X intensities were present in a wider area that formed two elongated zones in both seismic events. Specifically after the 17 August earthquake, X intensities occurred in an E-W zone that began at Yalova, were found again at Gölcük, passed through Izmit and stopped in Sapanca lake. The zone reappeared in Adapazari and terminated east of the town. After the 12 November 1999 earthquake, I_{EMS-98} = X contours were arranged in a similar E-W trending zone, which covered the areas east of Hendek, in Düzce and Kaynasli where constructions where totally damaged locally (Figures 7, 8). The estimation of the intensities attributed to the second earthquake was almost impossible to make (12 November 1999) in the wider area of Hendek, because constructions had already been damaged by the earthquake of 17 August 1999 and their vulnerability had increased. Also it was impossible to define the amount of increase of vulnerability of the constructions after the first (17 August) earthquake. The effect of both earthquakes was estimated approximately, incorporating the damage from both earthquakes. It was recorded that the first earthquake exhibited maximum intensities that reached I_{EMS98} = VIII in an E-W zone in the Hendek area, while after the second earthquake intensities locally approached I_{EMS98}=X. This may be partly attributed to the fact that the resistance of the constructions had already been weakened by the first earthquake and their vulnerability had already increased.

I_{EMS-98} = IX contours covered a wider E-W zone after each earthquake. This intensity zone coincides with the deformation zone, and is wider where pull apart basins, oversteps flower structures and other strike-slip deformation features occurred.

I_{EMS-98} = VIII intensities also developed in an E-W zone after each earthquake. In this case, intensities seem to have been significantly controlled

Figure 7: Reinforced concrete frame structure in Yalova which displayed first story column-hinge deformation, but did not collapse after the 17 November earthquake (grade of damage 5 – class of vulnerability D).

Figure 8: Reinforced concrete frame structure at Gölcük which displayed light structural damage but heavy damage to the infill brick walls after the 12 November earthquake (grade of damage 5 – class of vulnerability D).

by site effects and the high vulnerability and the remarkably poor performance of the constructions. More specifically, the distribution of VIII contours depended on the foundation soil response and mainly on the amplification of seismic waves when, for example, loose thin surficial formations overlaid the alpine basement. It also depended on the alpine basement geometry which controls the seismic energy propagation.

It is noteworthy that high intensities were also recorded at quite large epicentral distances, particularly in Istanbul, Eskisehir, Bursa and so on. These intensities appeared as islets within urban areas, which displayed lighter damage. At the suburb of Avcilar in Istanbul, $I_{EMS\text{-}98}$ = X intensities were attributed to (i) the frequency content of the seismic vibration (Lekkas et al. [1]), that is, the relatively high periods and the long duration of the vibration, (ii) the geological formation, and (iii) the relatively high natural period of the six-story constructions, most of which collapsed (Cranswick et al. [13]).

5 Conclusions

The earthquakes of 17 August and 12 November 1999 which struck Turkey and caused thousands of fatalities and widespread damage were attributed to the successive reactivation of two parts of the North Anatolian Fault Zone; these segments had not slipped before in the twentieth century. The overall rupture could be traced for a distance of 150 km. The fault rupture was accompanied by pull-apart basins, oversteps, en echelon arranged fractures, flower structures and other strike-slip related features on both a small and a large scale.

Damage recording and intensity evaluation were made according to the updated EMS-1998 scale, soon after both seismic events in the affected area.

According to the previous paragraphs, intensities exceeded I_{EMS98}=XI and even approximated XII in many urban blocks. X intensities occupied extended regions, whereas much wider areas displayed IX and VIII intensities. Intensity distribution map illustrates intensities from VII to XI because lower intensities were spread in vast areas impossible to cover.

All intensity contours, but mainly the $I_{EMS\text{-}98} \geq$ X, developed in an E-W orientation, which coincided with the fault strike. Intensity contours followed and became broader at strike-slip deformation structures as micro- and macro-pull-apart basins, flower structures and so forth. On the other hand, when the fault ruptured linearly, without these accompanying structures, intensity contours developed in an E-W elongated zone of significantly small width.

Moreover, intensity distribution also depended, apart from the two seismic vibrations and the vulnerability of the constructions, on the concomitant geodynamic phenomena, namely liquefaction, uplift, subsidence, settlements, lateral spreading and so on. Therefore, the two earthquakes were not solely responsible for damage occurrence. So it is the concomitant geodynamic phenomena which must also be considered seriously in future seismic events. The updated EMS-1998 scale does not incorporate such phenomena due to the rarity of actualistic models.

In the wider area of Hendek that was hit by both earthquakes (17 August and 12 November 1999), it was difficult to assess separately the participation of each seismic event in damage manifestation and, thus, in intensity estimation. Intensity evaluation was approximated in this area and is based on data and recordings collected mainly after the first earthquake, but also after the second. So it is apparent that in this area the recorded intensities do not correspond to the damage caused by the second event only, since the first earthquake had already vibrated constructions and had increased their vulnerability.

The recorded intensities were distributed similarly on both fault blocks as a consequence of the predominant horizontal movement of the NAFZ; opposite to a case of reverse or normal faulting (hanging wall and footwall) (Lekkas [14]) that intensities vary significantly on the two blocks of a rupture.

Finally, beside the meizoseismal area, islets of high intensities were observed in the wider area (e.g. Istanbul) as a result of the frequency content of the seismic vibration, as it was modified at that epicentral distance, and was coupled with soil response and the vulnerability and the characteristics of constructions.

References

[1] Lekkas, E., Dandoulaki, M., Ioannides, K., Lalechos, S. & Kiriazis, A. Izmit earthquake, Turkey 1999. Seismotectonic settings – Earthquake and ground motion characteristics – Geodynamic phenomena – Damage typology and distribution. *13th Hellenic Concrete Conference*, Special Issue, Rethimno, 1999.

[2] Stein, R., Barka, A. & Dieterich, H. Progressive failure on the North Anatolian fault since 1939 by earthquake stress triggering. *Geophysical Journal International*, **128**, pp. 594-604, 1997.

[3] Armijo, R., Meyer, B., Hubert, A. & Barka, A. Westward propagation of the North Anatolian fault into the northern Aegean: Timing and kinematics. *Geology*, **27(3),** pp. 267-270, 1999.

[4] Straub, C., Kahle, H.G. & Schindler, C. GPS and geological estimates of the tectonic activity in the Marmara Sea region, NW Anatolia. *Journal of Geophysical Research*, **102**, pp. 27587-27601, 1997.

[5] Aydin, A. & Nur, A. Evolution of pull-apart basins and their scale independence. *Tectonics*, **1**, pp. 91-105, 1982.

[6] Harding, T.P. Seismic characteristics and identification of negative flower structures, positive flower structures and positive structural inversion. *Bull. Am. Ass. Petrol. Geol.*, **69**, pp. 582-600, 1985.

[7] Lade, P. & Cole, D.Jr. Influence zones in alluvium over dip-slips faults. *J. Geot. Eng.*, ASCE, **110**, pp. 599-615, May 1984.

[8] Mann, P., Hempton, M.R., Bradley, D.C. & Burke, K. Development of pull-apart basin. *J. Geol.*, **91**, pp. 529-554, 1983.

[9] Grünthal, G. (ed.) European Macroseismic Scale 1992 (up-dated MSK-scale). Conseil de l' Europe, **7**, 79p, 1993.

[10] Grünthal, G. (ed.) European Macroseismic Scale 1998. Conseil de l' Europe, **15**, 99p, 1998.
[11] Kawase, H. The cause of the damage belt in Kobe: "The Basin-Edge Effect," constructive interference of the direct S-wave with the basin-induced diffracted/Rayleigh waves. *Seismological Research Letters*, **67**, pp. 25-34, 1996.
[12] Lekkas, E. New data for seismic hazard analysis. *Risk Analysis II*, ed. C.A. Brebbia, Wit Press: Southampton, pp. 245-255, 2000.
[13] Cranswick, E., Meremonte, M., Safak, E., Overturf, D., Frankel, A., Ozel, O. & Erdik, M. Damage site response and building response in Avcilar, west of Istanbul, Turkey. Seismological Society of America '00. *95th Annual Meeting*, Abstract, San Diego, California, 2000.
[14] Lekkas, E. Analysis of damage parameters of the Chi-Chi Taiwan earthquake. *Risk Analysis II*, ed. C.A. Brebbia, Wit Press: Southampton, pp. 419-432, 2000.

CHAPTER 12

Seismic strike-slip faults on a major boundary transverse to the Apenninic chain; the case of Molise (S. Italy) earthquake (31 October 2002).

S. G. Lozios, G. D. Danamos & E. L. Lekkas
Faculty of Geology, University of Athens, Greece.

Abstract

On 31 October 2002, a severe earthquake of Mw=5.9 struck the Molise province in southern Italy. The earthquake occurred in an area which is characterized by both an absence of significant neotectonic faults and low seismicity, since no historical strong earthquakes have been reported. Neighbouring seismogenic areas are located westward along the NW–SE normal seismogenic belt of the central and southern Apenninic chain, as well as eastward along the Gargano promontory of the Apulian platform, which is mainly deformed by E–W strike-slip faults. The Molise earthquake seems to be directly related to the second seismogenic source because the epicentral area is located at the westward prolongation of the E–W strike-slip Mattinata Fault which bounds the southern part of the Gargano promontory. Moreover, the preliminary fault plane solution, the distribution of the aftershock sequence and the damage show that the seismogenic fault is also a strike-slip one in the same E–W direction. The only evidence of surface faulting was the presence of two small ruptures trending E–W and N–S, accompanied by strike-slip right-lateral and left-lateral movement respectively. The kinematic data are compatible with the fault plane solution.

1 Introduction

On 31 October 2002, a strong seismic event occurred in the Molise province in southern Italy (about 60 km WNW of Foggia or about 115 km NNE of Naples), followed by a second of similar magnitude the next day, resulting in 29 casualties and heavy damage in the epicentral area. Most of the victims were found in a collapsed school at the community of S. Giuliano di Puglia, where 26 children

(aged three to ten years old) and one teacher lost their lives. The earthquakes were felt all over the Molise province but they caused damage only in certain villages in the wider epicentral area.

The magnitude of the main shock was M_w=5.9 (according to USGS) or M_w=5.7 (according to INGV – Instituto Nazionale di Geofisica e Vulcanologia) and that of the strongest aftershock, which occurred the following day, was M_w=5.8 (USGS) or M_w=5.7 (INGV). The foci are shallow since the focal depth for both shocks was about 10 km (U.S.G.S.) or 20 km (INGV).

The Italian peninsula is characterized by strong catastrophic earthquakes, such as the 1977 Umbria, central Italy, earthquake (M_w=5.6, 11 casualties), the 1980 Eboli earthquake, south of Naples, (M_w=7.2, 2,735 casualties), the 1976 Friuli earthquake, north-east Italy, (M_w=6.5, 976 casualties), the 1915 Avezzano earthquake, southern Italy, (32,000 casualties), the 1908 Messina Strait earthquake (82,000 casualties), the 1905 and 1783 Calabria earthquakes (5,000 and 50,000 casualties respectively) and the 1693 southern Italy earthquake (60,000 casualties in Sicily and 93,000 in Naples).

The seismic event of 31 October 2002, occurred in an area that does not host high seismicity, since no major historical earthquakes have been reported.

The purpose of this paper is to correlate the neotectonic structure of the affected area to the seismotectonic regime of the earthquake, the distribution of the geotechnic effects and the damage.

2 Geodynamic frame of the Italian peninsula

At the major area of the Italian peninsula several geodynamic units can be recognized, such as the "Alpine thrust system", the " Po plain", the "Apennine thrust system" and the "Calabrian arc" from north to south and the "Sardinia–Corsica block", the "Tyrrhenian extensional basin" and the "Adriatic block" from west to east (Figure 1).

The Apennines, which constitute the core of the Italian peninsula, south of the Po basin, belong to the southern branch of the alpine system of the Tethys which is characterized by tectonic movement and vergence of the large scale tectonic structures (folds, thrusts, etc.) towards the E-NE over the Apulian platform, which is considered as a part of the African plate (Aubouin [1], Disperati et al. [2], Elter & Scandone [3], Jolivet [4]). Southward, the Calabrian arc represents the boundary between the Apennine mountain range and the oceanic Mesozoic crust of the eastern Mediterranean (segment of the Tethys ocean). On the contrary, to the west of the boundary lies the oceanic basin of the Tyrrhenian Sea which represents a younger structure (Miocene – Upper Pliocene), (Jolivet [4], Meletti et al. [5]). Thus, a compressional geodynamic regime is recognized in the front of the Apennines towards the Adria plate (Apulian platform) and an extensional one to the west (Tyrrhenean basin).

The present seismotectonic regime of Italy is rather complex and bears important differences from the north to the south, as is obvious from the seismic and borehole breakout data (Mariucci & Muller [6]) as well as from the kinematic and dynamic data of the neotectonic faults. In particular, a more systematic

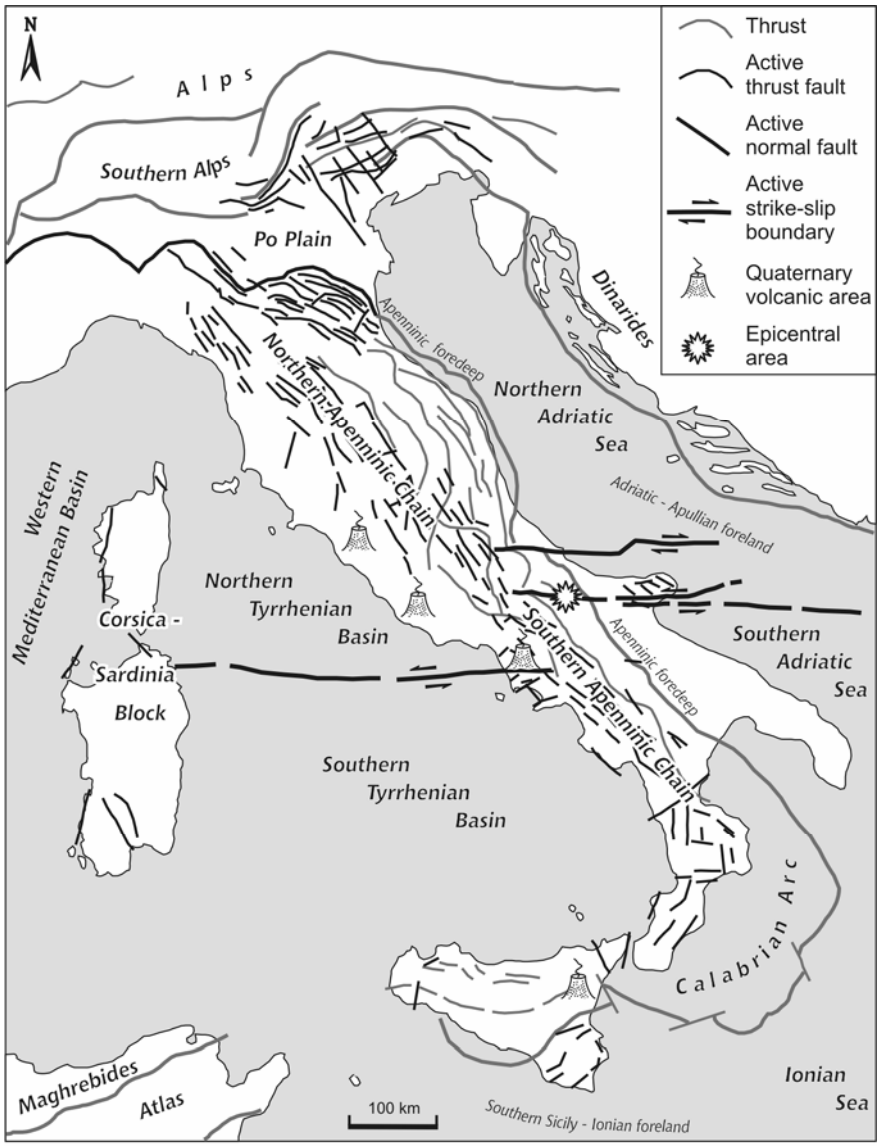

Figure 1: Schematic structural setting of Italy where the main geodynamic units and the E-W significant active strike-slip boundary (Favali et al. [8]) are presented.

variation of the tectonic regime is observed from SW to NE, as well as homogeneity in the central Apenninic belt and complexity to the north. Thus, at the northern Apennines (northern Adriatic foredeep), it seems that the Late Miocene uplift, and the following slab detachment and its southward migration along the

Apenninic chain, are accompanied by apparent normal or oblique-slip normal faults of NW–SE strike (NE–SW extension) in the upper crust (Figure 1). Deeper, however, where passive slab sinking occurs, strike-slip or thrust faults (NE–SW compression) dominate.

Along the Apenninic belt, the tectonic regime is mainly identified by NW–SE normal faults, resulting from the NE–SW extension that followed the upward flexure and the decompression of the Apennines (Mariucci & Muller [6], Meletti et al. [5]). In the southernmost Apenninic foredeep and in the Apulian foreland, the tectonic regime is expressed by both normal and strike-slip faults. In the Tyrrhenian coastal region the tectonic regime is characterized by normal or oblique-slip normal faults of basically NE–SW strike. In southern Italy, the tectonic regime is more complex in the wider area of the Calabrian arc because it is still controversial as to whether there is active subduction or persisting passive sinking of the Adria lithosphere. Both shallow and deep earthquakes occur in this area with focal mechanisms that show mainly strike-slip or transpressional zones rather than normal faulting.

These important changes of the seismotectonic characteristics along the Italian peninsula suggest a certain fragmentation of the foreland area through large-scale strike-slip zones that are developed across the Apenninic structure. These zones probably represent old transform faults such as those found in southern Sicily, in the Sicily channel, in the Gargano–Tremiti region and in the Central Adriatic Sea (Mariucci & Muller. [6]).

3 Geological frame and seismotectonic regime of the wider affected area

The wider affected area is located at the Gargano-Apulian peninsula, in southern Italy. The main alpine geological structure of this area is the thrust of the flysch-molasse type sediments of the external Apennines over the continental carbonate deposits of the Apulian platform (Aubouin [1], Jolivet [4]), (Figure 1). The latter corresponds to the main foreland of both the Apennines to the west and the Dinarides to the east.

The shallow Apulian platform (Gargano-Apulia), (Aubouin [1]) in the south-eastern part of the Italian peninsula is characterized by the deposition of thick-bedded neritic limestones from Triassic to Tertiary, mainly representing reef phases, some thousands of meters thick. Typical outcrops of these carbonate deposits, which are almost horizontal without large scale deformation, can be observed along the road from Bari to Foggia. These sediments represent the relative autochthonous sequence (Figure 2).

The para-autochthonous sediments of the external Apennines, which are thrusted over the Apulian platform to the east, represent a clastic sequence consisting of white-yellow and blue-grey marls with alternations of sandstones close to the front of the thrust. In the inner parts the alternations consist of white marls, sandstones, pelites and white marly limestones.

This clastic sequence represents syn-orogenic flysch-molasse type sediments, deposited at the Italian–Dinaric foredeep, which was developed around the

Apulian platform during the syn-orogenic stage of the Alpine orogen that followed the final collision between the Apulia (northern promontory of the African plate) and the European plate margins of the Apennines and Dinarides (Aubouin [1], Disperati et al. [2], Jolivet [4]).

This sequence is tectonised, folded and thrusted (Figure 2) with tectonic transport from SW to NE during the Upper Miocene – Lower Pleistocene (Aubouin [1], Disperati et al. [2], Elter & Scandone [3]).

From a seismotectonic point of view, the affected area lacks important neotectonic structures or high seismicity. Active faults relating to strong earthquakes can only be found both to the west in the wider Isernia region (Apenninic chain) and to the east in the Gargano promontory (Apulian platform), bearing significant seismotectonic differences in each case (Figure 3).

The wider Isernia region is located on an important geological boundary representing the geometrical and structural discontinuity separating the northern from the southern Apennines with major morphological, tectonic differences as well as significant changes in seismicity and the geophysical data (Di Bucci et al. [7]). This boundary might be regarded as a persistent segment boundary, forming a long-term barrier to the propagation of rupture of active fault systems in this area (Figures 1 and 3).

The general neotectonic structure shows that all along the core of the Apennines a subsequent major phase of SW–NE extension has overprinted the compressional structures since the Middle Pleistocene. This tectonic regime is still active today, and therefore the youngest structures of the Apennines show a general NW–SE orientation and are responsible for the strongest earthquakes in this region. Well-known active fault zones (Figure 3) bearing significant differences on both sides of the boundary between the northern and southern Apennines are (Di Bucci et al. [7]):

- The Aremogna – Cinque Miglia – Mt. Rotella fault system (ACRFS), which is composed of NW–SE normal faults that cut Pleistocene and Holocene sediments.
- The Upper Sargano Valley fault system (USFS), which consists of normal and left-lateral strike-slip NW–SE faults.
- The Boiano Basin fault system (BBFS), which shows a complex extensional pattern and consists of a system of NW–SE synthetic and antithetic Quaternary normal faults linked with shallow pre-Quaternary E–W high angle faults reactivated by the SW–NE active extensional stress field.
- The Carpino and Le Piane fault system (CLPFS), consisting of NNW–SSE normal faults and where the most recent tectonic activity is consistent with the extensional regime which has acted since the Middle Pleistocene in this part of the Apennines chain.

Known earthquakes (Figure 3) relating to these active faults are (data from INGV): the 1984 Sangro River Valley earthquake (M_S=5.5), the 1805 Boiano earthquake (M=6.6) and the 1456 Gruppo di Lavoro earthquake (M=7.1).

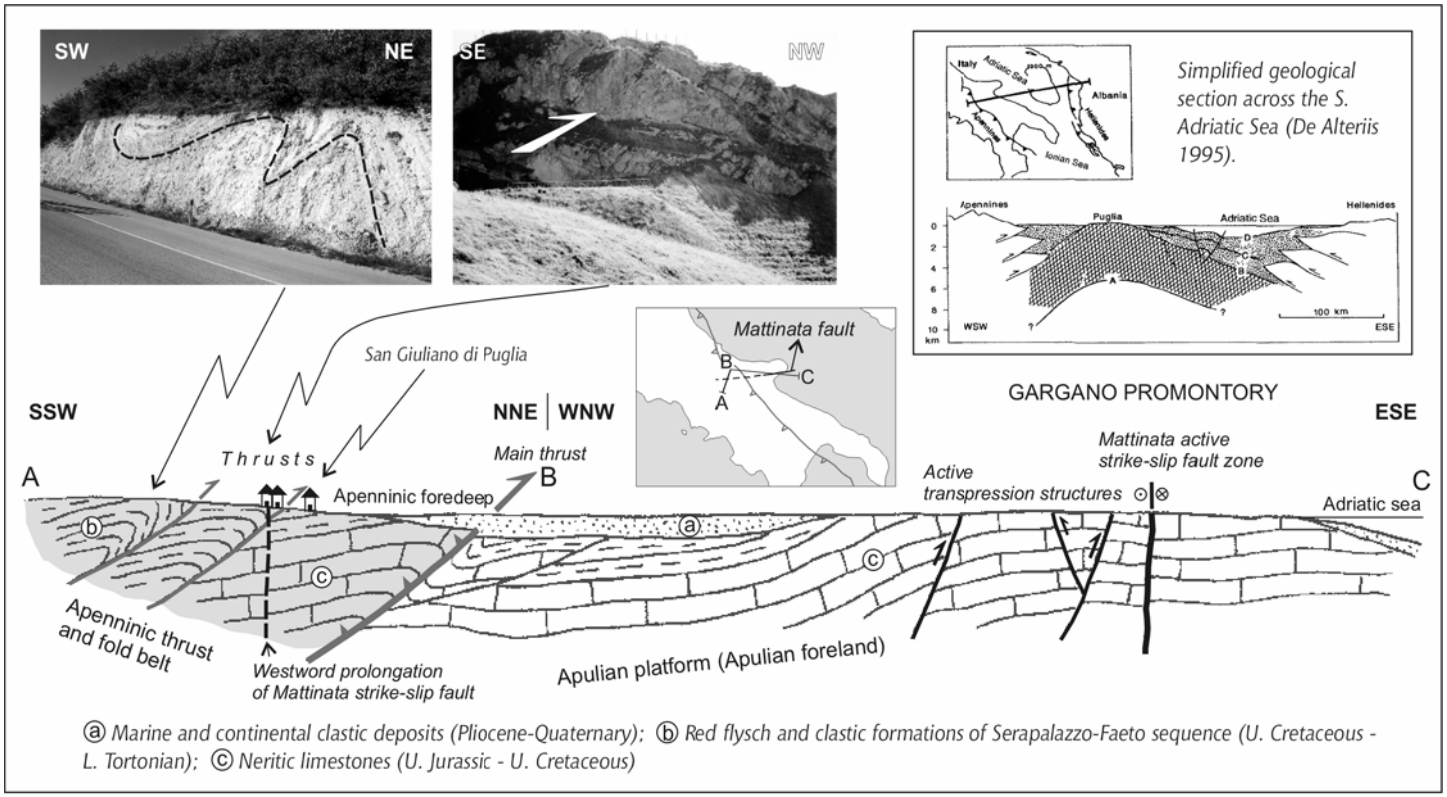

Figure 2: Geological and structural sketch from San Giuliano di Puglia to the Gargano promontory and Adriatic Sea.

The active structures of the Gargano Promontory dominate to the east of the affected area, which represents a structurally high area where Mesozoic rocks rise about 1000 m above sea level. Two main tectonic zones, trending E–W, can be observed. The first of these, known as the Mattinata fault, is located on the southern margin of the Gargano peninsula and the second is located on the northern margin, in the wider region of the Tremiti Islands (Figure 3). These zones also extend for some tens of kilometers at the bottom of the Adriatic Sea separating the northern from the southern part of the area and exhibiting significant morphological and seismotectonic differences (Favali et al. [8]).

The kinematic and dynamic data along the above zones show strike-slip faults but the sense of shear is still controversial (Billi [9], Favali et al. [8], Salvini et al. [10]). The Tremiti Islands Fault has been interpreted as right-lateral but the Mattinata Fault as right-lateral, left-lateral, right to left lateral or left to right lateral inverted, undetermined strike-slip or reverse, although the prevalent interpretation agrees with a left-lateral strike-slip fault (Billi [9]). The tectonic data along the fault surface reveal complex kinematics and indicate (Favali et al. [8]): (i) E–W strike-slip left-lateral fault, partialy transferred to NW–SE trending strike-slip left-lateral faults, (ii) minor reverse faulting (ENE–WSW compressional deformation), and (iii) pull-apart structures with E–W and NW–SE oblique-slip to dip-slip normal faults accompanied by second order left-lateral strike-slip E–W faults.

Although there are not enough seismological data for this region, the fault plane solutions of some recent earthquakes which occurred in the offshore area (three main shocks: 1986 M_b=4.2, 1988 M_b=5.3 and 1989 M_b=4.7), (Favali et al. [8]) are in accordance with the tectonic data and display strike-slip faulting accompanied by a small thrust component. It should also be noted that the epicentres of earthquakes reported in the central Adriatic Sea are roughly aligned along an E–W direction parallel to these strike-slip zones. For this reason, some authors interpret the Adriatic block as a single, rigid, almost aseismic block (Favali et al. [8]). It is also mentioned that medium-magnitude shallow earthquakes, due to NE–SW normal fault reactivation as the fault plane solutions show, have been reported at the N-NE part of the Gargano promontory such as that of 30September 1995 with M_w=5.2.

These E–W trending strike-slip zones are directly related to the evolution of the Gargano Promontory. This part of the Apulian platform has been uplifted by near vertical E–W or NW–SE faults since the Eocene. Most of these faults show evidence of early dip-slip movements compatible with uplift, and subordinate oblique to strike-slip motion due to younger reactivation. The structural analysis together with other geophysical and geological data reveal that the Gargano Promontory represents a push-up structure generated by the interaction of the E–W trending left-lateral strike-slip Mattinata fault system (MFS) southward and the E–W to NE–SW trending right-lateral strike-slip Tremiti Islands fault system (TIFS) northward (Favali et al. [8]).

It is underlined that this important tectonic zone, which is characterized by large-scale strike-slip faults and represents a seismically active deformation belt that cuts across the Adriatic basin, seems to be significant for the evolution not

only of the Adriatic block but also of the entire Italian peninsula as well as of the Tyrrhenian Sea (Favali et al. [8]). A possible westward prolongation of this tectonically active boundary up to the Tyrrhenian Sea, through the Apennines, is confirmed by important structures both in the Italian peninsula (boundary between the northern and the southern Apennines) as well as in the Tyrrhenian Sea (boundary between the northern and and southern Tyrrhenian Sea) and it has been interpreted as a transform fault (Figure 1).

Recent data from GPS velocities (Oldow et al. [11]) confirm this seismically active boundary and show that it is a quite complex structure. Therefore, it passes around the southern and eastern margins of the Tyrrhenian Basin, crosses Central Italy, extends into the Adriatic Sea and follows the western margin of the Dinaride tectonic belt. Along the Southern Apennines and the Adriatic coast the velocities of GPS measurements show movement towards the N, NNE and NW which are consistent with extension along the mountain belt and contraction across the foreland.

Submarine research and seismic profiles in the central Adriatic Sea reveal that E–W or NE–SW trending transpressional structures deform the sea floor, indicating recent activity, and together with the seismicity they provide a link between E–W trending faults of the Southern Dinaride belt and similarly oriented structures along the Adriatic margin of central Italy (De Alteriis [12]).

4 The earthquake parameters

The seismic sequence is emphasized by two main seismic events. The first and stronger of these (31 October) showed a magnitude of M_w=5.9 on the Richter scale (USGS) or M_w=5.7 (INGV), while the second one (1 November) bore a magnitude of M_w=5.8 (USGS) or M_w=5.7 (INGV). In both cases the earthquakes were shallow with a focal depth of the order of 10 km (USGS) or 20 km (INGV).

The two shocks and the aftershock sequence occurred in an area (a few km west of S. Giuliano di Puglia) that does not historically host major earthquakes and consequently is not classified in the current seismic codes.

The strongest historical and present-century earthquakes in the neighboring areas were (data from INGV): (i) the Apenninic sequence of December 1456, M=7.1 (about 50-60 km to the S-SW of the recent seismogenic source), which caused heavy damage, (ii) the Gargano sequence of July–August 1627, M=6.8 (about 40-50 km to the east of the recent seismogenic source), which caused damage estimated at 8-9 degree MCS, and (iii) the Matese earthquake of July 1805, M=6.6 (about 50-60 km to the W-SW of the recent seismogenic source), with damage estimated at 6 MCS (Figure 3).

The 1456 and 1805 strong events, as well as a great number of strong or medium earthquakes, occurred along the main normal faulting seismogenic belt that runs along the crest of the central and southern Apennines. On the contrary, the epicenter of the 1627 catastrophic earthquake was located near the western margin of the Gargano promontory. Weaker earthquakes have also been reported, mainly to the east (about 60-100 km from the recent seismogenic source), such

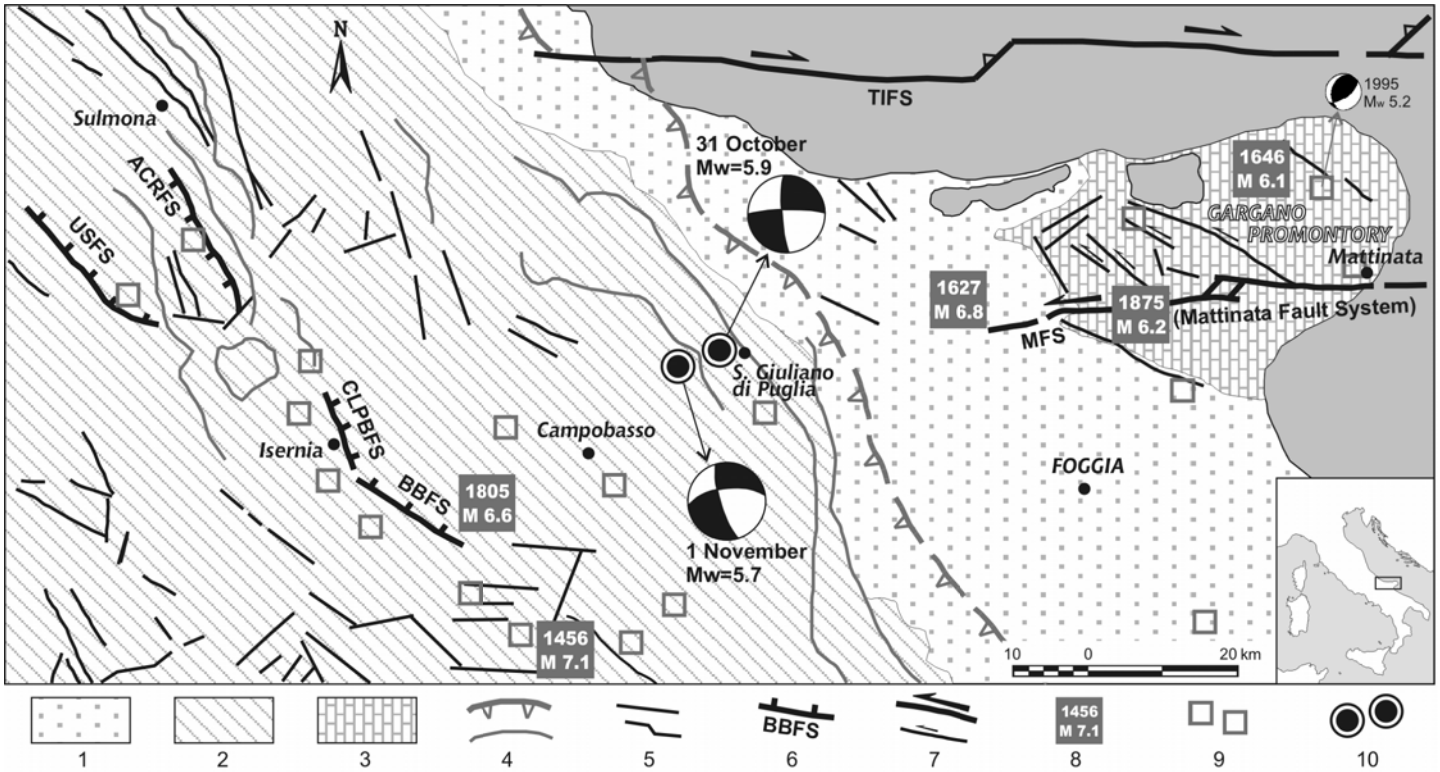

Figure 3: Seismotectonic regime of the wider affected area. [1. Marine and continental clastic deposits (Pliocene-Quaternary); 2. Parautochthonous clastic sediments of the ext. Apennines (Triasic-Tertiary); 3. Shallow neritic limestones of the Apulian platform (Triasic-Tertiary); 4. The main thrust of the Apennines over the Apulian platform and minor thrusts within the Apennines; 5. Active normal faults; 6. Significant active normal fault systems (see text); 7. Active strike-slip fault systems and faults; 8. The strongest catastrophic earthquakes; 9. Strong and medium earthquakes; 10. Main shock and strongest aftershock].

as the 1646 earthquake (M=6.1) at the NE part of the Gargano promontory and the 1875 earthquake (M=6.2) near the western part of the Mattinata Fault.

The moment-tensor solutions for both the main shock and the strongest aftershock (data from USGS and INGV) show that they occurred as the result of movement on a strike-slip fault with the two nodal planes trending N–S and E–W. Thus, according to the focal mechanism, the seismic fault would be either the N–S left-lateral fault or the E–W right-lateral one (Figure 4).

Elaboration of the aftershock sequence data, recorded by a local network (data from INGV), showed that the spatial distribution of the surface projection of the aftershocks follows an E–W narrow zone (about 30 km in length). This zone extends from the S. Giuliano region to the east up to the S. Angelo region to the west and represents the surface projection of the seismogenic source (Figure 4). The 3-D projection of the aftershock sequence shows that the depths of the aftershocks vary from about 10 to 23 km as well as that the seismogenic fault is almost vertical.

5 Tectonic structures, geotechnical effects and damage distribution

As the fieldwork in the wider epicentral area showed, no neotectonic structures related to active faults, were observed. The hilly relief of the area results in distinctive morphological axes in the NW–SE direction which in most cases coincide with thrusts, reverse faults and folds, as a result of the deformation caused by the nappe emplacement of the Apennines over the Apulian foreland. Minor morphological axes or other morphological anomalies (scarps, drainage network asymmetries, etc.) are found in the NE–SW or E–W direction, and are probably a result of the neotectonic deformation but they cannot be directly related to active faults.

Most of the villages hit by the earthquake were founded on the para-autochthonous clastic sequence that is thrusted over the Apulian platform. This sequence consists of alternations of marls, sandstones and marly limestones that are folded and crossed by thrusts or other discontinuities (Figure 2). The steep relief in combination with the lithology and the geometry of rock discontinuities (thrusts, folds, bedding, etc.) forms slopes with high instability and susceptible to landslides. Many of these phenomena occurred during the earthquake, were detected in the wider epicentral area and were usually represented by small-scale landslides and rock-falls. Their spatial distribution, although scattered, shows a secondary E–W zonation (Figure 4).

A large number of open cracks and extensional ruptures, from one meter to several tens of meters long and with different orientations, were observed in the affected area. These ruptures usually exhibited openings of the order of some mm or cm and a vertical displacement of several cm. All of these ruptures were the result of geotechnical effects that occurred during the earthquake, such as slope failures, surficial sliding and landslides, usually along steep slopes, road cuts, and so on.

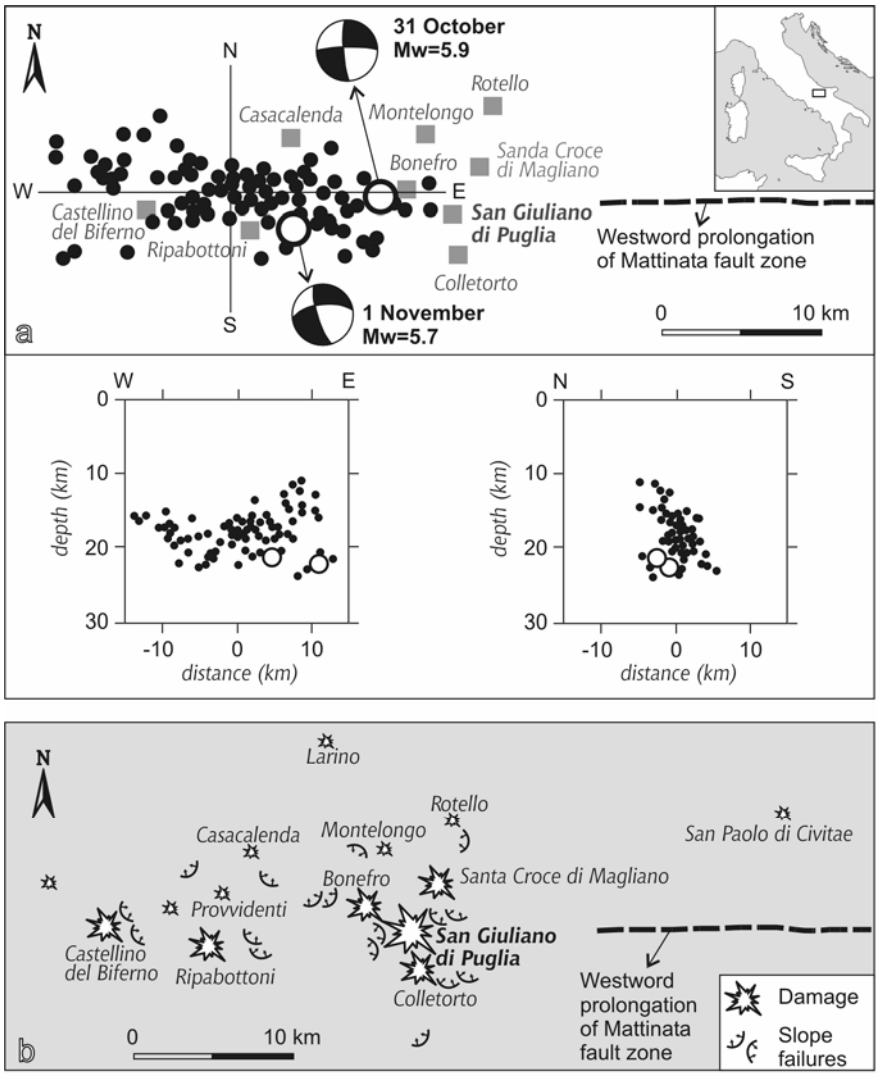

Figure 4: The spatial distribution of the aftershock sequence (a), as well as the distribution of the damage and the slope failures (b), are aligned along the same E-W direction, revealing the direction of the seismic fault.

In only two cases do the observed ruptures seem to be related to the seismic event. The first (Figures 5a,c) was located on the road that leads to S. Giuliano village, just before the entrance to the village (about 100 m from the houses of the eastern part of the village); it was approximately 20 m long and crosscut the road and the concrete retaining wall as well as the bedrock of clastic formations. The rupture bore a N80^{0}E strike and was accompanied by strike-slip right-lateral

offset of the order of only 1 cm. The second (Figures 5b,c) was located on the road from Colletorto village to S. Giuliano, with a N–S strike and a length of about 10 m. The kinematic data show a left-lateral strike-slip movement of the order of 3-5 mm. The geometric and kinematic features of these ruptures, and the fact that they don't seem to be related to landslides or other slope failures, lead to the conclusion that they probably represent seismic fractures, which coincide with the surface expression either of the seismic fault or of a secondary branch fault. On the other hand, the absence of similar ruptures shows that the mezoseismal area is also characterized by the absence of significant surface faulting. This is probably due to the small magnitude of the earthquake, the geotechnical characteristics of the geological formations and the conditions of the fault propagation to the surface.

The damage distribution is another factor which usually gives us much information about the seismotectonic characteristics of an earthquake. In this case the buildings of the affected villages were mainly old structures and rarely modern ones, and as was expected the old buildings suffered most damage. Human intervention without previous technical studies created favorable conditions for the collapse of these buildings in most cases, such as that of the school in S. Giuliano with such tragic results.

Most of the damage occurred in S. Giuliano di Puglia rather than Colletorto, Bonefro or Santa Croce di Magliano. Serious damage occurred to the west of Castellino del Biferno and at Ripahottoni about 20 km from S. Giuliano. Minor damage was also observed in other villages in the wider area, while the earthquake was felt as far as Lucera to the south-east and the Termoli to the north.

The distribution of the damage and the macroseismic intensities follows the S. Giuliano – S. Angelo axis (Figure 4) and is clearly aligned along an E–W direction, an observation that was also made for the aftershock distribution as well as for the geotechnical effects.

6 Discussion – conclusions

The Molise 31 October 2002, M_w=5.9, earthquake struck an area that is characterized by low seismicity, since no strong earthquakes have been reported. Moreover, as the fieldwork showed, there are no important neotectonic faults in the wider mezoseismal area. No evidence of significant surficial expression of the seismogenic fault was found in the affected area, either in the form of a reactivated fault surface or in the form of a zone of surface ruptures. The open cracks and the extensional ruptures, which are observed mostly along the roads and the steep slopes, are associated mainly with landslides and slope failures (Figure 4). The only exception was the presence of two ruptures, some tens of meters long, between Colletorto and S. Giuliano, which showed an approximately N–W or E–W direction and a left-lateral or right-lateral strike-slip offset of the order of 5 mm or 1 cm (Figure 5).

The main problem of the Molise earthquake concerns the kinematic and dynamic regime of the seismogenic fault as well as the seismic source that is related to this seismic sequence. The narrow region, characterized by high seismic-

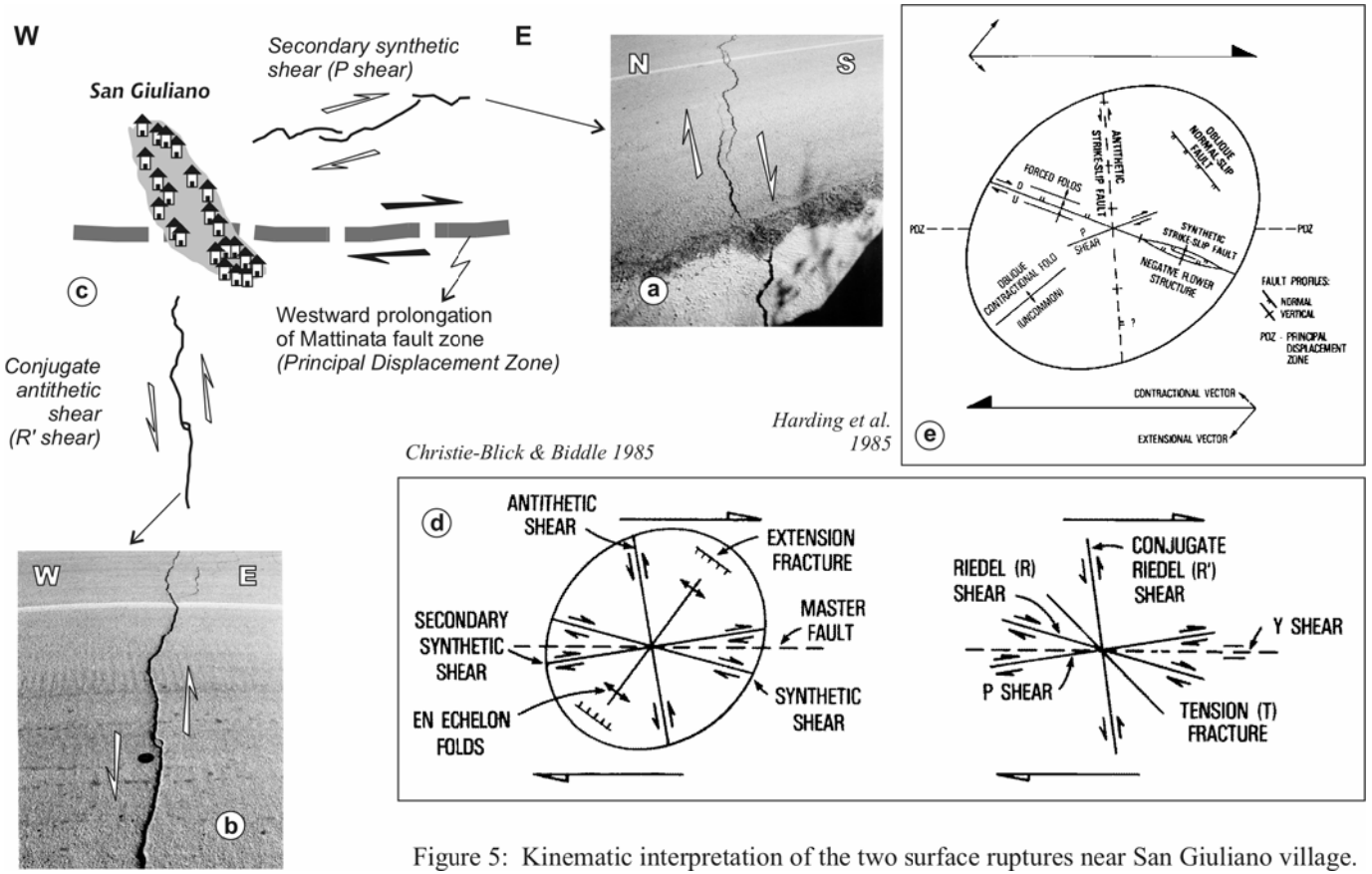

Figure 5: Kinematic interpretation of the two surface ruptures near San Giuliano village.

ity, is located about 60-70 km to the west (Figure 3) along the NW–SE normal seismogenic belt of the central and southern Apenninic chain (Di Bucci et al. [7]). Another seismogenic area (Figure 3), in a different geodynamic regime, however, lies about 80-100 km to the east, in the Gargano promontory. This area belongs to the Apulian platform and the Adriatic block and is characterized by E–W strike-slip faults (Favali et al. [8]). The prolongations of these faults to the west, to the Tyrrhenian Sea, form a zone which reveals an important geological boundary with fundamental lithospheric changes between the northern and southern parts (Figure 1).

The Molise earthquake seems to be directly connected to the eastern seismogenic area (Gargano promontory area) for the following reasons:

- The epicenters of the main shock and the aftershock sequence coincide with the westward prolongation of an E–W fault zone, which is the boundary between the southern margins of the Gargano promontory (known as the Mattinata fault system) and is characterized by left-lateral strike-slip movement (Figure 3).
- The focal mechanisms of the main shock and the strongest aftershock show a strike-slip fault that can be either N–S and left-lateral or E–W and right-lateral (Figure 4).
- The spatial distribution of the surface projection of the aftershock sequence depicts a distinctive E–W narrow zone and suggests that the seismogenic fault is the E–W one (Figure 4).
- The damage distribution and the macroseismic intensities follow the same E-W direction. Even the geotechnical effects, which present scattered distribution while they are controlled by high slope instability, show a secondary E–W zonation (Figure 4).
- From the two observed ruptures which seem to be related to the seismic event (Figure 5), the dominant was the $N80^0E$ one, with a right-lateral strike-slip offset that coincides with the fault-plane solution of the seismic fault. This rupture probably represents a secondary synthetic shear (P shear) due to the E–W strike-slip right-lateral shear along the seismic fault, which probably represents the principal displacement zone (PDZ), (Christie-Blick & Biddle [13], Harding et al. [14]), (Figure 5).
- From a kinematic point of view, the second N–S left-lateral strike-slip rupture is similar to the second of the nodal planes and probably represents the antithetic conjugate shear (R´shear) (Figure 5).

The correlation of the kinematics of the seismogenic fault to the kinematics of the Mattinata Fault zone is really obscure. The focal mechanism (as well as the observed E–W surface rupture) shows right-lateral movement for the E–W seismic fault, although the Mattinata Fault shows left-lateral movement. Because the Mattinata Fault System is a very complex fault zone, the fault segments could be interpreted as right- or left-lateral as well as right- to left-lateral or left- to right-lateral inverted (Billi [9], Favali et al. [8], Salvini et al. [10]).

References

[1] Aubouin, J. Alpine Tectonics and Plate Tectonics: Thoughts about the Eastern Mediterranean. *Europe from Crust to Core*, eds. D.V.Ager & M.Brooks, pp. 143-158, Wiley: London, 1976.

[2] Disperati, L., Liotta, D. & Carmignani, L. Short explanation to the terrane map of the northern Apennines (Italy). I.G.C.P. Project No 276, Terrane Maps and Terrane Descriptions. *Ann. Geol. des Pays Hell.*, **37**, pp. 211-217, 1996.

[3] Elter, P. & Scandone, P. Geologie des Chaines alpines issues de la Tethys. *Mem. du B.R.G.M.*, **115**, pp. 99-102, 1980.

[4] Jolivet, L. *La deformation des Continents.* Hermann, ed. des Sc. et Ar., 1997.

[5] Meletti, C., Patacca, E. & Scandone P. Construction of a Seismotectonic Model: The case of Italy. *Pure Appl. Geophys.*, **157**, pp. 11-35, 2000.

[6] Mariucci, M.T. & Muller, B. The tectonic regime in Italy inferred from borehole breakout data. *Tectonophysics*, **6781**, pp. 1-15, 2002.

[7] Di Bucci, D., Corrado, S. & Naso, G. Active faults at the boundary between Central and Southern Apennines (Isernia, Italy). *Tectonophysics*, **359**, pp. 47-63, 2002.

[8] Favali, P., Funiciello, R., Mattietti, G., Mele, G. & Salvini, F. An active margin across the Adriatic Sea (central Mediterranean Sea). *Tectonophysics*, **219**, pp. 109-117, 1993.

[9] Billi, A. Solution slip and separations on strike-slip fault zones: theory and application to the Mattinata Fault, Italy. *Jour. of Struct. Geol.*, **25**, 2003.

[10] Salvini, F., Billi, A. & Wise, U.D. Strike-slip fault-propagation cleavage in carbonate rocks: the Mattinata Fault Zone, Southern Apennines, Italy. *Jour. of Struct. Geol.*, **21**, pp. 1731-1749, 1999.

[11] Oldow, J.S., Ferranti, L., Lewis, D.S., Cambell, J.K., D'Argenio, B., Catalano, R., Pappone, G., Carmignani, L., Conti, P. & Aiken, C.L.V. Active fragmentation of Adria, the north African promontory, central Mediterranean orogen. *Geology*, **30(9)**, pp. 779-782, 2002.

[12] De Alteriis, G. Different foreland basins in Italy: examples from the central and southern Adriatic Sea. *Tectonophysics*, 252, pp. 349-373, 1995.

[13] Christie-Blick, N. & Biddle, K. Deformation and basin formation along strike-slip faults. "Strike-slip deformation, basin formation, and sedimentation" eds. K. Biddle & N. Christie-Blick, *Soc. of Ec. Pal. and Min.,* Spec. Publ. No. **37**, pp. 1-34, 1985.

[14] Harding, P.T. Vierbuchen, C.R. & Christie-Blick, N., Structural styles, plate-tectonic settings, and hydrocarbon traps of divergent (transtensional) wrench faults. "Strike-slip deformation, basin formation, and sedimentation" eds. K. Biddle & N. Christie-Blick, *Soc. of Ec. Pal. and Min.,* Spec. Publ. No. **37**, pp. 51-77, 1985.

Earthquake Geodynamics

Series: Advances in Earthquake Engineering Volume 12

Unless the geological, tectonic, seismological and engineering aspects of earthquakes are mastered, constructions will never be safe. A thorough knowledge of earthquake geodynamics is also vital if the safety/cost ratio of all constructions is to be increased.

Containing contributions from renowned geoscientists with first-hand experience, this book discusses various aspects of earthquake geodynamics in seismically active regions. The chapters include lessons learnt from earthquakes that have struck urban areas during the past two decades and cover a wide variety of topics including the analysis of seismic sequences, the study of surficial deformation and geophysical techniques for microzonation purposes.

Contents: The 1999 earthquake in Izmit - the study of actualistic strike-slip tectonic forms; The Gujarat, West India Earthquake (26 January 2001): A geodynamic episode in an intra-plate compressional regime; Contribution of GIS to analysis of the 7 September 1999 Athens Earthquake; The neotectonic macrostructures and the geological basement, the main factors controlling the spatial distribution of the damage and geodynamic phenomena resulting from the Kalamata (13 September 1986) and Athens (7 September 1999) earthquakes; A sequence of low magnitude earthquakes as a result of local tectonic activation: the case of the Psachna area, Evia Island, Greece; The 26 July 2001 Skyros (north Aegean Sea, Greece) earthquake; Active faults and seismic hazard assessment at municipality level - the case of Tenea (Corinthia, Greece); Parameters of intensity distribution in the Izmit and Duzce (Turkey) earthquakes; Seismic strike-slip faults on a major boundary transverse to the Apenninic chain; and the case of the Molise (S. Italy) earthquake (31 October 2002).

Other related titles in the Advances in Earthquake Engineering Series:

Earthquake Resistant Engineering Structures IV
Editors: G. LATINI and C. A. BREBBIA
ISBN: 1-85312-984-4 2003 400pp

Innovative Approaches to Earthquake Engineering
Editor: G. OLIVETO
ISBN: 1-85312-885-6 2002 336pp

WITPRESS
Email: witpress@witpress.com
www.witpress.com

ISBN 1-85312-996-8

9 781853 129964

ISBN: 1-85312-996-8
ISSN: 1361-617X